



UNIVERSITÉ DU QUÉBEC EN OUTAOUAIS

Department of Computer Science and Engineering

**Spectral properties of long-period fiber gratings
with nematic liquid crystals**

by

Aleksandra Czapla

Thesis submitted as partial fulfillment of the requirements for the doctorate
degree in Science and Information Technology

June 2015



UNIVERSITÉ DU QUÉBEC EN OUTAOUAIS

Département d'informatique et d'ingénierie

**Propriétés spectrales
des réseaux de fibres a longue période
dotées de cristaux liquides**

par

Aleksandra Czapla

Thèse présentée comme exigence partielle du programme de doctorat en
sciences et technologies de l'information

June 2015

Jury d'évaluation

Président du Jury: Dr Ahmed Lakhssassi, Professeur à l'UQO

Membre du Jury: Dr Larbi Talbi, Professeur à l'UQO

Membre du Jury: Dr Frédéric Lesage, Professeur à l'UQO

Membre du Jury: Dr Jacques Albert, Professeur à Carleton University

Membre du Jury: Dr Leszek Jaroszewicz, Professeur à Military University of Technology

Directeur de recherche : Dr Wojtek J. Bock, Professeur à l'UQO

Table of Contents

| | |
|---|------------|
| Acknowledgement | 6 |
| Résumé | 8 |
| Abstract | 9 |
| Chapter 1 INTRODUCTION | 10 |
| 1.1 Background for conducting the research..... | 10 |
| 1.2 Thesis motivation and objective | 12 |
| 1.3 Organization of the Thesis | 15 |
| Chapter 2 INTRODUCTION TO LONG-PERIOD FIBER GRATINGS (LPFGs) | 16 |
| 2.1 Optical fiber structure and fiber modes..... | 17 |
| 2.2 Spectral properties of LPFGs | 21 |
| 2.3 LPFGs sensing properties | 25 |
| 2.4 Fabrication methods of the LPFGs | 33 |
| Chapter 3 INTRODUCTION TO LIQUID CRYSTALS (LCs) | 37 |
| 3.1 State of matter and basic parameters | 37 |
| 3.2 Thermal and wavelength dependence of the refractive indices of LC..... | 39 |
| 3.3 Liquid crystal in an electric field..... | 41 |
| Chapter 4 LIQUID CRYSTAL LONG-PERIOD FIBER GRATINGS (LC-LPFGs) STATE OF ART | 43 |
| Chapter 5 SIMULATION OF THE LC-LPFGs | 49 |
| 5.1 Introduction to the simulation procedures..... | 49 |
| 5.2 LPFG transmission properties analysis..... | 58 |
| 5.2.1 Impact of the fiber parameters to the LPFG transmission properties | 58 |
| 5.2.2 Impact of the grating parameters on the LPFG transmission properties | 66 |
| 5.2.3 The temperature effect to the LPFG transmission properties..... | 71 |
| 5.3 LC-LPFG transmission properties analysis..... | 77 |
| 5.3.1 Impact of the LC layer thickness to the LC-LPFG transmission properties..... | 77 |
| 5.3.2 Impact of the LC layer refractive index on the LC-LPFG transmission properties..... | 82 |
| 5.3.4 The temperature effect to the LC-LPFG transmission properties | 85 |
| 5.3.5 Analysis of the LPFG placed in a capillary filled with an LC..... | 93 |
| 5.3.6 The external electric field effect on the LC-LPFG transmission properties..... | 99 |
| Chapter 6 EXPERIMENTAL STUDIES OF THE LC-LPFGs | 103 |
| 6.1 Materials and experimental procedure | 103 |
| 6.1.1 Selection and specification of host fibers and LC materials..... | 103 |

| | |
|--|------------|
| 6.1.2 LPFGs manufacturing methods | 106 |
| 6.1.3 Measurement of spectral properties | 113 |
| 6.1.4 Procedure of LC layer application on the LPFGs | 114 |
| 6.2. Temperature effect on individual tested LPFGs..... | 119 |
| 6.3 Impact of LC presence on the spectral properties of LPFGs | 126 |
| 6.4 LC-LPFGs designed for thermal tuning | 130 |
| 6.4.1 Towards tuning of the thermal sensitivity of LPFGs by using LC | 131 |
| 6.4.2 Switching the LC-LPFG transmission spectrum in specific temperatures | 142 |
| 6.4.3 Compensating of the thermal effect in LPFGs by a proper choice of the LC layer | 151 |
| 6.5 LC-LPFGs designed for electrical tuning | 155 |
| 6.5.1 Electrical modulation of the transmission properties for LPFG placed in an LC cell | 155 |
| 6.5.2 Electrical modulation of the transmission properties for the LPFG with a LC layer | 157 |
| 6.5.3 Enhanced LC-LPFG electrical properties by a properly chosen temperature of the operation | 168 |
| Chapter 7 CONCLUSION..... | 172 |
| 7.1 Original contribution and significance of the work..... | 172 |
| 7.2 Further research directions..... | 177 |
| References..... | 179 |
| PhD publication list..... | 188 |
| List of acronyms..... | 193 |

Acknowledgement

First of all, I would like to thank my supervisor Professor Wojtek J. Bock for his continuous help, support and invaluable advice during the course of this study. I thank him also for always having his door open, and his endless patience.

I am grateful to Professor Tomasz R. Woliński for his supervision though the study in Poland. Without his encouragement, guidance, and many fruitful discussions for almost a decade this Thesis would not have been completed.

I owe my deepest gratitude to Professor Roman Dąbrowski from the *Military University of Technology* in Warsaw for providing the liquid crystal materials and sharing his great knowledge on them with me. I would also like to thank Doctor Edward Nowinowski-Kruszelnicki from the *Military University of Technology* in Warsaw who gave me helpful hints about the topic of liquid crystals, and guided me in their application. He always found time for me whenever I needed to talk about my research.

Thanks must also go to all members of the *Photonic Research Center* at *Université du Québec en Outaouais* in Canada for their help and their constructive feedback contributed to this thesis. In particular, I would like to especially thank Predrag Mikulic for long-period fiber gratings fabrication for the purpose of this Thesis. I learned a lot thanks to our collaboration. Also I would like to thank Daniel Brabant for sharing his knowledge with me in the LPFG simulation field.

Appreciation must also go to all the members of the Optics and Photonics division at the Faculty of Physics, *Warsaw University of Technology* in Poland. Especially, I would like to say big thanks to all my colleagues and friends from *Optoelectronics Laboratory* for their support, useful, and indeed necessary discussions regarding our work. The joy and enthusiasm they had for their research was contagious and motivational for me.

I gratefully acknowledge the funding sources that made my Ph.D. work possible. During my work in Poland I received a Scientific Ph.D. Scholarship from *Warsaw University of Technology* (2007-2008) and a Scholarship founded by the European Union in the framework of the *European Social Fund through the Warsaw University of Technology Development Program* (2009-2011). My work was also supported by the

Foundation for Polish Sciences (FNP) Professor's Subsidy „MISTRZ”. I was also awarded the “Merit Scholarship for Foreign Students” founded by the *Fonds Québécois de la Recherche sur la Nature et les Technologies* which was mandated by the Ministère de l'Éducation, du Loisir et du Sport du Québec and made my work possible in Canada.

Finally, I would like to thank my all family for their understanding. Especially, thanks from the bottom of my heart to my parents, Aurelia and Lech, who supported me throughout my life. I am who I am now because they believed in me and gave me all their love and care. I would like also to thank Jamil Ben Alluch. His love, carefulness, encouragements, patience and help in every possible way (even 6 587 km away from me) was the incredible support for me. Our daughter, Maya, who came into this world during the course of this study, also deserves for a special attention. My sweet Maya thank you for all the comforting breaks (mostly random) during writing this Thesis, for your sweet naps and for your unconditional love.

Résumé

Ce travail de recherche se concentre principalement sur l'étude de structures uniques nommées Réseaux de Fibres à Longue Période à Cristaux Liquides (RFLP-CL).

La présence d'une couche active de cristaux liquides (CL) offre une flexibilité dans la conception de composantes photoniques basées sur les réseaux de fibres à longue période (RFLP). L'étude contenue dans cette Thèse, se penche sur un examen approfondi et exhaustif de ce concept. L'usage de RFLP-CL hybrides dans ce travail de recherche a pour objectif de profiter de deux classes différentes de CL : celles avec une biréfringence moyenne-basse, offrant la gamme de variation la plus élargie pour l'index des CL lors de l'étude des RFLP. Il faut noter que les propriétés de « double résonance » des RFLP sont exploitées dans le contexte des RFLP-CL. La combinaison des RFLP à « double résonance » avec des CL est étudiée pour la première fois, à la connaissance de l'auteur. Plusieurs propriétés spectrales intéressantes et uniques peuvent être atteintes avec les RFLP dotées d'une couche de CL. Par exemple, grâce aux propriétés électro-optiques des CL, les RFLP-CL démontrent une sensibilité électrique, en addition aux sensibilités déjà existantes dans les RFLP. Par conséquent, ceux-ci sont capables d'opérer entre deux états de bandes d'atténuation, correspondant aux états de voltage allumés et éteints du champ électrique. De plus, l'ajout de la couche de CL rend possible l'ajustement de la réponse thermique des RFLP dans une vaste gamme de sensibilités de température, allant de sa croissance significative jusqu'à sa compensation. Par ailleurs, l'amélioration des capacités de changement électrique des RFLP-CL suite à un choix propice de température opérationnelle peut également être atteinte. Simultanément, tous les résultats expérimentaux obtenus dans ce travail de recherche seront supportés par une analyse théorique. Afin d'atteindre cet objectif, un modèle de RFLP-CL, basé sur le concept du RFLP doté d'une couche fine, a été développé. À travers l'usage d'un tel modèle théorique, il est possible d'offrir une meilleure compréhension des principes opératoires derrière les RFLP-CL. Par exemple, les calculs théoriques ont permis l'explication de la réponse thermique mesurée lors des expériences en laboratoire ; le RFLP était situé dans un capillaire rempli avec des CL. À la connaissance de l'auteur, l'étude des RFLP placés dans un capillaire en verre n'a jamais été effectué jusqu'à maintenant. Il a été découvert que de telles propriétés thermiques uniques pour ces RFLP-CL proviennent de différentes sensibilités aux températures dans les modes paires et impaires. En outre, une attention spéciale a été portée à cette partie de l'étude dans le but de déterminer précisément comment les éléments conçus à base de RFLP-CL peuvent être modifiés afin de régler leur réponse à travers des températures ou champs électriques externes.

Abstract

In this work unique structures are studied, namely *liquid crystal long-period fiber gratings* (LC-LPFGs).

The presence of an “active” liquid crystal (LC) layer gives additional flexibility in designing photonic components based on long-period fiber gratings (LPFGs). The studies presented within this Thesis contain a comprehensive and extensive examination of this concept. In this work the use of hybrid LC-LPFGs is aimed at taking advantage of two different LCs classes: those with medium- and low-birefringence, providing in this manner the widest LC index range variation investigated so far with LPFGs. It should also be pointed out that properties of “double-resonant” LPFGs are well exploited here in the context of the LC-LPFGs. The combination of “double-resonant” LPFGs with LCs is investigated for the first time, to the author’s best knowledge. Many interesting and unique spectral properties can be achieved with LPFGs that have a LC layer. For example, thanks to the electro-optical properties of LC materials, *LC-LPFGs* will demonstrate electric sensitivity in addition to the sensitivities of the grating itself. Consequently, they will be able to operate between two states of the attenuation bands corresponding with the on- and off-voltage states of the electric field. Moreover, the addition of the LC layer will make it possible to adjust the thermal response of the grating under a very wide range of temperature sensitivities: starting from its significant increase up to its compensation. Furthermore, improving the LC-LPFGs electric switching capabilities by a making a proper choice of the temperature operational range can be achieved as well. Simultaneously, all experimental results achieved in this work are supported by theoretical analysis. In order to reach this goal a LC-LPFG model has been developed which is based on the concept of a LPFG coated with a thin layer. Through the use of such a theoretical model it is possible to provide a better understanding of the principles of operation behind the LC-LPFGs. For example, the theoretical calculations allowed to explain the LC-LPFG’s thermal response measured in the experiment, where the LPFG was placed into a capillary filled with LC. To the author’s best knowledge, the LPFG placed into a glass capillary filled with any liquid material was never theoretically studied so far. It was found that such unique thermal properties for this LC-LPFG comes from different sensitivities to temperature of modes with odd and even radial numbers. In addition, a special attention has been devoted in this part of the work to accurately determining how elements designed with LC-LPFGs can be modified to tune their response by temperature and/or external electric fields.

Chapter 1 INTRODUCTION

1.1 Background for conducting the research

Optical fibers were proposed for telecommunication transmission nearly four decades ago by Kao and Hockham. In 1966, Kao calculated that *“with a fiber of purest glass it would be possible to transmit light signals over 100 kilometers – compared to only 20 meters in the 1960s”* [1]. Nowadays, optical fibers are basic elements in some of the most important communications achievements such as high-speed internet. Optical fibers have also been applied in other fields. For example, they have been widely used in optical sensors since the early 1970s [2]. All around the world, projects related to fiber-optic sensors can be found. Throughout Europe, North America and Asia, especially China and India, fiber sensor networks are improving the ability to monitor tunnels, bridges, buildings, power lines or dams.

In addition, optical fibers with micro-periodic structures have recently generated a great interest in the scientific community. This is due to the fact that they provide new possibilities for light guiding and control that have not been obtainable with conventional optical fibers. Such structural features are also a key element in novel optical fiber sensing devices. One of the most mature classes of this kind of fiber device comprises long-period fiber gratings (LPFGs). Within a relatively short time it became obvious that LPFGs could be successfully incorporated into an optical communications network or into a fiber-optic sensing system [3-11]. This is because they provide a mechanism for producing a wavelength-dependent attenuation in the transmission spectrum, which can be controlled by external effects. Compared to other optical devices, LPFGs have a number of unique advantages such as low-level back reflection, compact construction, low insertion losses, resistance to harsh environments, immunity to electromagnetic interference and often greater sensitivity than conventional sensors. LPFGs have also found a variety of possible applications in optical communications as gain-flattening filters for erbium-doped fiber amplifiers (EDFAs) [12], as wavelength division multiplexing (WDM) systems [13] or as wavelength-selective optical fiber polarizer components [14-17].

Furthermore, LPFGs combined with liquid crystals (LCs) have been seen as promising structures for creating a new platform for tunable fiber devices. LCs are self-organized anisotropic materials that exhibit high electro-optic and thermo-optic effects associated with their birefringence, their dielectric anisotropy and the thermal dependence of their refractive indices (RIs) [18-26]. Therefore, the attractiveness of these structures result from the fact that they merge these unique LCs properties with LPFGs and extend in this

way the sensing capabilities of the LPFG itself. Consequently, a new class of photonic components, referred to here as liquid crystal LPFGs (LC-LPFGs), were born. Even though they are a relatively new area of research in fiber optics sensors, the results achieved so far brought to light the various advantages of such structures. Up to now, some publications concerning the experimental results of LPFGs surrounded by the LC were presented [28-35]. For example, in the [27] a modulation of the attenuation band intensity based on the electrical switching of a nematic liquid crystal (NLC) around a photo-induced LPFG was shown. In the [29] it was demonstrated that the cascade LC-LPFG structure might serve as an arbitrary loss filters that could compensate a non-uniform optical gain in an EDFA. Later, in [32] the idea of a coated LPFG with a thin LC layer (in the order of 1 μm) was brought forward. The host LPFG used in this research was fabricated by the CO_2 laser irradiation. The experimental results along with the theoretical analysis presented there, shown that the efficient thermal tuning can be achieved for such a LC-LPFG design. However, authors of this publication did not include the thermal response of the host fiber in their theoretical model (which can significantly contribute in the LC-LPFG thermal sensitivity). Also noteworthy is the successful use of LCs in creating LPFGs in holey fibers. An electrically controllable fiber-optic filter for a broad-band rejection has been shown by periodically poling a liquid-crystalline core in a hollow-core fiber [33]. As can be then concluded, it has been demonstrated that the LPFG and LC combination affords great design flexibility and shows promise to provide a variety features useful in the photonics field. However, there are still a number of design challenges to be met, as discussed in the next section.

1.2 Thesis motivation and objective

The main motivation of this work was to improve and to extend the LPFGs sensing abilities by merging them with LC materials. In this context the use of LC materials has gained a particular attention since their unique properties can provide a new highly-tunable all-in fiber structure, named here as a liquid crystal long-period fiber grating (LC-LPFG).

The experiments already carried out in the past [28-35] have shown that LC-LPFGs can realistically contribute to the creation of new photonic devices. However, their exact potential is still an open question and development in this area has only started to pick up speed. Fast, accurate and reliable measurements of physical parameters such as temperature, electric field or surrounding refractive index (SRI) are essential when it comes to ensuring the smooth operation of processes in many industrial or in security applications. It has become necessary to develop the technology to enable construction of effective and reliable LC-LPFG-based devices. In order to reach this goal, an understanding of the design factors for LC-LPFGs is necessary. With the ability to tailor the spectral characteristics of the LC-LPFGs (e.g., by a proper choice of fiber or LC materials or even by a proper choice of temperature range of operation) better, more sensing-efficient and application-specific elements could be obtained. For example, it has been shown that, for the highest sensitivity, the LPFG should be designed to couple light from the propagating core mode to a cladding mode at a wavelength near the phase matching turning point [53]. As a result a generation of dual resonant bands which shows sensitivities of opposite sign can be observed in the LPFG transmission spectrum. In this work this phenomenon will be exploited for the first time to measure LC-LPFGs thermal and electric responses. It was also previously demonstrated that by implementing of a thin layer of a high refractive index (HRI) material to the bare LPFG one can greatly expand the sensing capabilities over those offered by the LPFG surrounded by this material [36-52]. The spectral properties of this sensor type, which will be referred to as the HRI layer LPFG, can (in principle) be adjusted by varying the RI of the layer which is greater than that of the cladding. Following this idea, in the work presented here, such a LC-LPFG design is mainly investigated. This approach can solve the LC RIs magnitude problem, since most of LC materials have refractive indices higher than refractive index of silica glass. As a result, surrounding by these LC types the LPFG, which based on the silica glass fiber, will not provide require sensitivity [67-69].

Taking into account all of the above, the three most interesting and original objectives realized through these experimental studies are the following:

Objective 1.1: Thanks to the presence of a properly chosen LC layer, the thermal response of the LPFG can be adjustable over a very wide temperature sensitivity range: starting from a significant increase of the LC-LPFG thermal sensitivity down to its compensation and simultaneously providing the possibility to switch its spectral characteristics in specific temperature values.

Objective 1.2: The LC-LPFG will demonstrate electrical sensitivity in addition to the sensitivities of the grating itself and will be able to operate between two states of the attenuation bands corresponding with on- and off-voltage states of the electric field.

Objective 1.3: In the LC-LPFG it will be possible to tune the cladding modes propagation properties within the transition region by altering external factors (such as temperature or/and electric field), thus providing novel high-efficiency control of their optical properties.

Better understanding of the principles of operation behind LC-LPFGs is also needed. In order to reach this goal the LC-LPFG model has to be developed. Through the use of such a theoretical model, this work is aimed to determine how LC-LPFG design elements can be modified to tune their response by temperature and/or external electric field.

In the literature there is a lack of studies directly devoted to the LC-LPFG theoretical analysis. Nevertheless, in this work it will be shown that LC-LPFGs, in the majority of cases, can be analyzed as a structure based on the LPFG coated with an HRI layer. Such HRI layer-enhanced LPFG structure has been studied quite thoroughly in literature [36-52]. However, the results presented so far do not cover all the spectrum of issues when the LC-LPFG is theoretically analyzed. For example, the thermal sensitivity of the HRI layer LPFG (which include the thermal response of the layer and the host LPFG) was not theoretically investigated up to now. The LPFG placed into a glass capillary filled with any liquid material was also never theoretically studied so far, to the author's best knowledge. It seems therefore that there remains significant hurdles to overcome when it comes to establishing the LC-LPFG model.

In order to fill the gap of the current state of research, the three most original objectives that will concern the LC-LPFG theoretical studies, are the following:

Objective 2.1: Simulate as accurately as possible the LPFG transmission spectra with adequate parameterization of the LC layer on the bare grating.

Objective 2.2: Simulate the sensitivity effect to the temperature and/or external electric field for the LC-LPFG model composed by four layers.

Objective 2.3: Simulate the spectral properties of the LPFG placed in the capillary filled with LC by using the LC-LPFG models composed by five layers and the thermal response of such a designed structure.

The topics proposed above are very timely, since LC-LPFGs have reinvigorated research in the mainstream fields of fiber optics and LCs. Interest in the scope of this work has already been shown by support offered inter alia by:

- Scholarship awarded by the European Union in the framework of the European Social Fund through the Warsaw University of Technology Development Program (2009-2011),
- “Merit Scholarship for Foreign Students” awarded by the *Fonds Québécois de la Recherche sur la Nature et les Technologies* which was mandated by the Ministère de l'Éducation, du Loisir et du Sport du Québec (2008-2013).

It is also worth adding that studies for this Thesis were carried out at two collaborating research groups at the *Faculty of Physics, Warsaw University of Technology* in Poland and at *Centere de Recherche en Photonique, Université du Québec en Outaouais* in Canada. It has to be emphasized as well that this PhD Thesis is the first one, to the author's best knowledge, to be strictly devoted to studies of new highly-tunable all-in fiber structures such as LC-LPFGs.

1.3 Organization of the Thesis

Chapter 1 gives the background and motivation for conducting the research. It also presents the main objectives and the structure of the Thesis.

Chapter 2 describes some background on the fiber modes and gives the basic theory on the LPFGs with a special attention of their sensing properties. An overview of the fabrication techniques for LPFGs with the desired physical parameters is given there as well.

Chapter 3 introduces the basic properties of LC materials.

Chapter 4 provides an overview of the LC-LPFGs based devices reported previously in literature.

Chapter 5 presents the theoretical analysis of the LC-LPFG spectral properties. It starts with an introduction to the simulation procedures used in order to establish the LC-LPFG model. Later, the theoretical analysis of the LPFG with respect to its physical parameters (co-dopant percentages in the host fiber, specific grating parameters, etc.) is provided. Once the impact of these constraints is explained, the LC-LPFG-based devices are examined. A special attention in this part of the work is put into modeling the thermal and electric responses of the LC-LPFG. In addition, a separate section is devoted to studying the spectral properties and the thermal response of the LPFG placed in the capillary filled with a LC.

Chapter 6 starts to present the materials and procedures used during this research: host fibers and various LCs; methods to produce LPFGs, namely the arc discharge and the UV-laser based techniques; the experimental procedures to combine LPFGs with LCs; the experimental setups to conduct the temperature and external electric effects measurement. Next, the impact of the LC layer presence on the LPFG spectral properties is discussed. From this point on, a special attention is put to demonstrate the LC-LPFGs tuning possibilities by external factors such as temperature or/and the external electrical field. It is shown that the LC layer gives a great flexibility in adjusting the LPFG thermal sensitivity (starting from a significant increase of the LC-LPFG thermal response down to its compensation). In addition, by adding the LC layer to the LPFG structure a fast switching ability of the attenuation bands in specific temperature values can be obtained. Later, it is presented that the modification in depths and resonant wavelengths of the attenuation bands can be achieved when the LC-LPFG is electrically tuned. This effect is possible since the cladding modes' transition occurs when the external electric field is applied to the LC-LPFG. As a result, the LC-LPFG is able to operate between two sets of attenuation bands corresponding with on- and off-voltage states. At the end of this section it is also shown that LC-LPFGs electric sensitivity can be expanded by a properly chosen temperature of operation.

Chapter 7 concludes the Thesis. In addition, it highlights the problems encountered during the work and presents suggestions for further research work on the subject.

Chapter 2 INTRODUCTION TO LONG-PERIOD FIBER GRATINGS (LPFGs)

Fibers that consist of a periodic perturbation of the refractive index in the core and/or geometry are referred to as *fiber gratings*. Fiber gratings fall into two general classifications based upon the period of the grating: *fiber Bragg gratings* (FBGs) and *long-period fiber gratings* (LPFGs) [6,7]. The main difference between these two fiber gratings types are summarized in Tab. 2.1. Numerous physical parameters for this structures can be varied, including: the induced index change, the length, the apodization, the period chirp, the fringe tilt, etc. By varying these parameters, gratings can be made with extremely sharp spectral features and configurable dispersive characteristics.

Tab. 2.1 Basic differences between FBGs and LPFGs.

| fiber Bragg gratings FBG | long-period fiber gratings LPFG |
|--|---|
| have a sub-micron period | have period typically in the range 0.1-1 mm |
| couple light from the forward-propagating core mode of the optical fiber to a backward, counter-propagating | promotes coupling between the propagating core mode and co-propagating cladding modes |
| output spectra show that these grating devices act as narrow band-stop filters (causing attenuation at a single Bragg wavelength) | transmission spectra consist of several attenuation bands at different wavelengths. |
| In general, LPFGs are more sensitive to environmental perturbations than FBGs, which could be a disadvantage when manufacturing LPFG based telecommunications devices. However, this feature of LPFGs can be well exploit when they are intended to be used as a sensor component. | |

This work is dedicated to studying the second type of the fiber gratings: LPFG. The following chapter first introduces optical fibers on its own. Then, the LPFG structure is presented in order to give the reader the necessary fundamental understanding. A separate section is also dedicated to describing the basic sensing properties of the LPFG. The inherent sensitivity of the LPFG to the surrounding refractive index (SRI) acting on the fibre (which is not the case for the FBG since this fiber grating type cannot measure SRI without prior physical deformation of the fibre material) is the most important feature considered in this part. In addition, an overview of different techniques for LPFG fabrication is provided.

2.1 Optical fiber structure and fiber modes

Modes are fundamental concepts in optical fibers. The knowledge of their propagation characteristics is crucial to the design of numerous optical fiber based devices [70-74].

The mode theory is based on the electromagnetic wave behavior. The governing evolution equations for the electric and magnetic fields are provided by Maxwell's equations. These can be applied to analyze light propagation in optical fibers once the necessary assumptions have been established. By assuming that the optical fiber is linear, isotropic, homogeneous, lossless dielectric material without any sources such as currents, free charges and ferromagnetic medium, Maxwell's equations may be written as follows:

$$\nabla \times \vec{E} = -\partial \vec{B} / \partial t \quad (2.1.1a)$$

$$\nabla \times \vec{H} = \partial \vec{D} / \partial t \quad (2.1.1b)$$

$$\nabla \cdot \vec{D} = 0 \quad (2.1.1c)$$

$$\nabla \cdot \vec{B} = 0 \quad (2.1.1d)$$

where \vec{E} , \vec{H} , \vec{D} , \vec{B} are the electric field, magnetic field, electric displacement field and magnetic induction, respectively.

The material relations in the isotropic material are:

$$\vec{D} = \varepsilon \vec{E} \quad (2.1.2a)$$

$$\vec{B} = \mu_0 \vec{H} \quad (2.1.2b)$$

, where $\varepsilon = \varepsilon_0 n^2$ is the dielectric permittivity of the isotropic medium with the dielectric permittivity of free space ε_0 , and μ_0 is the magnetic permeability of free space. Standard wave equations can be solved from the above expressions to yield the general the wave phenomena of electromagnetic fields within optical fiber. From equations (2.1.1) and (2.1.2) can be obtained:

$$\nabla \times \vec{E} = -\mu_0 (\partial \vec{H} / \partial t) \quad (2.1.3a)$$

$$\nabla \times \vec{H} = \varepsilon (\partial \vec{E} / \partial t) \quad (2.1.3b)$$

Taking the curl of equation (2.1.3a) and using equation (2.1.3b) we get:

$$\nabla \times (\nabla \times \vec{E}) = -\epsilon\mu_0(\partial^2 \vec{E}/\partial t^2) \quad (2.1.4)$$

Using the vector identity $\nabla \times (\nabla \times \vec{A}) = \nabla(\nabla \cdot \vec{A}) - \nabla^2 \vec{A}$, and noting that $\nabla \cdot \vec{E} = 0$, provides one homogeneous wave equation:

$$\nabla^2 \vec{E} = \epsilon\mu_0(\partial^2 \vec{E}/\partial t^2) \quad (2.1.5)$$

Equation (2.1.5) is referred to as the wave equation or Helmholtz equation for \vec{E} . In the same manner, an equation for \vec{H} can be derived:

$$\nabla^2 \vec{H} = \epsilon\mu_0(\partial^2 \vec{H}/\partial t^2) \quad (2.1.6)$$

Subsequently, the time dependent harmonic fields with an $e^{i\omega t}$ dependence can be assumed, where ω is a single angular frequency. For a guided mode travelling in the z -direction (along the fiber axis) with propagation constant β , the electric and magnetic field vectors defined in cylindrical co-ordinates can be written as:

$$\vec{E} = \vec{E}_o(r, \phi)\exp[i(\omega t - \beta z)] \quad (2.1.7a)$$

$$\vec{H} = \vec{H}_o(r, \phi)\exp[i(\omega t - \beta z)] \quad (2.1.7b)$$

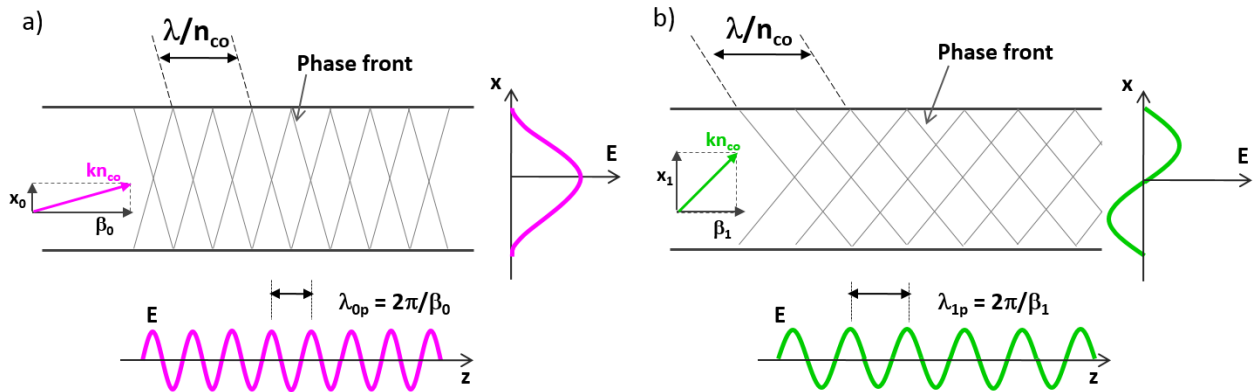


Fig. 2.1.1 Standing wave formation, which has a period corresponding to the wavelength $\lambda_0 = 2\pi/\beta$, for a guided mode: fundamental (a) and higher-order (b) modes.

Therefore, the modes have a spatial and time dependence proportional to $e^{i(\omega t - \beta z)}$, for the β along the fiber axis (component of k in the z -direction) equal to the $2\pi/\lambda_0$. This solution typically consists of a set

of electromagnetic field configurations that form a standing-wave pattern in a direction transverse to that varies periodically along the fiber's axis (as can be seen in Figure 2.1.1).

It is now suitable to define one more key parameter - the V -number (also known as the normalized frequency) which is expressed as follows:

$$V = \left(\frac{2\pi a}{\lambda} \sqrt{n_{co}^2 - n_{cl}^2} \right)^2 = a^2 k^2 (n_{co}^2 - n_{cl}^2) \quad (2.1.8)$$

V -number gives the information of the number of modes and of the range of propagation constants a fiber supports. Due to the presence of certain boundary conditions to the electromagnetic fields that must be met at the interfaces between the waveguide regions, there is only a discrete number of valid solutions corresponding to every V -number. Additionally, to *guided modes* propagating into the core of the optical fiber, there are also *cladding* and *leaky modes*, both of which utilize the waveguide nature of the core and cladding material. The penetration of low-order and high-order modes into the cladding region indicates that some portion is refracted out of the core. The refracted modes trapped in the cladding region (due to its dimension) are called *cladding modes*. Another class of modes propagating along the optical fiber is the *leaky modes*. A *leaky mode* has an electromagnetic field that decays monotonically (i.e., steadily) for a finite distance in the transverse direction (i.e., at a 90 degree angle to the plane or axis of the fiber), but becomes oscillatory beyond that finite distance.

Additionally, there are different types of modes depending on the electromagnetic field pattern of the radiation measured in a plane perpendicular to the propagation direction of the beam. Modes can be classified as:

- *transverse electric* (TE) modes: $E_z = 0$
- *transverse magnetic* (TM) modes: $H_z = 0$
- *hybrid modes*: $E_z \neq 0$ and $H_z \neq 0$ and are denoted as either HE or EH modes, respectively depending on whether the magnetic component, H_z , or the electric component, E_z , has a dominant effect on the magnitude of the transverse field.

The fiber modes are usually referred to as *linear polarization* (LP) modes using the called weakly guiding fiber approximation: $n_{cl}/n_{co} \cong 1$, first introduced by Gloge in 1971 [75]. This approximation is valid for conventional single mode (SM) fibers since their refractive index difference, $\Delta n = 1 - n_{cl}/n_{co}$, is of the order of 0.3% - 1%.

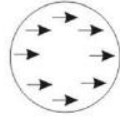



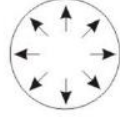

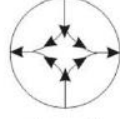

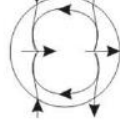



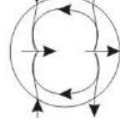

| LP mode designations | Traditional designations | Electric field distribution | Intensity distribution of E_x | |
|----------------------|---|--|--|---|
| LP_{01} | HE_{11} $\begin{cases} m=1 \\ l=0 \\ p=1 \end{cases}$ |  |  | |
| | |  |  | |
| LP_{11} | TM_{01} $\begin{cases} m=0 \\ l=1 \\ p=1 \end{cases}$ |  |  | |
| | | HE_{21} $\begin{cases} m=2 \\ l=1 \\ p=1 \end{cases}$ |  |  |
| | | |  |  |
| LP_{21} | HE_{31} $\begin{cases} m=3 \\ l=2 \\ p=1 \end{cases}$ |  |  | |
| | |  |  | |

Fig. 2.1.2 Relation between the electric field vectors and intensity profiles of the LP_m modes and conventional modes [70]

The LP modes are not exact modes of the fiber (except for the fundamental mode) but they are combinations of the modes found from the exact theory of the wave guide. The relation between the LP modes and conventional modes is presented in Fig. 2.1.2. Such modes are said to be degenerate. LP modes provide a way to visualize a mode with ease, since in one set of degenerative modes, only one electric and one magnetic field component are of importance [74]. The possible solutions depend on the arbitrary selection of the orientation of the electric field vector \vec{E} (the magnetic field vector \vec{H} is always perpendicular) and another set of solutions is obtained when the polarities of these field vectors are reversed.

2.2 Spectral properties of LPFGs

Long Period Fiber Gratings (LPFGs) consist of a periodic index modulation of the refractive index of the core of a single mode fiber (SMF). Typically, the periodicity of LPFGs ranges between 100 μm to 1mm (the remaining basic parameters that characterize LPFGs are presented in Table 2.2.1). As a result, dips are created in the transmission spectrum at wavelengths where there is a coupling between the core and co-propagating cladding modes. The positions of the resonances in wavelength are determined by the propagation constants of the core and cladding modes, which, in their turn, depend on the average constraints of the fiber grating structure such as: the refractive index (RI) profile, the cladding radius, and the RI of the surrounding medium. These parameters are determined by the initial parameters of the fiber itself and the average change in the fiber (dc component) prompted by the formation of the LPFG. The amplitudes of the resonances depend on the strength of modulation (ac component) of the fiber parameters in the LPFG.

Tab. 2.2.1 Basic parameters characterizing LPFGs.

| | | |
|---|---|--|
| 1 | Period of the LPFG, Λ | 100 – 1000 μm |
| 2 | Length of the LPFG, L | a few cm |
| 3 | Resonant wavelength, λ_{res} | center wavelength of the dip of the attenuation band |
| 4 | Full-width half-maximum of the attenuation band, FWHM | 10 – 60 nm |
| 5 | Loss of the attenuation band, L_{dB} | 10 - 35 dB |
| 6 | Index modulation within the core, Δn (depending upon the inscription method) | 10^{-4} – 0.1 |

There are several methods that can be used to analyze mode coupling in optical fibers; among them, the coupled-mode theory (CMT) is well developed and the one most often used to analyze LPFGs [6,7]. J.R. Pierce first developed this method in 1954 for the analysis of electromagnetic structures with regard to

electron beam waves [76], before it was adopted for use in optical waveguide theory. The basic concept of operation of LPFGs was first proposed by Vengsarkar *et al.* [8] and is illustrated in Figure 2.2.1a.

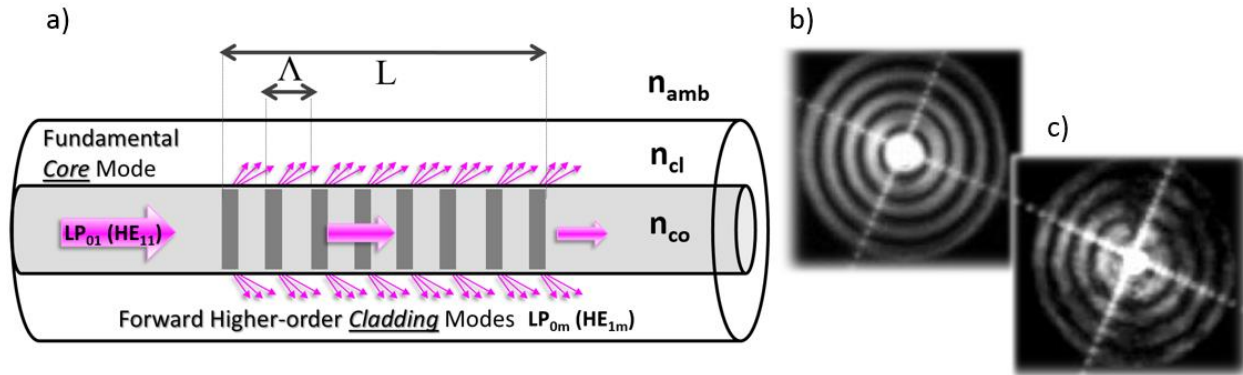


Fig. 2.2.1 (a) Coupling of a fundamental guided mode to a cladding mode in an LPFG. Distribution of the field of the cladding mode obtained for fiber segments in front of the grating, with lengths of (b) 1 cm and (c) 75 cm [62].

Light energy in the fundamental guided mode is perturbed by the presence of the grating in the fiber core and couples to co-propagating cladding modes (which are quickly attenuated, as is illustrated in Figures 2.2.1b and 2.2.1c), depending on the periodicity and amplitude of the RI variation of the LPFG. This is achieved by perturbing the phase of one mode such that it matches the phase of the other: the so-called ‘phase-matching condition’.

The phase-matching condition between the fundamental mode and the forward propagating cladding modes for the LPFG is given by:

$$\beta_{co} - \beta_{cl,m} = 2\pi/\Lambda \quad (2.2.1)$$

where β_{co} and $\beta_{cl,m}$ are the propagation constants of the forward fundamental core mode and the forward cladding mode of order m , respectively. Using the definition:

$$\beta = 2\pi n/\lambda = kn \quad (2.2.2)$$

where n is the effective mode RI and k is the free-space propagation constant, Eq. (2.1) can be transformed as follows:

$$\beta_{co} - \beta_{cl,m} = k(n_{co}^{eff} - n_{cl,m}^{eff}) = 2\pi/\lambda (n_{co}^{eff} - n_{cl,m}^{eff}) = 2\pi/\Lambda \quad (2.2.3)$$

Consequently, the resonant wavelength λ_{res} , for an attenuation band is given by:

$$\lambda_{res} = \Lambda(n_{co}^{eff} - n_{cl,m}^{eff}) = \delta n_m^{eff} \Lambda \quad (2.2.4)$$

where n_{co}^{eff} , $n_{cl,m}^{eff}$ and Λ stand for the effective RI of the core mode, the effective RI of the m th cladding mode and the period of the LPFG, respectively.

A SMF's cladding supports several different modes and numerous attenuation bands, centered at resonance wavelengths $\lambda_{res,m}$ that correspond to different cladding modes; they are formed in the LPFG transmission spectrum as is illustrated in Figure 2.2.2.

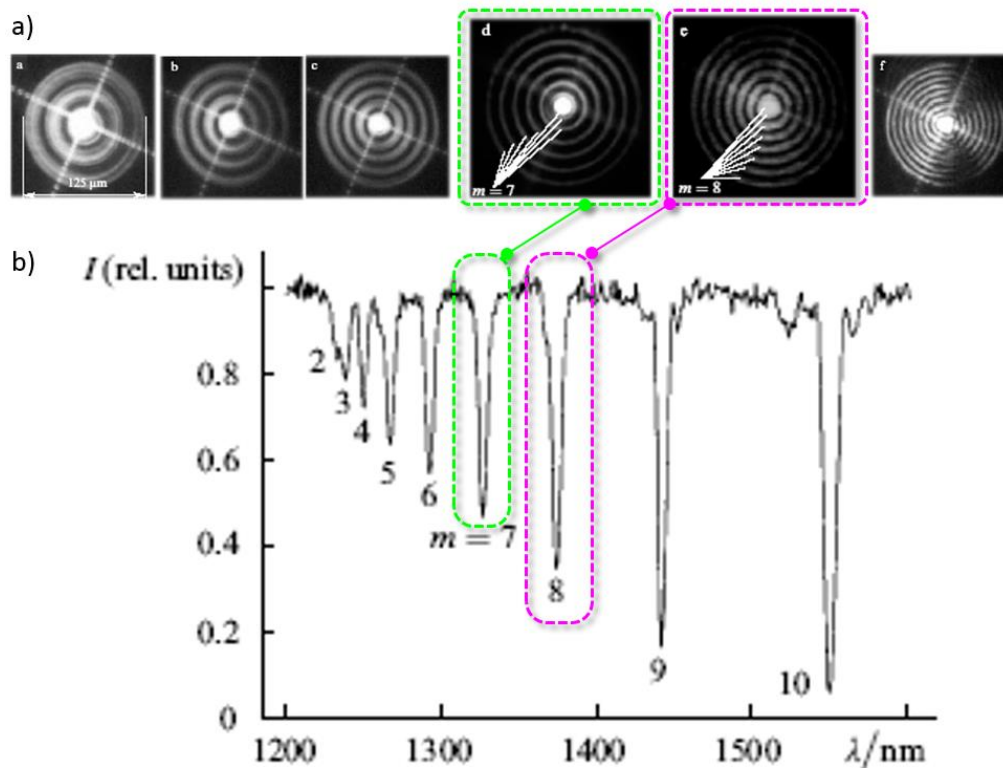


Fig. 2.2.2 (a) Near-field intensity distribution of HE_{1m} cladding modes: all the modes, as follows from theoretical consideration, have symmetry around the fiber axis, which corresponds to azimuthal number $l = 1$. The number of rings is equal to the radial mode number m . (b) Corresponding transmission spectrum of the LPFG [62].

A particular grating period can cause mode coupling at a predictable wavelength. Shorter LPFGs are generally required to couple with higher-order modes, while coupling with lower-order modes is more

easily achieved by using LPFGs with larger periods. The wavelength dependence of the effective indices is due to material and waveguide dispersion. From Equation (2.2.4), it can be shown that:

$$\frac{d\lambda_{res}}{d\Lambda} = \frac{(n_{co}^{eff}(\lambda) - n_{cl,m}^{eff}(\lambda))}{1 - \Lambda \left[\frac{n_{co}^{eff}(\lambda)}{d\lambda} - \frac{n_{cl,m}^{eff}(\lambda)}{d\lambda} \right]} \quad (2.2.5)$$

Material dispersion can be assumed to have the same overall effect on $n_{co}^{eff}(\lambda)$ and $n_{cl,m}^{eff}(\lambda)$. Thus, when the difference is taken, it is the waveguide dispersion which is the dominant contributor to the grating spectrum [16].

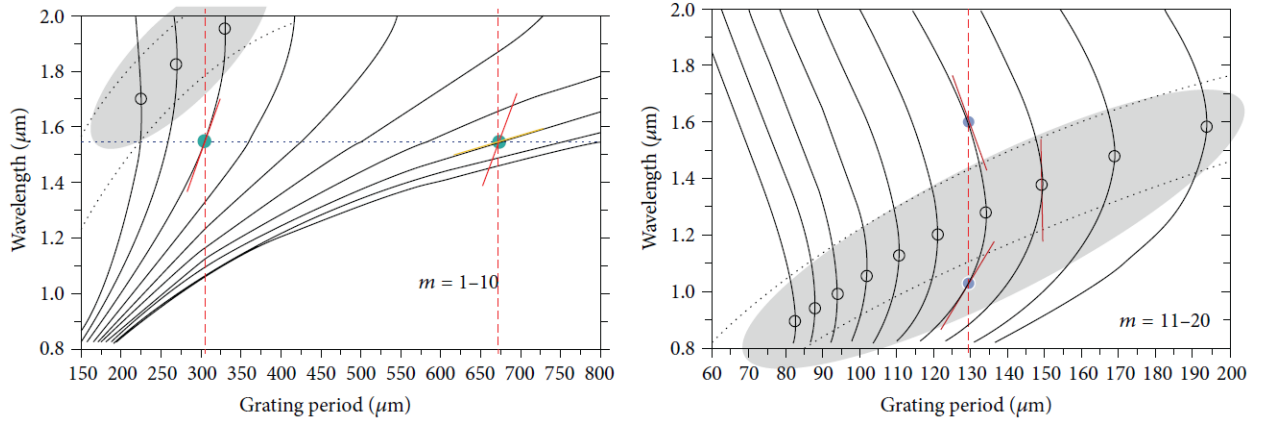


Fig. 2.2.3 Phase matching curves with designated turning points. The calculated relationship between resonance wavelength and LPFG period for m : (a) from 1 to 10, (b) from 11 to 20 cladding modes [52].

The plots in Fig. 2.2.3, so-called phase matching curves, describe the relationship between grating periodicity and wavelength where coupling takes place between guided and cladding modes [52]. It is clear that as the higher-order cladding modes are encountered, the slope of the resonant line changes from a positive value to a negative value at a particular mode. Thus, three types of LPFGs can be formed, depending on the grating period:

- 1) Positive linear-dispersion LPFGs: $\frac{d\lambda_{res}}{d\Lambda} > 0$ (2.2.6)

- 2) Negative linear-dispersion LPFGs: $\frac{d\lambda_{res}}{d\Lambda} < 0$ (2.2.7)

- 3) Quadratic-dispersion LPFGs: $\frac{d\lambda_{res}}{d\Lambda} = 0$ (2.2.8)

The solution to coupled-mode equations for two interacting co-propagating modes shows that the energy exchange law is sinusoidal at the exact resonance. The value of the minimum of the attenuation band, T_m ,

created by the coupling between the core mode and the m th cladding mode, can be expressed as follows [10]:

$$T_m = 1 - \sin^2(\kappa_m L) \quad (2.2.9)$$

where κ_m is the cross-coupling coefficient. According to the CMT, the resonance condition is achieved when κ_m is increased to maximize the power transfer to the cladding; it is increased until the condition $\kappa_m L = \pi/2$ is met, where $L = N \cdot \Lambda$ is the length of the grating and N represents the number of periods. As a result, in a filter based on an LPFG, a longer length of the grating does not always imply a better response; rather an optimum length should be determined. The optimum value of the number of periods can be estimated to be of $N_{opt} = \pi/2\kappa_m\Lambda$.

2.3 LPFGs sensing properties

The LPFG transmission spectrum, and the centre wavelengths of the attenuation bands, are sensitive to the local environment, like:

- applied tensile stress: can modify the effective indices of core and cladding modes through the elasto-optic effect and the grating period because of elongation (see e.g. [9, 11]);
- temperature: thermo-optic effect is responsible for the effective index change while thermal expansion for period modification in the case of the temperature changes (see e.g. [54-55, 111-118]);
- bending breaks the cylindrical symmetry of the LPFG: promoting coupling to the asymmetric azimuth cladding modes that are differently affected in their effective indices depending on the region of the fiber where they are confined (see e.g [56-58]);
- surrounding refractive index (SRI): the effective indices of cladding modes directly depend on the index contrast between the cladding and the surrounding medium being a boundary condition in the solution of the waveguide equation (see e.g. [52,62-69]).

These peculiar spectral features of LPFGs could make them potentially used in various applications. Although they were primarily introduced as devices for optical communications [8] (for which they have been used to develop band rejection filters, gain equalizers, optical amplifiers, fiber couplers, dispersion compensators [4]), they immediately show promise in multiple applications related to the sensing field [9, 59]. In particular, LPFGs represent above all one of the most promising fiber grating technological platforms, to be employed in a number of chemical applications because of their intrinsic sensitivity to

SRI changes [52]. Up until now great efforts have been made in order to enhance the performance of LPFGs in SMFs in terms of tuning capability and/or sensitivity. For instance several approaches have been proposed to achieve remarkable sensitivities such as cladding etching, LPFG design for coupling to higher order modes near their dispersion turning points or in-fiber complex configuration including multi-gratings [59-61]. Additionally, once the effects of depositing a thin HRI layer onto the LPFG have been discovered, great sensitivity enhancements in comparison to LPFGs itself have been obtained due to the so-called modal transition [36-53].

The center wavelength λ_{res} of an attenuation band is specified by the phase-matching condition (2.2.4) where:

$$\delta n_m^{eff} = n_{co}^{eff}(D, T, n_i) - n_{cl,m}^{eff}(D, T, n_i, n_{SRI}) \quad (2.3.1)$$

The equation above clearly demonstrate that the core n_{co}^{eff} and clad $n_{cl,m}^{eff}$ effective indices of the LPFG are dependent on a physical deformation D (bending, torsion, strain, pressure etc.), temperature, RIs of the external layers of the fiber n_i and to SRI. The strength of the LPFG sensitivity to environmental parameters is influenced by:

- the composition of the optical fiber,
- the period of the grating which determines a range of the modes which coupling take place within the investigated spectral range,
- the order of the cladding mode corresponding with the measured attenuation band. In this term the LPFG sensitivity reaches its maximum when the mode is close to so-called turning point (see Fig. 2.2.3). In these regions the slope of the phase matching curves changes from positive to negative and beyond this turning point. Therefore, for each grating period, there are two resonance wavelengths for each cladding mode. As a result, in the LPFG transmission spectrum with a suitably chosen value of the grating period, the dual resonant band can be observed which shows a sensitivity of opposite sign [124].

There is one common factor that relates sensitivity of the LPFG to all forms of external perturbation and is defined by [9]:

$$\gamma = (d\lambda_{res}/d\Lambda)/\delta n_m^{eff} \quad (2.3.2)$$

γ describes the waveguide dispersion and it is referred to as the general sensitivity factor. Typically, the LPFGs are investigated while grating is being kept straight (which is also the case of the research presented

within this Thesis). Therefore, the influence of bending and torsion can be neglected. The strain measurements were not included in this work and this effect is not discussed here (a detailed description of the LPFG strain sensitivities is provided e.g. in [53-54]. According with equation (2.3.2) the temperature sensitivity ($d\lambda_{res}/dT$) can be represented as follows [9]:

$$d\lambda_{res}/dT = \lambda_{res} \cdot \gamma \cdot (\alpha + \Gamma_T) \quad (2.3.4)$$

The temperature sensitivity factor Γ_T is determined by thermo-optic coefficients of the core/cladding materials ξ_{co}, ξ_{cl} , by the mode order and is expressed as follow:

$$\Gamma_T = (\xi_{co}n_{co}^{eff} - \xi_{cl}n_{cl,m}^{eff})/\delta n_m^{eff} \quad (2.3.5)$$

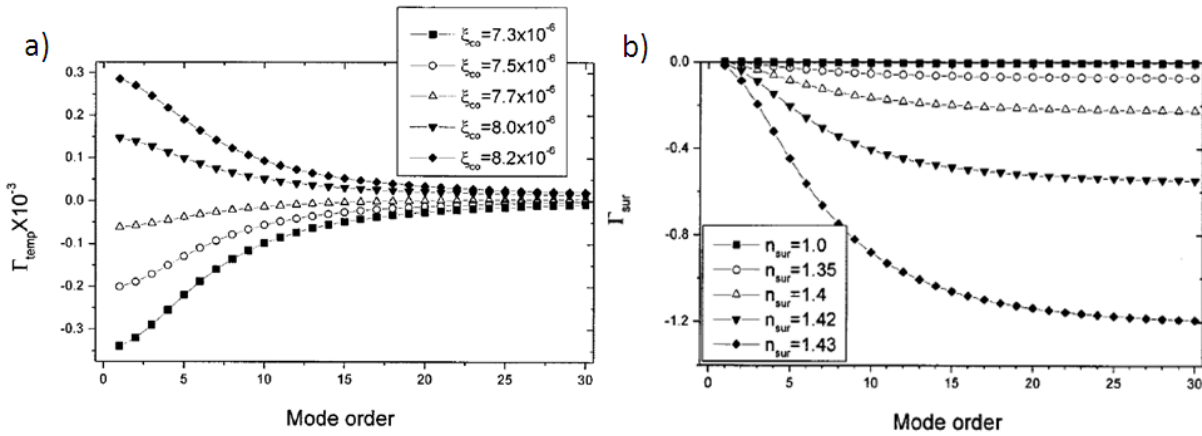


Fig. 2.3.1 Calculated values of sensitivity factor Γ_T for a series of thermo-optic coefficients (a) and sensitivity factor Γ_{SRI} for several values of $n_{SRI} < n_{cl}$ (b) plotted against the cladding mode order. The simulations were performed for B-Ge co-doped fiber to generate the resonance around 1500 nm [9].

Fig. 2.3.1a shows the temperature sensitivity factor Γ_T and the calculated temperature sensitivity $\frac{d\lambda_{res}}{dT}$ plotted against the cladding mode order for a series of thermo-optic coefficients. From this figure we can note that:

- For a given value of the thermo-optic coefficients, the absolute value of Γ_T decreases with an increasing mode order.
- Γ_T increases with an increasing difference between the thermo-optic coefficients of the core and cladding materials.
- The sign of Γ_T may be either positive or negative, as determined by $\xi_{co} - \xi_{cl} > 0$ or $\xi_{co} - \xi_{cl} < 0$. This feature is mainly associated with the initial composition of the fiber, e.g. the thermal

response of the LPFG based on standard fiber is opposite to those measured for the LPFG fabricated on the boron-germanium co-doped fiber (since boron doping can significantly decrease the thermo-optic coefficient of the core [55]).

In the context of the LPFG sensitivity to the SRI ($d\lambda_{res}/dn_{SRI}$) it is worth remembering that a strong coupling of the core mode with the co-propagating cladding modes should occur. This is important because, although the field of the core mode is negligible in the regions outside the cladding, the field of the cladding modes extends into the surroundings of the fiber. Therefore, the cladding mode structure will depend on the optical properties of the surrounding medium. The dependence of the resonant wavelengths on changes in the refractive index of the surrounding medium can be understood by the following equation:

$$d\lambda_{res}/dn_{SRI} = \lambda_{res} \cdot \gamma \cdot \Gamma_{SRI} \quad (2.3.)$$

where Γ_{SRI} is the SRI sensitivity factor.

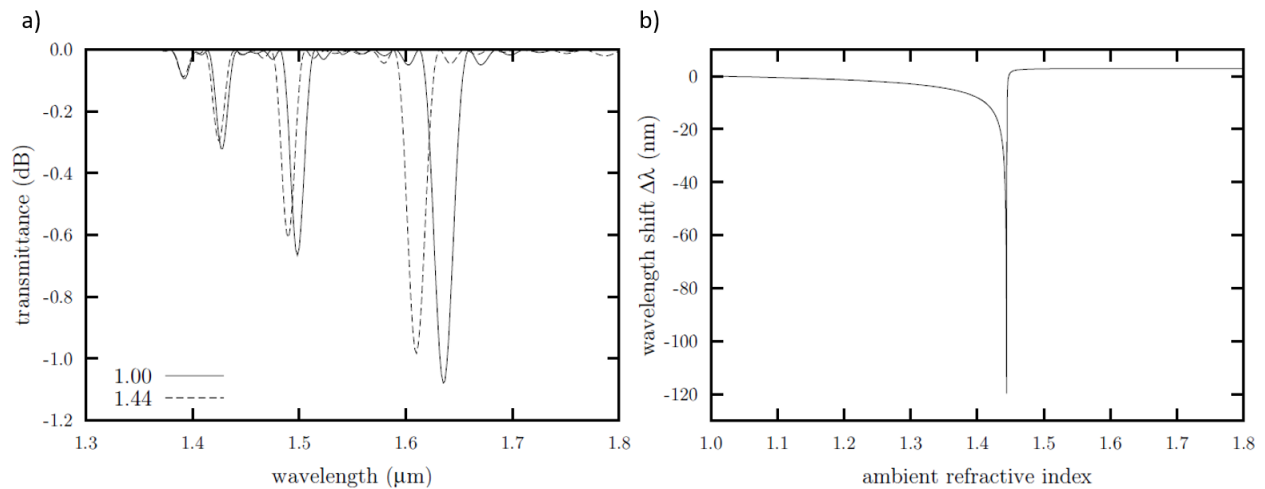


Fig. 2.3.2 a) Spectra of a bare LPG sensor element. The numbers in the legend refer to the SRI value.

b) Theoretically expected shift of the peak around 1630 nm. [36]

In Fig. 2.3.2a the calculated transmission spectra versus SRI for a typical LPFG is shown [36]. Fig. 2.3.2a presents a plot of the wavelength shift of the large attenuation band at about 1630 nm as a function of the SRI. From these results, it is clear that the LPFG sensitivity to the SRI should be separated into three main categories, depending on the magnitude of the SRI with respect to the RI of the fiber cladding:

REGIME 1: when $n_{SRI} < n_{cl}$ the cladding modes experience a TIR mechanism at the interface between the cladding and the surrounding medium. The LPFG sensitivity to the increase of the

SRI is evident as a shift in resonant wavelength of the attenuation band and a decrease in its depth. The latter effect is caused by successively smaller coupling coefficients. In this regime the Γ_{SRI} is expressed as follows [9]:

$$\Gamma_{SRI} = -\frac{u_m^2 \lambda_{res}^3 n_{SRI}}{8\pi r_{cl}^3 n_{cl} \delta n_m^{eff} (n_{cl}^2 - n_{SRI}^2)^{3/2}} \quad (2.25)$$

where u_m is the m th root of the zero-order Bessel function and the other symbols have their common meaning. Equation (2.3.4) also shows that the highest sensitivity of the LPFG to SRI variation is located around the value of the n_{cl} . Additionally, it is worth noting that the Γ_{SRI} is always negative here in contrast to the Γ_T , which can change its sign (as was explained above).

REGIME 2: when $n_{SRI} = n_{cl}$, the resonances disappear. This is due to the fact that once the value of SRI reaches that of the cladding, the cladding has an infinitely large radius. Consequently, the cladding modes are converted into radiation modes as a result of the lack of TIR at the cladding boundary.

REGIME 3: when $n_{SRI} > n_{cl}$, the resonances reappear but at longer wavelengths [29]. In this case, the modes are guided by Fresnel reflection and not by TIR and loose part of the energy at each reflection at the interface being called leaky modes [67-69]. As the SRI increases the modes become more confined and the dips more pronounced. However, the resonance wavelengths are insensitive to changes in the SRI because the phase of the partially reflected field at the surrounding-cladding interface does not change with the external index.

Although the LPFGs exhibit response to changes in the SRI, their sensitivity to this parameter is large only over a small region near the n_{cl} . This imposes a restriction to work with e.g. liquid crystals (LCs) since most of these materials has a higher value of RIs than the n_{cl} . Therefore, means to overcome those limitations were required. A further point is that the SRI sensitivity of the LPFG (especially in Regime 3) can be improved by depositing a layer of appropriate thickness. The basic concept of such a LPFG design is shown in Fig. 2.3.3a. In 2002, Rees *et al.* [37] first investigated the behavior of LPFGs with thin film layers in an experiment where a Langmuir-Blodgett technique was used to deposit tricosenoic acid. The shift of the attenuation bands in the LPFG spectrum was qualitatively discussed in regards to the average RI of the medium coating the fiber. It was pointed out that the deposition of a thin layer over the grating bare, with a refractive index exceeding that of the cladding, changes the position of the resonances. As the layer thickness increases, the average external refractive index also increases leading to a down shift of the resonances. Then, a point is reached where the resonances disappear. With further deposition the

resonances reappear. In [38] del Villar *et al.* presented a theoretical explanation of the sensitivity enhancement effect based on the transition of cladding modes from being guided in the cladding to being guided in the layer. The LP mode structures of the geometries of interest were obtained using a transfer matrix approach in the radial direction. It was explained that with the increase of the layer thickness, a cladding mode is allowed to be guided in the layer leading to a rearrangement of the cladding modes in which a cladding mode order will replace the position of the cladding mode with the precedent order (e.g., LP₀₈ replaces LP₀₇). This is a fast transition leading to the highest sensitivity (see Fig. 2.3.3b).

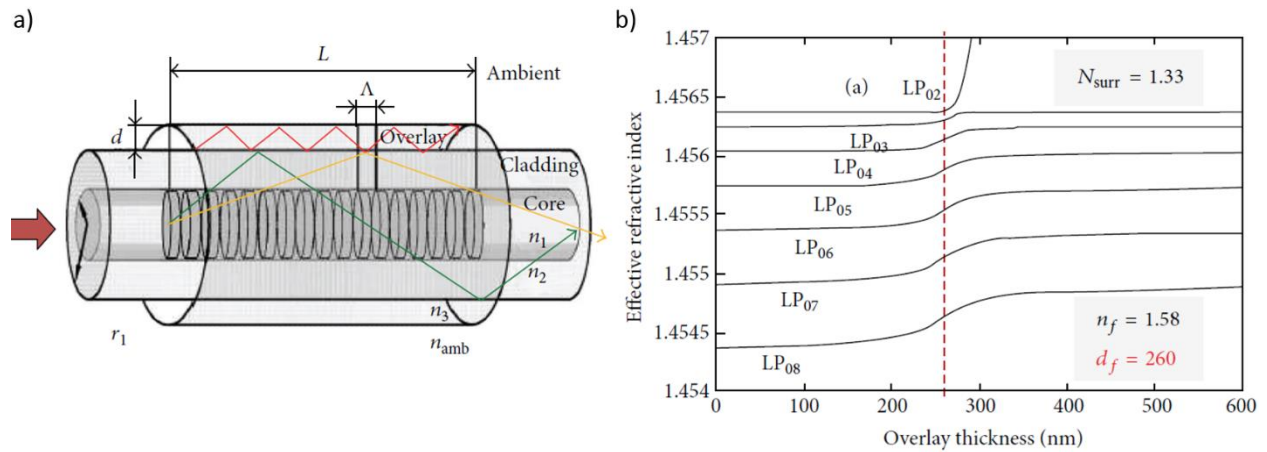


Fig. 2.3.3 a) A mode guided by the thin film (the ray trace in red). b) The fast transition region of cladding modes designated by the red dash line [52].

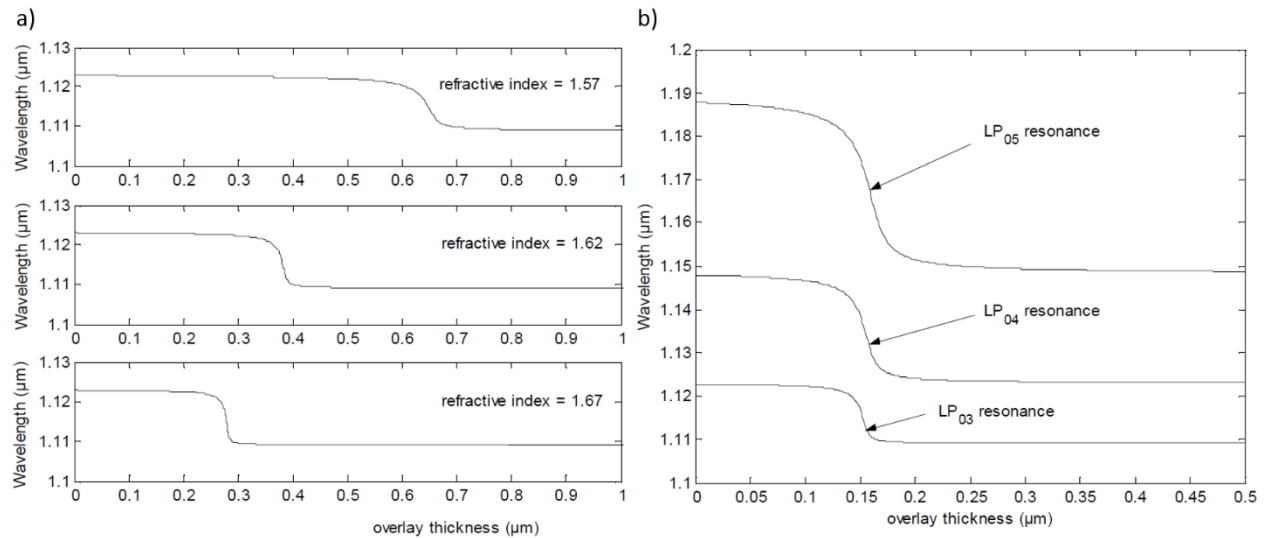


Fig. 2.3.4 The transition region: (a) Dependence of the optimum thickness on the layer RI (b) Resonance wavelength shift in 3rd, 4th and 5th cladding modes, as a function of the thickness of the overlay (RI layer: 1.67; Ambient index: 1.468) [39].

A more detailed paper by the same researchers was published soon afterwards [39]. The mode structures were analyzed this time over a larger effective refractive index interval in order to demonstrate the transition of several cladding modes from the cladding to the layer (see Fig. 2.3.4). Extending their analysis to coatings with absorbing layers (complex RI), del Villar *et al.* showed (experimentally and theoretically) [40]. It was found that additional phenomena are seen in this case of the characterized layers. Precisely, within the transition region, the complex part of modes propagation constants increases, which leads to a vanishing of the corresponding resonance peak in the spectrum (see Fig. 2.3.5 which shows the coupling strengths decrease effect in the transition region [42] - nonetheless, the resonances are still visible). In [43], del Villar comprehensive their previous analysis using a hybrid mode model. It was shown that the effect of EH-HE splitting occurs during the modes' transition.. Comparing the LP model with the hybrid mode model for the case of thin layers, it was pointed out that if the weak guidance condition is not fulfilled, low order modes should show a two-step transition rather than the one step transition predicted by the LP model.

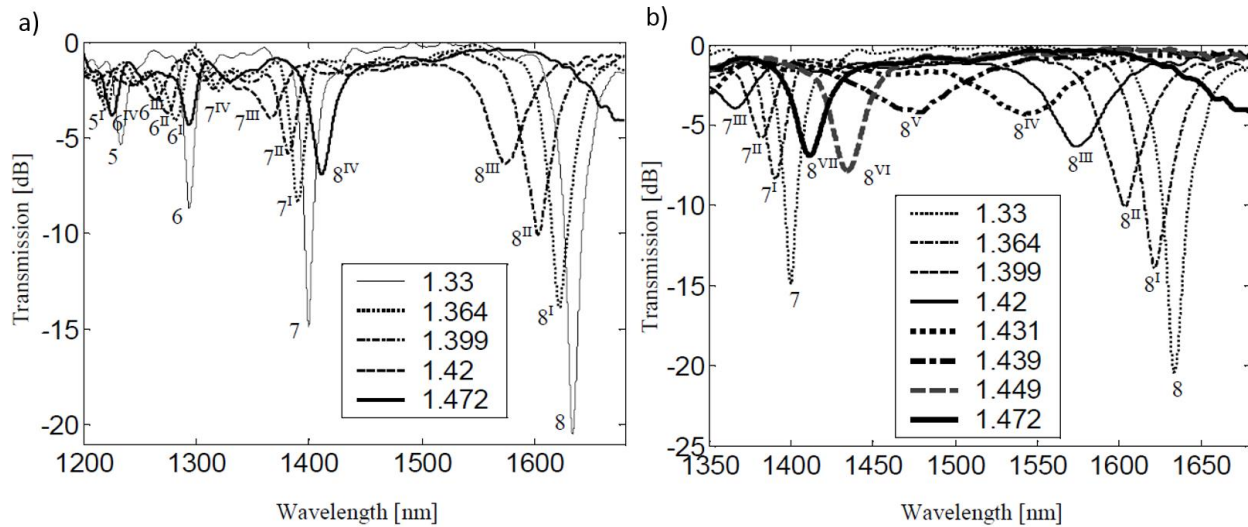


Fig. 2.3.5 The transition effect in the LPFG transmission spectrum coated with HRI versus different values of the SRI. In (b) zoomed on LP_{07} and LP_{08} cladding modes [42].

Significant contributions to this field were also made by Cusano *et al.* by publishing a theoretical analysis based on an LP mode model supported by experimental data [41]. A study of the dependence of the sensitivity on the layer thickness was presented. It was mentioned that HRI layers offer the opportunity to adjust the RI interval to highest LPFG sensitivity. In a subsequent paper more details on the mode fields were presented [42]. It was demonstrated that on transition, the higher order modes assume a mode field

similar to that of the next lower mode. In other words, the mode field of the transitioning mode shifts into the layer.

The study of coated LPGs and their use as sensors is a relatively new field. Therefore, it comes as no surprise that the vast majority of studies are limited to simplest case, namely a one-layer LPFG. An alternative to the one-layer LPFG is the multilayer LPFG. In these designs, one or more additional layers is interposed between the cladding and the polymer layer. One of the main advantages of the multilayer structure is the ability to adjust the transition interval and position. A problem might, of course, be the production and stability of a fiber structure with different multilayers. In tackling this daunting task it might be helpful to consider that – as pointed out with the one-layer sensor – different choices of parameters can yield very similar response characteristics. If it is possible to control either the layer thickness or its refractive index very well, the lack of control over the other parameter can be compensated in many situations. In a paper by del Villar *et al.*[44] it was presented that the deposition of two thin films in which the first layer has a smaller refractive index than the second layer forms a tunnel effect that leads to a more pronounced two step transitions. The resulting five layer geometry (core, cladding, first and second overlay, ambient environment) was theoretically analyzed. Another paper, published by Hochreiner *et al.* [36], described the design and response of one-, two- and three- layer LPFGs which were considered in the context of chemical sensing applications. It was proved through the theoretical calculations based on a hybrid mode model that the use of more than one layer greatly enhances the flexibility of sensor design and allows the response characteristics to be tuned for optimal performance. On the other hand, it is possible to use a first layer to increase the overall sensitivity and a second one being selective to a particular chemical or biologic component [44]. Thin films sensitive to specific components, such as, for pH measurement or for detection of Cl⁻, chloroform, hydrogen, methane, and ethanol, have also been used [46-51]. In this case, the sensitivity of the film increases if its refractive index approaches that of the cladding [46].

It is expected that future research on these subjects will contribute to a further increase in the sensitivity of sensors based on the LPFGs coated with the layer(s). In this work the concept of the LPFGs coated with liquid crystal layer is presented with brought forward the studies in this field.

2.4 Fabrication methods of the LPFGs

Several techniques are available in order to produce LPFGs. The most widely used method of introducing an index modulation along the fiber is realized by UV irradiation. In this method the LPFG is created by altering the core refractive index in a periodic manner. The earliest demonstration of efficient coupling between the guided mode and the cladding modes of a single-mode fiber was done by using this technology [8]. Typically, UV irradiation method uses wavelengths between 193 and 266 nm [77]. The lasers used are listed in Table 2.4.1. The pulsed KrF eximer laser at 248 nm provides plenty of power density [78], but the cw frequency argon ion laser at 244 nm exhibits a higher beam pointing stability and spatial coherence [79]. Therefore, depending on the application, the cw or pulsed lasers are favored. All procedures that rely on illumination by UV light require that the fiber first be made receptive to this irradiation, in other words the fiber must be made photosensitive prior to writing the grating.

Tab. 2.4.1 *UV lasers used for LPFG fabrications*

| Laser wavelength | Laser type | Regime | Ref. |
|------------------|------------------------------|-----------------|------|
| 193 nm | ArF eximer | pulsed ~tens ns | [79] |
| 244 nm | Argon ion frequency double | cw | [78] |
| 248 nm | KrF eximer | pulsed ~tens ns | [8] |
| 266 nm | Na: YAG frequency quadrupled | pulsed ~tens ns | [10] |

The photosensitivity of standard telecommunication fibers with the molar concentration of $\text{GeO}_2 \sim 3\text{-}5\%$ is not high enough for the efficient writing of gratings in them. The refractive index variation in such fibers does not exceed 5×10^{-5} even after a long exposure [3, 80-81]. Several models have been proposed for photo-induced refractive index changes. However, the mechanism of these changes is still not fully understood. It is believed that more than one process is involved in the photo-induced refractive-index changes, and hence, in the grating formation dynamics [80-81]. The only common element in these theories is that the GeO (germanium oxygen) defect concentration leads to index change in the glass. Those point defects are called *color centers* and are found to absorb in the range from 180 nm to 350 nm in silica. Presently, two main types of photosensitivity in germanosilicate fibers are used in order to fabricate the LPFGs [3]: type I and type IIa (compare in Table 2.4.2). The basic difference between photosensitivity's I and IIa type is the profile of changes of the induced refractive index. Type I photosensitivity is characterized by a monotonic increases in the refractive index with increasing the UV

dose (curve (1) in Figure 2.4.1a). In the case of type IIa the modulation of refractive index first increases, then decreases almost to zero, and then increases again towards the saturation (curve (2) in Figure 2.4.1a).

Tab. 2.4.2 Comparison of the types of photosensitivity achieved in the host fiber [3]

| Photosensitivity type I | Photosensitivity type II |
|--|--|
| Require molar concentration of GeO ₂ in the based fiber core: | |
| < 20% | > 20% |
| Photosensitivity the refractive index changes upon: | |
| Increasing concentration of GeO defect in the fiber core. | Increasing concentration of GeO defect in the fiber core and changes in the elastic stresses in the core-cladding complex. |

Tab. 2.4.3 Photosensitivity comparison of three different fibers [82]

| Fiber design | Fiber Δn | Δn_{mod} | Time to reach saturation |
|---|------------------|-------------------------|--------------------------|
| Standard fiber 4 mol % germania | 0.005 | 3.5×10^{-5} | 2h |
| High index fiber 20 mol % germania | 0.03 | 2.5×10^{-4} | 2h |
| Boron co-doped fiber 15 mol % germania | 0.003 | 7×10^{-4} | 10 min |

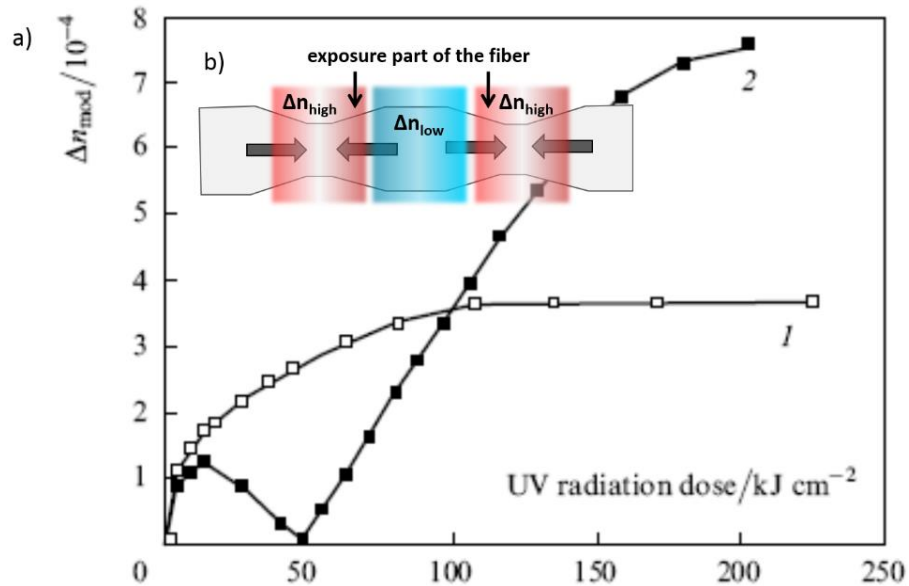


Fig. 2.4.1 a) Dependences of the modulation amplitude of the induced refractive index for gratings written in the fibers with the molar concentration of GeO₂ equal 12% (1) and 35% (2). [3]. b) Schema for mechanism of photosensitivity type II.

Fibers, other than the ones doped with germanium, can also exhibit the photosensitivity phenomena. For example, a B-Ge co-doped fiber produces large index modulations [55, 82]. A comparison of the relative photosensitivity of four different types of fibers is given in Table 2.4.3 [82]. The fibers were irradiated with a frequency-doubled cw argon ion laser until the grating formation saturated. The results showed that the incorporation of boron had an effect of enhancing photosensitivity (up to $7 \cdot 10^{-4}$ of induced refractive index changes) as compared with the fibers containing the same percentage of GeO_2 without the boron. Moreover, the UV exposure time required to achieve a saturation of the index change, Δn_{mod} is decreased by almost an order of magnitude. Several other techniques for improving optical fiber photosensitivity were presented as well, for example: flame brushing technique for thermally induced refractive index changes [80], hydrogen-loading technique for germanosilicate fibers [83] or even photosensitivity increasing by strain [84].

Aside of the LPFG fabrication methods based on the fiber irradiation with laser, the arc-induced technique deserved special attention. This method proved to be simple, flexible and having low cost. The biggest advantage of this method is that any type of fiber can be used for writing gratings in this way without any prior photosensitization (since it is predominantly the local heating of silica that creates the modulation in the fiber). Moreover, arc-induced gratings can stand temperatures as high as 1000°C for several days without significant deterioration in their spectrum [85]. Arc-induced gratings are fabricated by placing an uncoated fibre, under tension, between the electrodes of a splicing machine. The fibre is then submitted to an arc discharge with an electric current of 7 to 15mA and a duration ranging from 200ms up to 2 s. Afterwards the fibre is displaced by the grating period, typically, from $200 \mu\text{m}$ to 1mm and the whole process of arc-discharge/fibre displacement is then repeated 20 to 50 times. The main limitation of this method is that so far it was not possible to write LPFGs with grating periods shorter than $200 \mu\text{m}$ [86]. The reproducibility of this technique can be compromised by the degradation of the electrodes due to oxidation. However, the control of the position of the fibre in the arc discharge and the monitoring of the discharge parameters and of the ambient conditions would allow the technique to be used for mass production of gratings with precise and reproducible characteristics. The LPFGs produced by electric arc method have been studied for quite a long-time. Nevertheless, the mechanism of grating formation is still not well understood [87]. Humbert et al. [88] have studied the inscription of the LPFGs in standard telecommunication fiber (SMF-28, produced by *Corning*) using the electric arc fabrication process. Based on evidence provided by Raman and luminescence spectroscopy, it is suggested that the coupling arises due to an arc-induced local structural rearrangement and to a weak geometrical deformation of the glass structure, which modifies the refractive indices of the fiber core and cladding modes. In order to

understand the origin of the asymmetry of this perturbation, the studies of the temperature distribution in the arc that is applied to the fiber were done [87,89]. The results showed that wherever the fiber is positioned in the arc, there is always a temperature gradient. Therefore it should be expected that the temperature gradient in the arc could create some temperature gradient inside the fiber itself, the latter gradient being weaker due to thermal conductivity of the fiber. This temperature gradient inside the fiber is probably responsible for the asymmetric perturbation that forms the LPFG. In order to assess the symmetry of the perturbation, the near field of several arc-induced LPFGs was measured [87]. Figure 2.4.2a indicates that coupling occurs to the symmetric LP_{0j} cladding modes whilst its asymmetry in Figure 2.4.2b indicates that the perturbation leads to coupling to the LP_{1j} cladding modes. It can be then noted that in the case of the fibre co-doped with B/Ge the main mechanism of grating formation is not micro deformations but a reversible densification of the core that leads to coupling to symmetric cladding modes in opposition to the asymmetric ones due to the former mechanism [89-90].

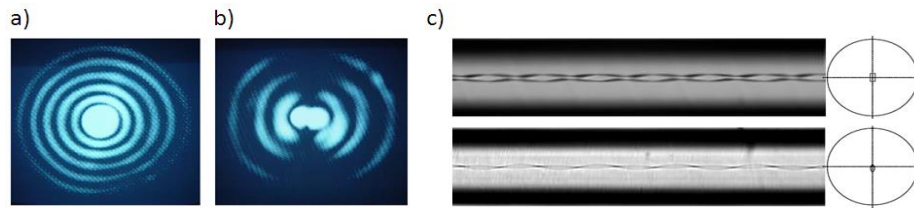


Fig. 2.4.2 Intensity distribution in the near field for the (a) LP_{07} cladding mode of a $415\ \mu\text{m}$ -LPFG written in the B/Ge fiber and (b) LP_{14} cladding mode of a $540\ \mu\text{m}$ -LPFG written in the SMF28 fiber [87]. In (c) The side and face images of the chiral LPFGs is shown [95].

Besides the illumination of the fiber by UV light and thermal annealing process, the LPFGs have also been achieved by structural deformation of the fiber, e.g. by using a mechanical apparatus [91], tapering the fiber [92], or deforming the cladding [93]. These techniques are extremely flexible: the grating periodicity and length are independent parameters, which can be individually adjusted to meet the desired LPFG characteristics. In addition, mechanical loading methods can introduce a significant birefringence in the fiber and, as a result, can produce a transmission spectrum that is highly polarization sensitive [94]. As an alternative to the typical profile of changes in the core refractive index, an LPFG with a chiral structure was also reported in [95] and is illustrated in Figure 2.4.2c. This structure may be created *via* glass micro forming as the fiber preform is being drawn. The fiber's refractive index is modulated by twisting a fiber preform with noncircular core cross section as it is passed through a miniature oven (see Figure 2.31). Dynamic gratings with controllable transmission characteristics have been implemented by using coil heaters [96], acousto-optic modulation [97], mechanical loading [98], and LCs (discussed in detail in Section 4).

Chapter 3 INTRODUCTION TO LIQUID CRYSTALS (LCs)

The study of liquid crystals (LCs) began in 1888 when an Austrian botanist named Fritz Reinitzer observed that a material known as cholesteryl benzoate had two distinct melting points. After his accidental discovery, Reinitzer did not pursue further study of LCs. The research was continued by German physicist Otto Lehmann, whose results were published in August 1889 in the *Zeitschrift für Physikalische Chemie* [18]. Today, thanks to Reinitzer, Lehmann and their followers, it is known that thousands of substances have a diversity of liquid crystalline phases. Some of them have been found to be very usable in a number of technical innovations, among which flat-panel LC displays and LC thermometers may be the best known. This section provides an introduction to the science of these materials.

3.1 State of matter and basic parameters

The LC state is a different state of matter observed between their solid and isotropic liquid states. As a result LC possess properties of both, the characteristics of solids long – range molecular orientation order and the ability to flow like liquids.

LC molecules usually have rod-like or disc-like shapes that encourage their collective alignment along a certain direction. There are many types of LC phases (called mesophases), depending upon the extent of order in the material [18-26]. In this work we will focus on nematic liquid crystals. This is the simplest example of the LC phase. In the nematic phase, elongated molecules possess long-range orientational order but their centers of gravity are distributed randomly.

One of the main parameters used to describe the alignment of LCs is the *director* \mathbf{n} . The \mathbf{n} defines an average direction of the molecular long axes in the LC phase. To specify the extent of the orientational order in the LC phase, the *scalar order parameter* S introduced by Tsvetkov (1942) is commonly used ($0 < S < 1$):

$$S = \frac{1}{2} \langle 3 \cos^2 \theta - 1 \rangle \quad (3.1)$$

where θ is an angle between the individual molecular long axis and the director \mathbf{n} , and the brackets indicate the average value (see Fig. 3.1a). In a perfectly oriented system, $S = 1$; and in an isotropic liquid state, with no orientation order, $S = 0$. The order parameter decreases as the temperature increases (see Fig. 3.1b). Since nematic LCs are thermotropic, the transition from one phase to another is induced by the

changing temperature. As a result, at temperatures higher than the clearing temperature (T_c), thermal motion will destroy the ordering of the LC phase, pushing the material into an isotropic liquid phase.

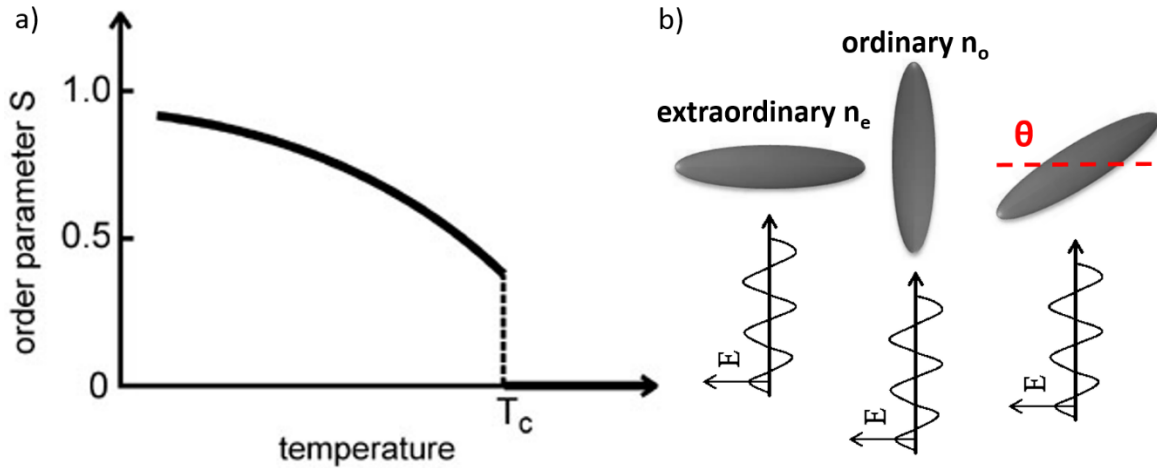


Fig. 3.1 Schematic representation of the LC order parameter dependence from temperature (a) and optical anisotropy in LC molecules (b).

One factor common to all LCs is *anisotropy* and this property is not observed in other fluids. This in turn means that all LCs will have a property known as *birefringence* Δn defined as:

$$\Delta n = n_e - n_o \quad (3.2)$$

In consequence LCs exhibit double refraction due to the fact that they possess two refractive indices: the *ordinary refractive index* (n_o) and the *extraordinary refractive index* (n_e), which are measured for the light wave where the electric vector vibrates perpendicular to or along the optical axis, respectively. Most LCs with a rod-like shaped molecules have positive birefringence in a range of 0.05 to 0.45.

The average refractive index of LC in an isotropic phase is equal to:

$$\langle n^2 \rangle = (n_e^2 + 2n_o^2)/3 \quad (3.3)$$

Much work has been done on measurement of the RIs of LCs using Abbe or Jellé-Leitz refractometers, hollow prism wedges, and a variety of other methods including the interference method for plane-parallel nematic LC cells [20]. In order to identify the birefringence of LCs, the Michel-Lévy interference color chart is often used [99-100]. This gives a quantitative analysis of the interference colors observed in LC cells under polarized light. Observation of the interference colors is possible due to the fact that the phase shift

accumulates as long as the light propagates in the LC birefringent material. The optical path for a wave travelling a distance d in a LC cell is nd . Hence the optical path difference (retardation) for the two wave components mentioned above will be [99]:

$$d(n_e - n_o) = d\Delta n \quad (3.3)$$

The resultant phase difference between the two components is equal to $2\pi d\Delta n/\lambda v$, where λv is the wavelength in vacuum. Therefore, according to the Michel-Lévy interference color chart (Figure 3.2), the polarization colors can be correlated with the actual retardation value, thickness, and birefringence of the LC.

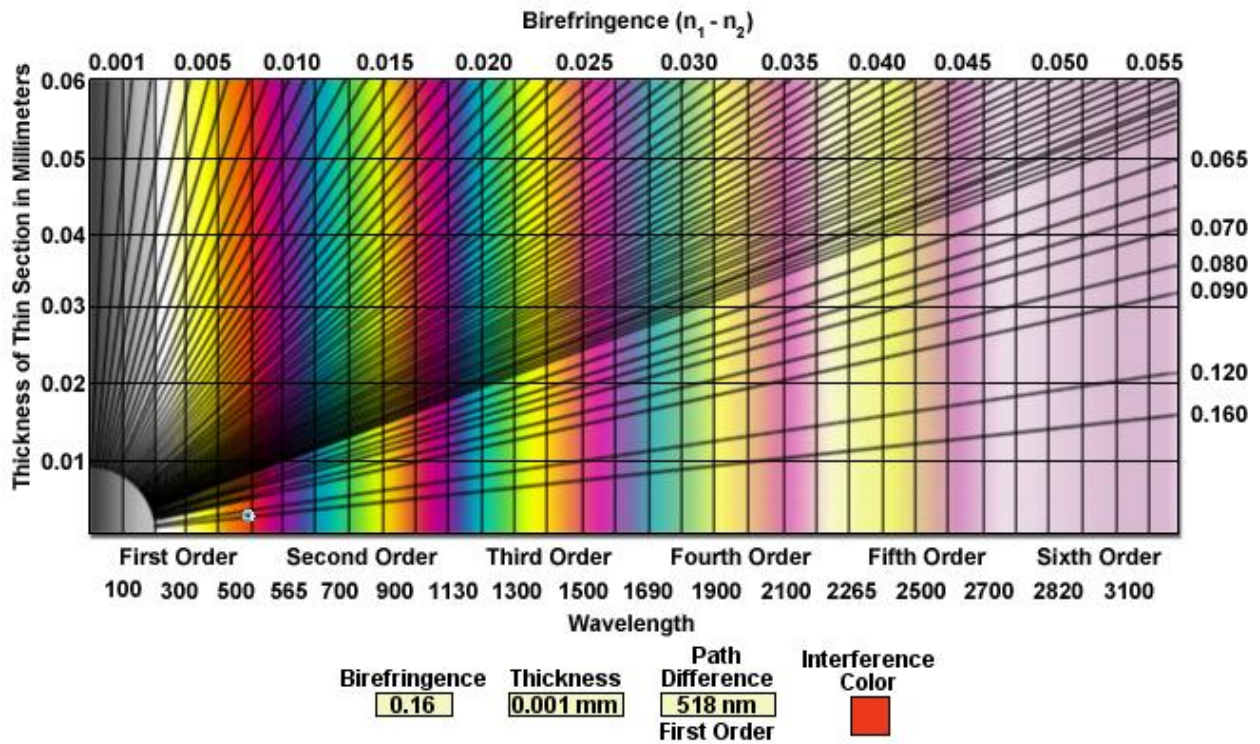


Fig. 3.2 Michel-Lévy birefringence chart [100].

3.2 Thermal and wavelength dependence of the refractive indices of LC

The RIs and the Δn of an LC are strongly dependent on the operating *wavelength* and *temperature* [20-21, 101]. As the temperature increases, the n_e decreases monotonously, but the n_o may decrease or increase depending on the crossover temperature of the LC employed [35]. In addition, LC exhibits at least

two phase transitions when they are thermally tuned. The transition from solid phase to mesophase appears in a melting temperature (T_m) and from the mesophase to isotropic phase in a clearing temperature (T_c), where long-range orientation order disappears (see Fig. 3.4). In addition, since nematic LCs are thermotropic, the transition from nematic phase to isotropic phase is induced by changing temperature

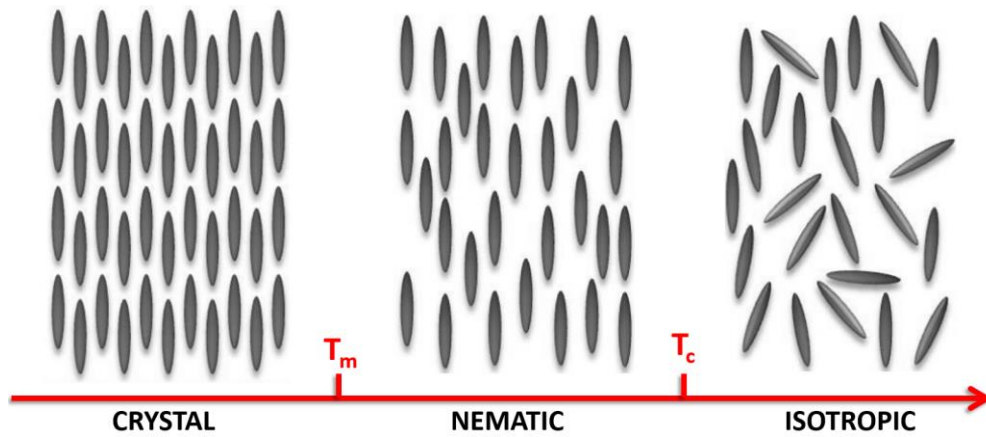


Fig. 3.4 Schematic representation of transitions in thermotropic LC: rising temperature causes the transitions from crystal, through nematic phases to isotropic phase.

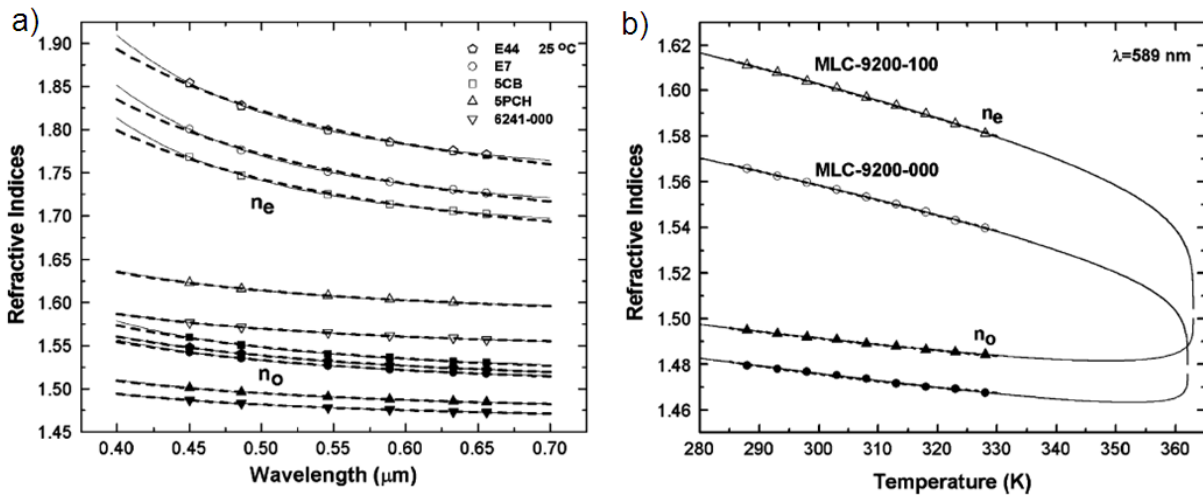


Fig. 3.4 Wavelength- and temperature-dependence of the refractive indices of LC [21].

As the wavelength increases, the RIs decrease. The decreasing rate depends on the molecular structures of the LC. The major absorption of a LC compound occurs in two spectral regions [20-21]: ultraviolet (UV) and infrared (IR). In the UV (100 – 400 nm) region, electronic transmission occurs. In the IR region, the RIs are insensitive to wavelength, except for the resonance enhancement effect near the local molecular vibration bands. Fig. 3.5 depicts the temperature- and wavelength-dependent RIs of some common LCs.

3.3 Liquid crystal in an electric field

It is well known that LCs are susceptible to an external electric field [22-23]. This is due to the fact that the dielectric constants parallel (ϵ_{\parallel}) and perpendicular (ϵ_{\perp}) to the director differ in value. The dielectric anisotropy $\Delta\epsilon$, defined as:

$$\Delta\epsilon = \epsilon_{\parallel} - \epsilon_{\perp} \quad (3.4)$$

is a physical quantity that describes how an electric field affects a dielectric LC medium.

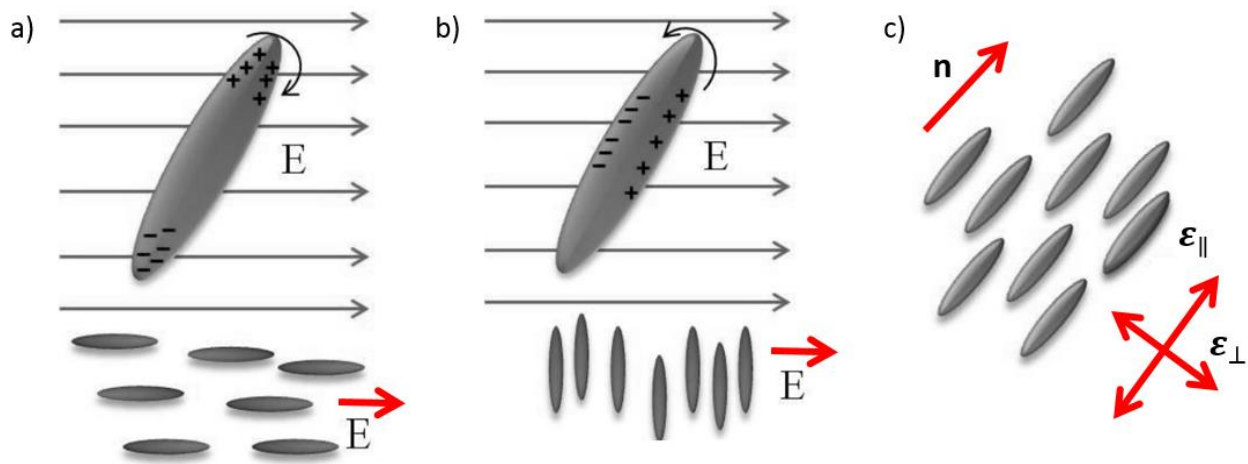


Fig. 3.6 Schematic representation of the positive (a) and negative (b) dielectric anisotropy, c) negative anisotropy in nematic LCs. In (c) dielectric constant are presented.

The $\Delta\epsilon$ is related to the polarity of the molecules, whereby its sign and magnitude depend on the direction of the permanent dipole moment in relation to the long axis of the molecule (see Fig. 3.6). If the direction of the permanent dipole moment coincides with the long axis of the molecule, the dielectric anisotropy is positive ($\Delta\epsilon > 0$). As a result the LC molecules will tend to orient along the electric field direction. If the dipole is perpendicular to the long axis of the molecules, the dielectric anisotropy is negative ($\Delta\epsilon < 0$) and LC molecules tend to orient perpendicular to the electric field direction. In addition, $\Delta\epsilon$ depends on temperature: typically decreases with an increase of the temperature. $\Delta\epsilon$ is frequency dependent as well. In the kHz frequencies region, most of nematic liquid crystals (NLC) can be described as a medium with no dielectric dispersion and instant dielectric response [24-25, 103]. However, NLC in the high frequencies region can be regarded as a dual frequency nematic (DFNs). For example, the most widely used NLC, pentylcyanobiphenyl (5CB) is DFN with a very high crossover frequency of 15 MHz [103]. The sign reversal of $\Delta\epsilon$ allows to control the LC molecules orientation by simply changing the frequency of applied voltage.

If the external electric field is applied to the LC sample with some uniform director structure, there is a gradual change of the director structure once the field strength exceeds some threshold value. This threshold phenomenon, typical only to LCs, is called Fredericks transition effect (or threshold). Taking as an example the homogenous LC cell (planar alignment), the threshold voltage value V_{th} can be defined as follows:

$$V_{th} = \pi\sqrt{K_{11}/\varepsilon_0\Delta\varepsilon} \quad (3.5)$$

where K_{11} is the splay elastic constant of LC. Therefore, by having a material with larger $\Delta\varepsilon$ a lower V_{th} is needed to make the LC respond to it. The K_{11} also affects the LCs performance. From the equation (3.5) it can be noted that a smaller value of K_{11} results in a lower V_{th} . However, a small K_{11} is unfavorable from the point of view of the response time, since the response time of LC is proportional to the visco-elastic coefficient K_{11}/γ_1 , where γ_1 is the rotational viscosity. In addition, in a planar cell, the reverse tilt domains (RTDs) refers to a spatially rapid variation of the LC director along a plane, and occurs [24-25]. Presence of the RTDs tend to diminish the quality of dynamics and uniformity of LC molecules reorientation: in one region the director has a positive polar orientation, and in an adjacent region a polar orientation is negative – a domain wall then separates the two regions [25]. It was shown that the contrast between the domains can be decreased with an increase of the temperature of operation [24]. Moreover, RTDs can be obviated by introducing a small uniform pre-tilt angle relative to the planar orientation. Presence of this angle also avoids the Fredericks threshold effect [26].

Chapter 4 LIQUID CRYSTAL LONG-PERIOD FIBER GRATINGS (LC-LPFGs) STATE OF ART

The investigation of LC-LPFGs, as documented by the literature review, has been limited. It seems that there is still a lot of work to be done in order to improve the efficiency of their tunability. However, LPFGs, when combined with LCs, already show clear promise for creating new platforms for various fiber devices. Such devices will have a response time in the millisecond range (depending on the type of LC used) and will be tunable by a variety of external factors. These features could be of great interest especially in the sensing and optical fiber communication fields.

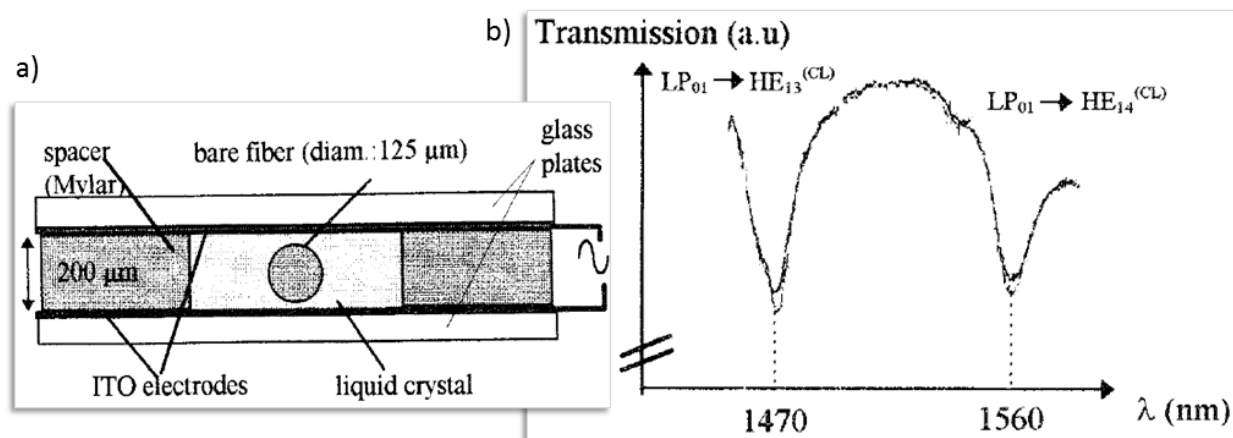


Fig. 4.1 a) The experimental setup used in modulating the LPFG by LC surrounding; b) Comparison of the spectrums with and without electric field [27].

Taking advantage from the LPFG sensitivity to the SRI, the tunable optical filters could be realized by controlling the RI of the surrounding region. From this reason the LCs are attractive candidates as a coating materials for the gratings, since their RIs can be controlled through temperature, optical, electrical, and magnetic fields. Moreover, the choice of the LCs as a practical and functional material was driven by a variety of available LC materials with different physical and optical properties and by a well-established fabrication technology. One of the first examples of LPFG tuning by using LC was demonstrated in 1998 by Duhem *et al.* [27]. They proposed a modulation of the attenuation band intensity based on the electrical switching of a nematic liquid crystal (NLC) around a photo-induced LPFG as shown in Figure 4.1. Due to the development of ultra-wide band gain amplifiers, broadband gain flattening devices were needed. The LPFG appears to be a good candidate for gain flattening applications. However, most of the

conventional filters based on LPFGs are static elements and are therefore not suitable for dynamic control of an optical network. To overcome this shortcoming, in 2001 Yin *et al.* presented a device based on an ultrathin LPFG etched by hydrofluoric acid (HF), which was surrounded by a dye-doped NLC for tuning the resonant wavelength [28]. It has to be pointed out that the ultra-thin cladding increases the sensitivity of the LPFG to the SRI. The experimental results of tuning the ultra-thin LPFG by photo-induced LC molecular reorientation are presented in Figure 4.2. The NLC in the outer cladding of the proposed LC-LPFG is switched by a polarized Ar⁺ laser. However, the tuning range of the resonance peak in this case is not wide enough for wideband applications because of the limitation in power of the Ar⁺ laser.

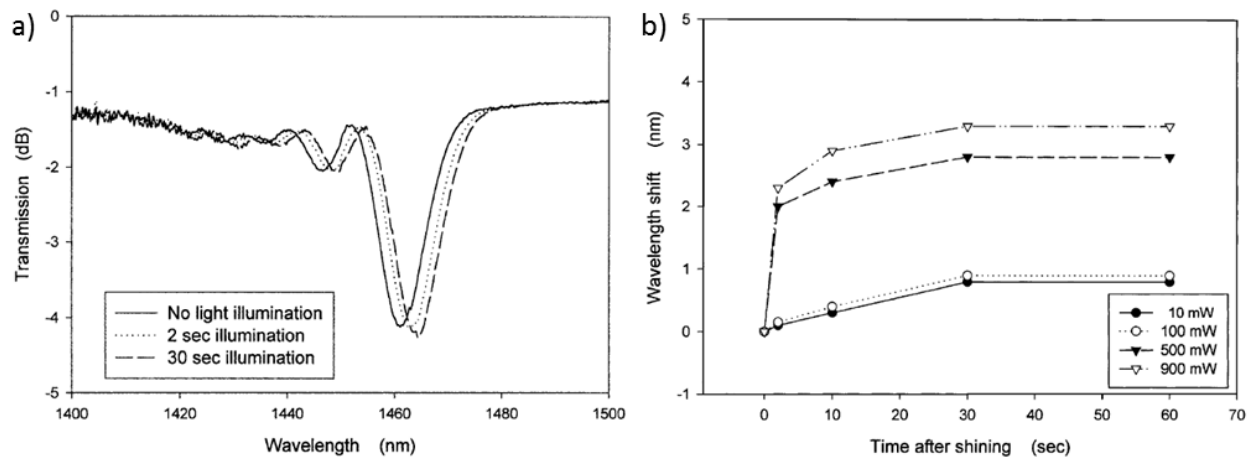


Fig. 4.2 a) All-optical tuning of the LPFG transmission spectrum surrounded by a dye-doped low-RI LC. b) Wavelength shift of ultra-thin LPFG with different Ar⁺ laser powers [28].

Furthermore, a cascade structure of LPFGs with LC as the surrounding medium was proposed by H-R Kim *et al.* [29] for arbitrary loss filters that could compensate a non-uniform optical gain in an EDFA. The results show that the interference effects in cascaded LPFGs can be suppressed using an extended LC cladding (Figure 4.3a) and the amount of the reflection can be controlled by an electric field across the LC cladding (Figure 4.3b). Again, Yin *et al.* proposed an HF-etched ultra-thin LPFG surrounded by a low-RI LC material for sensor applications [30]. This structure provides a resonant wavelength red shift of 46 nm in the temperature range from 48°C to 70°C. The corresponding tuning efficiency is approximately 2.1 nm/°C. This compares favorably with the tuning efficiency of a conventional LPFG (based on an SMF with a diameter of 125 μm) using the thermal effect, which is less than 0.1 nm/°C or the tuning efficiency of 0.8 nm/°C for an LPFG with a polymer cladding [31].

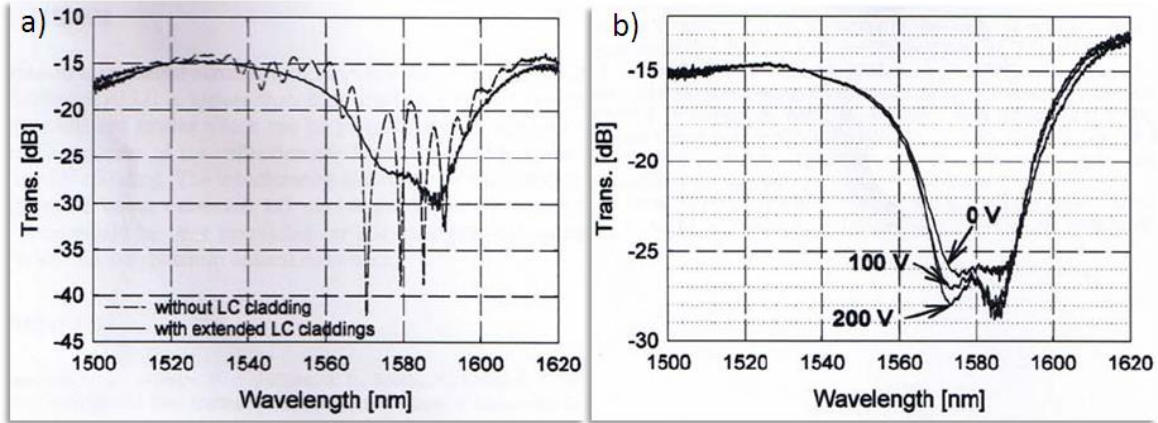


Fig. 4.3 Transmission spectra of cascaded LPFGs as a function of wavelength at different surrounding conditions: (a) with extended LC claddings; and (b) in the presence of various applied voltages [29].

Next, the idea of a coated LPFG with a thin LC layer (in the order of $1\ \mu\text{m}$) was brought forward by Luo *et al.* [32]. Figure 4.4a presents CCD photographs of bare and LC-coated LPFGs. In this experiment the host LPFG was fabricated using CO₂ laser irradiation on Corning SMF-28 fibers, with a grating period of $620\ \mu\text{m}$. The LC served as a LPFG cladding material (MDA-98-3699, Merck Chemicals, Darmstadt, Germany) has a refractive index larger than that of silica. Although the RI of the LC layer is higher than that of fiber cladding, the sensitivity of the LPFG can be improved by depositing the layer at an appropriate thickness (similarly as for the LPFG coated with HRI layer described in Section 2.3).

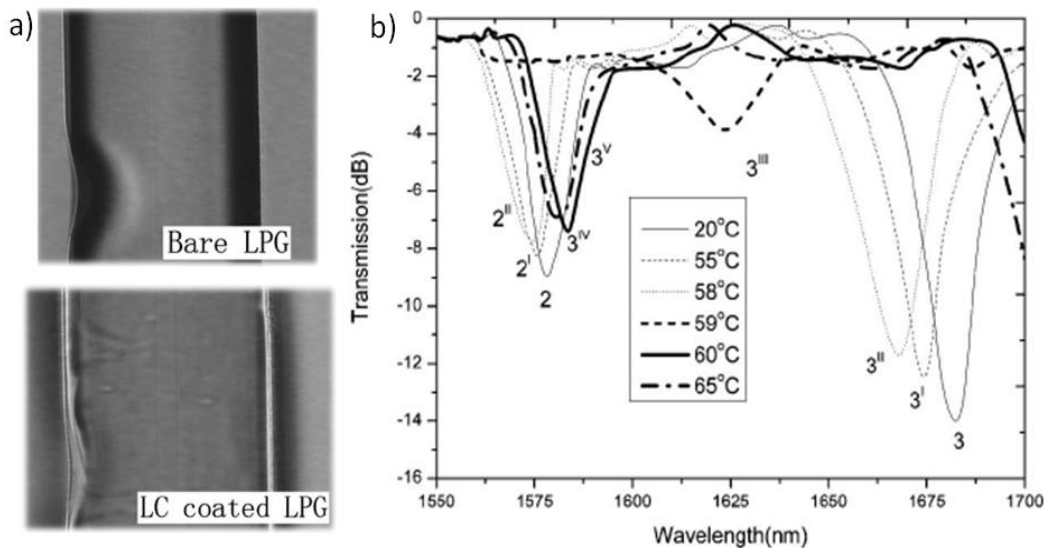


Fig. 4.4 a) CCD photographs of bare and LC-coated LPFGs (fabricated by CO₂ laser irradiation on the Corning SMF-28 fibers; $\Lambda = 620\ \mu\text{m}$). The LC material is MDA-98-3699 (prod. by Merck Chemicals, Germany). b) The transmission spectrum of an LC-coated LPFG versus temperature [32].

By thermal tuning such a LC-LPFG design (providing this way change of the LC layer RI from 1.477 to 1.515) the effect of transition between cladding modes and layer modes was observed. As a consequence, a shift in the attenuation band in the transmission spectrum for the LC-coated LPFG of more than 80 nm was achieved (Figure 4.4b). In [32] the theoretical analysis is provided, as well as for this LC-LPFG. However, authors did not include the thermal response of the host fiber in their model which can significantly contribute in the LC-LPFG thermal sensitivity.

Also noteworthy is the successful use of LCs in creating LPFGs in holey fibers. An electrically controllable fiber-optic filter for a broad-band rejection has been demonstrated by periodically poling a liquid-crystalline core in a hollow-core fiber [33]. The periodically poled LC crystal core was achieved by means of an external long-period-combed electrode. As illustrated in Figure 4.5, a maximum dip in transmission loss of approximately 15 nm bandwidth and 6 dB band rejection was obtained for a non-polarized light with a combed 250 V external voltage modulation. Unfortunately, since the LC was introduced into the core fiber, the proposed filter is characterized by a high level of signal attenuation.

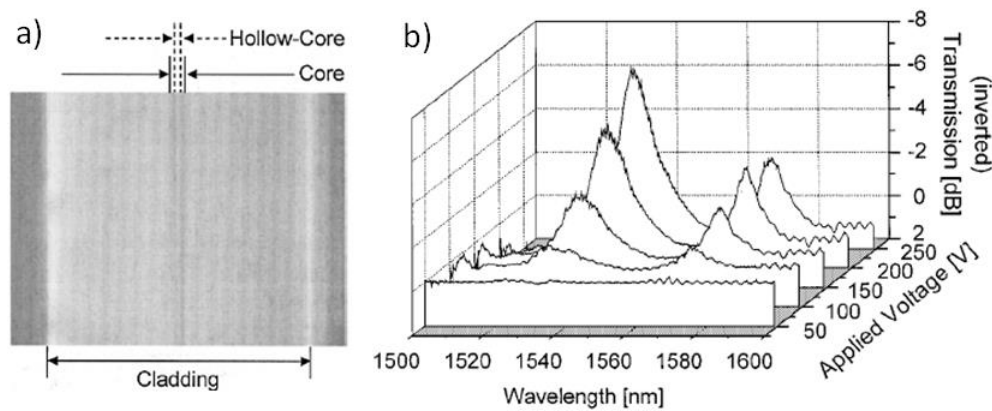


Fig. 4.5 a) Image of an LC-filled hollow-core fiber. b) Transmission spectra of an LC-LPFG with $\Lambda = 483 \mu\text{m}$ according to the applied voltages [33].

The optically [104], mechanically and electrically [34] tuned LPFGs, in a solid core photonic crystal fiber (PCF) with filled with LC, have also been presented. The effect of an optical tuning was achieved by infiltrating the PCF with an LC mixture consisting of nematic LC molecules and light-sensitive 4-methoxyazobenzene (4MAB) [104]. With the aid of photo-induced isomerization of 4MAB, the RI of the LC mixture was modulated by exposing the PCF to a blue laser. The periodic index perturbation along the fiber was obtained by placing the PCF under an amplitude mask. Figure 4.6 shows polarized microscope images of this photo-induced LPFG. Its resonance wavelength and dip depth can be controlled by the

appropriate selection of blue-laser irradiation times, period numbers, and 4MAB concentrations. In addition, the photo-induced LPFG is erasable under green-laser illumination.

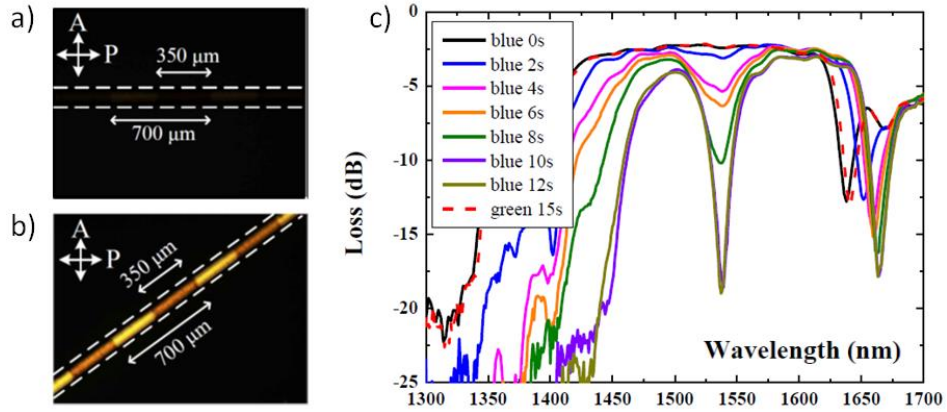


Fig. 4.6 Polarized microscope images of the LPFG when the axis of the photonic liquid crystal fiber (PLCF) was placed at an angle of (a) 0° and (b) 45° with respect to the polarizer. (c) Transmission spectra of the photo-induced LPFG for various blue-laser irradiation times and the LPFG erased by a green laser [104].

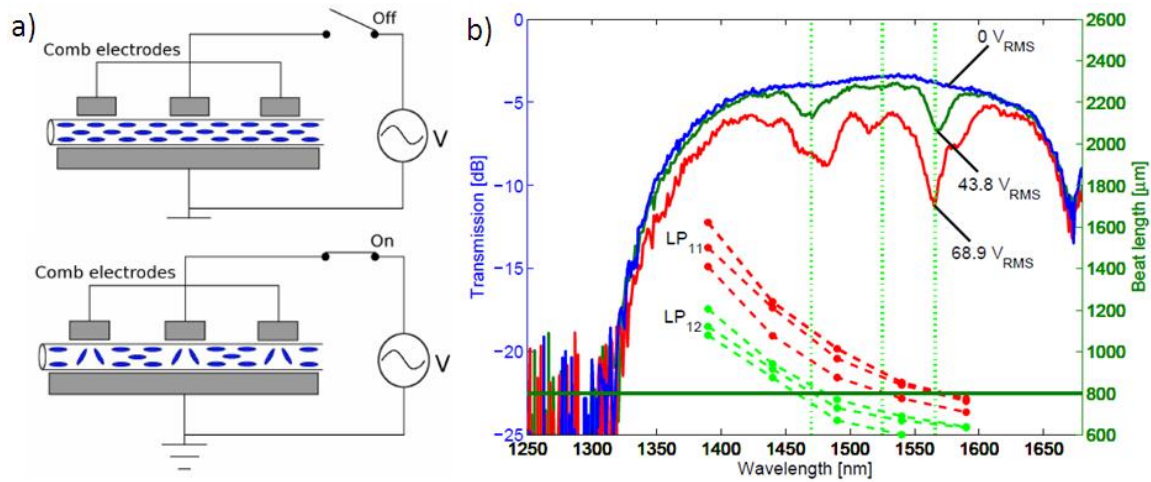


Fig. 4.7 a) Illustration of a single capillary tube filled with a planarly aligned liquid crystal, sandwiched between a comb electrode b) Transmission spectrum of electrically tunable LPFGs with $\Lambda = 800 \mu\text{m}$ in the E7 filled PCF [34].

The mechanical method to induce the LPFG use a periodic pressure applied on the length of the photonic liquid crystal fiber (PLCF) [34]. The basic fabrication procedure consisted of placing the PLCF on a flat surface and pressing it with a brass block with periodically cut V-grooves (see Fig. 4.7). A periodic variation of the RI of LC was achieved in [34] by using a comb electrode. Both the strength and the resonance wavelength of these LPFGs in PLCF were highly tunable due to the presence of the electrical field.

Furthermore, a method presented to induce the LPFG in the PLCF just by exploiting the properties of the LC material and the fiber to create a loss in a narrow wavelength band was presented in [35]. In this experiment the LC splay alignment was obtained. The spectrum shows a notch in the transmission at a wavelength of 1160 nm in the PBG from 1070 to 1360 nm (Figure 4.8). The 3 dB width of the notch is 21 nm. This notch in the transmission spectrum is caused by a cladding mode with a cutoff at this wavelength. The fiber cladding therefore becomes transparent at this wavelength, and light cannot be confined in the fiber core. Thermal tuning of such grating induced on the PLCF was demonstrated as well. Nevertheless, it has to be noted that for LPFGs based on PLCFs the wavelength operation range is limited. This is due to the fact that the presence of the LC changes the guiding properties of the PCF from the modified TIR to the photonic band-gap (PBG) mechanism. As a result, in the PLCF only selected wavelengths are guided.

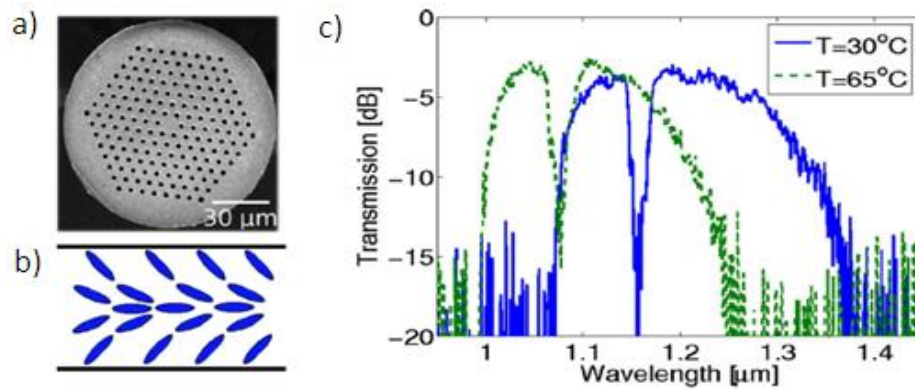


Fig. 4.8 a) SEM image of PCF end facet. b) Splay alignment of the MDA-00-3969 LC c) Transmission spectrum of the PCF filled with LC for different temperatures [35].

Chapter 5 SIMULATION OF THE LC-LPFGs

In this part of the work, the theoretical concepts that helped to understand the LC-LPFGs properties will be presented. The process developed to find correspondence between the experimental and theoretical LC-LPFGs transmission spectra required the solving of three main tasks:

1. Simulation of the LPFG transmission spectra has to be performed as accurately as possible.
2. Adequate parameterization of the LC layer on the LPFG has to be done.
3. The LC-LPFG sensitivity to the environmental factors (like temperature or/and external electric field) has to be taken into consideration.

The main software tool chosen in order to analyze the problems listed above is OptiGrating v.4.2. This software is specifically designed for modeling integrated and fiber optic devices that are assisted by optical gratings. It employs LP mode approximation and coupled-mode theory. The model of the grating and the fiber is based on the fiber datasheet, and the grating period which is determined during the fabrication process. In Section 6 the LC-LPFGs theoretical analysis presented here will be put into context of the achieved experimental results.

5.1 Introduction to the simulation procedures

In the first step of the simulation process, the LC-LPFG model has to be prepared accurately by adjustments of its structural parameters. Based on the experimental LC-LPFG studies (presented in Section 6), a numerical model of the LC-LPFG has been developed where:

- the simulated structures (see Fig. 5.1.1) are composed by three layers in the case of the LPFG (corresponding with the fiber core and the fiber clad surrounded by the third layer of air), by four layers in the case of the LPFG coating with a thin LC layer (corresponding with the fiber core, the fiber clad and the LC layer surrounded by the fourth layer of air) and by five layers in the case of the LPFG placed in the silica glass capillary with inner LC layer (corresponding with the fiber core, the fiber clad, the LC layer, the silica glass layer surrounded by the fifth layer of air).

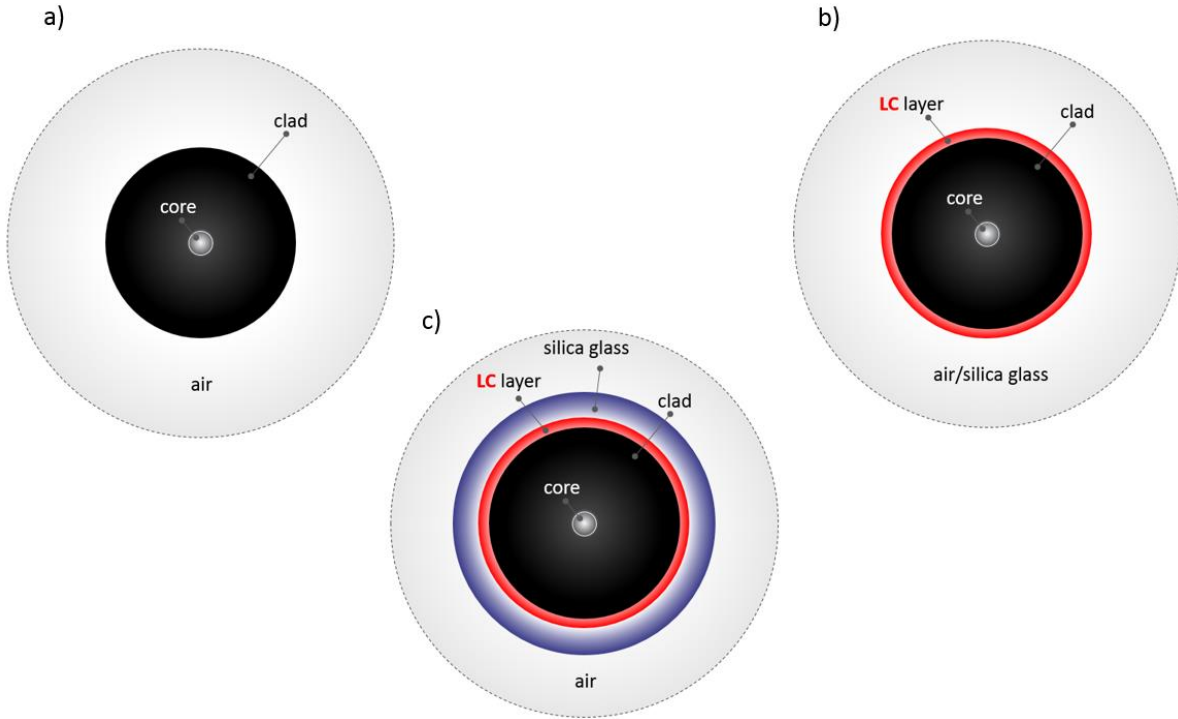


Fig. 5.1.1 Graphic representation of three (a) four (b) or five (c) LC-LPFG layer models

- the model of the fiber is based on fiber's datasheets (presented in Tab. 6.1.1) used in the experimental work; explicit fiber parameters are fit to the specification of the germanium doped *Corning* SMF-28 fibers and boron co-doped photosensitive *Fibercore* PS1250/1500 fiber.
- the model of the grating can be represented by the formula that combines a grating shape function, an average index modulation function, a period chirp function, and an apodization function:

$$n(x, y, z) = n_0(x, y, z) + \Delta n_0(x, y, z) + \Delta n \cdot P(x, y) \cdot A(z) \cdot f(\Lambda(z)/\cos\theta, z) \quad (5.1)$$

where $n_0(x, y, z)$ and $\Delta n_0(x, y, z)$ are the waveguide refractive index and the average index modulation function, Δn is the index modulation amplitude, $P(x, y)$ is the photosensitivity profile of fiber, θ is the grating tilt angle and $f(\Lambda(z)/\cos\theta, z)$ is the grating periodic shape function. For the LPFGs study within this work the following assumptions and simplifications are done:

- no period chirp is included $\Lambda(z) = \Lambda$,
- no apodization is included $A(z) = 1$,

- no grating tilt angle is included $\theta = 0$,
- the uniform average index is set $\Delta n_0(x, y, z) = \Delta n_0$,
- the uniform photosensitivity profile in the core is set to $P(x, y) = 1$ if $r \leq r_{co}$, where r_{co} is the fiber core radius, and is 0 otherwise,
- the profile of the index modulation within one grating period is assumed to be shaped of sin as follows $f(\Lambda(z)/\cos\theta, z) = f(\Lambda, z) = \sin(\frac{2\pi}{\Lambda}z)$.

Under those circumstances equation (5.1) becomes:

$$n(x, y, z) = n_{co} + \Delta n_0 + \Delta n \cdot \sin(\frac{2\pi}{\Lambda}z) \text{ for } r \leq r_{co} \quad (5.2a)$$

$$n(x, y, z) = n_{cl} \quad \text{for } r > r_{co} \quad (5.2b)$$

- the Sellmeier model [106] for pure silica is used in order to determine the fiber n_{cl} dispersion. The Sellmeier equation is defined as follows:

$$n^2 - 1 = \frac{A_1\lambda^2}{\lambda^2 - \lambda_1^2} + \frac{A_2\lambda^2}{\lambda^2 - \lambda_2^2} + \frac{A_3\lambda^2}{\lambda^2 - \lambda_3^2} \quad (5.3)$$

where the Sellmeier parameters in this case are: $A_1 = 0.6961663$, $A_2 = 0.4079426$, $A_3 = 0.897479$, $\lambda_1 = 0.0684043$, $\lambda_2 = 0.1162474$, $\lambda_3 = 9.896161$.

- In order to establish the n_{co} dispersion properties, the dopants in the fiber core also have to be taken into consideration. These dopants are Germanium (GeO_2) which increases the RI, and Boron (B_2O_3) which decreases the RI. According to [123] it is assumed that SMF-28 core fiber consists of 3.1 mol% of GeO_2 , while for the PS1250/1500 core fiber it is suspected that it consists of 10% of GeO_2 and 20% of B_2O_3 , like in [89,122]. Then the Sellmeier parameters for:

SMF-28 core fiber are $A_1 = 0.7028554$, $A_2 = 0.4146307$, $A_3 = 0.897454$, $\lambda_1 = 0.0727723$, $\lambda_2 = 0.11460853$, $\lambda_3 = 9.8961609$.

PS 1250/1500 core fiber are $A_1 = 0.6935408$, $A_2 = 0.4052977$, $A_3 = 0.9111432$, $\lambda_1 = 0.0717021$, $\lambda_2 = 0.1256396$, $\lambda_3 = 9.896154$.

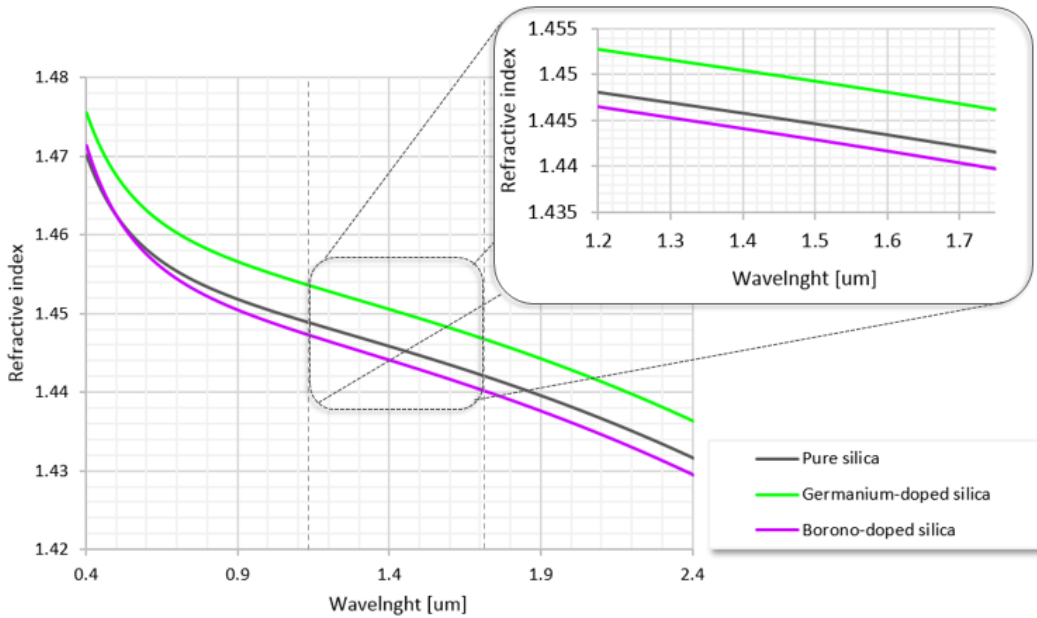


Fig. 5.1.2 Dependence of refraction index and wavelength for fused silica, Germanium-doped silica and Boron-Germanium-doped silica.

- the extended Cauchy formula is used in order to determine the dispersion properties of the LCs [23].

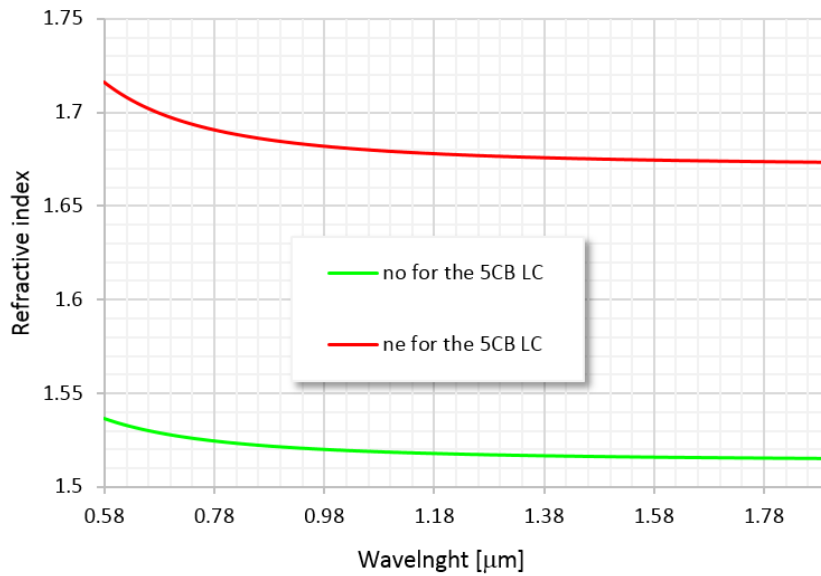


Fig. 5.1.3 Dependence of refraction indices and wavelength for 5CB LC.

This model takes into account the birefringence of LCs and thus provides an empirical way of describing the relationship of RIs to the wavelength of light. The extended Cauchy model can be expressed as follows:

$$n_o = A_o + B_o/\lambda^2 + C_o/\lambda^4 \quad (5.4a)$$

$$n_e = A_e + B_e/\lambda^2 + C_e/\lambda^4 \quad (5.4b)$$

where A_i, B_i, C_i are the three Cauchy coefficients for the ordinary ($i = o$) and extraordinary ($i = e$) RIs obtained by fitting experimental RIs measurements for the particular LC material. In Fig. 5.1.3 the dispersion characteristic for 5CB LC used in the experimental work is shown.

Once the parameters of the desired LC-LPFG have been selected, the numerical simulations can be performed. In the simplest terms, the simulation process takes place as follows:

- ➔ the propagation constants of the fundamental and cladding modes are calculated to determine the effective refractive indices of the core and cladding modes,
- ➔ the coupling coefficient is found for coupling between specific modes,
- ➔ the complete transmission spectrum is obtained by using Coupled Mode Theory (CMT).

The attenuation peak shape and intensity is dictated by the value of the coupling coefficient and the electric field profiles of the coupling modes, whereas the wavelength locations of loss bands depend on the relative magnitudes of the effective mode indices for a fixed grating period (from the phase-matching condition presented by the Equation 2.2.1). The numerical simulations in this work are performed mainly by using the Optigrating v.4.2 software (Optiwave Systems, Inc., Ottawa, ON, Canada). OptiGrating v.4.2 is based on the CMT. The program has built-in mode solvers providing modal constants and fields needed to formulate the Coupled Mode Equations (CMEs). CMEs are solved by using Transfer Matrix Method (TMM). The general idea of TMM is that the grating structure is divided into a number of uniform grating sections, which have an analytic transfer matrix. The transfer matrix for the entire structure is obtained by multiplying the individual transfer matrices. As a result the CMEs can be solved with the initial values.

At this stage the selection of modes is critical in the reduction of computational effort. The calculation of the modes in a cylindrical multilayer waveguide becomes a difficult and time consuming task. For the sake of simplicity, a theoretical model presented here is based on the LP-mode approximation. LP modes are adequate for a description of the LPFG under the assumption of weak guidance [38-42]. Therefore, the presence of a layer of a RI which shows an unimportant contrast with the cladding (as is the case for the

LB LC mixtures used in the experimental work presented here) will not affect results in a significant way. As the LC layer (like for MB LCs and HB LCs) on the cladding shows a higher contrast, error present in the results will increase, but they will remain qualitatively correct. It was also proven in [105] that the high contrast between ambient and cladding refractive indices don't have to play a significant role in the results.

LP modes of arbitrary azimuthal number can be calculated for structures with arbitrary azimuthal or radial refractive-index profile. It is assumed that the structure simulated here presents no azimuthal variation of the perturbed index profile. In other words, resonant bands corresponding to coupling from the guided core mode to a discrete set of symmetrical cladding modes appear in the LPFG transmission spectrum. It can be explained by the fact that the efficiency of coupling between these types of modes occurs where there is significant overlap between its electric field profiles. The efficiency of coupling to the asymmetric modes is small, and thus in general no attenuation bands are visible. As a result, there are only interactions between LP_{mn} modes where $m = 0$.

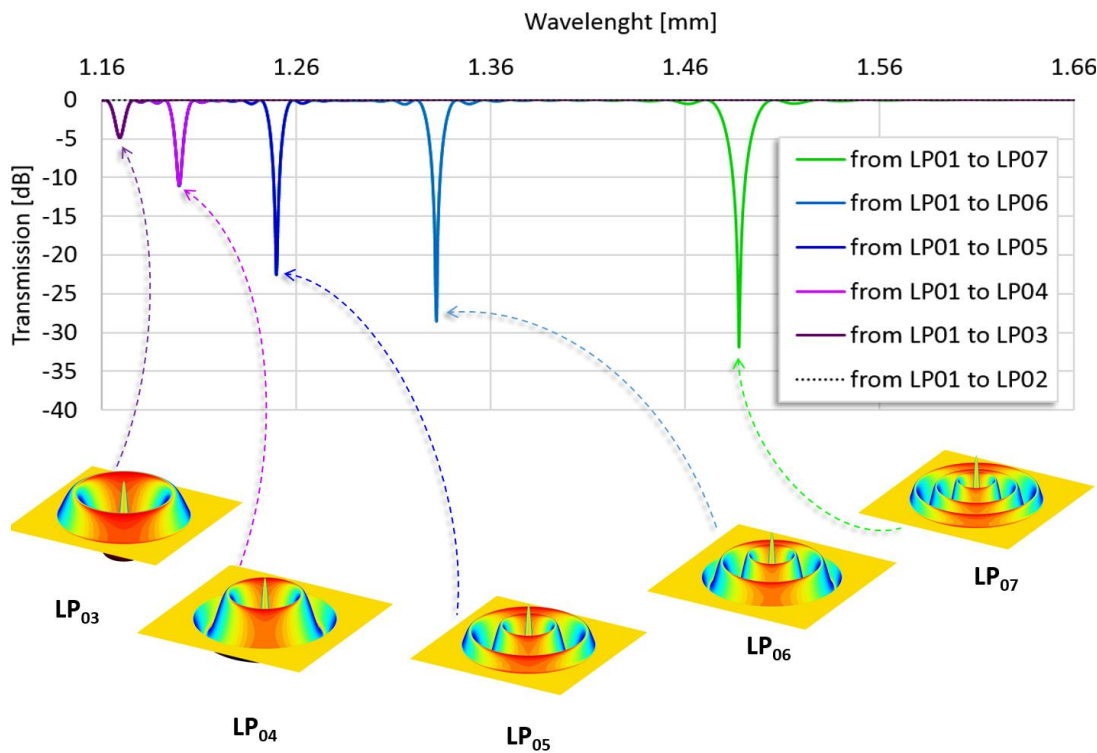


Fig. 5.1.4 LPFG transmission spectra calculated versus number of modes taking into account in the simulation (main parameters of the LPFG: $\Lambda = 368 \mu\text{m}$, $L = 28800 \mu\text{m}$; fiber properties are set for the PS1200/1500 fiber used in the experimental work) with theoretical intensity profile for the LP_{03} - LP_{07} cladding modes.

Another important factor which has to be deliberated is the mode's designation. The notation used here for the LP_{mn} modes (m – azimuthal number, n – orbital number) is as follows: core mode LP_{01} , first-order cladding mode is LP_{02} , second-order cladding mode is LP_{03} , and so forth. Fig. 5.1.4 presents LPFG transmission spectra calculated for different numbers of modes taken into account in the simulation. As can be seen, this process allowed to clearly define the number of the mode corresponding with the particular attenuation band. In addition, it was found that taking into account the first thirteen modes will provide sufficient results for all the LC-LPFG cases studied here.

It have to be noted that the accuracy of the LCs properties, grating constraints and fiber parameters given in the specification sheets or by producers, is often insufficient for precise simulation of the LC-LPFG transmission spectrum. Typically, such parameters as refractive index of clad (in the case of silica clad) or grating period are quite well-defined. On the other hand, the values of core and cladding radius, dopant concentration, LC dispersion properties may have large relative uncertainties. That is why some adjustment of LC-LPFG parameters are always needed. Here, this was mainly achieved by fitting the measured and simulated transmission spectra.

In order to determine LPFG parameters, first the simulation transmission spectra were fit to those measured within the experiment. This step allows to specify the fiber dimension and refractive indices values of its core and clad. Estimated fiber parameters stay in agreement with Corning and Fibercore specifications. The LPFG parameters, namely period, length, index of the modulation could also be assessed at this point. Since the LPFG parameters are modified during the grating writing process the method of their fabrication was also taken into account (see Section 6.1.2). Additionally, by fitting the simulated transmission spectra to the experimentally measured LPFG thermal response, it was possible to approximate the thermo-optic coefficients of the host fibers.

The LC layer parameters were also found by comparing both, experimental and simulated LC-LPFG transmission spectra (measured in air and versus temperature and/or electric field). Precisely, it is important to find two parameters of the LC layer: its thickness and refractive index. The accuracy of the LC layer thickness measurement under the experimental work (see Section 6.1.4) is limited and allowed to determine its value to be of few micrometers. For this reason, the greatest attention was paid to estimating the value of the LC layer thickness. When the LC layer refractive index is considered, their refractive indices' thermal characteristics were available. However, they were measured for the wavelength of 589 nm. These characteristics will be different for spectral range studied here (typically

from 1200 nm to 1600 nm). Precisely, since LCs are dispersive materials their refractive indices will be lower in the infrared range compared to values given in the visible range (dispersion should not have significant impact on the magnitude of the LC RIs thermal response). The Cauchy coefficients were known only for 5CB LC. Thus, due to the lack of complete information about the dispersion properties for the rest of the LCs, it was assumed that the shape of the dispersion characteristic will be the same as for 5CBLC. These characteristics are only offset by a corresponding difference in RI measured for wavelength 589 nm (like is presented in Fig. 5.1.4 for the 1702 LC).

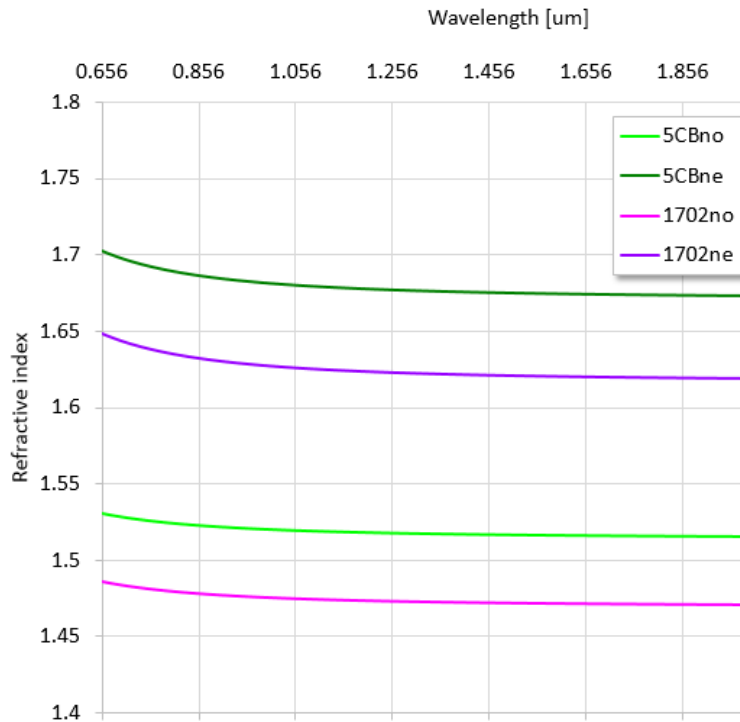


Fig. 5.1.4 Dispersion characteristic for the 5CB LC (known) and for the 1702 LC (estimated)

This will introduce the error into the calculation. Nevertheless, this assumption should be adequate for the description of the LC-LPFGs transmission properties and should provide qualitative valid outcomes. In the simulation it is also assumed that the LC molecules' orientation order on the bare LPFG is perfect. Obviously, this situation never occurs in the reality. The order of the LC alignment will be mainly affected by the n_o value. Precisely, the lower the LC alignment order, the higher the value of the effective LC RI will be. Based on the causes listed above, the LC n_o values were also slightly adjusted for each of the samples (this difference between particular LC-LPFGs was however not higher than 0.02%). In order to consider n_e values of the LCs, the LC-LPFG have to be in the presence of an external electric field. In this case there is one more issue which has to be deliberated. Since two parallel electrodes were used in the setup for the experimental work, the anisotropy to the LC layer could be introduced by an electric field

(detailed discussion of this effect is provided in Section 5.3.5). In simulations the isotropic refractive index distribution of the LC layer was assumed. This will introduce the error into the calculations. Conversely, the LC layer anisotropy effect was included in terms of decreasing the n_e value when the LC-LPFG is considered in the on-voltage state. This parameter could be estimated when the simulated electric responses of the LC-LPFGs were fit to those measured in the experiment. The anisotropy of the LC layer should play a role in the results presented henceforth. However, the influence of the LC layer refractive index plays a more important role. Consequently, there is a correspondence between the theoretical and the experimental results.

In conclusion, the LC-LPFG simulation is a challenging task, even more when their thermal and/or external electric field are/is considered as well. Its complexity and lack of detailed dates requires that certain simplifications be established within this work. Nevertheless, it has to be emphasized that the primary purpose of the LC-LPFG simulations performed here is to determine their principle of operation rather than exactly match the results. It will be shown in Section 6 (where the LC-LPFG model described here has been confronted with experimental results) that the performed calculations allowed to qualitatively analyze the LC-LPFG tuning.

5.2 LPFG transmission properties analysis

The LPFG transmission spectra have to be simulated as accurately as possible. However, this task can be quite complicated. It will be presented that even very small deviations of the LPFG parameters can result in significant changes in the transmission spectra. The attenuation bands are determined by the parameters of the fiber itself (e.g., cladding/core radius and RI, dopant concentration), and by the changes in the fiber induced by the formation of the LPFG (e.g., grating period, fiber length, change in the core-cladding RI difference). Below, the impact of these parameters on the LPFG transmission spectra is examined carefully.

5.2.1 Impact of the fiber parameters to the LPFG transmission properties

The main fiber parameters which define the LPFG transmission spectrum are:

- a) radius of the fiber core,
- b) radius of the fiber clad,
- c) refractive index of the fiber core,
- d) refractive index of the fiber clad.

If one of the fiber parameters listed above is changed, the propagation constants of all modes are modified. For example, a variation in the refractive index of the fiber core, will strongly affect the core mode and weakly affect the cladding modes. In contrast, a variation in the radius of the fiber clad, has no influence on the core mode but has strong impact on the cladding modes. The changes in the mode's propagation constants shift the corresponding resonance wavelengths by different values, which are specific for each parameters. As a result, the LPFG transmission spectrum is modified. Therefore, in order to find a correspondence between the experimental and the theoretical LPFG spectra the knowledge about the fiber properties used in the grating production has to be as accurate as possible. Unfortunately, in practice, the accuracy of the fiber data given in the specification sheets is often insufficient in order to easily reproduce the transmission spectra of a LPFG. Moreover some additional changes might be induced during the grating writing process. As a result, directly comparing the experimental data with the theoretical calculation becomes an impossible task. Nevertheless, it is possible to adjust, with acceptable accuracy, some of the fiber's parameters and to obtain adequate correspondence between the experimental and the theoretical results.

In order to study the impact of fiber parameters, a series of simulations was performed (as summarized in Tab. 5.2.1 and Tab. 5.2.2). The LPFG transmission spectra are calculated several times versus the changes of one of the parameters. The intervals of the parameters' changes were set to be 0.5% for the core and clad radius while for the core refractive index the interval of variation of 0.001% was selected. The following assumptions are taken in order to simplify the process and to avoid having too many arbitrary parameters to optimize:

- the refractive index of the clad and its dispersion properties are set in all simulations as for the pure silica glass, since all tested fibers in the experimental work had such an outer cladding. Consequently, only three parameters are chosen to study the impact of their variation, namely: the fiber core radius, fiber clad radius and core refractive index. The reason why they were selected is that they may have large relative uncertainty. That is why some adjustment of these fiber parameters is always required.
- the maximum variations in the core and clad radius are set within the limits of the reasonable changes according with the specification in the fiber data sheets.
- the fiber core dispersion properties are set as for the PS1200/1500 fiber used in the experimental work.
- one of the main purposes of this analysis is to be able to track the displacement of the resonance wavelengths when the fiber parameters are changed. Regarding the depth of the attenuation bands, there are many factors that influence this value, mainly associated with the grating structure. For this reason, the variation of the attenuation bands' depth will be discussed in section 5.2.2.
- it is assumed that the LPFG designed here operates in the air (thus in all simulations one external layer is added with thickness of 20 μm and with refractive index of 1) and under unperturbed conditions (the environmental temperature is set to be 25°C).

In addition, two cases of the LPFGs are studied, and chosen to match the experimental constraints (their basic parameters are presented in Tab. 5.2.1). The main difference between them is the period magnitude of the grating. The first LPFG model (designated in the Tab. 5.2.1 as a case 1) belongs to the group of gratings where coupling occurs at relatively low-order modes. In the example demonstrated here, explicit coupling of the modes takes place up to the LP_{07} mode over a wavelength range 1200-1750 nm. For the second LPFG model (designated in the Tab. 5.2.2 as a case 2) the coupling takes place for the higher-order modes showing a turning point in the wavelength range of interest. It should be emphasized here that all

the cladding modes can exhibit a turning point. However, for the lower-order modes this lies outside of the wavelength range of interest. This feature (discussed in the Section 5.2.2) will strongly affect the cladding mode's properties and as a consequence, LPFG spectral dependence from on the fiber parameters.

Tab. 5.2.1 *Specification of the basic parameters study LPFG models*

| Case of the study LPFG model | 1 | 2 |
|------------------------------|---------------------|---------------------|
| period | 368 μm | 226.8 μm |
| index modulation | 0.00023 | 0.00017 |
| length of the grating | 28700 μm | 28700 μm |

Tab. 5.2.2 *Specification of the fiber parameters variation applied to the LPFG models*

| No. of the simulation series | r_{co} [μm] | r_{cl} [μm] | n_{co} | n_{co} | Dispersion properties for the fiber core |
|------------------------------|---|---|--|----------|--|
| 1 | Change in value by 0.5% from 3.72400 μm to 3.91399 μm | 61.5 | case 1: 1.4494 case 2: 1.4502 | 1.444033 | set for the PS1200/1500 fiber |
| 2 | 3.8 | Change in value by 0.5% from 60.5775 μm to 63.3450 μm | case 1: 1.4494 case 2: 1.4502 | | |
| 3 | 3.8 | 61.5 | case 1: change in value by 0.001 % from 1.449327530 to 1.449443482 case 2: change in value by 0.001 % from 1.450127490 to 1.450272510 | | |

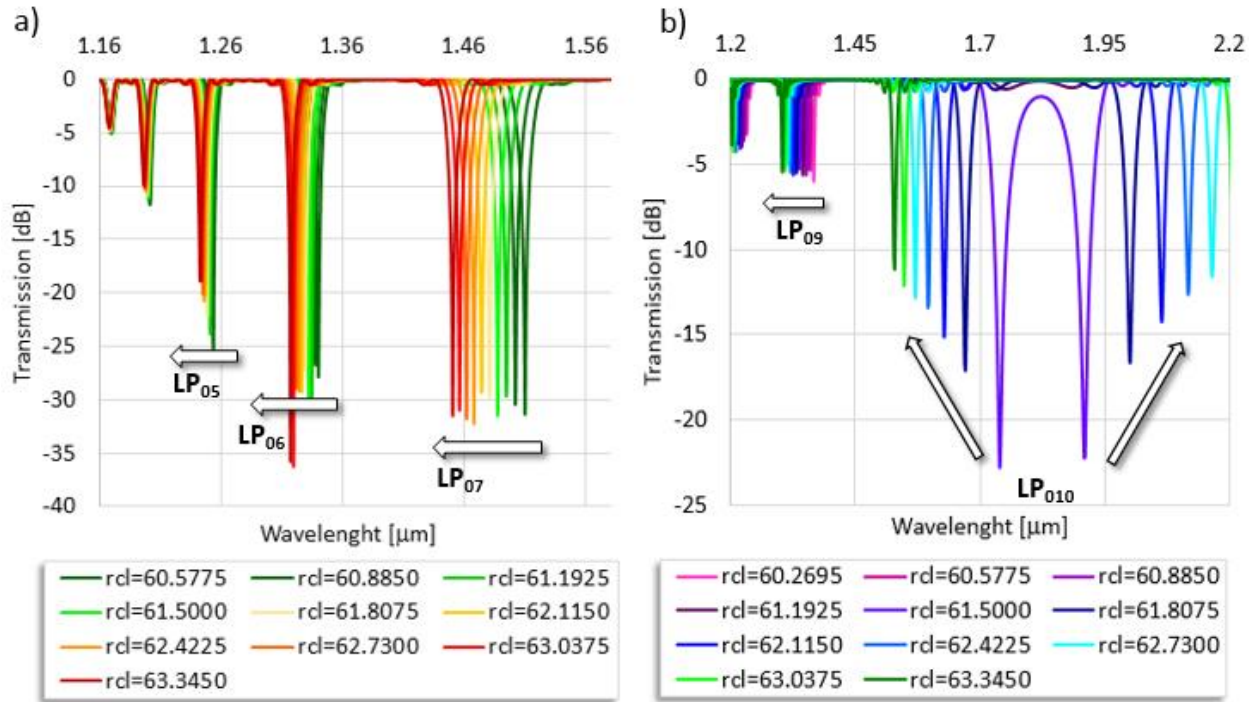


Fig . 5.2.1 Calculated LPFG transmission spectra versus radius of the clad for the gratings define within the case 1 (a) and case 2 (b).

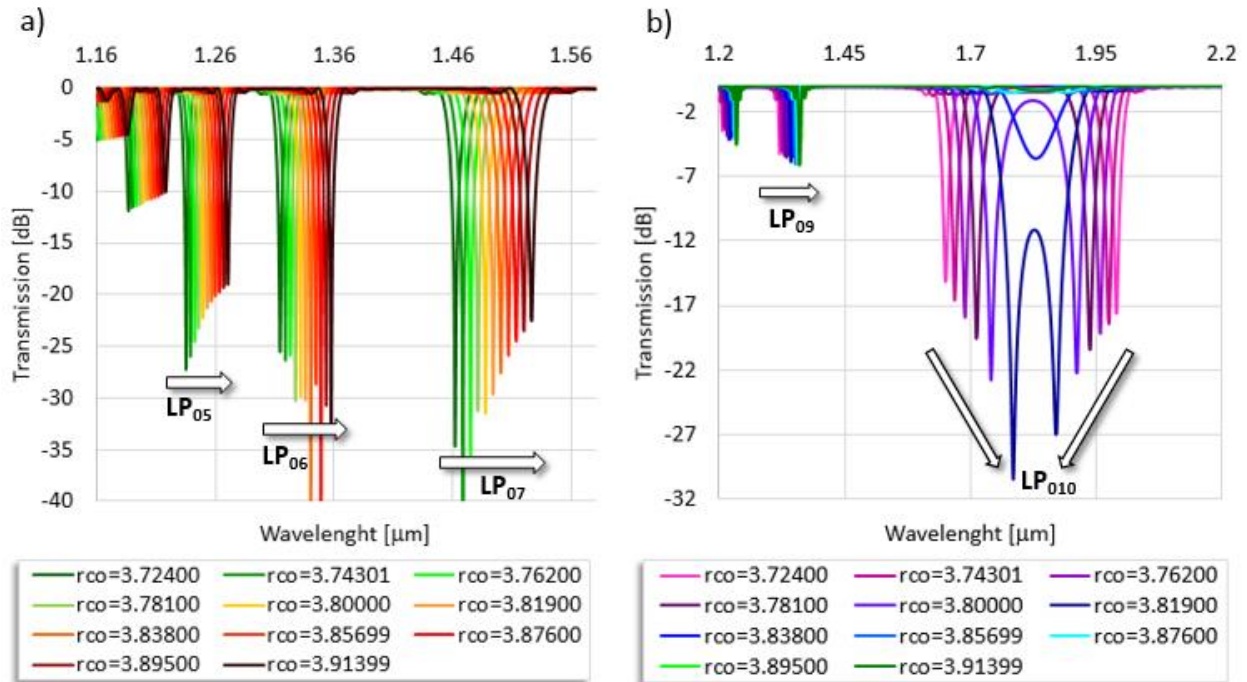


Fig . 5.2.2 Calculated LPFG transmission spectra versus radius of the core for the gratings define within the case 1 (a) and case 2 (b).

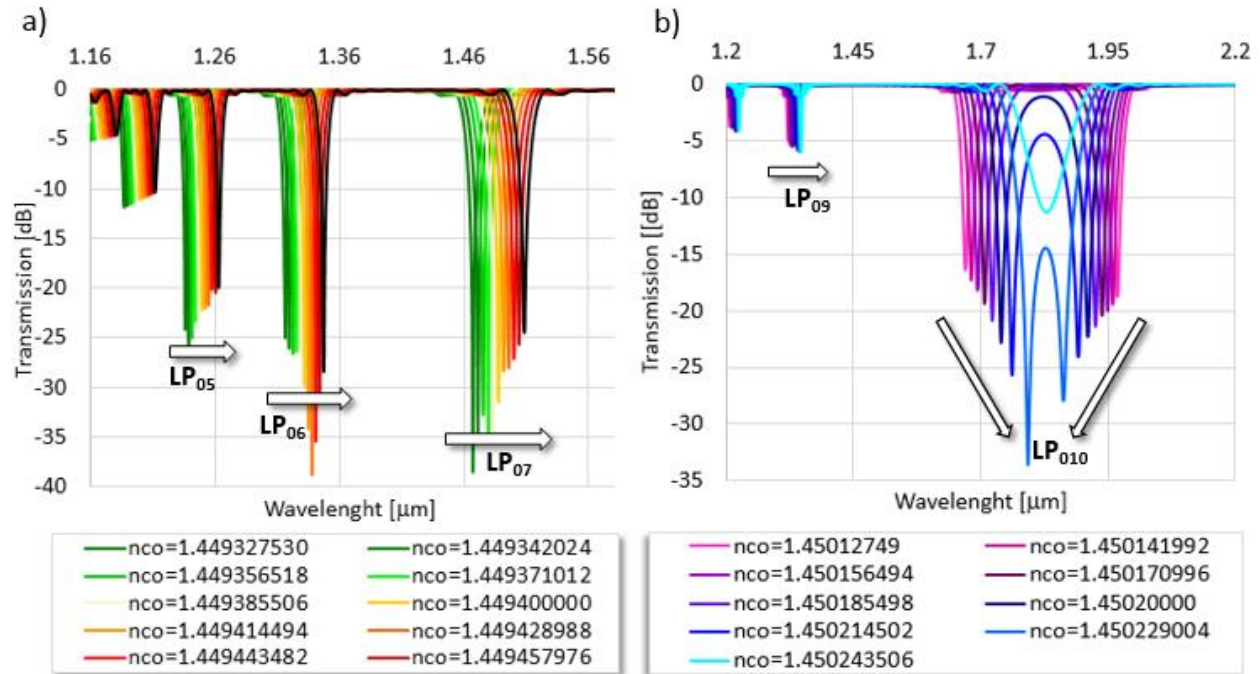


Fig . 5.2.3 Calculated LPFG transmission spectra versus refractive index of the core for the gratings define within the case 1 (a) and case 2 (b).

In Figs from 5.2.1 to 5.2.3, the calculated LPFG transmission spectra versus different fiber parameters are presented. The following conclusions can be drawn from the study conducted above (summarized in the Tab 5.2.3):

- Even very small deviations of fiber grating parameters can result in significant changes in the transmission spectra. For example, in Figure 5.2.2a, the results of the simulations for the LPFG calculated versus the r_{cl} magnitude are presented. It is apparent that the shift of the attenuation band corresponding with the LP₀₇ mode is of the order of 20 nm when the r_{cl} changes just by $\sim 2.77 \mu\text{m}$.
- The result obtained for the LPFG defined in case 2, shows that the proper adjustment of the fiber parameters can open a transmission window and break up one of the attenuation bands into two transmission peaks. An explanation of the reason behind the formation of dual resonant peaks in higher-order cladding modes will be presented in the Section 5.2.3.
- The impact of the fiber parameters' variation is also different for a particular band in the transmission spectrum of the LPFG. Each attenuation band corresponds with a different mode order. For each particular mode there is a fractional power in both the core and the cladding. The resulting ratio leads

to a higher sensitivity of the resonance wavelength to the fiber parameters changes in the case of the higher-order modes (see Fig. 5.2.4a). In addition, for the mode with a high enough order, the coupling results in the dual resonant attenuation band. As is clearly visible from the Fig. 5.2.4b, such an attenuation band exhibits the highest changes resulting from the fiber parameters' variation at their phase matching turning point.

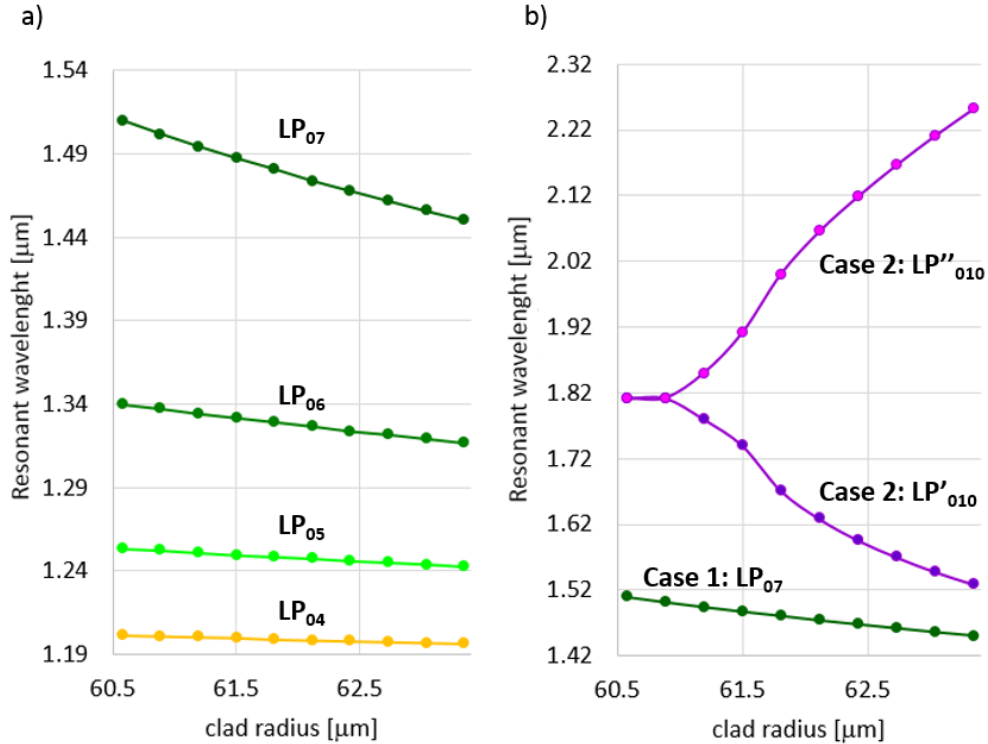


Fig. 5.2.4 a) Dependence of resonance wavelengths on the clad radius variation for the LPFG defined within case 1. The attenuation bands correspond to the cladding modes LP₀₄-LP₀₇.

b) Comparison of the resonant wavelengths' evolution with the clad radius variation for the LPFG defined within case 1 and for the LPFG defined within case 2 (note the dual-resonant attenuation band corresponding with the LP₀₁₀ cladding mode).

- Due to the fact that a variation of the r_{cl} has no influence on the core mode but has strong impact on the cladding modes, the attenuation bands will shift to the longer wavelengths. This effect occurs up to a point when in the LPFG spectrum the attenuation band, characterized by the phase-matching turning point, will appear in the wavelength range of interest. As a result, by increasing the r_{cl} the splitting of the attenuation band is observed. In contrast, variations of the r_{co} and n_{co} , weakly affected the cladding modes but have strong impact on the core mode. Therefore, the changes in the modes' propagation constants shift the corresponding resonance wavelengths in the opposite way than it is

observed in the case of the r_{cl} variations (in accordance with the phase-matching condition). The behaviors described above are shown in the Fig. 5.2.5b and the Fig. 5.2.6b.

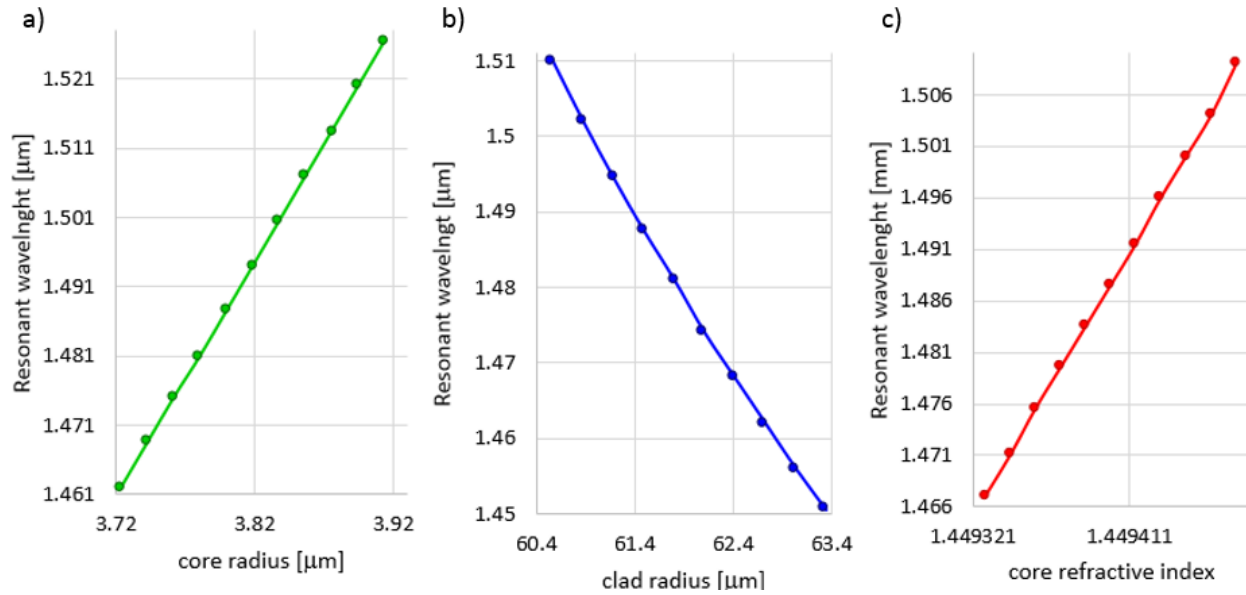


Fig. 5.2.5 Dependence of the resonance wavelengths on the core radius (a), clad radius (b) and core refractive index (c) for the LP_{07} mode.

Tab. 5.2.3 Summarized results of the fiber parameters impact on the LPFG transmission spectrum study

| Case of the study LPFG model | Fiber parameter | cladding modes | Max. shift of the attenuation band [nm] | Direction of the shift |
|------------------------------|-----------------|---------------------|---|------------------------|
| 1 | r_{co} | LP ₀₄ | 31.5 over the r_{co} variation of 0.18999 μm | positive |
| | | LP ₀₇ | 64.4 over the r_{co} variation of 0.18999 μm | positive |
| | r_{cl} | LP ₀₄ | 5.0 over the r_{cl} variation of 2.7675 μm | negative |
| | | LP ₀₇ | 59.5 over the r_{cl} variation of 2.7675 μm | negative |
| | n_{co} | LP ₀₄ | 25.0 over the n_{co} variation of 0.000145 | positive |
| | | LP ₀₇ | 41.5 over the n_{co} variation of 0.000145 | positive |
| 2 | r_{co} | LP ₀₉ | 34.29 over the r_{co} variation of 0.095 μm | positive |
| | | LP _{010'} | 133.7 over the r_{co} variation of 0.095 μm | merge into one |
| | | LP _{010''} | 120.3 over the r_{co} variation of 0.095 μm | |
| | r_{cl} | LP ₀₉ | 56.6 over the r_{cl} variation of 1.845 μm | negative |
| | | LP _{010'} | 211.0 over the r_{cl} variation of 1.845 μm | move apart |
| | | LP _{010''} | 341.1 over the r_{cl} variation of 1.845 μm | |
| | n_{co} | LP ₀₉ | 22.0 over the n_{co} variation of 0.000102 | positive |
| | | LP _{010'} | 121.7 over the n_{co} variation of 0.000102 | merge into one |
| | | LP _{010''} | 97.7 over the n_{co} variation of 0.000102 | |

5.2.2 Impact of the grating parameters on the LPFG transmission properties

The main grating parameters which define the LPFG transmission spectrum are:

- a) grating period Λ
- b) grating length L
- c) refractive-index modulation in the fiber core Δn_{co}

In order to study the impact of these parameters on the LPFG spectral properties, first the fiber parameters have to be defined. The core and cladding radii with the core and clad refractive indices are set for the model of the fiber given in the Tab. 5.2.4. When this is done the LPFG transmission spectra are calculated versus different grating parameters. The details of the performed simulations are presented in Tab. 5.2.5.

Tab. 5.2.4 *Specification of the fiber parameters*

| r_{co} [μm] | n_{co} | r_{cl} [μm] | n_{cl} | Dispersion properties |
|----------------------------|----------|----------------------------|----------|-------------------------------|
| 3.8 | 1.450200 | 61.5 | 1.444033 | set for the PS1200/1500 fiber |

Tab. 5.2.5 *Specification of the grating parameters variation applied to the LPFG models*

| Λ [μm] | L [μm] | Δn_{co} |
|------------------------------------|--|--|
| change in value from 340 to 190 | 47854 | 0.00017 |
| Case 1: 226.8 Case 2: 350.0 | | case 1: change in value by 0.00001 from 0.00010 to 0.00022 case 2: change in value by 0.00002 from 0.00010 to 0.00022 |
| | change in value from 40000 to 60000 | 0.00017 |

At first, accurate modelling of the LPFGs requires the correct identification of the grating periodicity. In order to verify the impact of the period variation on the LPFG transmission spectrum, several sets of the period values are considered. The first one is in the range from 400.0 μm to 350.0 μm . In this region the coupling occurs to the lower order cladding modes LP_{01} – LP_{07} . As is depicted in Fig. 5.2.6, decreasing of the period value results in a negative shift of the attenuation bands across the wavelength range.

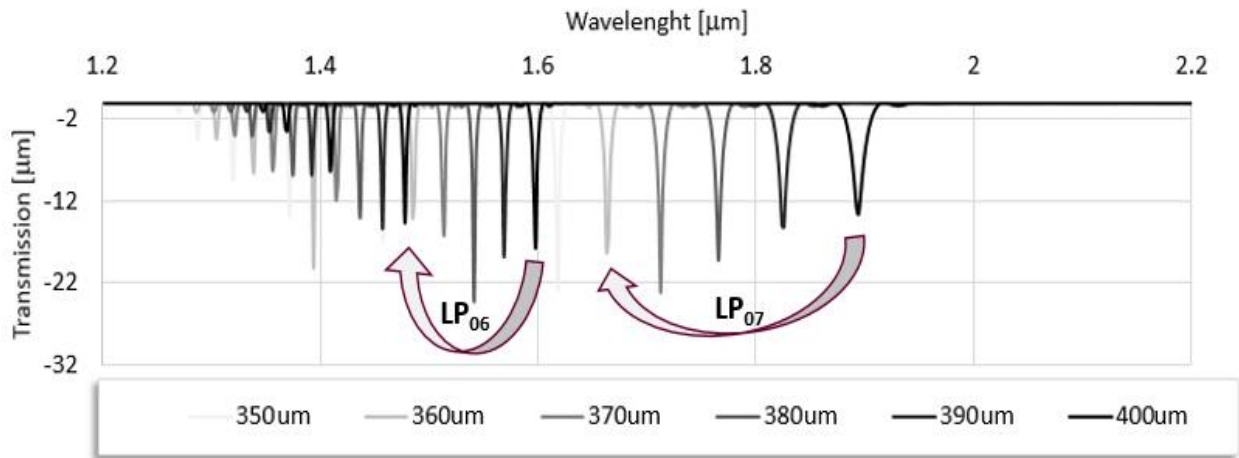


Fig. 5.2.6 Transmission spectra of the LPFG versus period which conditions appearance of the lower-order modes

For shorter periods, coupling takes place to the higher order cladding modes. The behaviour for such modes shows a turning point in the wavelength range of interest. Explicitly, this phenomenon is observed for the LPFG model presented here in the period ranges from 330.0 μm to 334.0 μm , from 269.5 μm to 272.0 μm , from 225.0 μm to 228.0 μm , from 190.0 μm to 196.0 μm . As is shown in Fig. 5.2.7 in each of these period ranges, the coupling of modes from LP_{08} to LP_{011} occurs sequentially. As a consequence, a new attenuation band appears each time in the LPFG transmission spectrum. Then, with a continuous decrease of the period value, the band splits into two peaks, which move apart in opposite directions. It is also worth adding that the wavelength at which the turning point occurs decreases with decreasing the grating period (marked in Fig. 5.2.7 by the grey dash line). Therefore, it is possible to select a period where the coupling to a single cladding mode occurs at two wavelengths.

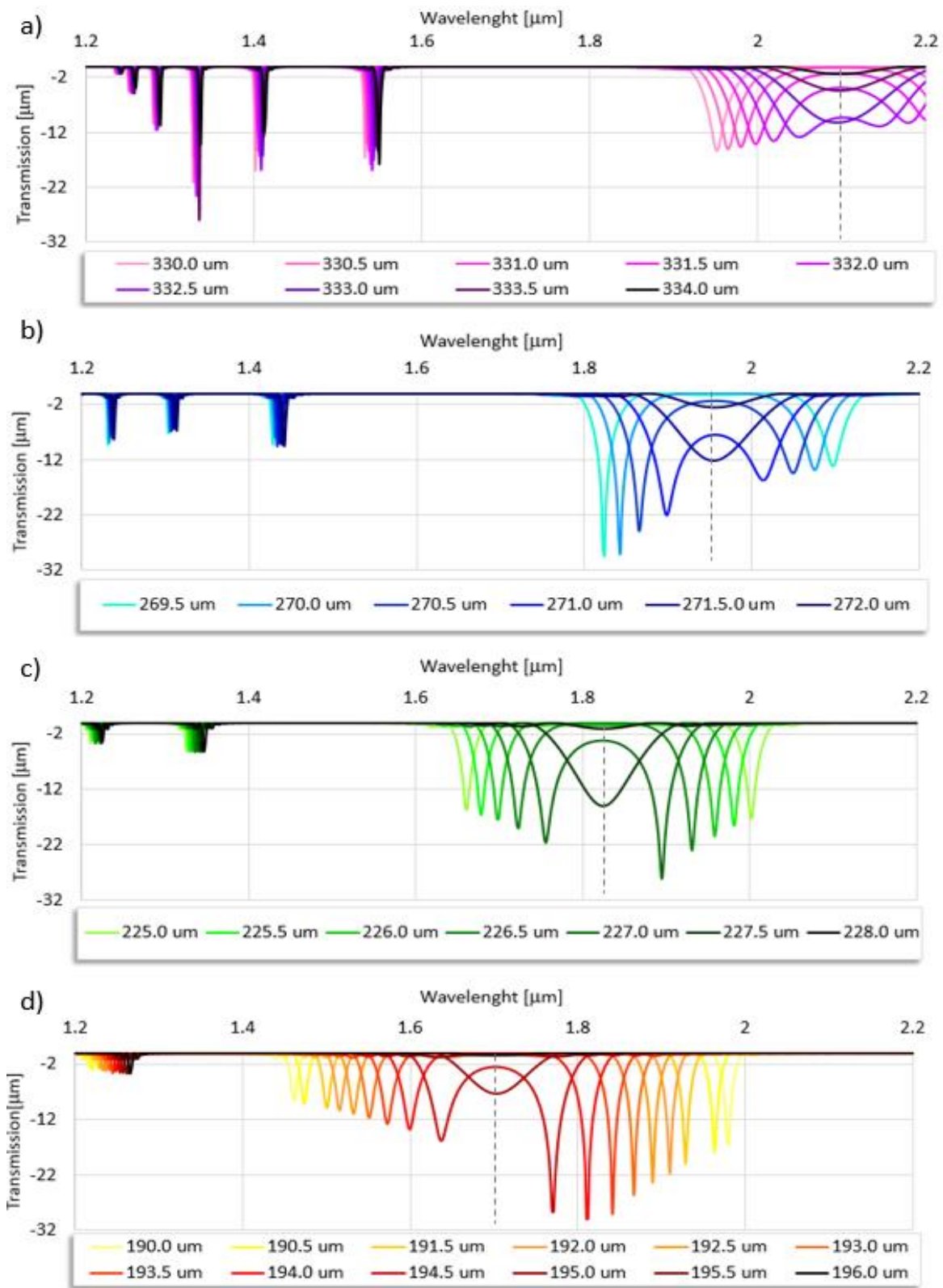


Fig. 5.2.7 Transmission spectra of the LPFG versus period which conditions appearance of the higher-order modes

While the period of the LPG determines its resonant wavelengths (as was just shown above), the grating length affects the depth of the attenuation bands. The cross coupling coefficient between the core mode and the cladding mode that couples at that resonance wavelength is also a factor influencing the transmission spectrum - this effect is governed in the simulations by the refractive-index modulation in the fiber core Δn_{co} because the coupling coefficient is directly proportional to this value. A simple formula [10] permits to have an approximate idea of the expression for the transmission minimum T_m (maximum of transmission loss) of a resonance attenuation band:

$$T_m = \cos^2(\kappa L) = \cos^2(\pi \Delta n_{co} \eta L / \lambda) \quad (5.2.1)$$

where κ is the coupling coefficient, η is the overlap integral and λ is the resonant wavelength. It can be inferred that the first maximum of the LPFG attenuation band corresponds to $\kappa L = \pi/2$. Therefore, during the LPFG fabrication, the rise of the attenuation band should be observed and then its decline after the coupling factor κL had passed through the $\pi/2$ value. Such a behavior was observed in the simulation when the LPFG transmission spectra were calculated versus the grating length (Fig. 5.2.8) and the refractive-index modulation in the fiber core Δn_{co} (Fig. 5.2.9 and Fig. 5.2.10).

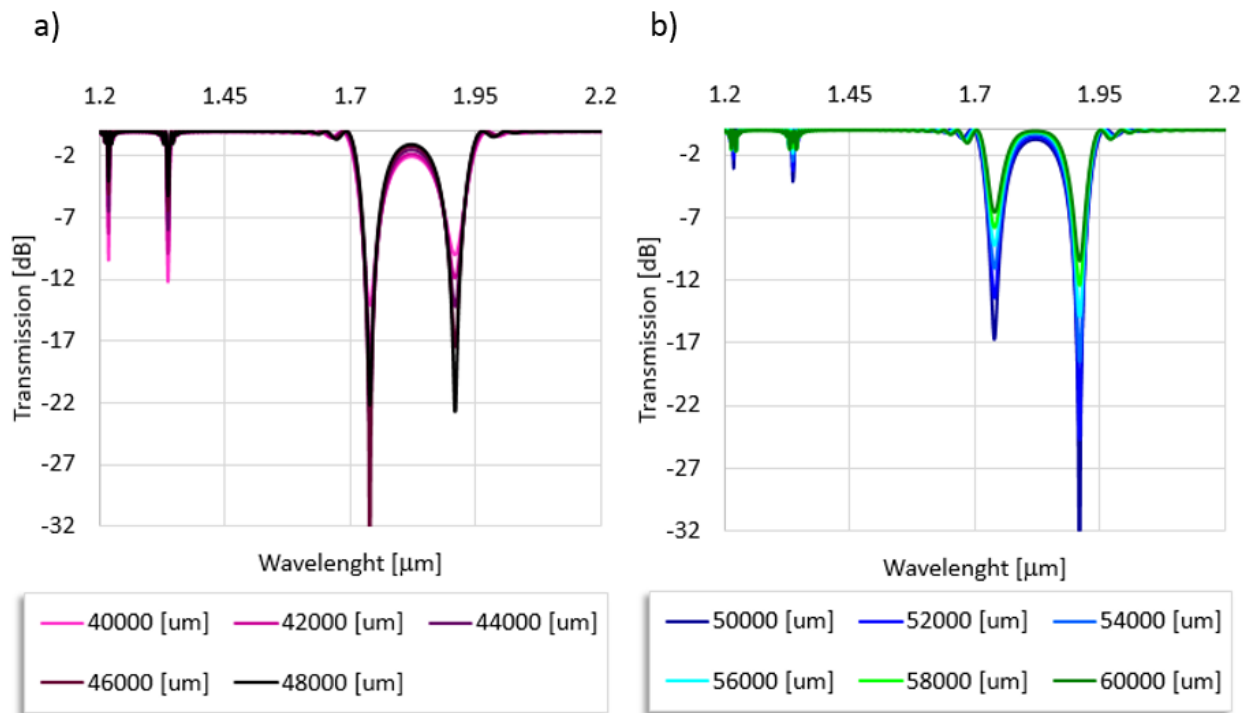


Fig. 5.2.8 Transmission spectra of the LPFG with period of 226.8 μm versus grating length

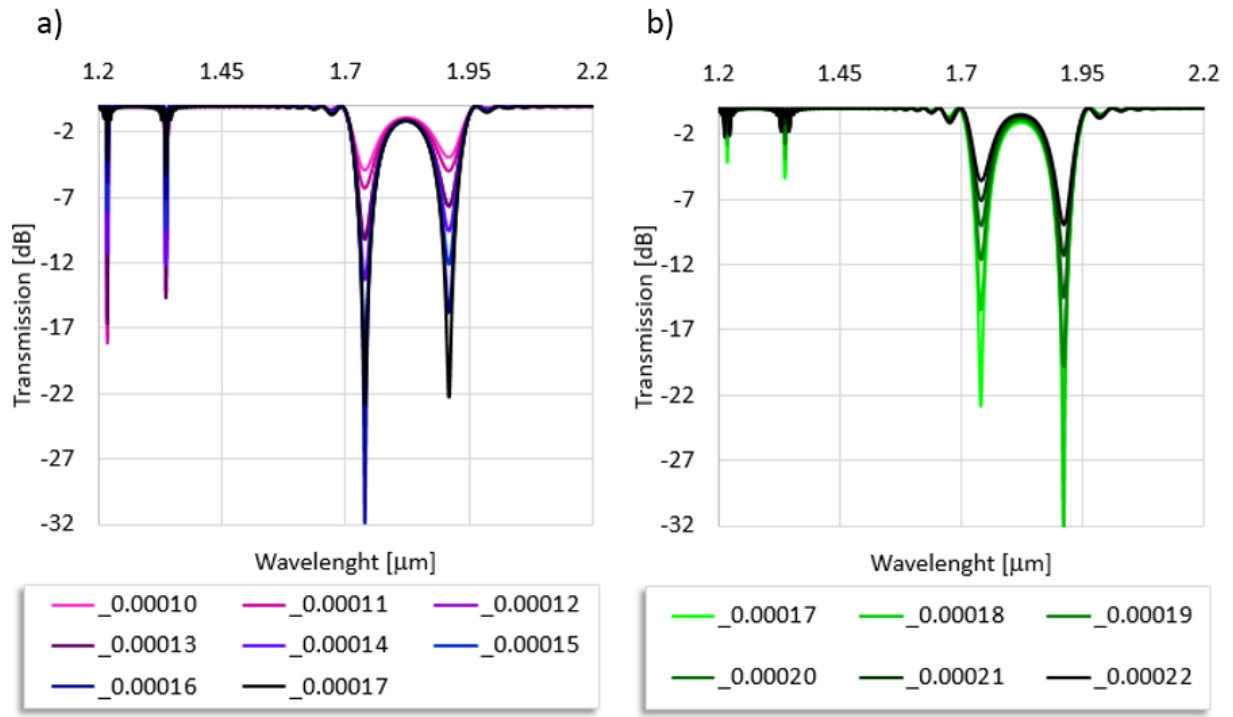


Fig. 5.2.9 Transmission spectra of the LPFG with period of 226.8 μm versus refractive-index modulation in the fiber core Δn_{co}

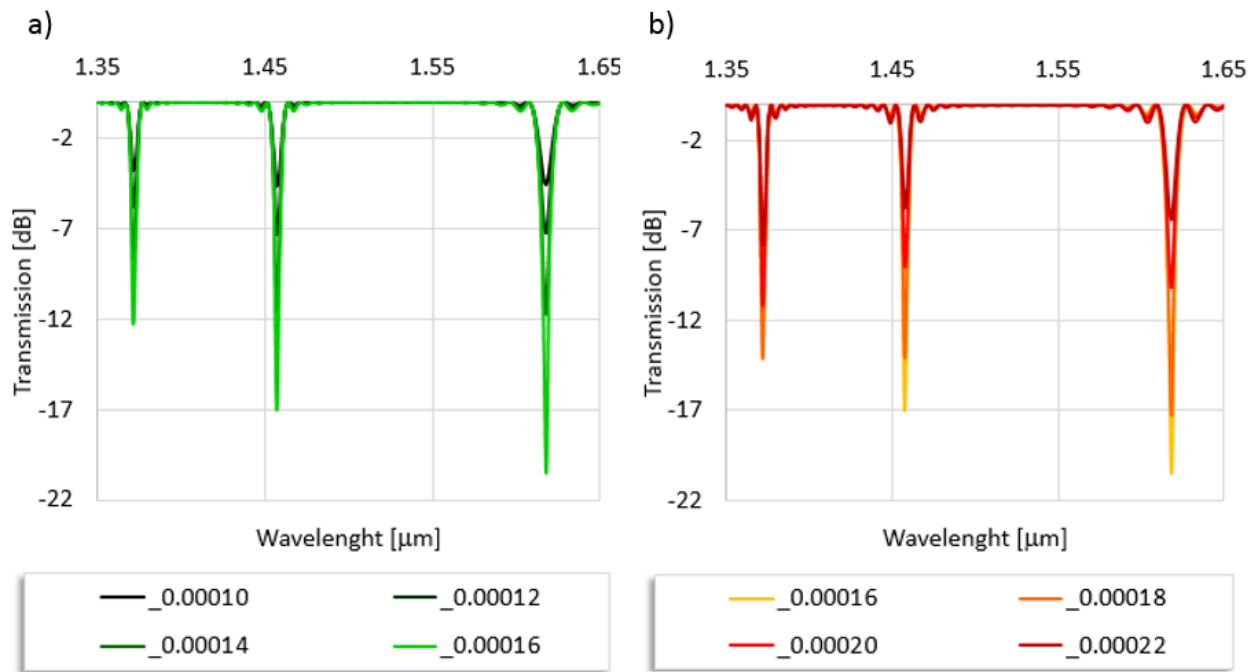


Fig. 5.2.10 Transmission spectra of the LPFG with period of 350.0 μm versus refractive-index modulation in the fiber core Δn_{co}

5.2.3 The temperature effect to the LPFG transmission properties

The most complete form of the temperature effect on the LPFG can be expressed as follows:

$$\frac{d\lambda_0}{dT} = \frac{d\lambda_0}{d(\delta n_{eff})} \left(\frac{n_{eff,co}}{dT} - \frac{n_{eff,cl}^{(m)}}{dT} \right) + \Lambda \frac{d\lambda_0}{d\Lambda} \frac{1}{L} \frac{dL}{dT} \quad (5.2.2)$$

,where T , λ_0 , Λ , L are temperature, wavelength, period of the grating and length of the grating, respectively. The $n_{eff,co}$ and $n_{eff,cl}^{(m)}$ are the effective indices for the core and m clad modes. The δn_{eff} is defined as follow:

$$\delta n_{eff} = n_{eff,co} - n_{eff,cl}^{(m)} \quad (5.2.3)$$

The first term on the right-hand side of the equation 5.2.2 is the material contribution, and is related to the change in the differential effective refractive index of the core and the cladding arising from the thermo-optic effect. This contribution is dependent upon the composition of the fiber and is strongly dependent upon the order of the cladding mode. This effect can be governed in the simulations by the thermal coefficients' modulation in the fiber core ξ_{co} and clad ξ_{cl} . The second term mainly denotes the change in grating periodicity (the so-called waveguide contribution) and can be taken into consideration in the LPFG models by defining the thermo-optic expansion coefficients of the core α_{co} and α_{cl} clad values. Nevertheless, It will be later shown that variation in α_{co} and α_{cl} for study here gratings will not affect the transmission spectrum.

The simulated LPFG transmission spectra vs temperature were obtained in two steps:

STEP 1: The temperature induced changes in the core and clad refractive indices have to be found first. The new values for refractive indices of the core $n_{co,T}$ and clad $n_{cl,T}$ corresponding with certain values of the ambient temperature T are calculated as follows:

$$n_{co,T} = n_{co,T_{REF}} + (T - T_{REF})n_{co,T_{REF}}\xi_{co} \quad (5.2.4a)$$

$$n_{cl,T} = n_{cl,T_{REF}} + (T - T_{REF})n_{cl,T_{REF}}\xi_{cl} \quad (5.2.4b)$$

where T_{REF} is a reference temperature; $n_{co,T_{REF}}$ and $n_{cl,T_{REF}}$ are refractive indices of the core and clad at T_{REF} ; ξ_{co} and ξ_{cl} are thermo-optic coefficients for the core and clad, respectively.

STEP 2: The transmission spectra in OptiGrating are simulated according to these new values for refractive indices of the core $n_{co,T}$ and clad $n_{cl,T}$ corresponding to certain values of the ambient temperature T .

The temperature distribution along the LPFG is assumed to be uniform (constant value along the distance). Three types of LPFG models are chosen in order to investigate their thermal sensitivity: LPFG with a period of 226.8 μm based on the PS1200/1500 fiber, LPFG with a period of 368.0 μm based on the PS1200/1500 and LPFG with a period of 368.0 μm based on the SM-28 fibers. The detailed description off all parameters and their variation applied to the models is given in Tab 5.2.6 and Tab. 5.2.7.

Tab. 5.2.6 Specification of the basic parameters set in the LPFG models

| | | |
|-------------------------------|--------------------------------------|---|
| Fiber parameters | r_{co} [μm] | 3.8 |
| | r_{cl} [μm] | 61.5 |
| | n_{co} [at 25°C] | 1.4494 |
| | n_{cl} [at 25°C] | 1.44403 |
| | Type of the clad glass | Pure Silica |
| Grating parameters | Length [μm] | 28800 |
| | In. Mod. | 0.00023 |
| Temperature parameters | ξ_{cl} [$1/^\circ\text{C}$] | 8.3×10^{-6} (set for fused silica glass) |
| | α_{co} [$1/^\circ\text{C}$] | 5.5×10^{-7} |
| | α_{cl} [$1/^\circ\text{C}$] | 5.5×10^{-7} |
| | Temperature distribution | Uniform |

Tab. 5.2.7 Specification of the parameters variations applied to the LPFG models

| | | |
|-------------------------------|-----------------------------------|---|
| Fiber parameters | Type of the core glass | Boron co-doped silica or Germania doped silica |
| Grating parameters | Period [μm] | 226.8 or 368.0 |
| Temperature parameters | ξ_{co} [$1/^\circ\text{C}$] | 6.5×10^{-6} , 7.0×10^{-6} , 7.5×10^{-6} , 8.6×10^{-6} |

As can be seen above, only the temperature-induced refractive indices' changes are considered here. This is justified by the fact that the period of the studied gratings is greater than $100 \mu\text{m}$. In addition, for the optical fibers studied here, the thermal-expansion coefficient ($\sim 10^{-7} [1/^\circ\text{C}]$) is much smaller than the thermo-optic coefficients which induce changes in the core and clad refractive indices ($\sim 10^{-6} [1/^\circ\text{C}]$). Consequently, the waveguide contribution in the equation (5.2.2) should not have a significant impact on the LPFGs transmission spectra.

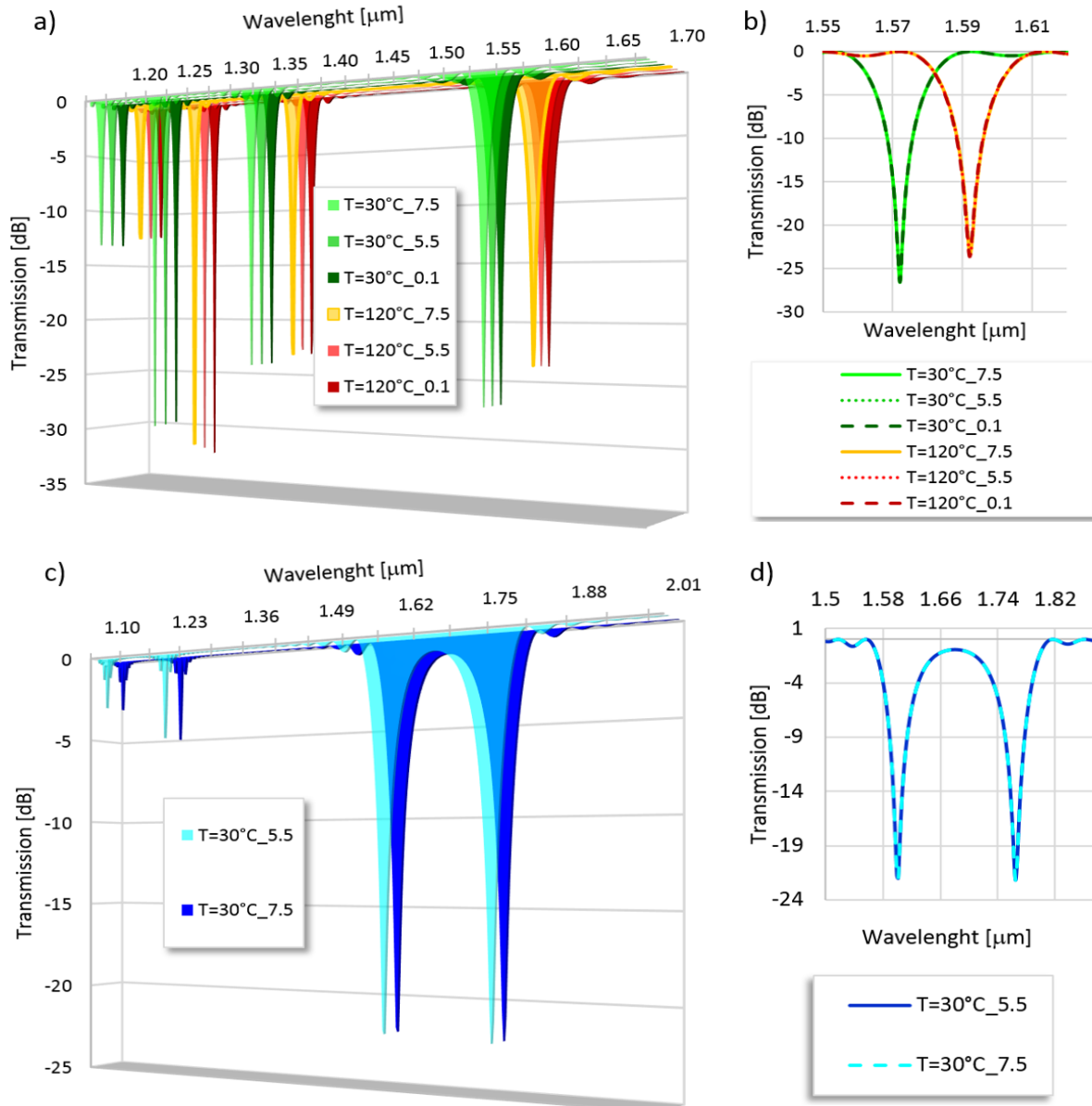


Fig. 5.2.11 Transmission spectra of the LPFG based on the SM-28 fiber with $\Lambda=368 \mu\text{m}$ (a-b) and based on the PS1200/1500 with $\Lambda=226.8 \mu\text{m}$ (c-d) vs thermal expansion coefficient α_{co} (α_{cl} is set constant equal to $5.5 \times 10^{-6} [1/^\circ\text{C}]$).

In order to confirm this statement, the LPFG transmission spectrum versus the thermo-optic expansion coefficient of the core α_{co} (the thermo-optic expansion coefficient of the clad α_{cl} is set constant equal to 5.5 [1/°C]) as calculated. It is clear from Fig. 5.2.11 that the LPFG transmission spectra simulated for different values of the α_{co} coincide with each other very well.

An important consideration is the level of the ξ_{co} and ξ_{cl} values when the LPFG thermal sensitivity is analysed. More specifically, the temperature sensitivity of a LPFG mainly comes from the difference between the thermally induced changes in the core and clad refractive indices, Δn_{co-cl} . In Fig. 5.2.12 the Δn_{co-cl} versus temperature is calculated for four different ξ_{co} values:

- Scenario 1: $\xi_{co} = 6.5 \times 10^{-6}$ [1/°C]
- Scenario 2: $\xi_{co} = 7.0 \times 10^{-6}$ [1/°C]
- Scenario 3: $\xi_{co} = 7.5 \times 10^{-6}$ [1/°C]
- Scenario 4: $\xi_{co} = 9.0 \times 10^{-6}$ [1/°C]

The value of the ξ_{cl} is set for fused silica glass in all simulations, equal to be of 8.3×10^{-6} [1/°C]. One can therefore state that the Δn_{co-cl} thermal characteristics will allow the prediction of the polarity and magnitude of the resonant wavelength shift induced by the temperature.

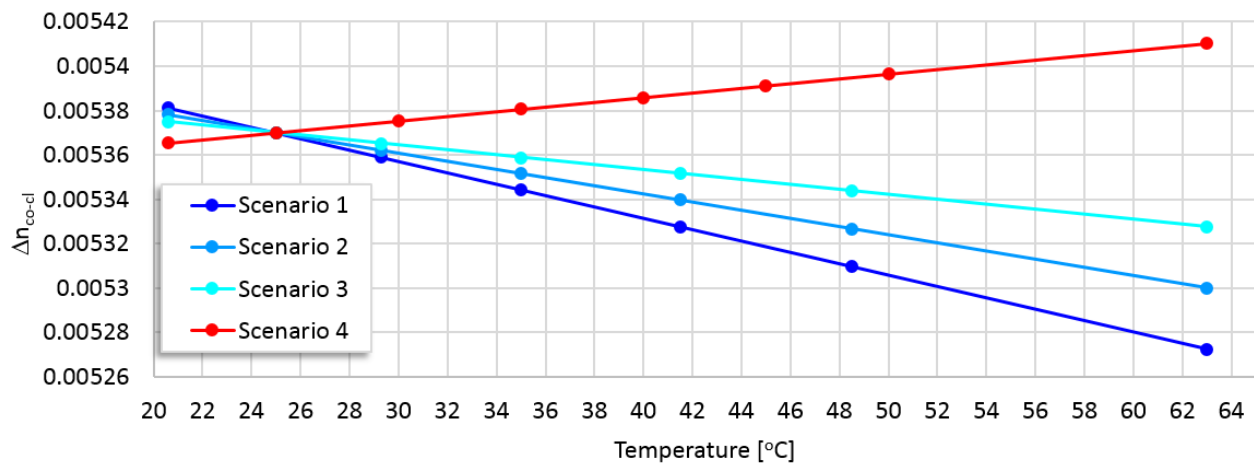


Fig. 5.2.12 The difference between the thermally induced changes in the core and clad refractive indices versus core thermo-optic coefficients.

The Δn_{co-cl} value is associated with the type of dopants in the fiber glass core which alters the temperature dependence of the refractive index. These dopants are Germanium (GeO_2), and Boron (B_2O_3). In Fig. 5.2.13 the LPFG responses versus the temperature are calculated for different host fibers: boron co-doped PS1200/1500 (Fig. 5.2.13a) and germanium doped SMF28 (Fig. 5.2.13b) for which Scenario 2 and Scenario 4 are respectively applied to the model. The period of this grating is $368 \mu\text{m}$. In addition, in Fig. 5.2.14, the thermally induced evolution of the LPFG transmission spectrum is shown where the grating period is $226.8 \mu\text{m}$ period and the host fiber is PS1200/1500 fiber.

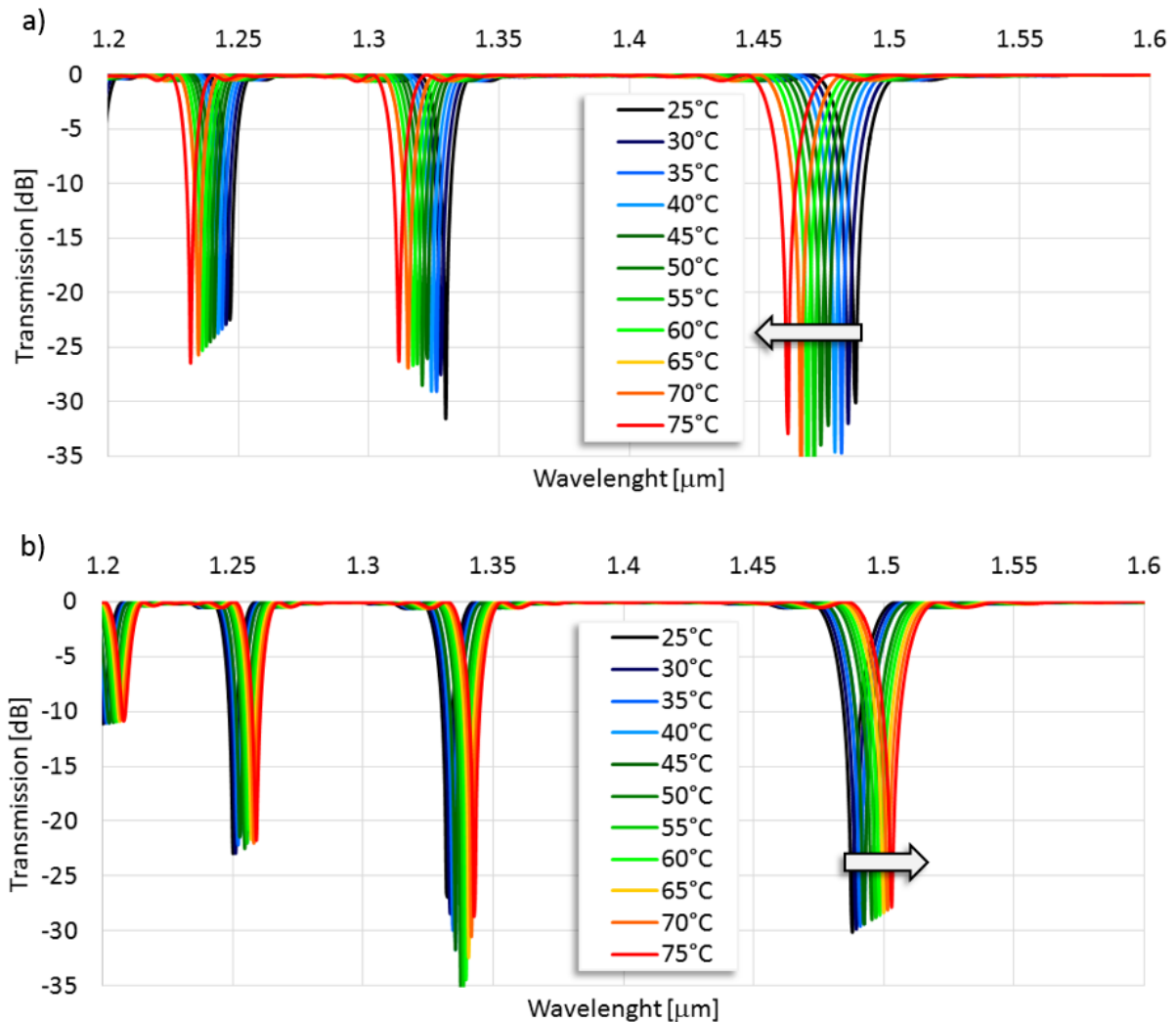


Fig. 5.2.13 Transmission spectra versus temperature obtained for the LPFG a) with $\Lambda = 368 \mu\text{m}$, based on the boron co-doped fiber calculated according with the Scenario 2 ($\xi_{co} = 7 \times 10^{-6} [1/^\circ\text{C}]$) b) with $\Lambda = 368 \mu\text{m}$, based on the germanium co-doped fiber calculated according with the Scenario 4 ($\xi_{co} = 9 \times 10^{-6} [1/^\circ\text{C}]$)

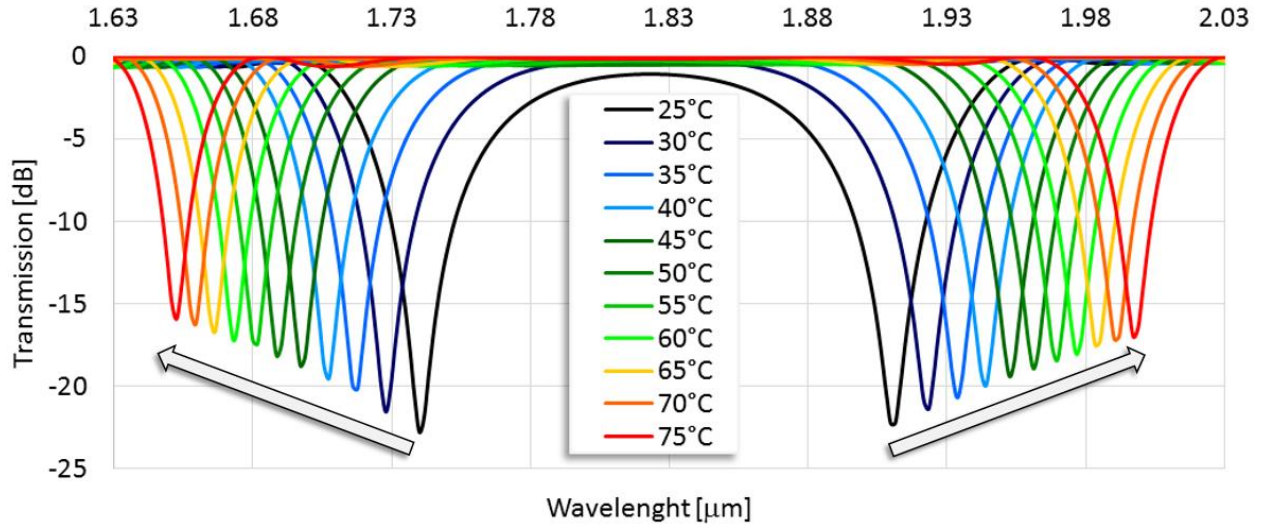


Fig. 5.2.14 Transmission spectrum versus temperature obtained for the LPFG with $\Lambda = 226.8 \mu\text{m}$, based on the boron co-doped fiber calculated according with the Scenario 2 ($\xi_{co} = 7 \times 10^{-6} [1/^\circ\text{C}]$)

As can be noticed from the Figures presented above, the behaviour of the thermal tuning of LPFGs:

- in terms of the material contributions (defined by the ξ_{co} and the ξ_{cl}), is in conformity with the results obtained experimentally (see Section 6.2). In other words, the LPFGs manifests:
 - a blue shift of the attenuation bands vs temperature when ξ_{co} and ξ_{cl} were set for PS1200/1500 fiber,
 - a red shift of the attenuation vs temperature when ξ_{co} and ξ_{cl} were set for SMF28 fiber.

The exact value of Δn_{co-cl} can be found by direct comparison of the results obtained in experiment and in simulation. However it has to be emphasized that it is impossible to find precise values of ξ_{co} and ξ_{cl} this way. Dopant concentration in the fiber core are frequently unknown or unspecified. The ξ_{cl} value is just a guess from the range of values reported in the literature for silica glass (according with [111-118] it can vary form $7.8 \times 10^{-6} [1/^\circ\text{C}]$ to $1.45 \times 10^{-5} [1/^\circ\text{C}]$). Nevertheless the thermal sensitivity can be successfully modeled with the method described above, providing adequate correspondence between experimental and theoretical LPFG transmission spectra.

5.3. LC-LPFG transmission properties analysis

Here, the LPFG designs based on four and five-layer geometries (presented in Fig. 5.1.1) are investigated, where the layer on the bare grating is the LC. As has been proven through the experimental work (presented in the Section 6.4 and Section 6.5), the application of such a LC layer on a bare LPFG permits the improvement of the sensitivity in a significant way.

As a matter of fact, the presence of a thin LC layer induces strong changes in the cladding modes' distribution, leading to a lowering of the modes bounding factor. Due to the refractive-reflective regime at the cladding-overlay interface, the cladding modes in a LC coated LPFG are bound within the structure comprising the core, the cladding and the LC layer. This means that a relevant part of the optical power carried by the cladding modes is localised within the LC layer. The field enhancement in the LC layer depends strongly on the features, like refractive index and thickness of the LC layer. The aim of the work presented in this Section is to select suitable values of these parameters, in order to increase the sensitivity of the LC-LPFGs for a specific application. In addition, a valuable advantage of the LC-LPFGs is that the properties of the LC layer can be adjusted not only by modifying the parameters like thickness or refractive index, but also by variable temperature and/or electric field. The theoretical analysis of these effects is also presented below.

5.3.1 Impact of the LC layer thickness to the LC-LPFG transmission properties

In order to study the effect of the LC layer thickness, two grating periods are defined, namely 226.8 μm and 350.0 μm , (the remaining parameters for these LC-LPFG models are presented in Tab. 5.3.1). The fiber parameters chosen for the construction of the LC-LPFG models are also shown in Tab. 5.3.1. The dispersion properties of the fiber are stated for the PS1200/1500 fiber. The 5CB LC used in the experimental work is investigated here. Its dispersion properties are included according with the Cauchy model. It is also anticipated that the planar orientation of the LC molecules is present on the bare LPFG. As a result, only the ordinary refractive index n_o of the 5CB LCs is concern now.

Tab. 5.3.1 Specification of the parameters chosen for the construction of the LC-LPFG models

| Grating parameters | | Fiber parameters | |
|-----------------------------|---------|----------------------------|----------|
| Λ [μm] | 226.8 | n_{co} | 1.450200 |
| | 350.0 | n_{cl} | 1.444033 |
| Δn_{co} | 0.00017 | r_{co} [μm] | 3.8 |
| L [μm] | 47900 | r_{cl} [μm] | 61.5 |

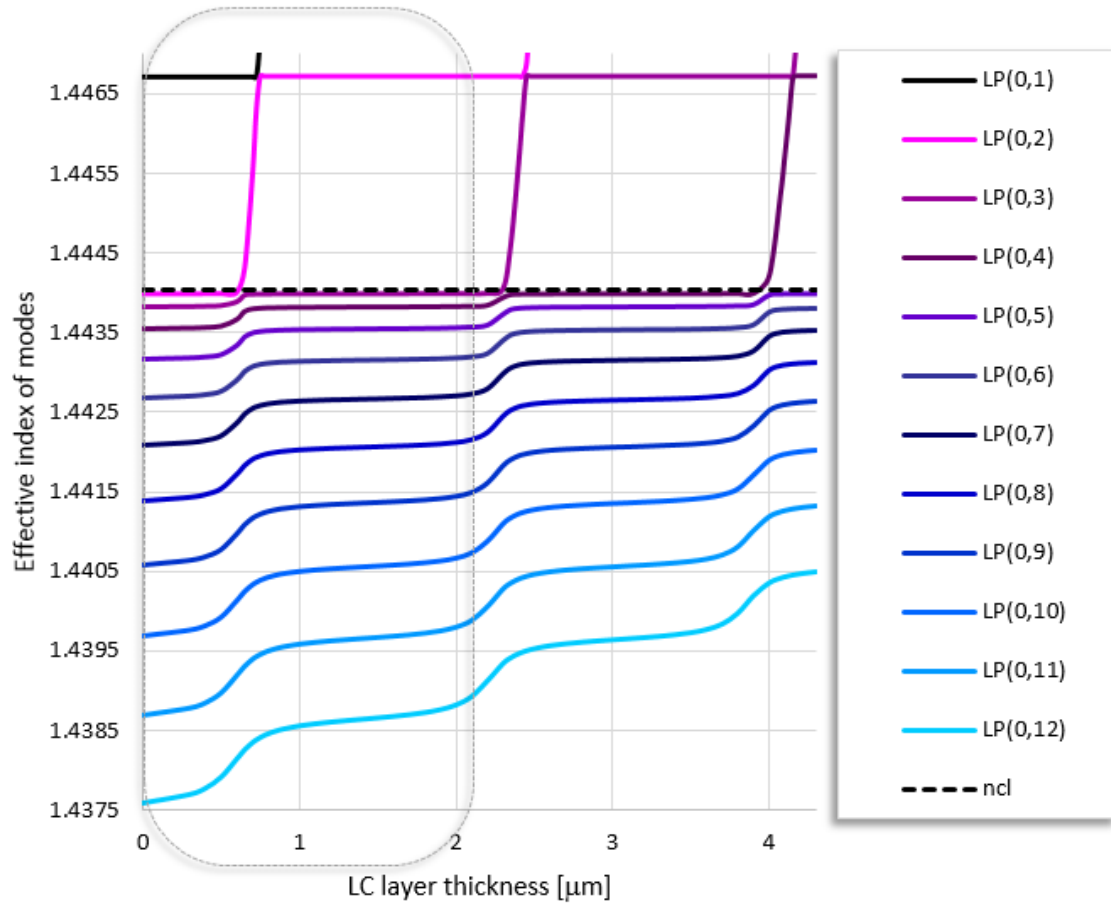


Fig. 5.3.1 Mode structure plot versus layer thickness with the fixed LC layer refractive index for n_o of the 5CB LC.

In Fig. 5.3.1, the effective index of the core mode and the first eleven cladding modes are represented as a function of the overlay thickness for a fixed wavelength of 1550 nm. This plot (referred here later as a mode structure plot) is very useful from a design perspective because it helps to identify the responsive regions of the LPFG with much less computational effort. The LC layer thickness varies from 0.0 μm to 4.3 μm . In addition, the evolution of the LC-LPFG transmission spectra is calculated for the thickness range indicated in the Fig. 5.3.1 by the gray dashed line.

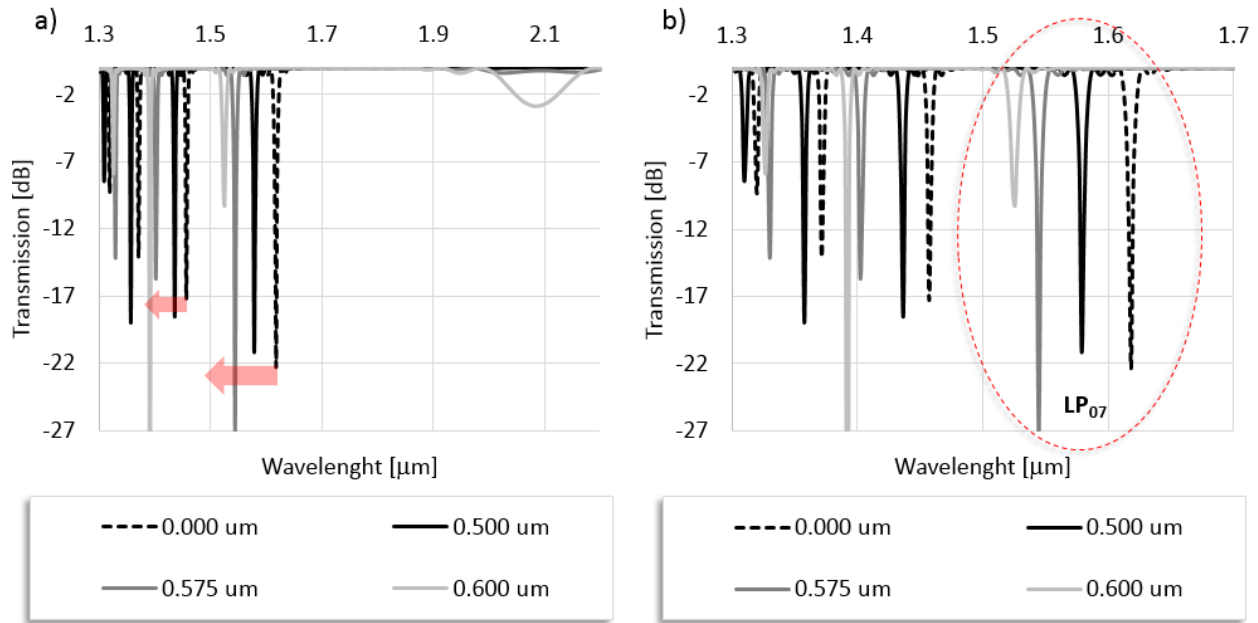


Fig. 5.3.1 Evolution of LPFG transmission spectrum versus 5CB layer thickness for the grating with $\Lambda=350 \mu\text{m}$ – before transition of the LP07 mode to the LC layer

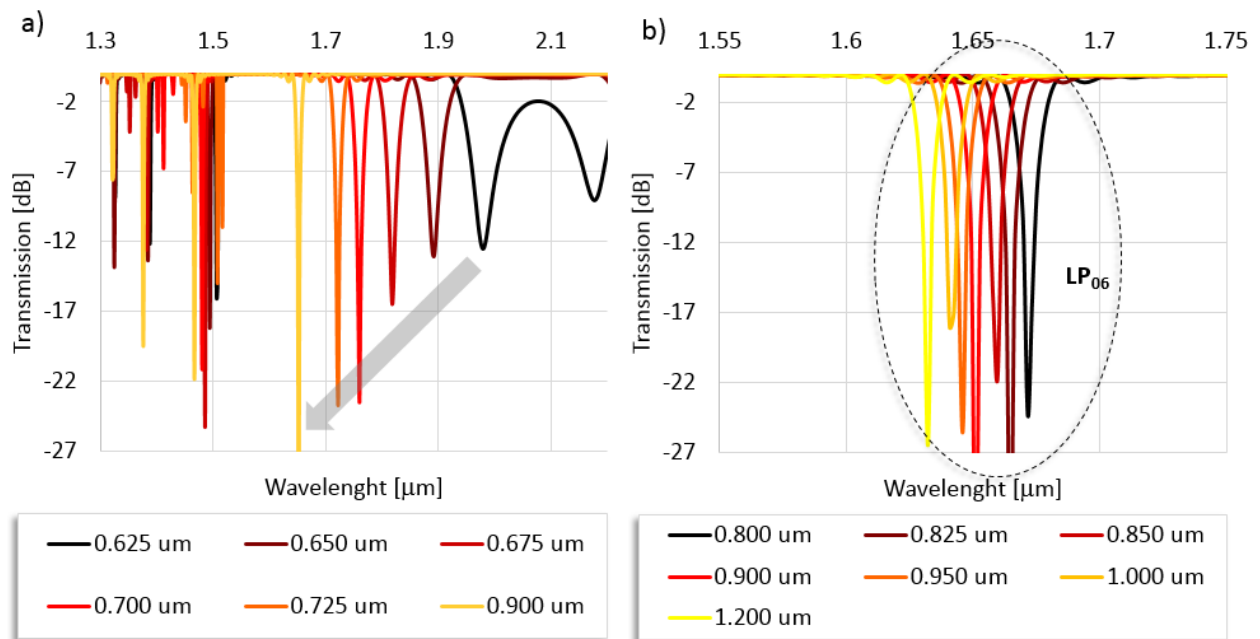


Fig. 5.3.2 Evolution of LPFG transmission spectrum versus 5CB layer thickness for the grating with $\Lambda=350 \mu\text{m}$ – after transition of the LP07 mode to the LC layer

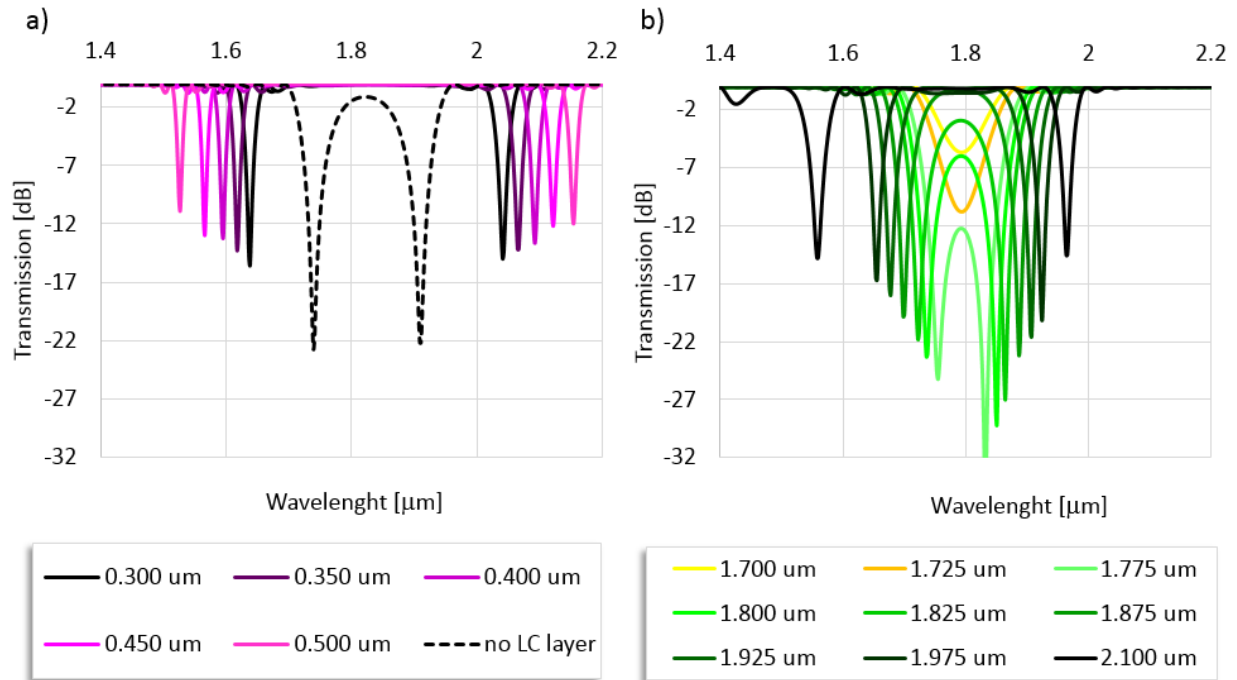


Fig. 5.3.3 Evolution of LPFG transmission spectrum versus 5CB layer thickness for the grating with $\Lambda=226.8 \mu\text{m}$

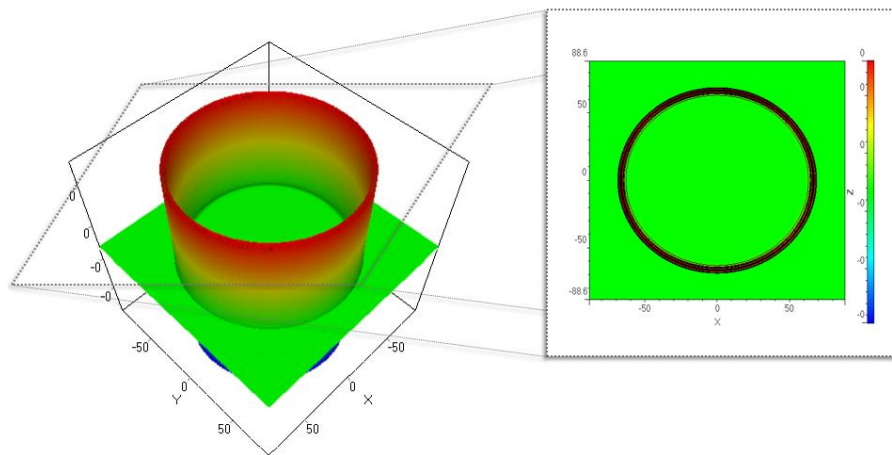
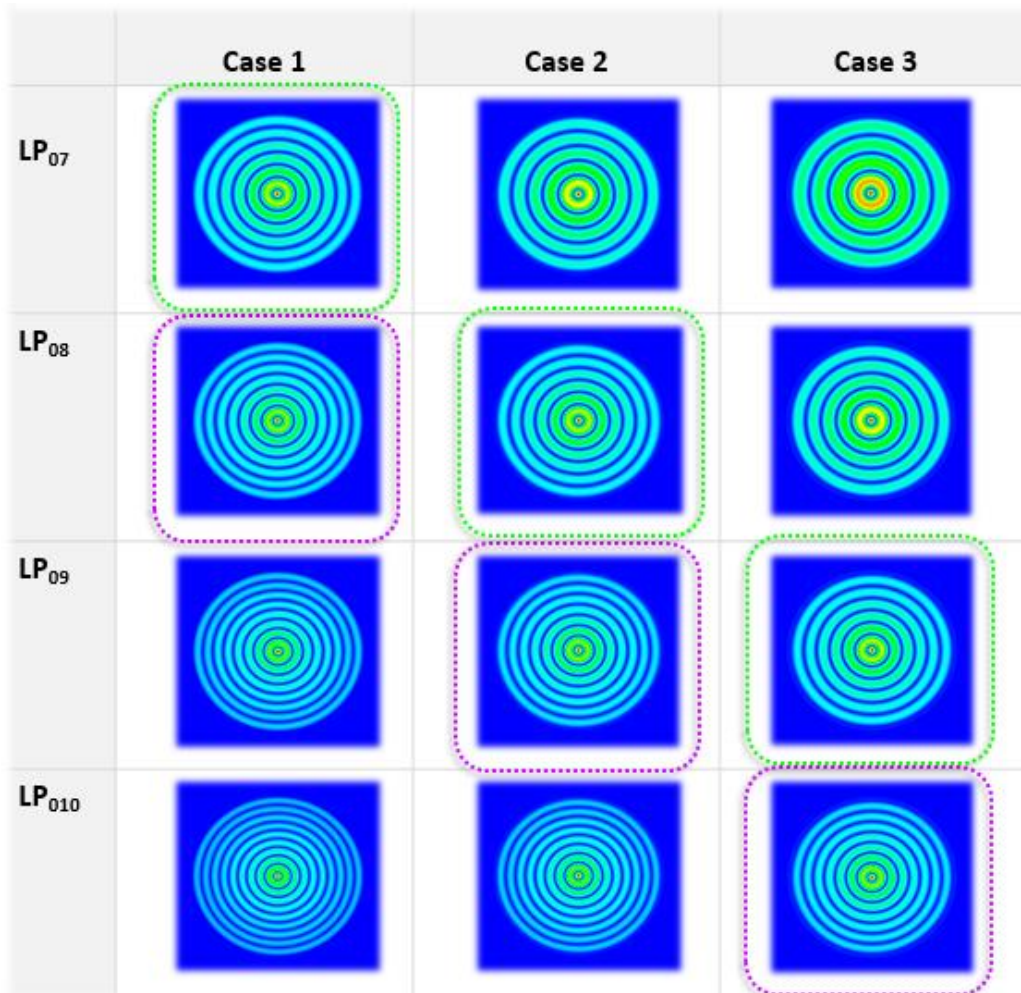


Fig. 5.3.4 Theoretical intensity profiles of LP_{02} cladding mode field calculate when is guided in the 5CB LC layer with the thickness value of $3.3 \mu\text{m}$.

As can be noticed from the performed calculation, if a LC layer of higher refractive index (like is the case for the 5CB LC) than the cladding is added to the LPFG model, as its thickness increases, the cladding modes shift their effective index to the higher values. When the LC layer is thick enough, one of the cladding modes is guided by the LC layer (the example of the intensity profiles of such a mode is shown in Fig. 5.3.4). This causes a reorganization of the effective index for the rest of modes (like it is presented in

Figs. 5.3.1 – 5.3.3). Higher order cladding modes than the one guided by the overlay, will shift their effective index value towards the effective index of the immediate lower order cladding mode. As the LC layer thickness increases, the effective index distribution before the LC layer is added to the LPFG structure, is recovered (visible e.g. in Fig. 5.3.3). This phenomenon repeats itself as the LC layer thickness becomes greater. This means that if the thickness continues to be increased, more modes are guided by the LC layer and new reorganizations of the cladding modes take place. The immediate consequence of the shift in effective index is that it leads to a displacement in the attenuation bands, as is clearly shown in Fig. 5.3.1 and Fig. 5.3.2. The attenuation band corresponding with the seventh mode shifts the wavelength to that of the sixth mode; the same is true for the fifth mode that shifts the wavelength to the attenuation band of the fourth mode, and so forth.

Tab. 5.3.2 Theoretical intensity profiles for the LP_{07} - LP_{10} cladding mode fields calculated for three different thickness values of the 5CB LC layer, which are $0.3\ \mu\text{m}$ (case 1), $1.3\ \mu\text{m}$ (case 2) and $3.3\ \mu\text{m}$ (case 3).



This phenomenon can be also represented in terms of the mode profile switching to the profile of the lower-order mode. In Tab. 5.8, the LP_{07} - LP_{10} modes field profiles are calculated. Three cases are considered: the overlay of $0.3\ \mu\text{m}$ (before transition to guidance of a LP_{02} mode into the LC layer), the overlay of $1.3\ \mu\text{m}$ (after transition to guidance of a LP_{02} mode into the LC layer) and the overlay of $3.3\ \mu\text{m}$ (after transition to guidance of a LP_{02} and LP_{03} modes into the LC layer). As is visible, the field profile for the $LP_{0,10}$ mode from the case 3 corresponds to the field profiles of the $LP_{0,9}$ from the case 2 and $LP_{0,8}$ from the case 1. The field profile for the $LP_{0,9}$ mode from the case 3 corresponds to the field of the $LP_{0,8}$ from the case 2 and the $LP_{0,7}$ from the case 1, and so forth.

It seems therefore that by selecting an adequate thickness of the LC layer, the sensitivity of the cladding modes can increase dramatically. The same is true for the resonance wavelength values observed in the LC-LPFG transmission spectrum. The shift of the attenuation bands will be at its maximum when the effective index of the mode is half way between its original effective index and the original effective index of the next lower cladding mode before covering the grating with LC. As a result, it can be inferred that there is an optimum value of the LC layer thickness, corresponding to the successive reorganization of the cladding modes. The optimal value of the LC layer thickness is also associated with the order of the cladding mode. The transitions of higher order modes start at lower LC layer thickness values than those of the lower order modes. Clearly, it is not possible to obtain an optimal thickness value for each mode at the same time. Nevertheless, even if the optimal LC layer thickness is not perfectly fixed for a cladding mode, there is an appreciable range of values that still permits to achieve high sensitivities, e.g. as a function of the external electric field. This fact will also be proved in the next Section.

5.3.2 Impact of the LC layer refractive index on the LC-LPFG transmission properties

In order to examine the variation of the LC layer refractive index these same fiber parameters are set for the construction of the LC-LPFG models like in those presented in the Tab. 5.3.1. The variation of the LC refractive index is studied from 1.430 to 1.720 which is assumed to match the maximum range of the LC refractive indices values used in the experimental work (its specification is presented in Tab. 6.1.2). The dispersion properties are set for the 5CB LC, therefore this setting will introduce the deviation in the results from the situation when other LCs are concerned. Nevertheless, this assumption should be adequate for the general description of the impact of the LC layer refractive index variation on the LC-LPFGs transmission properties and should provide qualitatively valid outcomes.

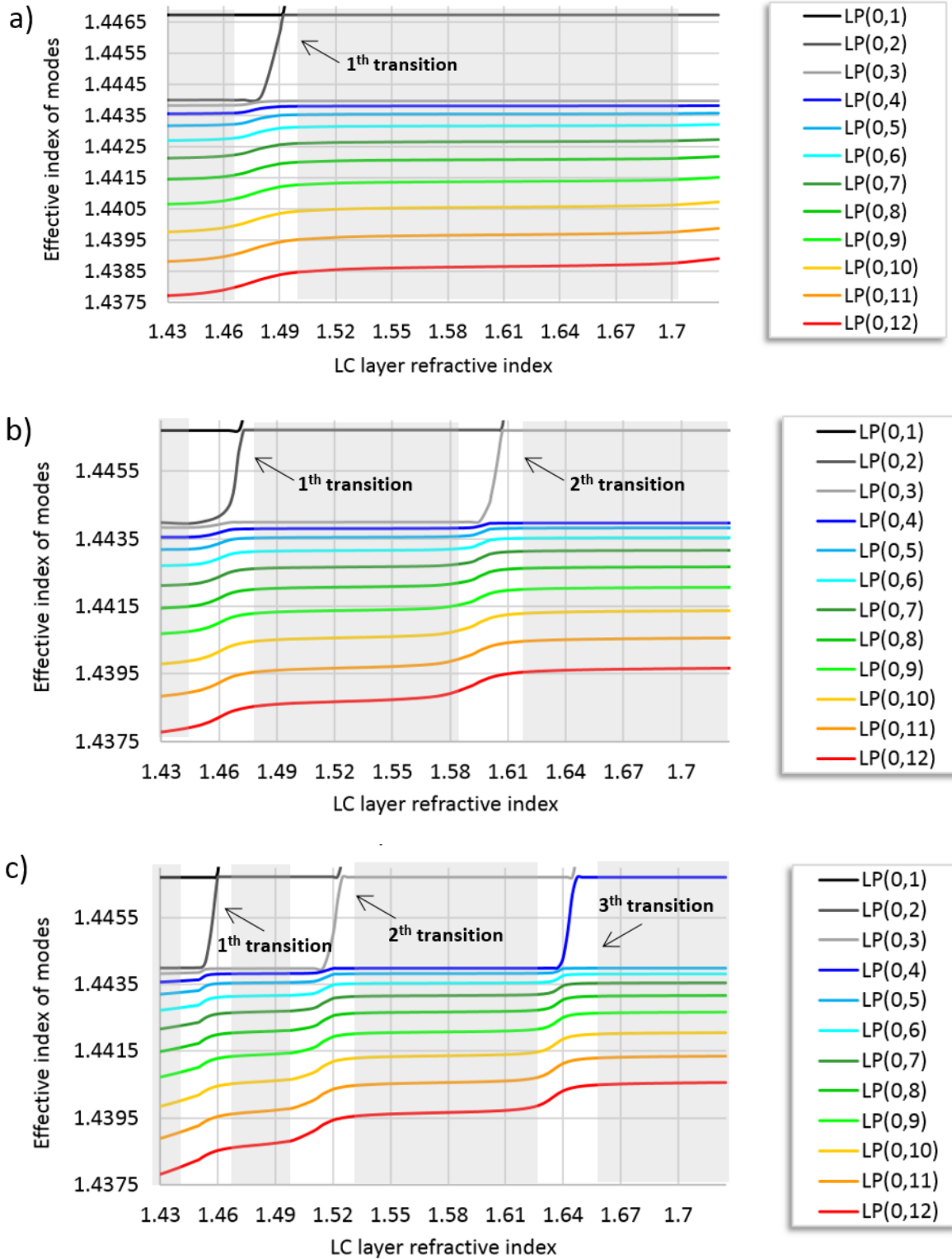


Fig.5.3.5 Mode structure plot versus LC layer refractive index for the thickness layer fixed to be 1.0 μm (a), 1.5 μm (b) and 2.3 μm (c).

Tab. 5.3.3 Values of the LC layer refractive index where the transition of cladding modes takes place, as estimated for the LP₀₇ mode.

| No. of the cladding modes transition | LC layer thickness | | |
|--------------------------------------|--------------------|-------------------|-------------------|
| | 1.0 μm | 1.5 μm | 2.3 μm |
| 1 | 1.495 | 1.474 | 1.459 |
| 2 | - | 1.608 | 1.525 |
| 3 | - | - | 1.646 |

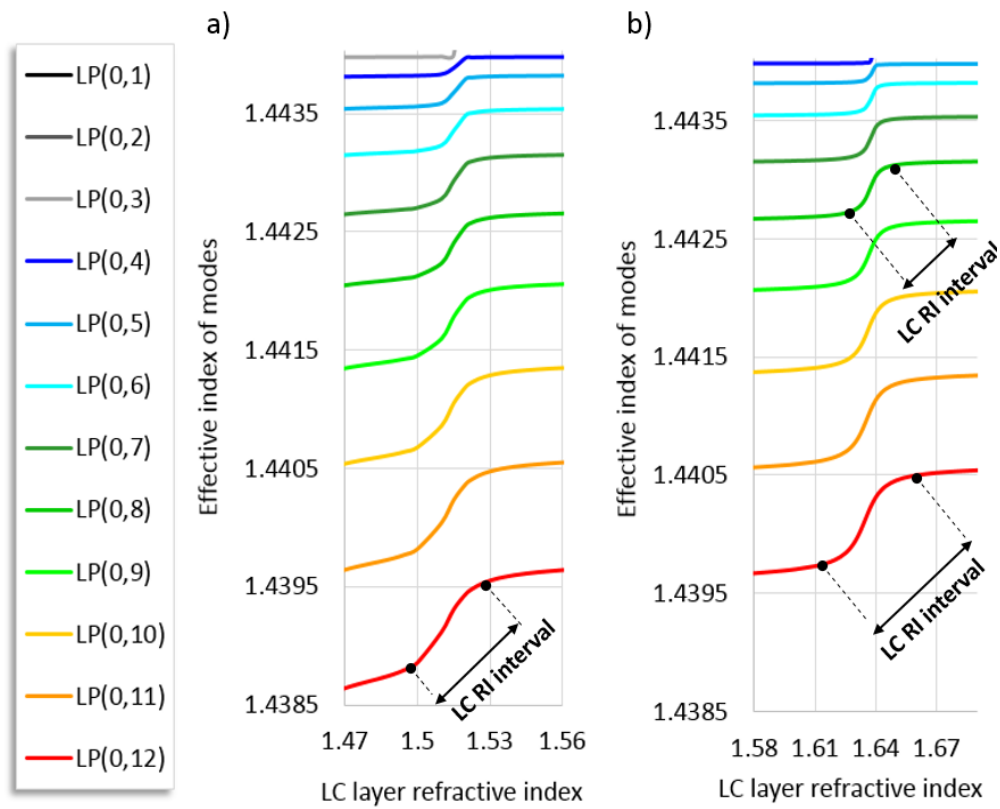


Fig. 5.3.6 Mode structure plot versus LC layer refractive index ranges where the 2nd (a) and 3rd (b) transition occur. The LC layer thickness is fixed to be 2.3 μm .

In Fig. 5.3.5 the mode structure plot versus refractive index is calculated when the thickness is fixed to be of 1.0 μm , 1.5 μm and 2.3 μm . The following remarks can be drawn from the study conducted above:

- With a higher value of the LC layer thickness, the number of cladding modes transitions increases with the variation of the LC refractive index, reflecting simultaneously the increasing number of modes that can be guided in the LC layer. (see Fig. 5.3.5 Tab.5.3.3).
- It appears that the LC refractive index interval of the transition increases with the mode order and the number of the transition (see Fig. 5.3.6).
- The transitions of higher order modes start at a lower LC refractive index than those of the lower order modes (see Fig. 5.3.6).
- The guiding starts faster if the LC layer refractive index is higher (see Tab. 5.3.3). Consequently, the transition to guidance of a cladding mode into the LC layer is faster. This implies a higher variation of the effective index of the cladding modes as a function of external perturbation, and a higher shift in the attenuation bands.

These trends clearly manifest that the thickness interval in which the transition will take place depends strongly on the LC layer refractive index. As was mentioned in the previous Section, an optimal value of the LC layer thickness exists. However, even if the LC thickness is not fixed perfectly, e.g. just by using different LCs as a grating layer, its value can be compensated. In addition, the transition region where the LC-LPPG demonstrates the highest sensitivity can be dynamically tuned by an external perturbation. e.g. by temperature or/and external electric field. From the calculations presented above, it can also be deduced that in order to be able to measure the attenuation bands associated with the modes within:

- the 1th transition the LB LC mixtures are well suited,
- the 2th and the 3th transitions the MB LCs are a wise chosen.

5.3.4 The temperature effect to the LC-LPPG transmission properties

In this section a unique feature of the LC layer, namely its thermal sensitivity is analyzed in the context of its impact on the LC-LPPG sensing properties. Two types of LCs are studied here in order to provide a general idea how the LC-LPPGs thermal sensing capabilities can be designed. These LCs are MB 5CB and

LB 1550 (described in detail in the Section 6.1.1). In all simulations the LC molecule's planar orientation on the bare grating is assumed, therefore only the n_o thermal characteristics is considered. The Grating and fiber parameters chosen for the construction of the LC-LPFG models are shown in Tab. 5.3.1.

Regarding the LC-LPFG sensitivity to the temperature, there are many factors that influence this value. Nevertheless, three of them are critical in order to optimize the LC-LPFG thermal sensing properties as may be required for specific applications. This factors are:

1. Host fiber

As was presented in the Section 5.2.2 the thermal responses of the LPFGs based on the boron co-doped PS1200/1500 fiber and germanium doped SMF28 fiber are opposite. This rule is no longer valid after adding the LC layer to the LPFG structure.

Tab. 5.3.4 *Specification of the models used in order to study the impact of the host fiber to the LC-LPFG thermal sensitivity*

| Type of the host fiber | PS1200/1500 | SMF28 |
|--|---|---|
| Core material dispersion properties | set for boron co-doped glass | set for germanium doped |
| Clad material dispersion properties | set for fused silica glass | |
| ξ_{co} | $6.9 \times 10^{-6} [1/^\circ\text{C}]$ | $9.0 \times 10^{-6} [1/^\circ\text{C}]$ |
| ξ_{cl} | $8.3 \times 10^{-6} [1/^\circ\text{C}]$ | |
| Grating period [μm] | 368 | |
| LC material | 5CB | |
| LC layer thickness [μm] | 2.2 | |
| Temperature range variation [$^\circ\text{C}$] | 20.3 – 27.2 (nematic phase of the 5CB LC) | |

In Fig. 5.3.7 the LC-LPFGs transmission spectra versus temperature calculated for different host fibers are shown (a detailed description of the LC-LPFGs parameters applied to the simulation is presented in the Tab. 5.3.4). As can be seen, both LC-LPFGs models show the attenuation band shift toward shorter wavelengths versus temperature. This effect can be explained by the fact that in the study, the

temperature range of the attenuation bands exhibits the blue shift with increasing RI of the LC layer, regardless of the grating host fiber type. Taking this into consideration, the 5CB LC layer added to the LPFG based on the SMF28 fiber can change the thermal sensitivity sign (according with the n_o thermal characteristics for the 5CB LC) due to the temperature induced n_o variation. The change of the thermal sensitivity sign can be also achieved for the LPFG based on the PS1200/1500 just by choosing the 1550 LC mixture as a LC layer. It is possible, since the value of n_o mainly decreases with an increasing temperature for the 1550 LC (this statement will be proved later in the following section).

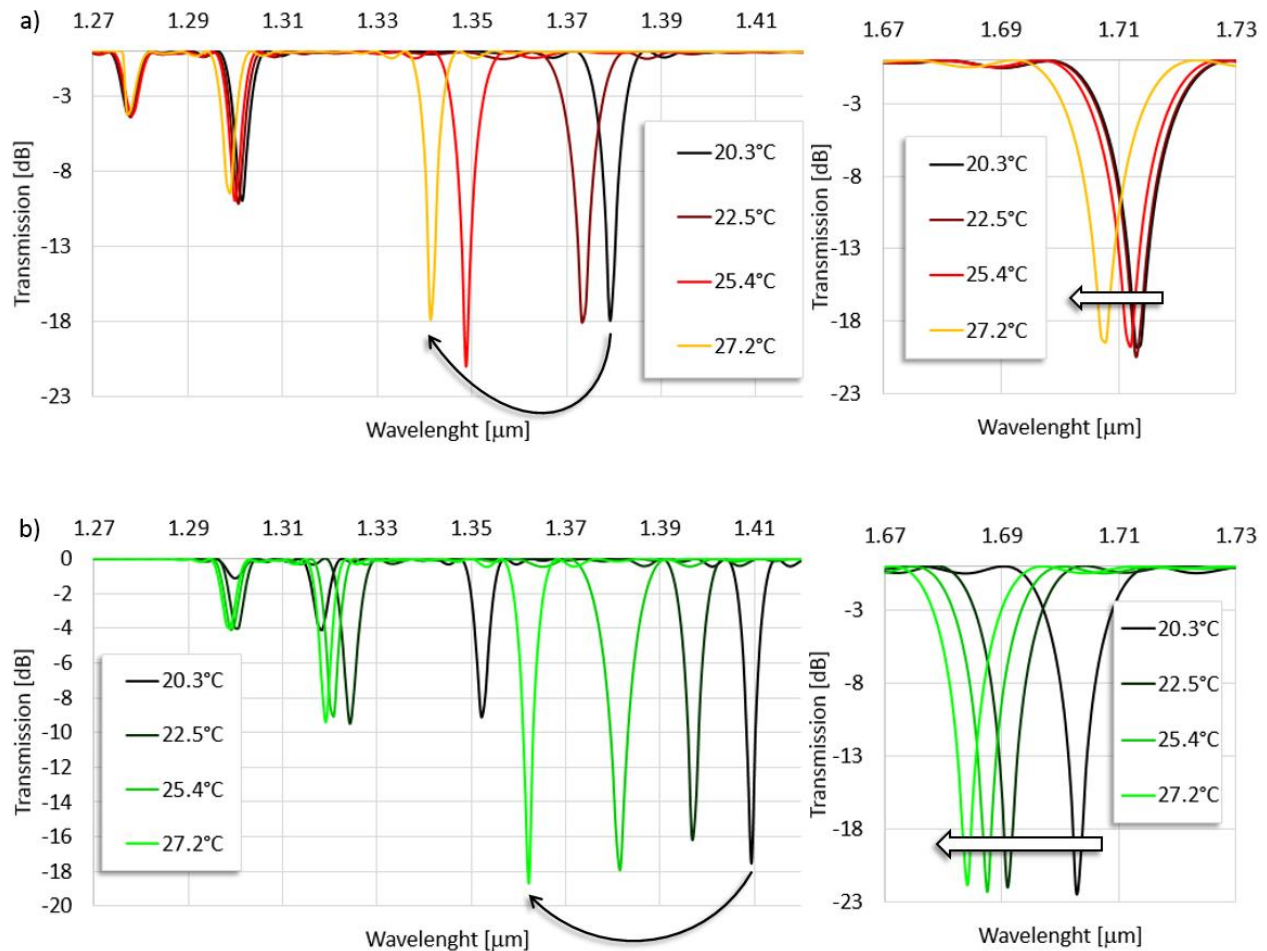


Fig. 5.3.7 Transmission spectrum of the LPFG with 5CB LC layer versus temperature calculated for the SMF28 host fiber (a) and PS1200/1500 host fiber (b).

2. LC layer thickness

The LC layer thickness will define the temperature induced LC RIs variation range where the mode transition phenomenon can take place. Consequently, by properly defining this value, the tuning of the

LC-LPFGs can be adjusted to fall in a more suitable region of the temperature variation and in terms of the thermal tuning magnitude. In Fig. 5.3.8, the LC-LPFG mode structure plot versus temperature is shown, as calculated for three different values of the 5CB LC layer thicknesses.

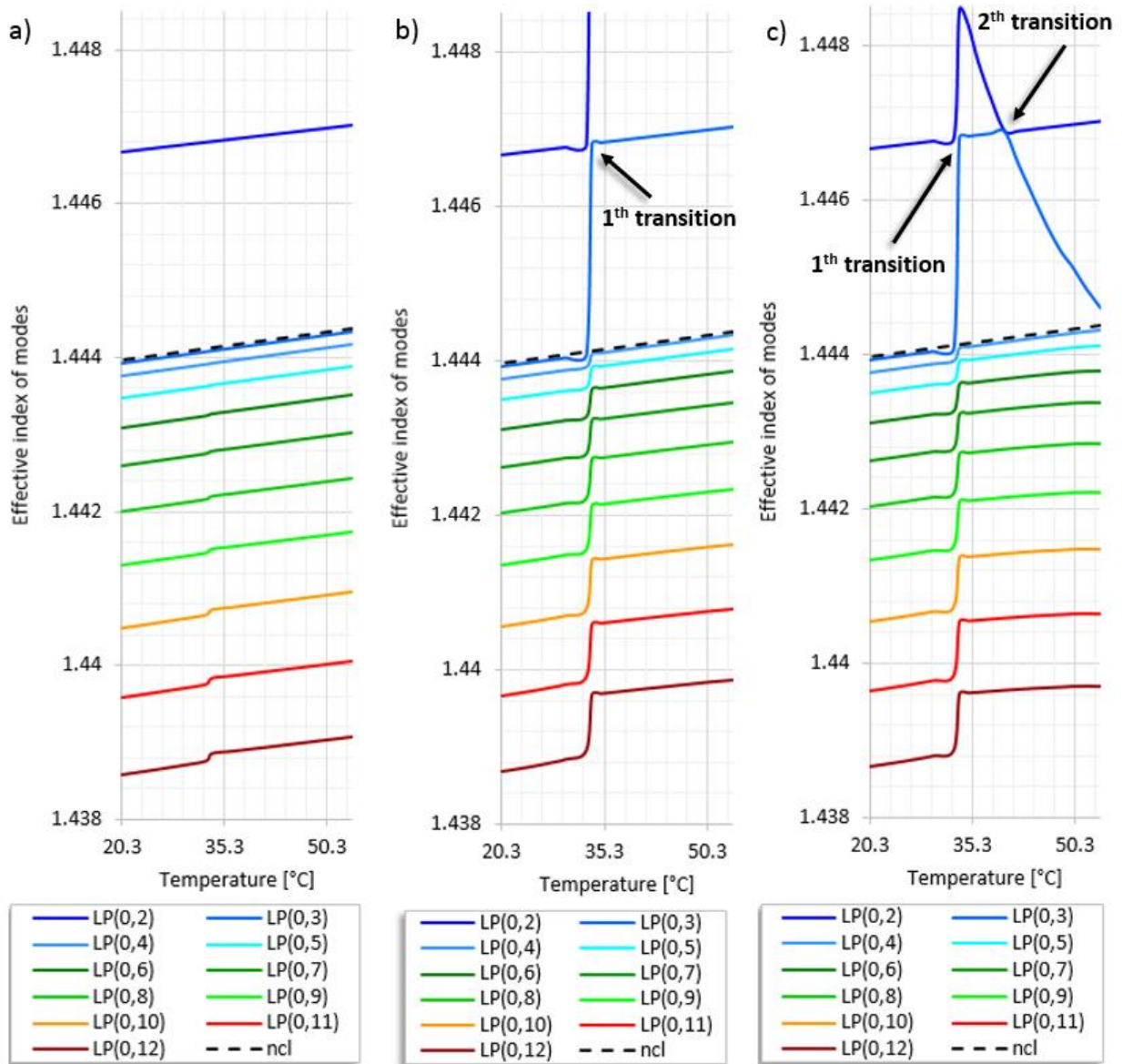


Fig. 5.3.8 Mode structure plot versus temperature for the LPFG with 5CB LC calculated for the LC layer thickness of $1.5 \mu\text{m}$ (a), $2.0 \mu\text{m}$ (b) and $1.886 \mu\text{m}$ (c).

As can be seen, for all cases of the LC layer thicknesses, the modes exhibit the highest thermal sensitivity around the temperature corresponding to the phase-transition temperature T_c of the 5CB LC. At T_c the

jump in the n_o value occurs (the Δn_o at this point is 0.0385). This feature of the LCs results in the thermal “switching” of the LC-LPFG transmission spectrum around T_c (clearly shown in Fig. 5.3.9).

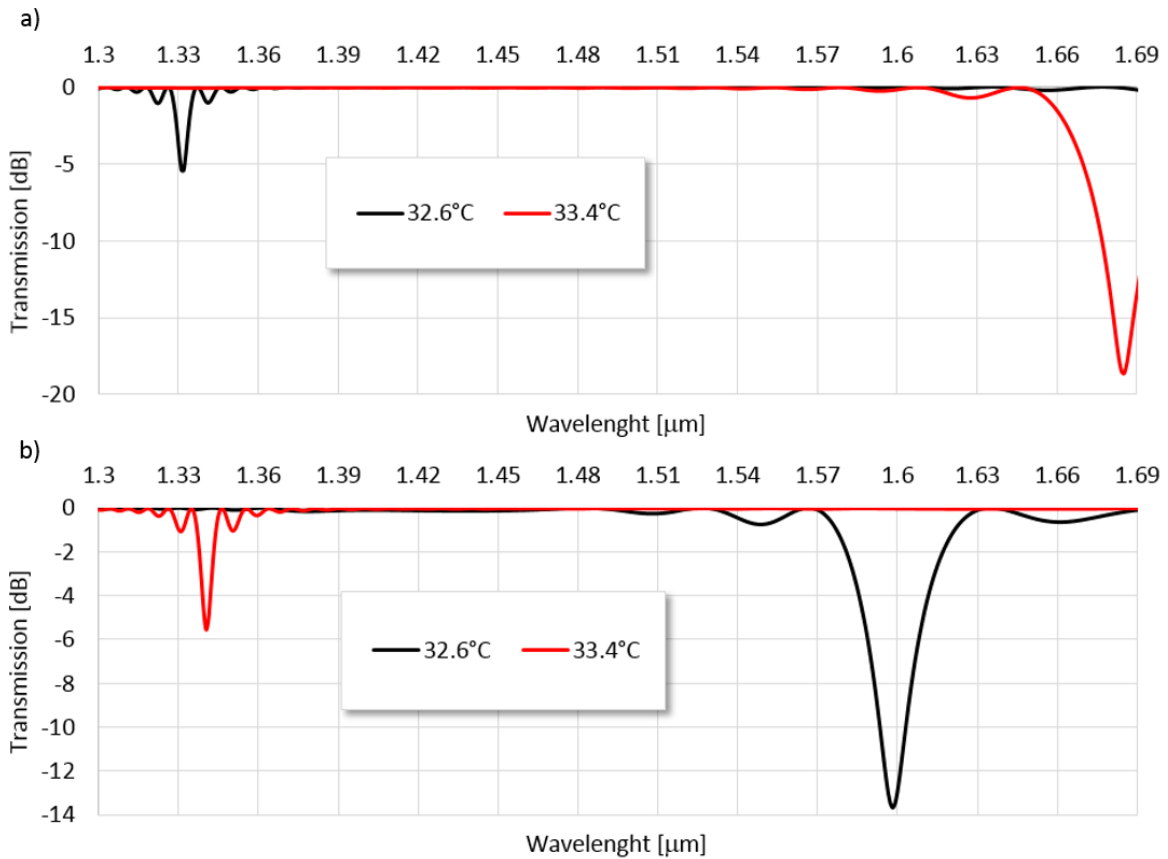


Fig. 5.3.9 Simulation of the thermal switching of the LC-LPFGs transmission spectra. The effect is modeled for the LPFG coated by the 5CB LC layer with thickness of 1.5 μm (a) and 2.0 μm (b). The grating has a period of 226.8 μm and is based on the PS1200/1500 fiber.

It can also be noticed from Fig. 5.3.8 and Fig. 5.3.9 that for the LC layer with:

- 1.5 μm thickness, the efficiency of the thermal tuning cladding modes is the smallest (Fig. 5.3.8a). In this case there are no transitions to the LC layer of any cladding mode. Nevertheless, even in this case the change in the cladding modes is visible around T_c and still can provide fast thermal switching of the LC-LPFG transmission spectrum (see Fig.5.3.9a).
- 2.0 μm thickness at T_c , the second cladding mode LP_{02} transition into an overlay mode occurs while all the other subsequent cladding modes have their modal RI value transitioning toward the next lower order cladding mode (Fig. 5.3.8b). Consequently, the example of the LC-LPFG presented here has wider range of thermal tuning around T_c by selecting a thicker LC layer thickness. In addition, thicker the LC

layer on the LPFG locate the attenuation band of interest into a more suitable region of the LC-LPFG transmission spectrum (Fig. 5.3.9b).

- 1.886 μm thickness at T_c , similar to the layer with a 2.0 μm thickness, the transition of the LP_{02} cladding mode occurs (Fig.5.3.8c). In addition, for 1.886 μm layer thickness, the second reorganization in the cladding modes can be observed with the further temperature increase. Around 40°C, the LP_{02} mode starts to “move” being guided in the fiber cladding structure, providing again a supplementary range of the LC-LPFG increased sensitivity to the higher temperature values. Nevertheless, the LC-LPFG thermal tuning will be less dynamic in this case. This can be explained by the fact that the n_o for the 5CB LC continuously increases with an increasing temperature in contrast to the fast jump in its value at T_c .

3. LC thermal characteristics

The LC thermal characteristics will define fundamental thermal sensing properties of the LC-LPFG like e.g. direction of the attenuation shift versus temperature, or temperature where the fast thermal switching of the attenuation band can be achieved. In Fig. 5.3.10 the LC-LPFG transmission spectra versus the temperature are presented. The LC layer parameters are set to the 1550 LB LC .All the remaining parameters set in this simulation are shown in Tab. 5.3.5. Taking advantage from the unique properties of this LC material it will be demonstrated that the LC-LPFG thermal tuning ability can be designed in a very wide range.

Tab. 5.3.5 *Specification of the models used in order to study the impact of the LC thermal characteristics on the LC-LPFG thermal sensitivity*

| | |
|--|---|
| Type of the host fiber | PS1200/1500 |
| Core material dispersion properties | set for boron co-doped glass |
| Clad material dispersion properties | set for fused silica glass |
| ξ_{co} | $6.9 \times 10^{-6} [1/^\circ\text{C}]$ |
| ξ_{cl} | $8.3 \times 10^{-6} [1/^\circ\text{C}]$ |
| Grating period [μm] | 226.8 |
| LC material | 1550 |
| LC layer thickness [μm] | 2.0 |

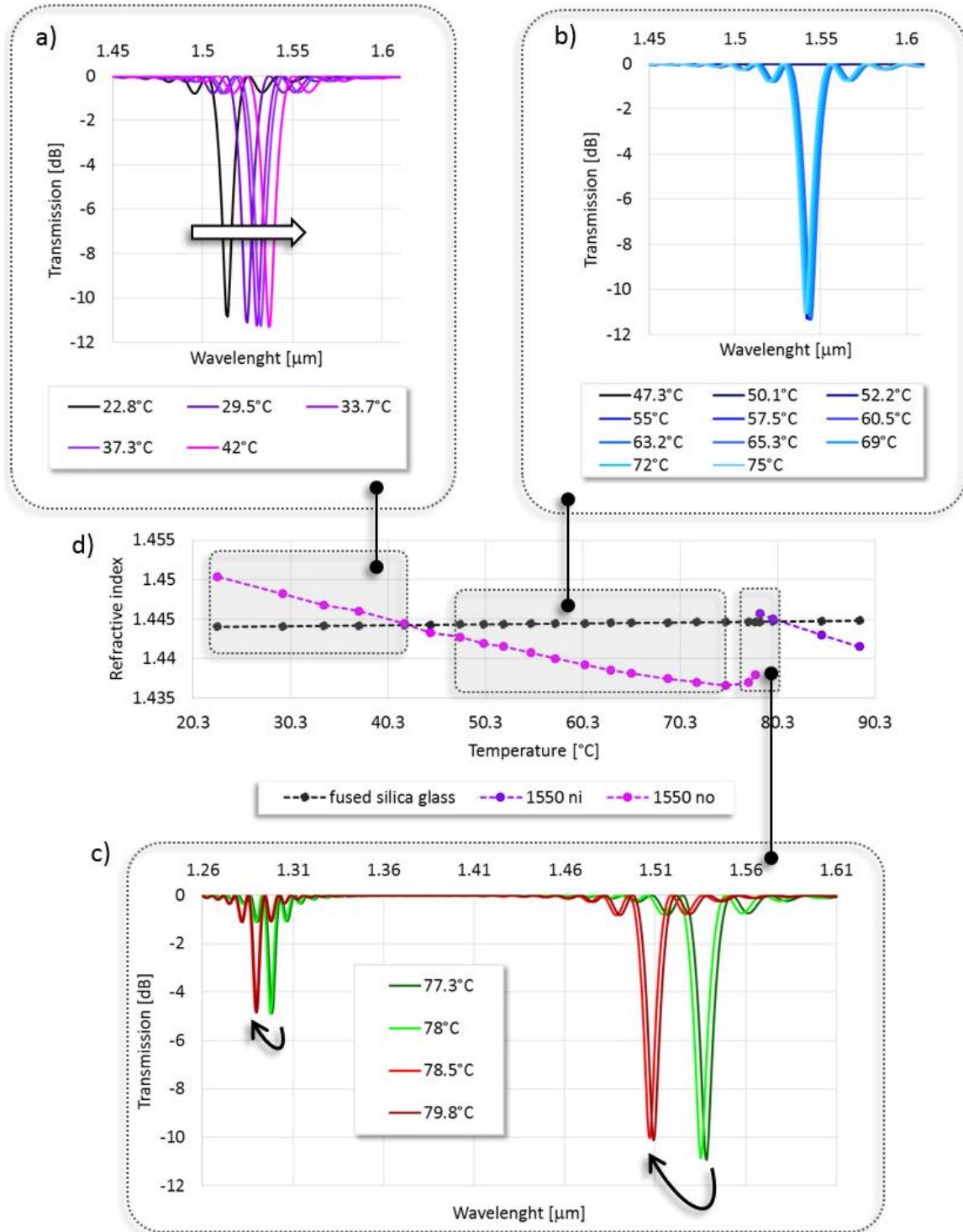


Fig. 5.3.10 The transmission spectra versus temperature of the LC-LPFG coated with 1550 LC layer (a-b). The LPFG studied here had a period of $226.8 \mu\text{m}$. Parameters of the host fiber are adjusted to the PS1200/1500 fiber. The thickness of the LC layer was assumed to be of nm. In (d) the n_o thermal characteristics for the 1550 LC is shown.

Through careful examination of the results presented above, the following conclusions can be made:

- The slope of the n_o thermal characteristic can change the direction of the attenuation band shift previously associated with the type of the host fiber, as was already shown in the example presented in the simulations of the LPFG based on the SMF28 fiber coated by the MB 5CB LC layer (Fig. 5.3.7). Here the change of the thermal characteristic sign can be observed for the LPFG based on the PS1200/1500 fiber and functionalized with an additional layer of LB LC 1550 (Fig. 5.3.10a). This effect takes place in the temperature range from 22.8°C to 42°C where the n_o value decreases with temperature and still is higher than n_{cl} .
- Since the opposite shift of the attenuation bands versus temperature can be observed for the LPFG in air and with the LC layer, it can be predicted that the temperature compensation effect should be also possible to obtain by a proper LC-LPFG design. In Fig. 5.3.10b it is clearly visible that the attenuation band seems to be almost unaffected by the temperature changes in the range from 47.3°C to 75°C (note that in these temperatures $n_o < n_{cl}$). This effect can be explained by the fact that, for this attenuation band, the impact of the temperature itself (LPFG based on PS1200/1500 exhibits shifts towards lower wavelengths with temperature) and LC layer's presence (decreasing n_o with temperature cause shifts towards higher wavelengths) on the LPFG properties are almost cancelled out. These theoretical results will be also experimentally proved in Section 6.3 for the LPFG coated with the LB LC 1800.
- In Fig. 5.3.10c (corresponding with T_c for the 1550 LC) the thermal switching of the attenuation bands spectral position takes place around a temperature of 78°C, where the fast change in the n_o value occurs (the Δn_o at this point is 0.0078). This same effect was shown for the LPFG with 5CB LC layer (Fig. 5.3.9) but at temperature of 33°C.

The above theoretical analysis shows that, thanks to the presence of a properly chosen LC layer, the thermal response of the grating can be adjusted over a very wide temperature sensitivity range: starting from a significant increase of the LC-LPFG thermal sensitivity down to its compensation. Simultaneously, the LC-LPFG provides a possibility for fast switching of its spectral characteristics in specific temperature ranges. The experimental work which proved the above statement is presented in Section 6.3.3.

5.3.5 Analysis of the LPFG placed in a capillary filled with an LC

When the LPFG is placed inside a glass capillary filled with the LC is analyzed, the five-layer geometry has to be employed to achieve an accurate simulation. Since the refractive index of the middle LC layer is studied here over the interval 1.4-1.6, only the two cases need to be considered:

Case 1: If the LC layer has a refractive index smaller than that of the cladding it would act as a barrier, separating the cladding from the capillary layer. This barrier will determine the magnitude of the refractive index interval needed for the transition.

Case 2: If the first LC layer has a refractive index higher than that of the cladding, it will act as a guiding structure. The glass layer will, depending on its refractive index and thickness, contribute to the guiding effect.

The five-layer geometry is chosen in order to match the experimental constraints imposed by the use of a silica glass capillary to form the LC layer on a bare grating. Therefore, the thicknesses of the LC and glass layers are defined according to the specification of the capillary used for the experimental work.

- The radius of the capillary is 134 μm , therefore the space between the inside surface of the capillary and the surface of the fiber is fixed to be of 4.5 μm .
- The outside diameter of the capillary is 195 μm , thus the glass layer thickness is set to be of 59 μm .
- The refractive index of the glass capillary is also fixed to be equal to the refractive index of the silica glass.

The refractive index of the silica glass capillary is assumed to be equal to the refractive index of clad fiber. As can be noticed, in this configuration there is a variation of one parameter left to investigate, namely the LC refractive index of the middle layer. In Fig. 5.3.12 the mode structure plot versus refractive index calculated for such a design structure is presented. In addition, the mode structure plot versus refractive index calculated for the LPFG with this same LC layer thickness, but without the outer layer of the capillary is shown in Fig. 5.3.11. This allows to determine the effect of the capillary presence in the LC-LPFG structure.

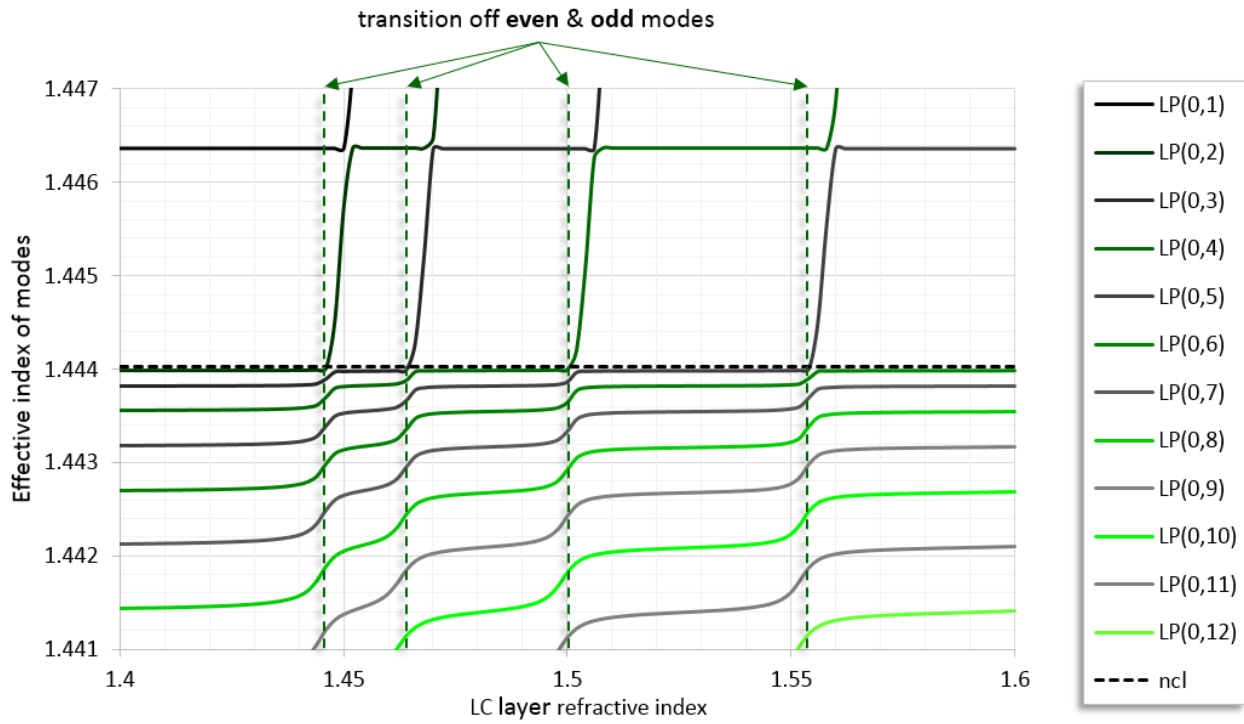


Fig.5.3.11 The mode structure plot versus refractive index calculated for the LC-LPFG with LC thickness layer of $4.5 \mu\text{m}$.

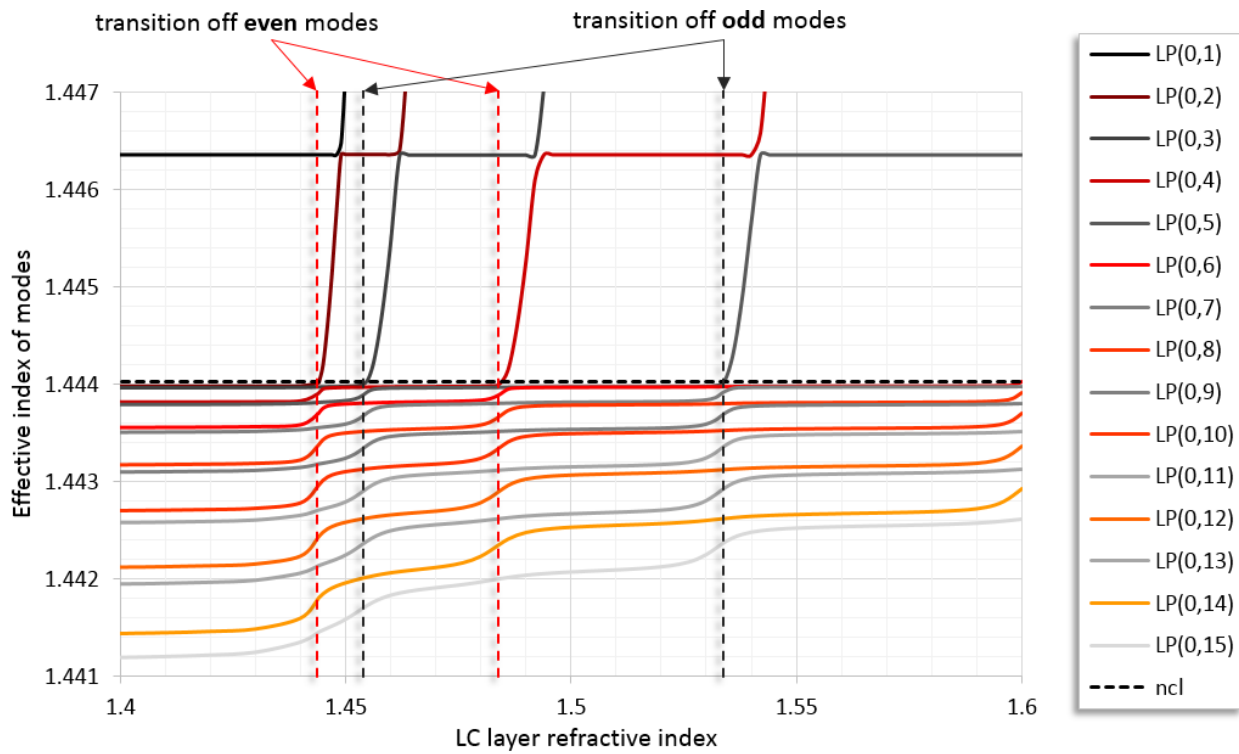


Fig.5.3.12 The mode structure plot versus refractive index calculated for the LPFG placed in the capillary filled with the LC.

From the results presented above, it can be immediately noted that the presence of the capillary fundamentally changes the modes' characteristic. Precisely, this outer layer separates them into two groups of modes with even and odd radial numbers: the transition for the modes with even and odd radial numbers occur at different moments with the LC layer refractive index variation. This effect could be explained by the fact that the capillary layer acts on the modes similarly like a fiber cladding. Since the field distribution of the modes with odd radial numbers radiate deeper into the fiber cladding, they are more affected by the presence of this additional layer. As a result, their transition is "slowed down". Comparing Fig. 5.3.11 with Fig. 5.3.12 it can be also seen that the presence of the capillary within the LC-LPFG structure causes:

- lowering the refractive index value for which the 1st transition takes place,
- increasing the effective index of modes,
- narrowing the distance between the modes (especially between the pairs of adjacent even and odd modes). This implies that more of the attenuation bands will be visible in the spectral window,
- increasing the refractive index interval over which the transition occurs. However, by following simultaneously the adjacent modes (with even and odd radial numbers) the refractive index interval is actually smaller. This implies a higher variation of the effective index of this cladding modes pair as a function of the LC layer refractive index.

These novel effects observed in this work have obvious uses for the development of new sensors. Using this approach, the sensitivity of the LC-LPFG can be increased considerably. In order to confirm this statement, the thermal response of such LC-LPFG design will be investigated now. The LB LC mixture 1110 parameters are set for a LC layer in order to meet the experimental conditions for the results presented in Sections 6.4.1 and 6.4.2). Its thermal characteristic measured at wavelength of 589 nm and estimated for the wavelength of 1550 nm (in accordance with the requirements of the simulation for which the values of the refractive index have to be given in the infrared range) are shown in Fig. 5.3.14. The parameters for the host grating were set for the UV-induced LPFG with period of 386 μm (presented in detail in Tab. 6.1.6). The simulated transmission spectra for this LC-LPFG design are presented in Fig. 5.3.13. They were calculated separately for three different temperature ranges corresponding with the nematic (Fig. 5.3.13a) and isotropic (Fig. 5.3.13c) phases of the LC and close to it clearing temperature T_c which matches to the LC phase-transition temperature (Fig. 5.3.13b).

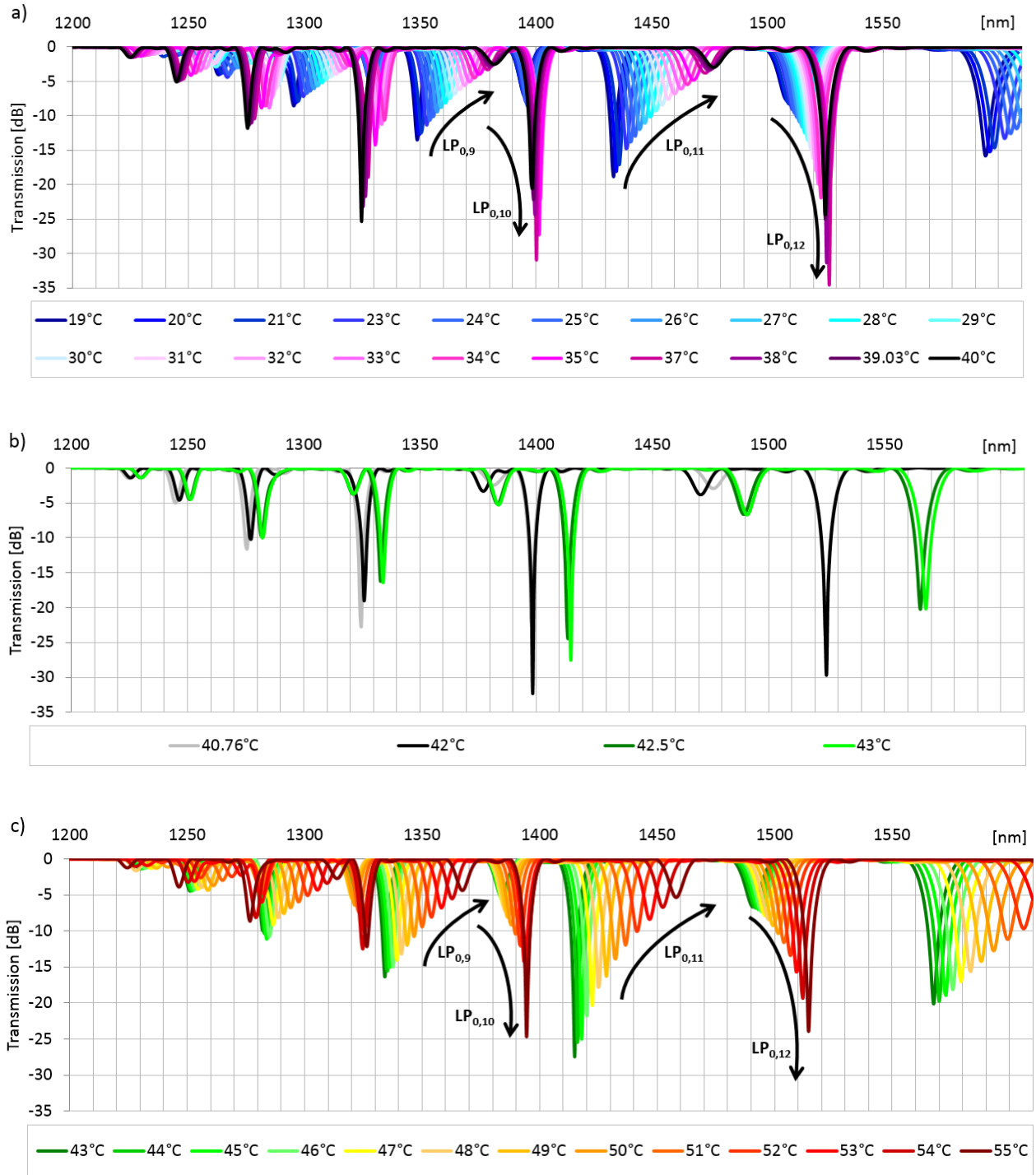


Fig.5.3.13 Simulated thermal response for the UV-Induce LPPG (grating period 368 μm ; based on the PS1250/1500 fiber) placed in the capillary filled with 1110 LB LC.

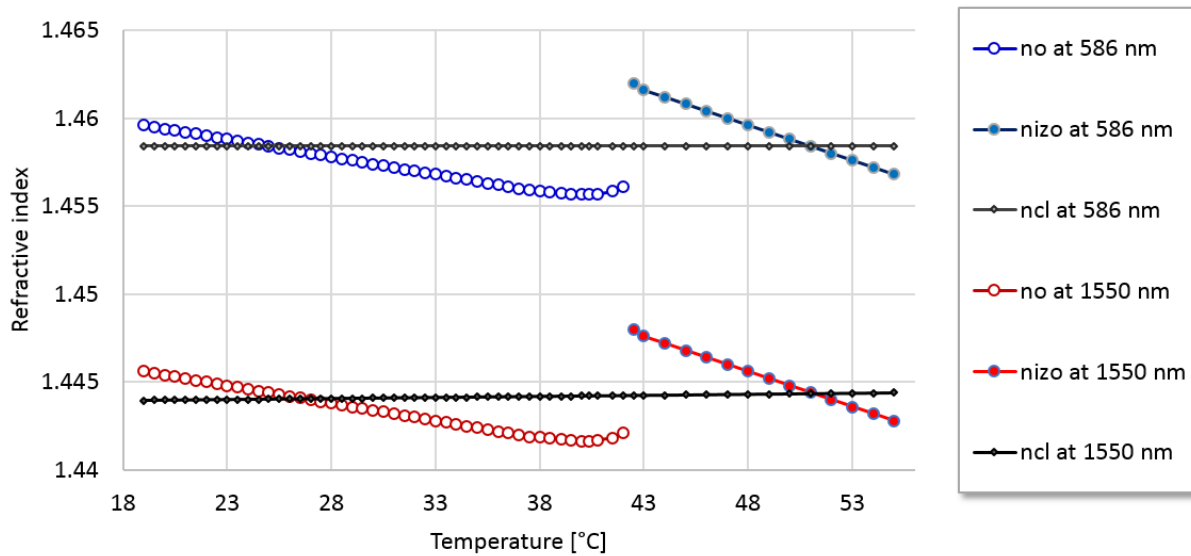


Fig. 5.3.14 The 1110 LC thermal characteristic measured at wavelength of 589 nm and estimated for the wavelength of 1550 nm.

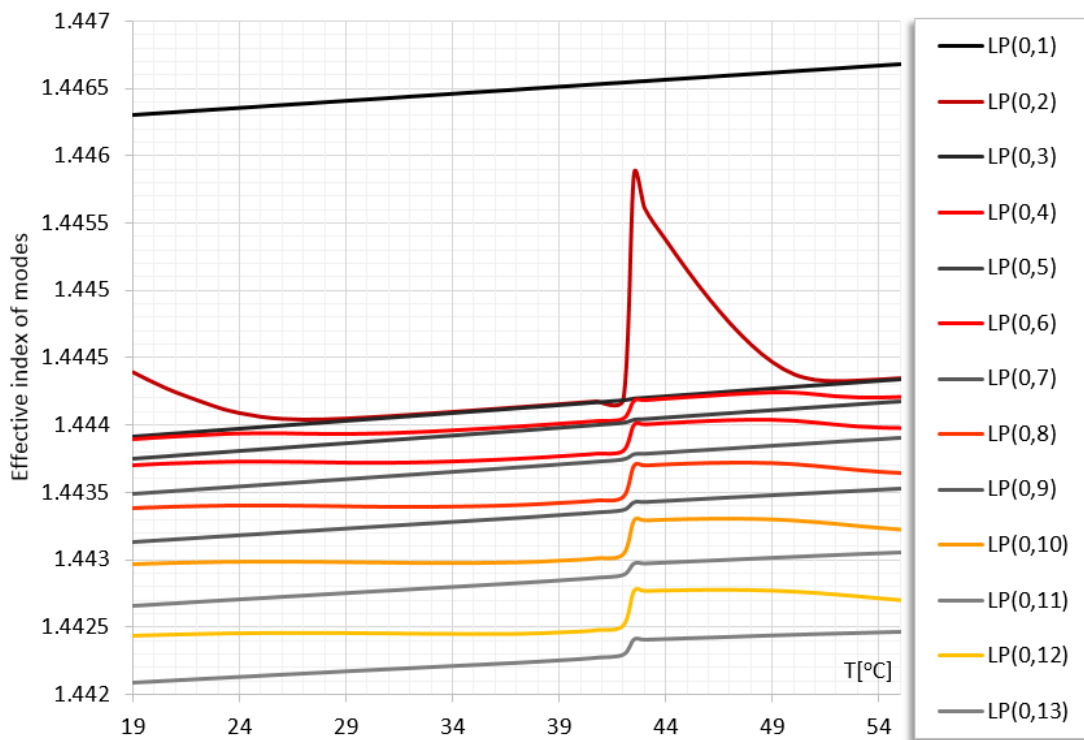


Fig.5.3.15 The mode structure plot versus temperature calculated for the UV-induced LPFG placed in the capillary filled with the 1110 LB LC.

From the results presented above it can be seen that:

- the attenuation bands that correspond with the modes with odd radial numbers are characterized by a higher thermal sensitivity than those associated with the modes with even radial numbers. This is due to the fact that the variation of the effective index of these cladding modes as a function of temperature is different for modes with odd and even radial numbers (as is clearly seen from the mode structure plot versus temperature calculated for this LC-LPFG – presented in Fig. 5.3.15).
- LC-LPFG tuning in the isotropic phase and in the nematic phase occur in the similar way (compare Fig. 5.3.13a and Fig. 5.3.13c). This feature could be achieved thanks to the unique thermal characteristic of the 1110 LC used here (see Fig. 5.3.14). Namely, the 1110 LC n_o values coincide with the 1110 LC n_{iso} values.
- close to T_c of the LC, a fast switching of all attenuation bands occurs (Fig. 5.3.13c). This is due to the fact that at T_c a jump in the LC refractive index values occurs.

In addition, for attenuation bands associated with the lower-order modes (in the left side of the calculated transmission spectra) some irregularity in their thermal tuning can be noticed. This effect is caused by the fact that for certain temperatures, modes with even and radial numbers have their effective indices very close to each other. As a result, the characteristic of the lower-order modes changes from a mode with an odd/even radial number to a mode with an even/odd radial number mode during this transition. In order to verify this statement let's examine carefully the LC-LPFG thermal tuning occurring close to T_c . In the Fig. 5.3.16 are shown simulated LC-LPFG transmission spectra corresponding to two temperature values:

- 42°C which is the temperature within a nematic phase of the 1110 LB LC (Fig. 5.3.16a),
- 43°C which is the temperature within an isotropic phase of the 1110 LB LC (Fig. 5.3.16b).

The LC-LPFG transmission spectra were calculated several times, successively increasing the number of the modes taken into account in the simulation. It seems that with a decreasing mode order, the attenuation bands associated with the modes with odd radial numbers diminish in intensity for the temperature range corresponding to the nematic phase. For the temperature range corresponding to the isotropic phase this effect occurs for attenuation bands associated with the modes with even radial numbers. Simultaneously, the distance between a pair of modes with even and odd radial numbers decreases with decreasing of their order. This phenomenon is visible when the LC-LPFG transmission spectra were calculated for both temperature values. Finally, the lower order modes change their

characteristic from a mode with an odd radial number to an even radial number at 42°C or from a mode with an even radial number to an odd radial number at 43°C (designated in Fig. 5.3.16 by grey dash circles).

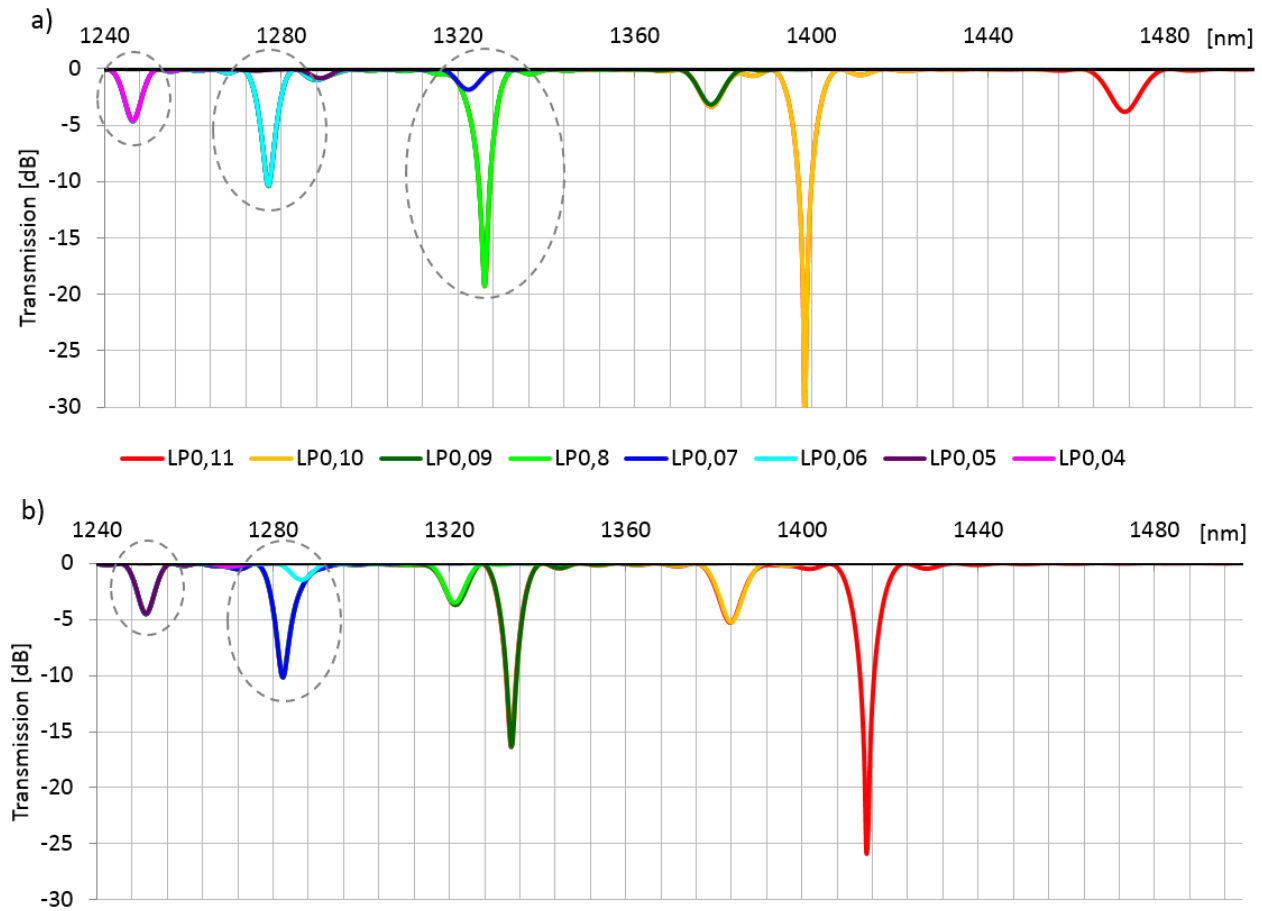


Fig. 5.3.16 Transmission spectra versus number of modes taken into account in the simulation calculated for the UV-induced LPFG (grating period 368 μm ; based on the PS1250/1500 fiber) placed in the capillary filled with 1110 LB LV at 42°C (a) and at 43°C (b).

5.3.6 The external electric field effect on the LC-LPFG transmission properties

In this section a general description of the LC-LPFG model used to investigate their electric properties is presented (a detailed theoretical explanation of the individual experimental results is provided in Section 6.5). In addition, the theoretical studies of the external electric field effect on the LC-LPFG transmission properties are limited to the case where the LPFG is coated with a thin LC layer. As it will be shown, such a design provides the most promising results and was therefore mainly explored within the experimental work on this project.

An electric field applied to the LC-LPFG reorients the LC molecules and modifies this way the LC layer RI. Consequently, such modifications in the LC layer RI should have an impact on the LC-LPFG transmission spectrum. However, the impact of these changes will be strongly dependent on the thickness of the LC layer. For example, if the grating is placed in the LC cell, the LC layer can be assumed to be infinite. As a result, for gratings surrounded by MB LCs, the cladding modes can be guided only by Fresnel reflection and, consequently, variations in the RIs of the LC will change only the strength of a mode coupling. A strong improvement in the LC-LPFGs electric sensitivity can be obtained by reducing the LC layer thickness to the thickness of order of few μm . For this LC-LPFG design, when the presence of the electric field increases, the LC layer RI cladding modes effective indices are shifted to the higher values. Simultaneously to this effect, a down shift of the resonances occurs. Based on this mechanism, the LC-LPFG electrically tuning becomes possible also in terms of the spectral shift of the attenuation bands.

For this LC-LPFG configuration care must be taken in order to achieve the required electrical control by proper choice of the LC material serving as a layer and by suitable adjustment to its thickness. As was already presented in the Sections 5.3.1 and 5.3.3:

- With the increase of the LC layer thickness, a cladding mode is allowed to be guided in the layer, leading to a rearrangement of the cladding modes. As a result, a lower order cladding mode will replace the position of the cladding mode with the precedent order (e.g., $LP_{0,9}$ replaces $LP_{0,10}$, etc.). This is a fast transition leading to the highest sensitivity.
- With the increase of the LC layer thickness, the lower RI of the LC layer is required to reach the transition region.
- The higher cladding modes order, the faster the transition will occur (providing this way a higher sensitivity).

Since the LCs are anisotropic materials composed of rod-like molecules, their optical properties strongly depend on the molecules' long range orientation order. Thus, the birefringence ($\Delta n = n_e - n_o$) of the LC is one of the most important parameters in the context of the LC-LPFGs electrical control. For the LCs investigated experimentally the Δn magnitude is from 0.0611 to 0.170 (note that the LCs considered here are only these which possess the positive dielectric anisotropy, see Tab. 6.1.2). Therefore, the electric field will change the RI of the LC layer by the value which usually should lead to the transition of the lowest-order cladding mode (higher effective index) to be mode guided within the LC layer. As the lowest-order

cladding mode transfers to a guided one within the overlay, a reorganization of other cladding modes occurs as well. As a result, the LC-LPFG is able to operate between two states of the attenuation bands, namely:

- the off-voltage state corresponding with the planar LC layer orientation on the bare LPFG,
- the on-voltage state corresponding with the orthogonal LC layer orientation on the bare LPFG.

It will be presented in Section 6.5, that by properly choosing the LC-LPFG components and by considering the issues listed above, the LC-LPFG effective tuning by the electric field is experimentally obtainable. It is worth mentioning that thanks to the presence of the electric field it is possible to achieve:

- a blue shift of the attenuation band in the LC-LPFG transmission spectrum,
- a red shift of the attenuation band in the LC-LPFG transmission spectrum,
- a fade of the attenuation band in the LC-LPFG transmission spectrum.

In addition, the electrical properties of the LC-LPFG could be adjusted by a proper choice of the ambient temperature. A detailed theoretical explanation of these LC-LPFG features is also provided in Section 7.5.

At the end of this section there is one more issue that has to be discussed when the LC-LPFG electrical properties are studied. In most of the cases, increasing the supplied voltage resulted in the LC molecules reorientation according with the electric field direction. In the experimental work, a setup with two parallel electrodes was used (see Fig. 6.1.5). As a result, the electric field is perpendicular to the LPFG axis. In practice it means that the LC molecules will not reorient in the same way within the LC layer with respect to the cross section of the LPFG. This electrically induced anisotropy in the LC layer may increase the birefringence and the Polarization Dependent Losses (PDL) of the LC-LPFG. Within this work, the LC-LPFG polarization properties were not investigated. The effect of the LC layer birefringence on the LC-LPFG spectral properties is difficult to be determined and needs additional study. What can be expected, is that the separation of the resonant wavelength can occur if the impact of the anisotropic LC layer will be strong enough. This separation is related to the change in the mode's effective indices, which would now be depended on the incident polarization state.

The isotropic refractive index distribution within the LC layer was assumed in the simulations. This apparently might introduce an error into the calculations. However, it has to be noted that the LC layer is the only portion of the fiber cross section that is birefringent (the core and clad region of the host fiber are supposedly insensitive to the state of polarization light), and is also relatively small compared to the

fiber dimensions. Secondly, the LC birefringence affects only the LPFG in terms of its sensitivity to the RI to the LC layer. The pre-tilt of the LC director, the imperfect polarization state, and/or a geometrical effect resulting from the cylindrical shape of the optical fiber are additional factors, which can also decrease the effect of the LC layer anisotropy. For these reasons, the resonant wavelength separation induced by the LC layer anisotropy does not have to be so large. It is suspected that the measured transmission spectra for different states of polarization will rather overlap with each other. Let's keep also in mind that even the LPFGs written in nominally non-birefringent optical fibers do acquire some local birefringence, which depends on a number of factors such as the writing process, inscription conditions, and type of the fiber. Moreover, in the theoretical model presented here, the LC layer anisotropy effect was included in terms of decreasing the n_o value for the LC-LPFG considered to be in the on-voltage state. This parameter could be estimated when simulated electric responses of the LC-LPFGs were fit to those measured in the experiment. Then, the fitting procedure was as follows:

- first, the LC layer thickness value was estimated by matching the simulation results to the experimentally measured LC-LPFG transmission spectrum in the off-voltage state (the LC layer refractive index correspond in this case with the n_o value of the LC)
- secondly, the refractive index of the LC layer in the on-voltage state could be found by matching the simulation results to the experimentally measured LC-LPFG transmission spectrum in the on-voltage state

The LC layer anisotropy should be considered in future work. However, the magnitude of the LC refractive index plays a more important role. Therefore, even if the LC layer anisotropy was not directly simulated, the LC-LPFG model presented here should still allow for a qualitative description of the LC-LPFG electric properties.

Chapter 6 EXPERIMENTAL STUDIES OF THE LC-LPFGs

In this chapter the experimental results are presented which show that LC-LPFGs can provide many novel and useful features, especially in the sensing field. First, the materials used during this research, the host fibers, the various LCs and the methods to produce the LPFGs are described here. Furthermore, the experiments performed to characterize the thermal sensitivity of the LPFGs themselves are presented. These results are analyzed in consideration of the type of the host fiber and physical parameters of the grating. Next, the response of the LPFGs to LC layer presence is investigated. From this point on, a special attention is put to the exploration of the tuning of the LC-LPFGs by external factors such as temperature or/and the external electrical field. The results obtained within this part of the work demonstrate that LC-LPFGs can open up the road to new detection schemes.

6.1 Materials and experimental procedure

6.1.1 Selection and specification of host fibers and LC materials

The host fiber is chosen according to the method of production of a LPFG. It is possible to produce the LPFGs in all of the studied fibers through an electric arc method. As far as the UV method is concerned, the use of a photosensitive fiber is required. The manufacturing of the LPFGs by exposure to UV-irradiation was performed with the PS1250/1500 fiber. This fiber offers the possibility of writing the grating directly, without any hydrogenation procedure. Co-doping this fiber with boron enhances its photosensitivity. As a result the UV exposure time required to obtain saturation of the index change is greatly decreased. The boron and germanium concentration for PS1250/1500 fiber were not disclosed by the manufacturer, but according to [89] the core of the fiber may contain 10% of GeO_2 and 20% of B_2O_3 in addition to SiO_2 . The host fibers that could be used for the fabrication of the LPFGs, together with their physical specifications, are presented in Tab. 6.1.1.

Tab. 6.1.1 Specification of the host fibers for fabrication the LPFG

| No. | Name | Physical parameters | Producer |
|-----|-------------|---|----------------|
| 1 | SM-28 | core/clad radius: 4/62.5 μm coating diameter: 250 μm | <i>Corning</i> |
| 2 | PS1250/1500 | Boron germanium co-doped core/clad radius: 3.7/62.5 μm coating diameter: 245 μm | <i>Corning</i> |

As an outside layer for the LPFG, two different classes of the LCs could be used:

- with a medium birefringence (MB): two commonly-known nematics (5CB and 6CHBT) and one prototype nematic mixture (1702).
- with a low birefringence (LB): four prototype nematic mixtures (1110, 1550, 1550A, 1800b).

Tab. 6.1.2 *Electro-optical properties of the tested LC materials (measured at 589 nm and ~25°C).*

| No. | Symbol | Clearing temperature, T_c [°C] | Ordinary refractive index, n_o | Extraordinary refractive index, n_e | Birefringence, Δn | Dielectric anisotropy, $\Delta\epsilon$ |
|-----|--------------|----------------------------------|----------------------------------|---------------------------------------|---------------------------|---|
| 1 | 1110 | 42 | 1.4594 | 1.5058 | 0.0406 | <0 |
| 2 | 1550 | 77.3 | 1.4614 | 1.5225 | 0.0611 | 3.2 |
| 3 | 1550A | 71 | 1.4592 | 1.5168 | 0.0594 | >0 |
| 4 | 1800b | 70 | 1.4567 | 1.5134 | 0.0567 | <0 |
| 5 | 6CHBT | 43 | 1.52 | 1.67 | 0.15 | 8 |
| 6 | 5CB | 33 | 1.54 | 1.71 | 0.16 | 16.1 |
| 7 | 1702 | 86 | 1.4909 | 1.6599 | 0.17 | 48.4 |

The refractive indices' thermal characteristics (measured at 589 nm) for all the investigated LCs are presented in Fig. 6.1.1. As can be seen, for MB LCs, both the ordinary RI (n_o) and the extraordinary (n_e) RI are always higher than the RI of silica glass (n_{SiO_2}). In the case of LB LCs the n_o in the specific temperature ranges is lower than n_{SiO_2} , which makes these LC types especially interesting for silica glass fibers. Another important parameter that should be considered when the LC is chosen as an LPFG modulating external layer is the dielectric anisotropy ($\Delta\epsilon$). The key point is that the sign of the $\Delta\epsilon$ determines the alignment of the LC molecules in the E-field presence: for $\Delta\epsilon > 0$, the LC molecules tend to orient along the E-field direction, while for $\Delta\epsilon < 0$, they are oriented perpendicularly. Table 6.1.2

provides a summary of the optical properties for all the tested LC materials. Each of the LC mixtures used in experiments was b(MUT) in Warsaw by the group of Professor Roman Dąbrowski.

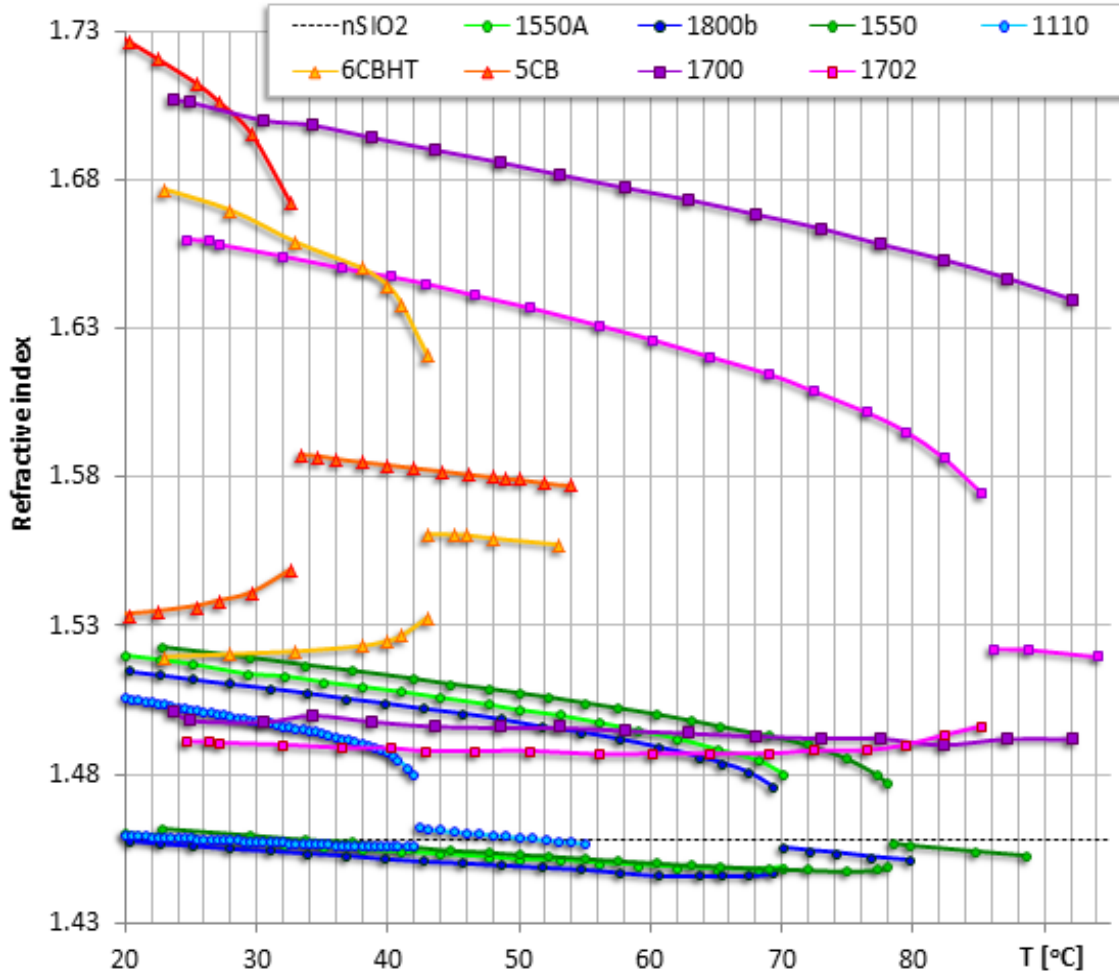


Fig. 6.1.1 Refractive indices of LC mixtures as functions of temperature.

6.1.2 LPFGs manufacturing methods

All LPFGs investigated within this work were manufactured at the *Photonics Research Center (PRC)* at *UQO*. These LPFGs were fabricated by one of two methods: electric arc discharge or ultraviolet (UV) laser irradiation. The fabrication procedures with schematic diagrams of the setups used for this purpose (Figs. 6.1.2 and 6.1.3) are as follows:

- electric arc discharge method

In the case of LPFG writing with the arc technique, a partial stress relaxation take place. The LPFG manufacturing process using this cost-effective method is as follows:

- a bare fiber without its protective coating is placed between the electrodes of a fusion splicer and fixed to a translation stage controlled by a motor,
- the fiber in a straight position is to moves past the electrodes of a fusion splicer (point-by-point writing) after each discharge has occurred. Then the strength of the grating is increased to its desired level by repeating the entire process a specific number of times,
- the number of periods is increased to the desired level by repeating the entire process with a specific number of times.

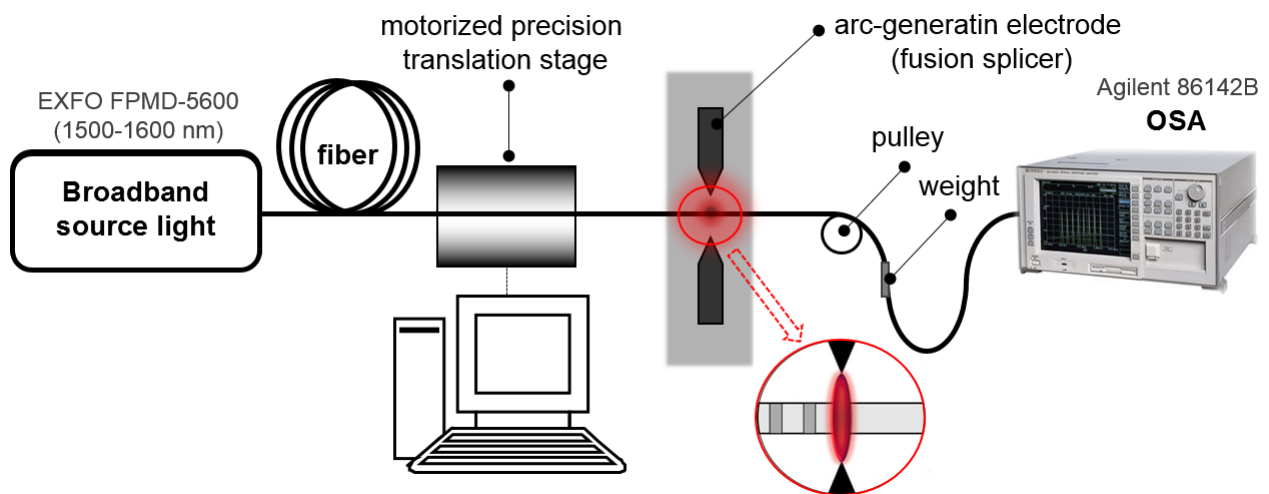


Fig. 6.1.2 Computer-assisted arc discharge apparatus for manufacturing LPFGs at PRC-UQO.

During the process of fabrication an optical spectrum analyzer is used to monitor the output characteristics. A schematic diagram of the fabrication setup is presented in Figure 7.1.2. The electric arc

discharge method is based on the periodic melting of the fiber while a pulling weight stretches it, therefore creating a periodically tapered fiber. The grating period is mainly determined by the moving step of the translation stage that is controlled by a computer and by some other factors such as: arc intensity, arc duration time, pulling weight.

- **UV laser irradiation method**

For the LPFGs fabrication with this method the source of the UV light was provided by an Excimer laser (PulseMaster GSI Lumonics). The Eximer laser is supplied by a special mixture of gases (helium, krypton and fluorine) which results in emission of a 248 nm wavelength light beam. At this UV wavelength used for irradiation of boron co-doped fiber, the core experiences the highest absorption, and at the same time the silica cladding is transparent, so that the color-center model of refractive index modulation should be valid.

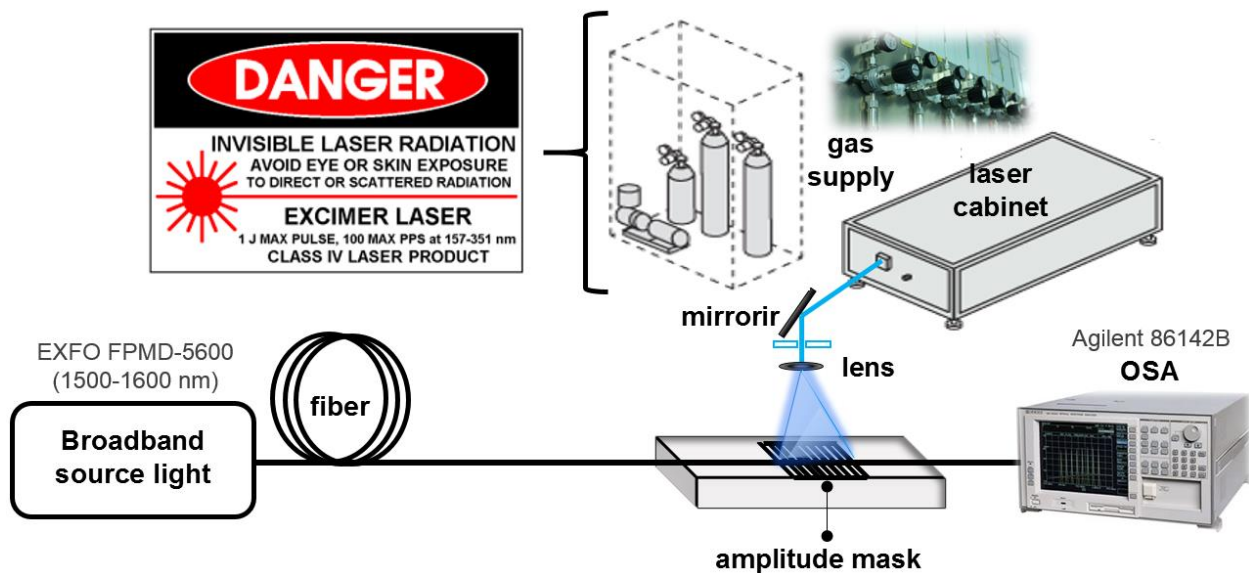


Fig. 6.1.3 Experimental setup at PRC-UQO for manufacturing LPFGs by UV laser irradiation.

The experimental setup for the inscription of the LPFGs by UV laser is shown in Figure 6.1.3 and the procedure is as follows:

- a segment of PS1250/1500 fiber with polymer coating removed is spliced between two segments of SMF-28 and such prepared fiber is placed in contact with the amplitude mask,
- the fiber is irradiated by a UV light and the exposure is repeated until the index modulation has reached a sufficient level to provide the desired attenuation depth in the LPFG transmission spectrum.

The specification of the amplitude mask is given in Tab. 6.1.3. The major advantage of using this amplitude mask method is that a large number of identical gratings with the required period may be easily mass produced by placing more fibers behind the amplitude mask.

Tab. 6.1.3 *The specification of the amplitude mask*

| | | | | | | | | | | | | | | |
|---|----------|----------|----------|----------|----------|----------|----------|----------|----------|-----------|-----------|-----------|-----------|-----------|
| | 1 | 2 | 3 | 4 | 5 | 6 | 7 | 8 | 9 | 10 | 11 | 12 | 13 | 14 |
| Λ[μm] | 680 | 600 | 515 | 437 | 368 | 378 | 358 | 311 | 265 | 227 | 171 | 169 | 135 | 131 |

In Table 6.1.4 a summary of physical specifications and manufacturing methods of the LPFGs studied within this work is given. The lengths of the gratings fabricated within the fibers were typically around few centimeters. The grating period range investigated for the arc-induced LPFGs was from 400 μm to 222 μm and for the UV-induced LPFGs was from 368 μm to 226.8 μm .

Tab. 6.1.4 *Specifications of tested LPFGs*

| No. | Period | Host fiber | method |
|------------|---------------|-------------------|---------------|
| 1 | 400 | SMF-28 | Electric arc |
| 2 | 375 | PS1250/1500 | Electric arc |
| 3 | 222 | PS1250/1500 | Electric arc |
| 4 | 368 | PS1250/1500 | UV laser |
| 5 | 358 | PS1250/1500 | UV laser |
| 6 | 226.8 | PS1250/1500 | UV laser |

In Tab. 6.1.5 a comparison of the approaches described above is shown. The electric arc method offers simplicity, flexibility and low cost of fabrication. One of the greatest benefits of this technique is that a photosensitive fiber (PSF) is not required. The second method, based on a UV laser, is assumed to be superior in terms of achieving fabrication repeatability and good quality symmetrical coupling [87,89]. Moreover, an important advantage of using an amplitude mask method in the case of the UV irradiation technique is that a number of gratings with the required period may be easily mass produced by placing more than a single fiber behind the amplitude mask. If we compare the thermal stability, the gratings produced by the electric arc technique are much more stable at high temperatures [88]. This is due to the fact that the LPFGs inscribed by UV laser are based on the photosensitivity phenomena. Under the

influence of UV irradiation, defects in the glass structures are created and consequently, the RI is changed. Each defect contributing to the change in the RI is stable only up to a certain temperature (associated with a specific activation energy value), after which the defect is reversed and the RI modulation decreases. In addition, the electric arc technique limits the minimum period of the gratings that may be fabricated. In this case the electrodes of the fusion-splicing machine expose a region of fiber with a length of the order of $200\ \mu\text{m}$ to the arc. The UV technique makes it possible to produce the LPFGs with a much shorter fiber grating period and is restricted only by the amplitude mask specifications. In terms of the outside shape of the LPFG, the grating made by the UV technique is smooth while the grating made by the electric arc discharge can be characterized by a periodical deformation of the structure. The main mechanisms responsible for the formation of arc-induced gratings can be summarized as periodic modification of the glass structure (densification), relaxation of drawing-induced or viscoelastic stress and geometric modulation (tapering) of the fiber [87]. The tapering effect is unavoidable when the arc-based technique is used. Some tension must be applied to the fiber during the LPFG fabrication process, which is the main reason for tapering when the fiber is exposed to the arc discharge. In Fig. 6.1.4 are presented the scanning electron microscope (SEM) images of two fibers [121]: the LPFG based on and with period of $345\ \mu\text{m}$ and the LPFG based on the and with period of $221\ \mu\text{m}$. They were fabricated at PRC, like all LPFGs investigated in this work. It can be seen in Fig. 6.1.4 that the SMF28 fiber is slightly tapered and that its average diameter is reduced due to the arc discharges, while the PS1250/1500 fiber shows no modification of its diameter. However, the diameter reduction of the SMF28 fiber is less than expected, at $1\ \mu\text{m}$ in the overall radius of the fiber for less tapered regions, and $2.5\ \mu\text{m}$ for more tapered regions.

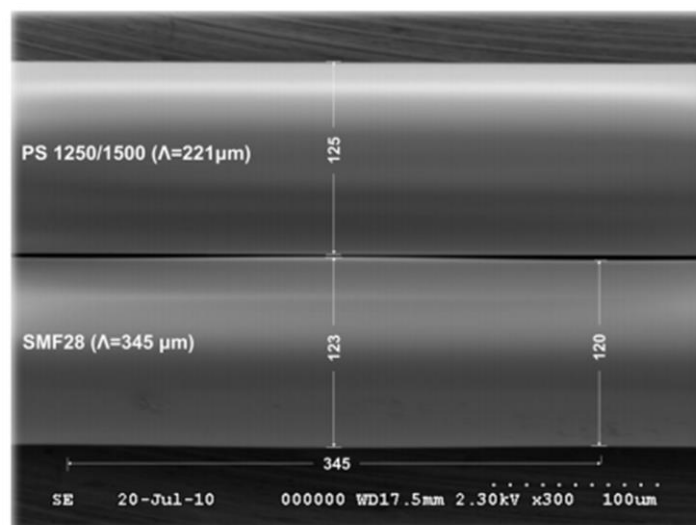


Fig. 6.1.4 Scanning electron microscope (SEM) images of the arc-induced LPFGs.

The values are given in μm [121].

In order to compare the impact of fabrication methods described above on the LPFG transmission spectrum, three gratings with periods of 378 μm , 368 μm and 358 μm were fabricated (all of them were produced on this same fiber type, PS1200/1500 fiber). The first one was induced by the arc discharged method, while the rest were written by the UV irradiation. Their transmission spectra are shown in Fig. 6.1.4. It can be seen that both these methods allowed to obtain good quality LPFGs, with transmission of the last resonance reaching below -20 dB. Taking only into account the Λ value, it should be expected that the transmission spectrum of the LPFG with a longer period will be shifted to a longer wavelength (as was discussed in detail in the Section 6.2.2). This is true only for gratings produced by this same technique of fabrication (in this example for the UV-induced LPFGs with period of 368 μm and 358 μm), as is visible in Fig. 6.1.5a. When the transmission spectrum of the UV-induced LPFG with a period of 368 μm is compared to the arc-induced LPFG with period of 378 μm , the opposite shift is measured, as is presented in Fig. 6.1.5c. This effect can be explained by assuming that the UV-induced LPFGs had in fact longer “effective periods” than those fabricated by arc discharge. The difference between the spectra can be also explained by the fact that the arc discharge induced tapering of the fiber. As a result, a decrease in the core and cladding diameters occurs. That hypothesis is in accordance with previously performed simulations where the impact of fiber and grating parameters on the LPFG transmission spectra and was carefully examined. As was shown in Section 5.2.2 shortening of the grating period, induces a blue shift of the resonance wavelengths for each of the cladding modes. Despite the fact that a decrease in the cladding diameter contributes to a red shift, the dominant effect remains the decrease of the core (as was presented in Section 5.2.1). This in turn reduces the effective refractive index of the guided mode and can lead to a higher blue shift of the resonances. Consequently it can be anticipated that the attenuation bands measured for the arc-induced LPFGs transmission spectra will be shifted to a shorter wavelengths than those produced by the UV irradiation method. The phenomenon described above has also been proven by achieving a good agreement between the measured and simulated data for the LPFGs presented in Fig. 6.1.5d. The parameters assumed for the simulations of these LPFGs are shown in Tab. 5.1.6. The small reduction in the core radius and cladding radius was assumed for the arc-induced LPFGs written with the arc method. This reduction (compared to the parameters set for the UV irradiated LPFG) is 0.05 μm for the core and 0.3 μm for the cladding radius. Additionally, in order to achieve an accurate fit, for the UV-written LPFG slightly higher refractive index of the core was used for the simulation. This grating was probably irradiated with a high dose of UV light, which in terms of simulation modeling is represented by a higher refractive index of the core.

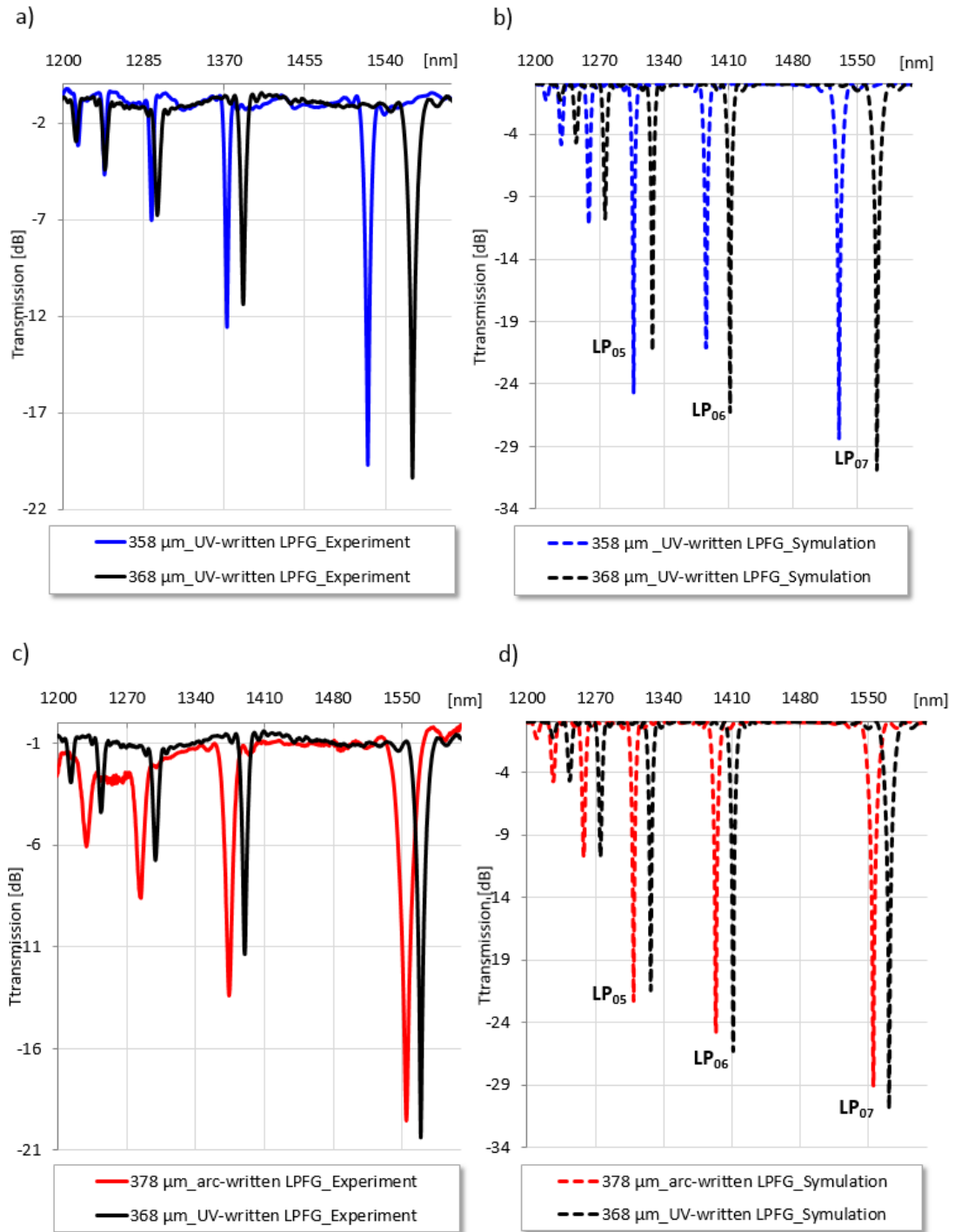


Fig. 6.1.5 Measured (a,b) and calculated (b,d) transmission spectra of the LPFGs based on PS1200/1500 fiber versus their fabrication method. The LPFGs were written with a slightly different period Λ (378 μm for the arc-induced LPFG; 368 μm and 358 μm for the UV-induced LPFG). In all cases the fiber host was PS1250/1500 fiber.

Tab. 6.1.6 Simulation parameters used for the LPFGs models discussed in terms of the fabrication method.

| Fabrication method | Electric arc technique | UV laser technique |
|----------------------------|------------------------|--------------------|
| Host fiber | PS1250/1500 fiber | |
| Length [μm] | 32500 | 35000 |
| Period [μm] | 375 | 368 and 358 |
| In. Mod. | 2.1×10^{-4} | |
| r_{co} [μm] | 3.9 | 3.95 |
| r_{cl} [μm] | 61.5 | 61.8 |
| n_{co} | 1.4494 | 1.44954 |
| n_{cl} | 1.44403 | |

Tab. 6.1.5 Comparison of the two techniques for fabricating the investigated LPFGs.

| | Electric arc technique | UV laser technique |
|-------------------------------------|---|---|
| Key element | Fiber fusion splicing machine | UV laser |
| Procedure of fabrication | SIMPLE. Cost-efficient. Does not require photosensitization of the fiber. | DEMANDING. In general, consists of 3 steps: pre-fabrication treatment; writing by UV laser; post-fabrication treatment. Fiber must be photo-sensitized. |
| Thermal stability | Very stable (up to temperatures causing deformation of the glass) | Low stability (the grating starts to disappear even at around 100°C) |
| Outside shape of the grating | Nearly smooth surface | Smooth surface |
| Min. period | 200 μm | \ll 200 μm |
| Reproducibility | Low | High |
| Inscription by | Point-by-point | Amplitude mask |

6.1.3 Measurement of spectral properties

The optical transmission spectrum of the fibers and fiber devices was monitored by using the Ando AQ-6315E optical spectrum analyzer (OSA) for the part of the research conducted in Poland at the Warsaw University of Technology (WUT). When the study was carried out in Canada at the Photonics Research Center (PRC) at Université du Québec en Outaouais (UQO) the output signal was analyzed by using the Agilent 86142B OSA. The maximum resolution for both OSAs was of 0.05nm.

Depending on the requirements, four different sources of light were used during the experiments:

- Halogen lamp for the range of wavelengths from 1200 nm to 1700 nm (WUT)
- SC source for the range of wavelengths from 1000 nm to 1750 nm (WUT)
- Agilent 83437 broadband light source for the range of wavelengths from 1160 nm to 1610 nm (UQO)
- Agilent 83439A Erbium ASE source for the range of wavelengths from 1500 nm to 1600 nm (UQO)

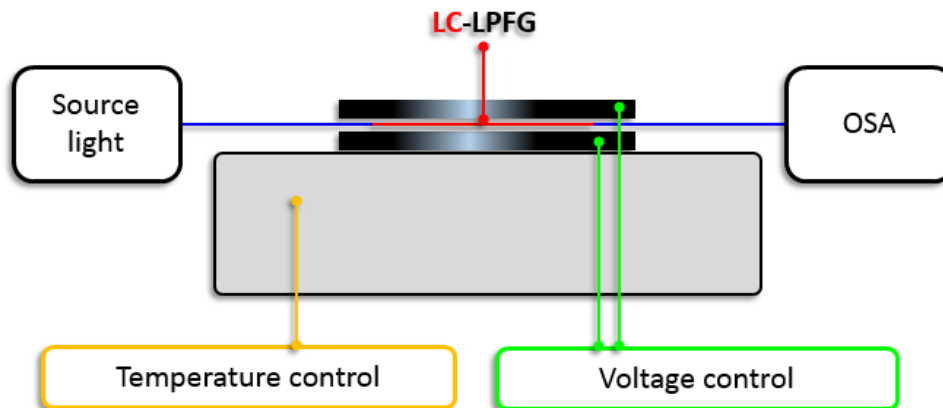


Fig. 6.1.6 *Experimental setup to investigate spectral properties of LC-LPFGs under the influence of temperature and external E-field.*

The experimental setup for the measurement of the LC-LPFGs under the influence of temperature and external E-field is presented in Fig. 6.1.6. The LC-LPFG was placed in a Peltier module. Temperature regulation was within the 10°C -120°C range according to the Testo 735 precise thermometer (0.05°C resolution and 0.1°C accuracy). Each measurement was performed after stabilization of the temperature by the Peltier module. In order to apply an external electric field to the samples, the Function Generator (1μHz-10MHz) with an amplifier and two electrodes were used. Then the electrical control was achieved within the 0V to 1000V typical range with a frequency of 2 kHz.

6.1.4 Procedure of LC layer application on the LPFGs

The external LC cladding of the LPFGs was formed by using three methods:

- 1st method:

In the first step the tested LPFG was placed in an empty cell. At this point the LPFG transmission spectrum was measured in order to have a base comparison value. The next step was to fill the cell with LC by using the capillary forces. The construction of the LC cell is presented in Figure 6.1.7. The space between the plates was $\sim 140 \mu\text{m}$. In order to achieve planar orientation in the LC cell, the anti-parallel rubbing was used. Indium tin oxide was deposited on inner surface of the plates to apply an electric field across the cell. To achieve the optical control of the orientation of the LC, the LC cell was operated between the crossed polarizers in such a way that it appeared bright when no voltage was applied.

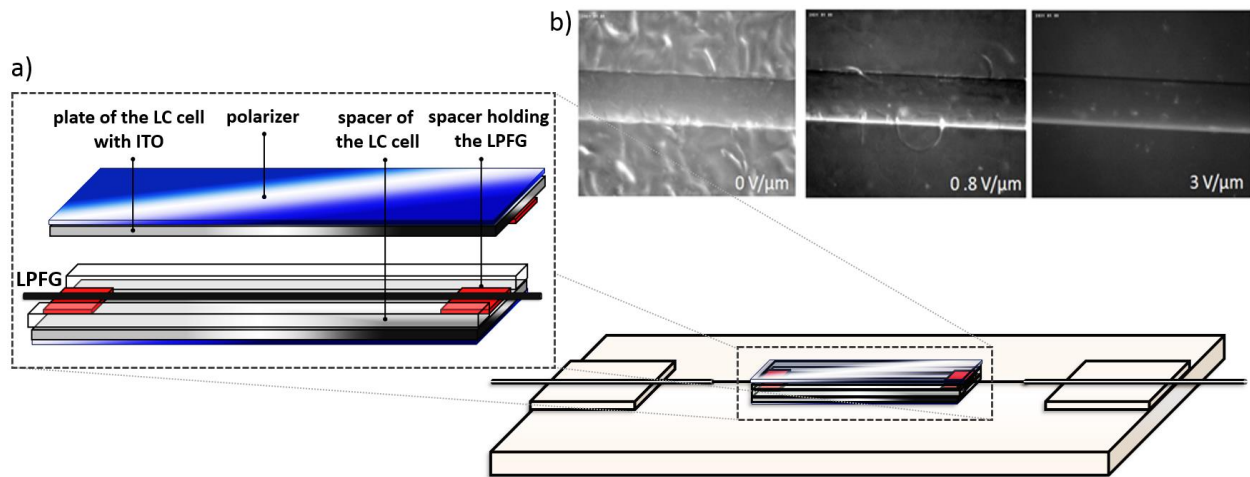


Fig. 6.1.7 a) LC cell b) Pictures of the arc-induced LPFG (with $\Lambda = 400 \mu\text{m}$) placed in the LC cell (filled with 5CB) for different values of the external field are shown.

- 2nd method:

A bare LPFG was introduced into a capillary with a radius of $\sim 134 \mu\text{m}$. Then the capillary was filled with the LC mixture by using the capillary forces (as is presented in Figs. 6.1.8 and 6.1.9). Due to the small space between the inside surface of the capillary and the surface of the fiber ($\sim 4.5 \mu\text{m}$) and the flow-induced orientation during the capillary filling process, it is assumed that the planar and the axial LC alignments dominate over the radial geometry.

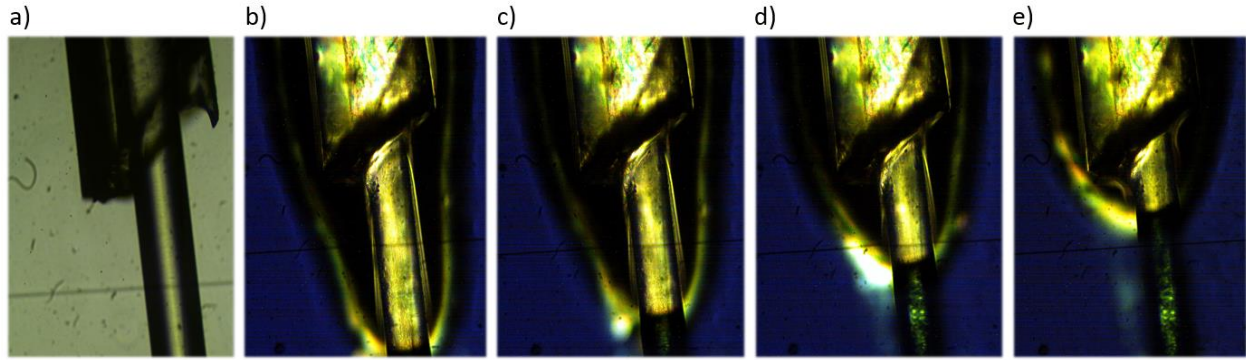


Fig. 6.1.8 In (a) the LPFG introduced into the capillary. In (a-c) filling capillary process with the 6CHBT LC.



Fig. 6.1.9 An LPFG inside a capillary filled with the LC

- 3rd method:

A thin layer of the LC was initially formed on the bare LPFG. The surface tension of the LC makes it easy to coat it uniformly on the LPFG by making the LC behave as if it were a skin. The presence of the LC layer on the surface of the LPFG was observed when the sample was placed between the polarizers, as is shown in Figs 6.1.10 - 6.1.12. The LC nematic phase is birefringent. Hence under the polarized light, some different colors can be observed for different LC layers. These colors are related to the optical path difference $\Delta n \cdot d$, where Δn is the optical birefringence of the LC sample and d is the sample thickness. Since the Δn of the investigated LCs is known, the LC layer thickness estimation should be possible - according to the Michel-Levy interference chart [99-100]. Unfortunately, this method is not accurate enough for the needs of this work. The clear variation of the LC thickness can be referred from the pictures presented above (especially when we look at Fig. 6.1.10 and Fig 6.1.11, on which the LPFG was coated with this same LC material, namely 5CB LC). However, based on the Michel-Levy interference chart its thickness could be estimated to be from ~ 0.5 to ~ 2.0 , from ~ 1.5 to ~ 3.0 and from ~ 4.0 to ~ 6.0 for samples presented in Figs. 6.1.10, 6.1.11, and 6.1.12, respectively. More precise determination of the LC layers could be done with help of the LC-LPFG simulations, as was described in Section 5 and carried out in Sections 6.3 – 6.5.

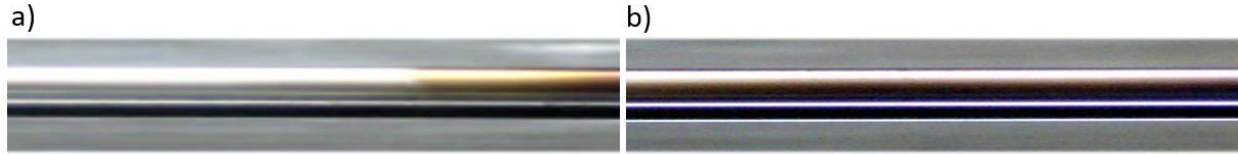


Fig. 6.1.10 Pictures of the LPFG coated with 5CB LC. In (a) the border between the fiber surface and the LC layer is shown. In (b) middle section of the LC-LPFG is presented.

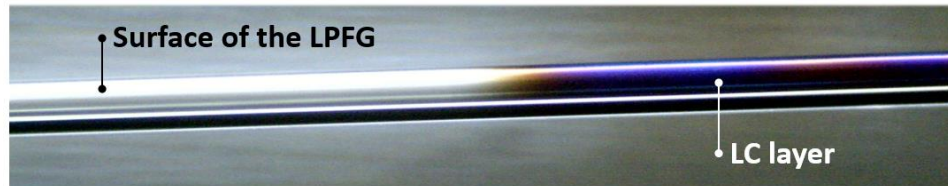


Fig. 6.1.11 Pictures of the same LC-LPFG sample presented in Fig. 6.1.10, but coated once again with the 5CB LC.

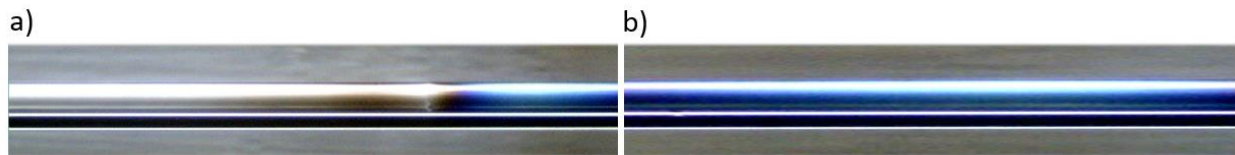


Fig. 6.1.12 Pictures of the LPFG coated with 1550 LC. In (a) the border between the fiber surface and the LC layer is shown. In (b) middle section of the LC-LPFG is presented.

The degree of ordering of the LC alignment is of prime importance since it has a significant effect on the LC RI value. The LC orientation on the bare LPFG will mainly be determined by the anchoring conditions (especially for the LPFGs coated by the LC layers). Therefore, in order to provide a better alignment of the LC molecules, the LPFGs were first rubbed several times along the fiber axis using a cotton swabs. As a result, the LC molecules tend to align along the fiber axis. In reality, a certain non-zero tilt angle of the LC molecules with respect to the fiber axis will always exist. The LC order orientation depends from many factors, such as LC surface tension, LC elastic constants, a solid-LC contact angle, LC dielectric anisotropy, dipole and rigidity of the LC molecules and many others [26]. Nonetheless, when LCs are deposited on the glass layer surfaces they are in general coated with appropriate layers, which can give a uniform and repeatable alignment. Therefore, for the LC-LPFGs prepared according with the 3rd method a good alignment of the LC layer should be possible to achieve. In order to verify this statement the LC layer alignment was examined under a polarizing optical microscope. The LPFG coated with the 6CHBT LC layer was placed between the crossed polarizers. First, the LC-LPFG axis was parallel to the first polarizer axis (Fig. 6.1.13 – the white arrow represents the polarizer axis direction), and then rotated about 45 degrees

(Fig. 6.1.14). As can be noticed, when the LC-LPFG axis was parallel to the first polarizer axis the light almost complete faded out (Fig. 6.1.13b). This direct observation confirms that a nearly planar alignment has been obtained. In the case of the LC-LPFGs prepared according with the 2nd method it has to be noted that the planar orientation of the LC is supposed to occur only due to the capillary filling process. For the capillary filling process the LC orientation close to the capillary walls and the LPFG surface is determined by the anchoring conditions while in the centered part of these boundaries, the LC molecules are oriented parallel to the axis of the capillary (flow-induced orientation). This statement is in accordance to the results presented in [103, 119] where it was demonstrated that the glass cylindrical cavities of dimension 2 – 6 μm infiltrated with the LCs present already a good alignment. When the geometry of the host fiber is considered in this context, for the UV-induced LPFGs the overall impact to the LC alignment can be negligible. The arc-induced LPFGs are characterized by the structural deformation. However, for the arc-induced LPFGs studied within this work, significant variations of the fiber cladding dimension were not observed. It can be therefore assumed that this effect should not have an important impact on the LC alignment as well. It is, thus, reasonable to assume that satisfactory LC planar alignment is present on the bare LPFG. Consequently, for the LC-LPFGs prepared in this way, the effective refractive index of the LC can be approximated by a value close to the LC n_o .

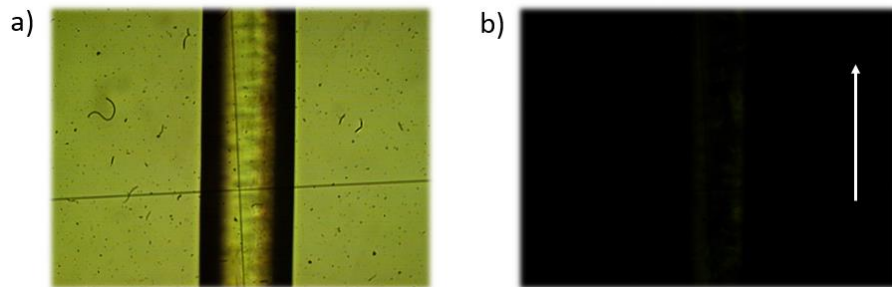


Fig.6.1.13 LPFG with the 6CHBT LC layer placed in the polarizing optical microscope observed in not polarized light (a) and the when LC-LPFG axis was perpendicular to the first polarizer axis (b).

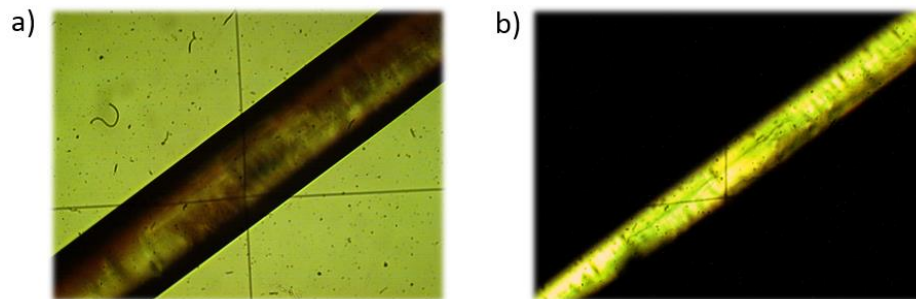


Fig.6.1.14 LPFG with the 6CHBT LC layer placed in the polarizing optical microscope observed in not polarized light (a) and when the LC-LPFG axis was at 45 degree to the crossed polarizers (b).

In addition, the orientation of the LC molecules was also investigated by simply measuring the transmission spectrum of the LPFGs with 1800b LC layer with and without the presence of the E-field. Note that since the 1800b possess the $\Delta\epsilon < 0$, presence of the E-field should just induce a better planar orientation of the LC molecules. Moreover, the E-field impact to this LC-LPFG transmission spectrum was recorded at two different ambient temperatures: 36.5°C and 65.3°C. As can be seen from Fig. 6.1.15, the transmission spectra look almost identical, regardless of the presence of the E-field. Therefore, it is reasonable to assume that the orientation of the LC molecules is homogenous.

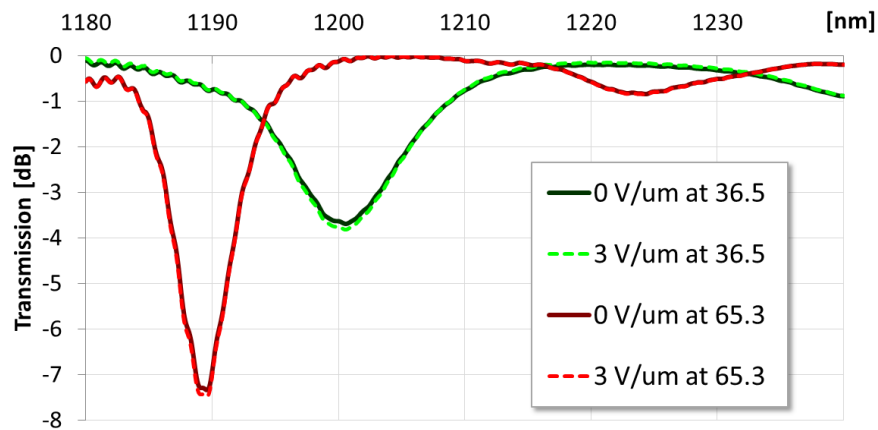


Fig.6.1.15 Transmission spectra of the LPFG functionalized with 1800b LC layer versus E-field measured. The E-field impact to the LC-LPFG spectral properties was recorded two different ambient temperatures.

6.2. Temperature effect on individual tested LPFGs

The temperature sensitivities of the LPFGs and the differences between gratings written in diverse fibers can be explained on the basis of the thermo-optic coefficients of the core and the cladding materials (as was discussed in details in Section 5.2.3). The presence of boron in the core of the PS1250/1200 fiber alters the temperature dependence of the n_{co} . The difference in thermo-optic coefficients of boron co-doped fiber is also opposite to the coefficient difference of SMF-28 fiber. Consequently, it is expected that for:

- LPFGs based on PS1250/1500 fiber the blue shift of the attenuation bands vs temperature should occurred,
- LPFGs based on SMF-28 fiber the red shift of the attenuation bands vs temperature should happen.

In Figure 6.4 measured thermal sensitivities for the:

- UV-induced LPFG based on PS1250/1500 with period of 368 μm ,
- arc-written LPFG based on PS1250/1500 with period of 375 μm ,
- arc-written LPFG based on SMF-28 fiber with period of 400 μm ,

are presented. Consecutively, in order to estimate the thermo-optic coefficients for the investigated host fibers, transmission spectra for the UV- (based on the PS1250/1500 fiber) and the arc-induced (based on the SMF-28 fiber) LPFGs were simulated. In Figs. 6.2.2 and 6.2.3 these simulations are presented along with the corresponding experimental results. The method of calculation of the temperature effect on the LPFG transmission spectra was described in Section 5.2.3. Due to the lack of complete data about the fiber properties (such as the core radius or dopant concentration in the core determining its refractive index), a custom LPFG model had to be developed (grating and fiber properties used in the model for grating based on PS1250/1500 fiber are summarized in Tab. 6.1.6 while for the grating based on the SMF-28 fiber they are provided in Tab.6.2.2). This was mainly achieved by fitting the measured and simulated transmission spectra. As a result the cladding modes corresponding with the observed attenuation band could be correctly determined. In addition, to achieving an accurate fit of the LPFG transmission spectra, the fabrication method was taken into account. Therefore, for the LPFG based on the PS1250/1500 fiber the core and clad were slightly reduced when its transmission spectrum was simulated for the arc discharged method (compared to the UV irradiation technique) - explanation can be found in Section 7.1. Finally, it was possible to estimate the values of the thermo-optic coefficients for the core of $6.6 \cdot 10^{-6}$ and

$8.6 \cdot 10^{-6}$ for the PS1250/1500 and SMF-28 fibers, respectively (temperature parameters settings are given in Tab. 6.2.3).

Tab. 6.2.1 Thermal sensitivity for arc-written and UV-written LPFGs.

| Specification of the LPFG | Order of the mode, m | K_T^m [nm/°C] | Correlation coefficient, R^2 |
|--|------------------------|----------------------|--------------------------------|
| Host fiber: SMF-28 Method: electric arc $\Lambda = 400 \mu\text{m}$ | 7 | 0.1608 ± 0.0128 | 0.9985 |
| Host fiber: PS1250/1500 Method: electric arc $\Lambda = 375 \mu\text{m}$ | 7 | -0.4887 ± 0.0390 | 0.9817 |
| Host fiber: PS1250/1500 Method: UV laser $\Lambda = 368 \mu\text{m}$ | 7 | -0.5039 ± 0.0403 | 0.9992 |

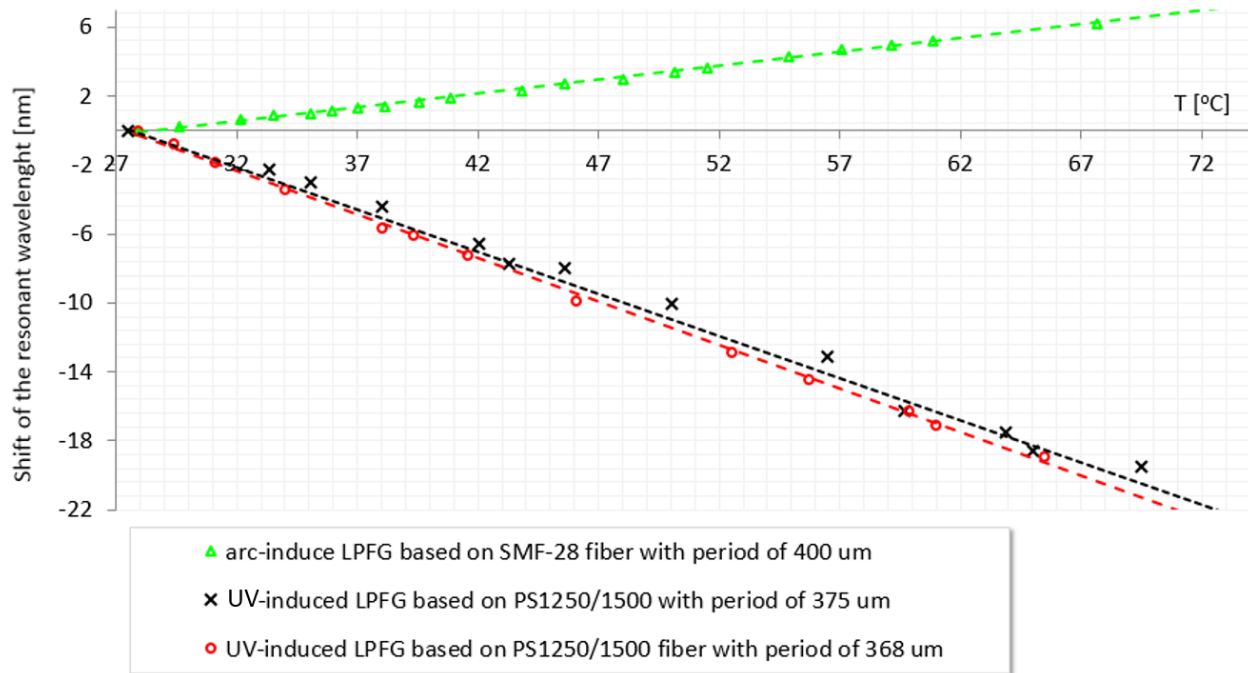


Fig. 6.2.1 Thermal sensitivity LPFGs write with different methods: arc-written LPFGs based on SMF-28 ($\Lambda = 400 \mu\text{m}$) PS1200/1500 ($\Lambda = 375 \mu\text{m}$) fibers; UV-written LPFG based on PS1200/1500 fiber ($\Lambda = 368 \mu\text{m}$).

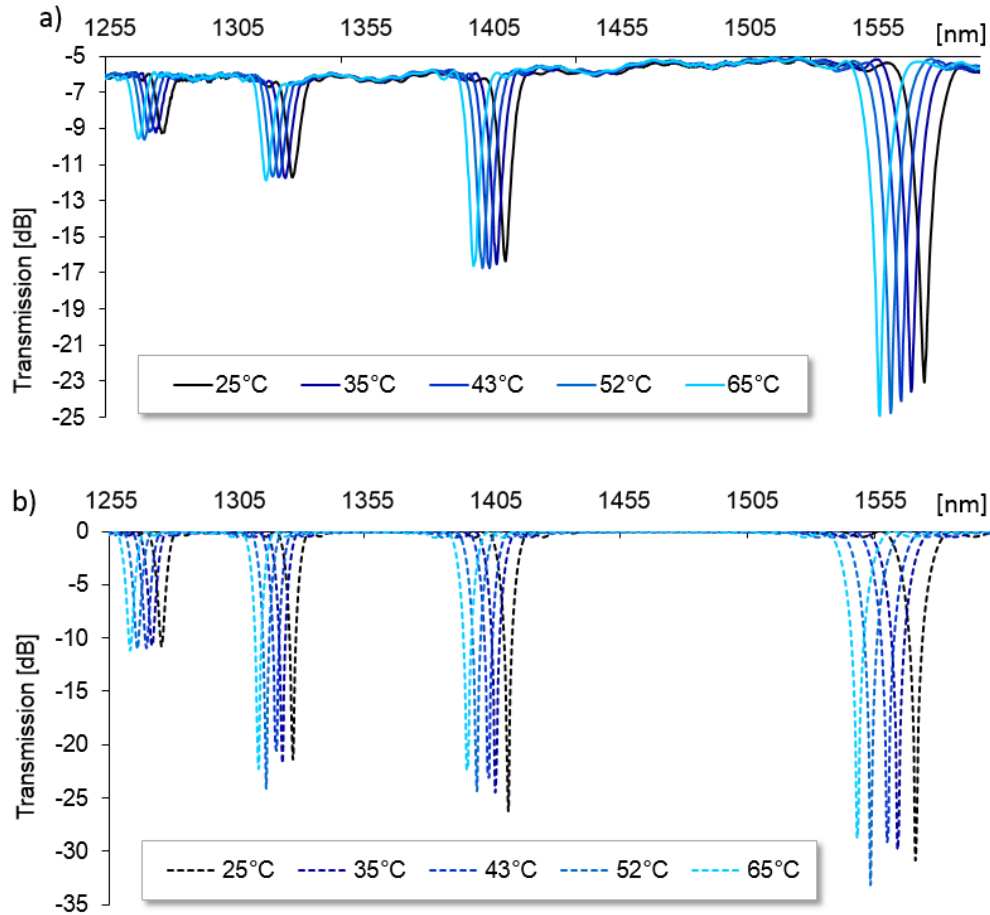


Fig.6.2.2 Measured (a) and calculated (b) transmission spectra versus temperature for the UV-induced LPFG based on the PS1250/1500 fiber with period of 368 μm .

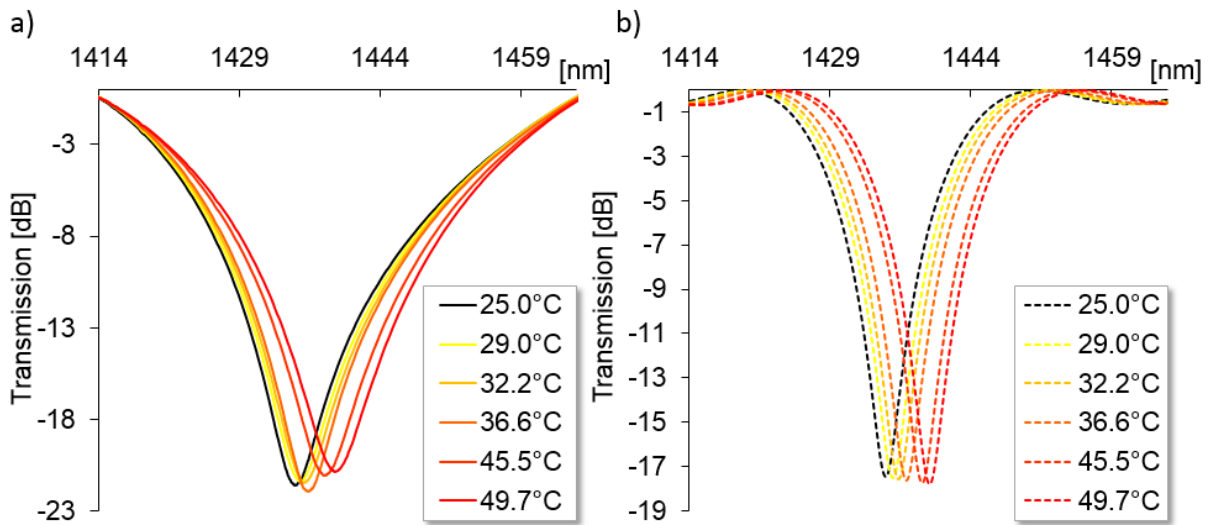


Fig.6.2.3 Measured (a) and calculated (b) transmission spectra versus temperature for the arc-induced LPFG based on the SMF-28 fiber with period of 400 μm .

Tab. 6.2.2 Specification of the fiber and grating and temperature parameters applied to the LPFG model based on the SMF-28 fiber.

| Fiber parameters | |
|-------------------------------------|----------------------------|
| r_{co} [μm] | 4.00 |
| n_{co} | 1.44900 |
| r_{cl} [μm] | 62.5 |
| n_{cl} | 1.44403 |
| Core material dispersion properties | set for germanium doped |
| Clad material dispersion properties | set for fused silica glass |
| Grating parameters | |
| Grating period [μm] | 400 |
| Ind. Mod. | 0.000198 |
| Lenght [μm] | 34000 |

Tab. 6.2.3 Specification of the temperature settings applied to the LPFG models

| Temperatures settings | | |
|--|----------------------|----------------------|
| Type of the host fiber | PS1250/1500 | SMF-28 |
| Temperature range variation [$^{\circ}\text{C}$] | 25-65 | 22-65 |
| ξ_{co} [$1/^{\circ}\text{C}$] | 6.6×10^{-6} | 8.6×10^{-6} |
| ξ_{cl} [$1/^{\circ}\text{C}$] | 8.3×10^{-6} | |

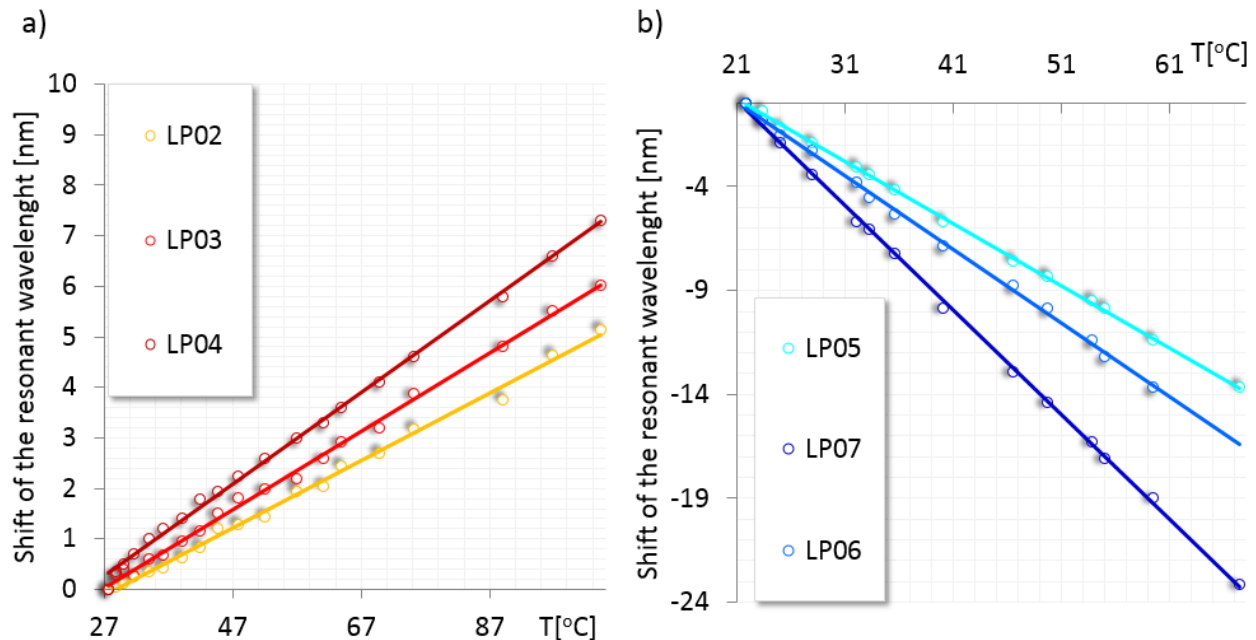
As can be seen from the results presented above, the predicted LPFGs behaviour versus the temperature was confirmed by the theoretical and experimental work. It is also important to notice that:

- the difference in the magnitude of the temperature sensitivities between the LPFGs based on PS1200/1500 fiber and the on SMF-28 fiber is clearly visible. This is due to the fact that the difference in the thermo-optic coefficients of the core and cladding materials for PS1200/1500 is

several times higher than for the SMF-28 fiber (according to the simulations carried out, this difference was 1.7 and 0.3 respectively for PS1200/1500 fiber and SMF-28 fiber).

- the LPFGs based on PS1250/1500 fiber written using the two methods show very similar temperature-sensing properties. Therefore, it can be stated that the temperature sensitivity in general is not so dependent on the fabrication method.
- regardless of the fabrication methods, LPFGs based on the PS1250/1500 fiber always shows a negative shift with an increase in temperature (while for the LPFG based on SMF-28 fiber), which indicated once again that the fiber properties have the main impact to the LPFGs thermal characteristic.

The thermal sensitivity is also different for a particular band in the transmission spectrum of the LPFG. Each attenuation band corresponds with a different mode order. For each particular mode there is a fractional power in both the core and the cladding. The resulting ratio leads to a higher sensitivity of the resonance wavelength in the case of the higher-order modes. As a result, the thermal sensitivity of the attenuation bands increases with the order of the cladding mode as well, as is shown in Fig. 6.2.4. Thermal sensitivities correspond with the coupling to the different cladding modes for the arc- and the UV-induced LPFGs are summarized in Table 6.2.4.



Tab. 6.2.4 Thermal sensitivity for arc-written (host fiber SMF-28; $\Lambda = 770 \mu\text{m}$) and UV-written (host fiber PS1250/1500; $\Lambda = 368 \mu\text{m}$) LPFGs versus mode order corresponding with the measured attenuation bands.

Tab. 6.2.4 Thermal sensitivity for arc-written and UV-written LPFGs versus mode order corresponding with the measured attenuation bands.

| Specification of the LPFG | Order of the mode, m | K_T^m [nm/°C] | Correlation coefficient, r |
|--|----------------------|--------------------|----------------------------|
| Host fiber: SM-28 Method: electric arc $\Lambda = 770 \mu\text{m}$ | 2 | 0.067 ± 0.009 | 0.996 |
| | 3 | 0.077 ± 0.011 | 0.997 |
| | 4 | 0.090 ± 0.014 | 0.998 |
| Host fiber: PS1200/1500 Method: UV laser $\Lambda = 368 \mu\text{m}$ | 5 | -0.287 ± 0.038 | 0.999 |
| | 6 | -0.354 ± 0.040 | 0.998 |
| | 7 | -0.504 ± 0.042 | 0.999 |

The LPFG temperature sensitivity depends also on the Λ of the grating, which strongly affects the order of the coupled cladding mode. In Figure 6.2.5 the measured (a) and the simulated (b) temperature response of the UV-induced LPFG with period of 226.8 is shown (parameters assumed for this LPFG simulation are given in Tab. 6.2.5 while temperature setting are this same like those presented in Tab. 6.2.3).

Tab. 6.2.5 Specification of the fiber and grating parameters applied to the UV-induced LPFG model with period of 226.8 μm based on the PS1250/1500 fiber.

| Fiber parameters | |
|-------------------------------------|----------------------------|
| r_{co} [μm] | 3.975 |
| n_{co} | 1.449333 |
| r_{cl} [μm] | 59.235 |
| n_{cl} | 1.44403 |
| Core material dispersion properties | set for boron doped glass |
| Clad material dispersion properties | set for fused silica glass |
| Grating parameters | |
| Grating period [μm] | 226.8 |
| Ind. Mod. | 0.000132 |
| Lenght [μm] | 47855 |

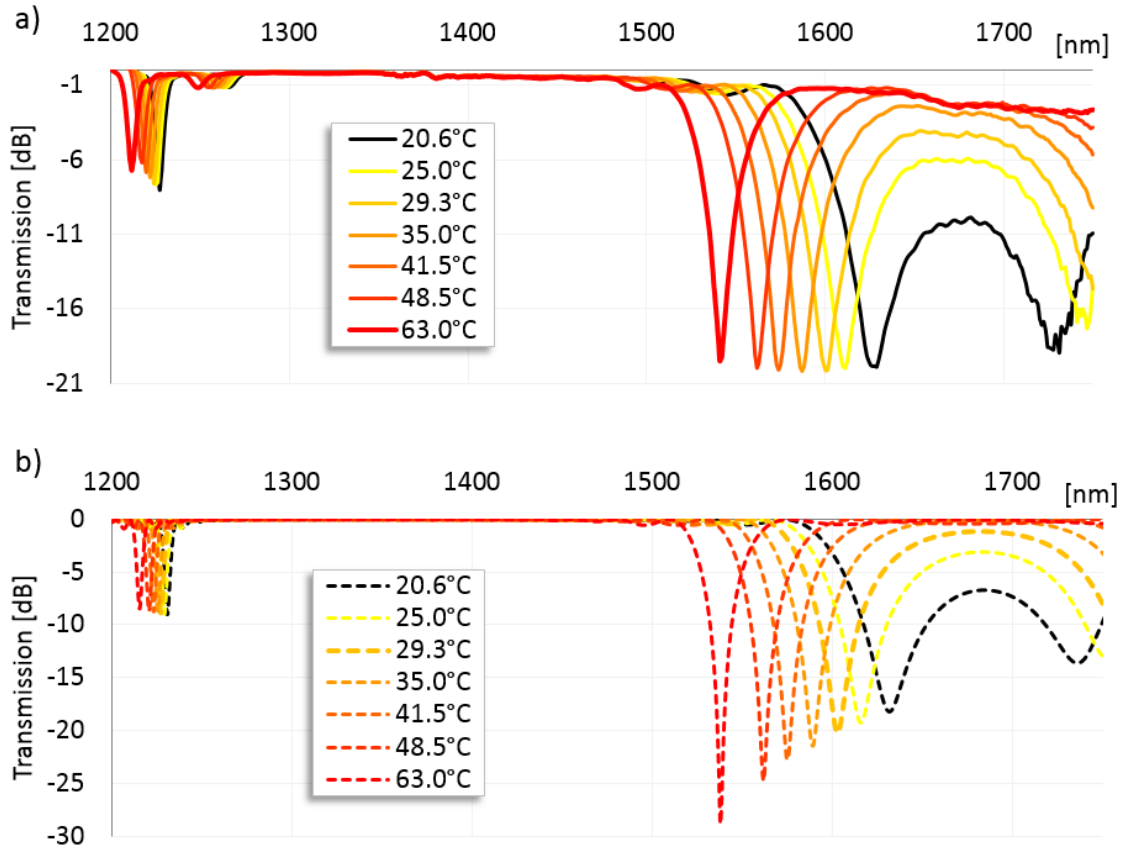


Fig. 6.2.5 Measured (a) and calculated (b) transmission spectra versus temperature for the UV-induced LPFG based on the PS1250/1500 fiber with period of 226.8 μm .

This grating exhibits a dual-peak in the transmission spectrum (associated with coupling of the $\text{LP}_{0,10}$ mode) which moved apart with increasing temperature. This property leads to unique sensing features of such LPFGs. The enhanced sensing capability becomes evident when it is noted that it is possible to double the sensitivity by referencing the measurement of the wavelength shift of one peak to another within such dual-peak structure. Nonetheless, even by measuring the temperature response of only one of the peaks of these bands, the high temperature sensitivity can be recorded. The thermal sensitivity, measured for the left-side peak of the attenuation band corresponding with the $\text{LP}_{0,10}$ mode, was determined to be $-3.0673 \pm 0.06 \text{ nm}/^\circ\text{C}$. By comparing this result to the thermal sensitivities shown in Tabs. 6.2.1. and 6.2.4 it' becomes clear that by increasing the period of the grating its sensitivity increases as well.

6.3 Impact of LC presence on the spectral properties of LPFGs

The presence of the LC layer on the LPFG will reorganize the effective indices of the cladding modes. The change in the attenuation bands position induced by adding the LC layer to the LPFG structure will be now determined by its thickness and by its refractive index. As was already described in Section 5.3, varying one of these parameters leads to a transition of the cladding modes from the cladding to the LC layer. Consequently, the reorganization of the remaining cladding modes happens to reconstruct the mode structure present before the transition. According to this phenomenon, we should expect displacement of the attenuation bands after coating with the LC layer the bare LPFG.

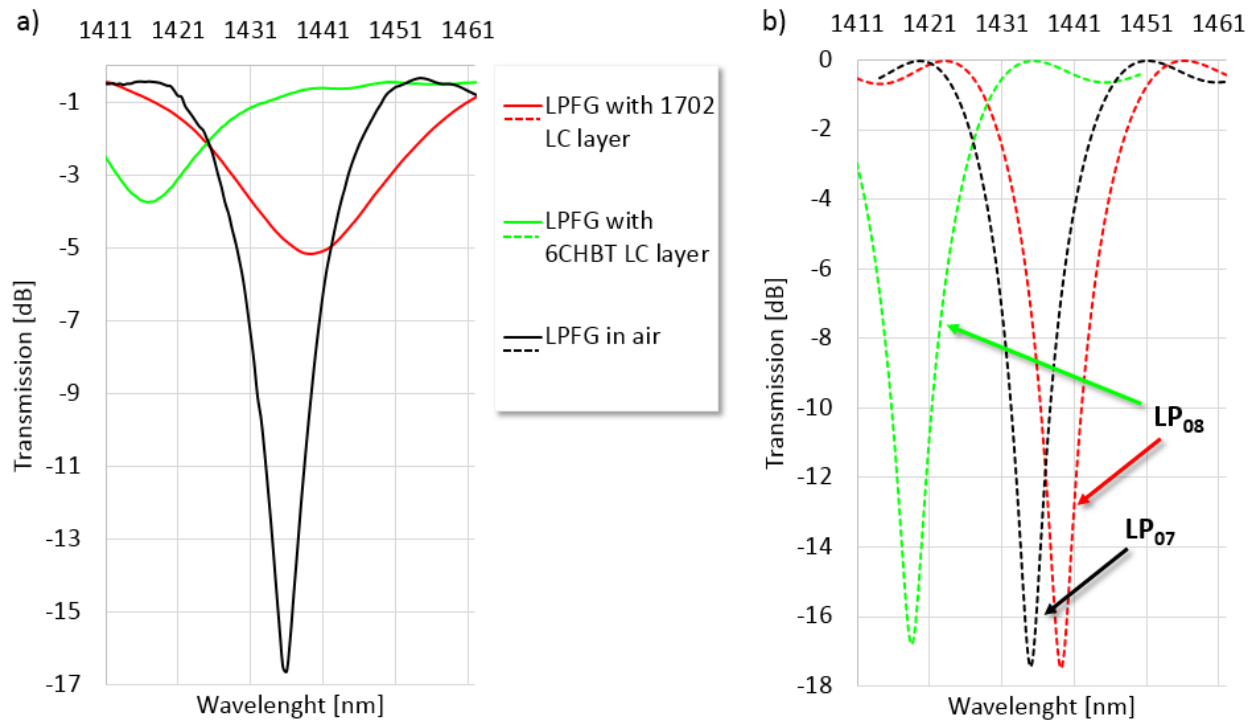


Fig. 6.3.1 Measured (a) and simulated (b) LPFG spectrum in air, with 1702 LC layer and with 6CHBT LC layer. The thickness for both LC layers was estimated to be of 2 μm .

In Fig. 6.3.1a the transmission spectra of the same host LPFG (arc induced, based on the SMF-28 fiber, with period of 400) measured in air, with 1702 LC and 6CHBT LC layers are presented. With help of the LC-LPFG transmission spectra simulations (presented in Fig. 6.3.1b) the thickness of the LC layers in both cases was found to be of 2.0 μm . By comparing transmission spectra for the LPFG in air and with 1702 LC layer it can be noticed that, indeed, the displacement of the attenuation band happens. This is due to the

fact that by adding the 1702 LC layer to the grating structure the reorganization of the modes occurs (since n_o for the 1702, estimated at a 1550 nm wavelength to be of 1.48, is higher than n_{cl}). Through the theoretical calculation it was found that visible attenuation in the spectral window corresponds with the resonance of the LP₀₇ mode and LP₀₈ mode when it's measured in air and with 1702 LC layer. From Fig. 6.3.1 it can be also seen that the resonant wavelength for the LPFG coated with 6CHBT LC is blue shifted compared to what was recorded when the LPFG was with the 1702 LC (the mode order corresponding with attenuation band measured for the LPFG with the 6CHBT LC layer is the same like for the 1702 LC layer). Such an effect could be expected since the n_o for the 6CHBT (estimated at 1550 nm wavelength to be of 1.507) is slightly higher than that for the 1702 LC and this difference should induce a blue shift. However, the magnitude of this displacement is not so large. This is due to the fact that the LC layer parameters which meet the transition region are characterized by the narrow variation range. Therefore, the measured attenuation bands in the LC-LPFG transmission spectrum will be usually those that already had time to recover after transition of the cladding modes.

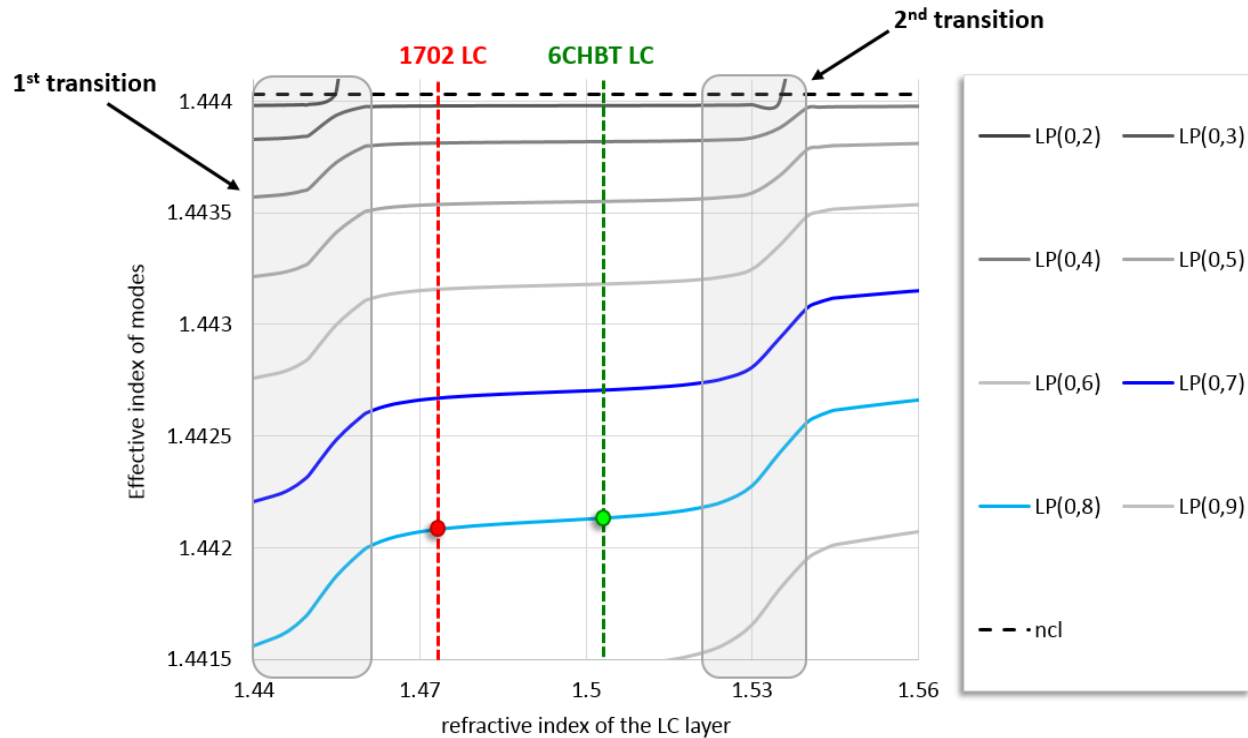


Fig. 6.3.2 Mode structure plot versus LC layer refractive index. The LC layer thickness is fixed to be 2 μm .

The interpretation of the LC layer impact on the LPFG transmission properties presented above have been proved through the calculation of the mode plot structure versus LC layer refractive index (Fig. 6.3.2). The

host fiber parameters were set for the SMF-28 fiber. The thickness of the LC layer was fixed in the simulation to be of 2 μm . Therefore, in regards to the result shown in Fig. 6.3.1 and accordingly to the Fig. 6.3.2 it can be stated that for the LPFG with the:

- 1702 LC layer the measured LP_{08} mode resonance is just after the 1st transition and in the moment when it is recovering the LP_{07} mode resonance vanished from the spectral window.
- 6CHBT the measured LP_{08} mode moved closely to the 2nd transition which should be reached for higher refractive index values.

From the results discussed above, it can be concluded that the scope of the LCs RIs investigated within this work will allow to obtain the transition effect of cladding modes. Detailed LCs properties are shown in Tab. 6.1.2. Additionally, in Fig. 6.3.3 the mode plot structure (with the same parameter settings as the one shown in Fig. 6.3.2) calculated for the wide range of the LC layer RI variation is shown. Ordinary and extraordinary (for the cases when the impact of the electric field on the LC-LPFG properties was investigated) RIs values for all the LCs studied here are marked with dashed lines (with the exception of the extraordinary refractive index values for the 1800b and 1110 LCs since they are characterized by the negative dielectric anisotropy). From Fig. 6.3.3 it can be also noticed that:

- the closer the LC refractive index is to the n_{cl} , the wider is the shift of modes effective refractive indices as a function of the relative variation of the layer refractive index (as was explained as well in Section 5.3.2). This behaviour is opposite to the effect of varying the overlay thickness, where the modes' effective refractive index shift is wider for higher layer refractive indices. Therefore, if the design is aimed for a material of variable refractive index (which is the case of the LCs for which their RIs can be adjusted e.g. by temperature or/and external electric field) the best choice is a refractive index close to that of the cladding of the LPFG.
- It has to be also pointed out that the cladding modes' distribution, obtained after coating the grating with a LC layer, is not frequently within the transition region (which is characterized by the highest sensitivity). This can later be compensated by choosing a different LC layer thicknesses (see Fig. 6.5.3 in Section 6.5.2) or by varying the LC layer RI by temperature and external electric field (see Section and Section). It also has to be kept in mind that the possible range of detection bandwidth is restricted near to the transition region. There is an additional phenomenon of vanishing attenuation bands. This limits the range of the LC layer-refractive index values if the LC-LPFG design is aimed for a detection of wavelength shift. Nonetheless, significant modification in

amplitude can be also exploited in the same manner as wavelength shift in a variety of sensor applications.

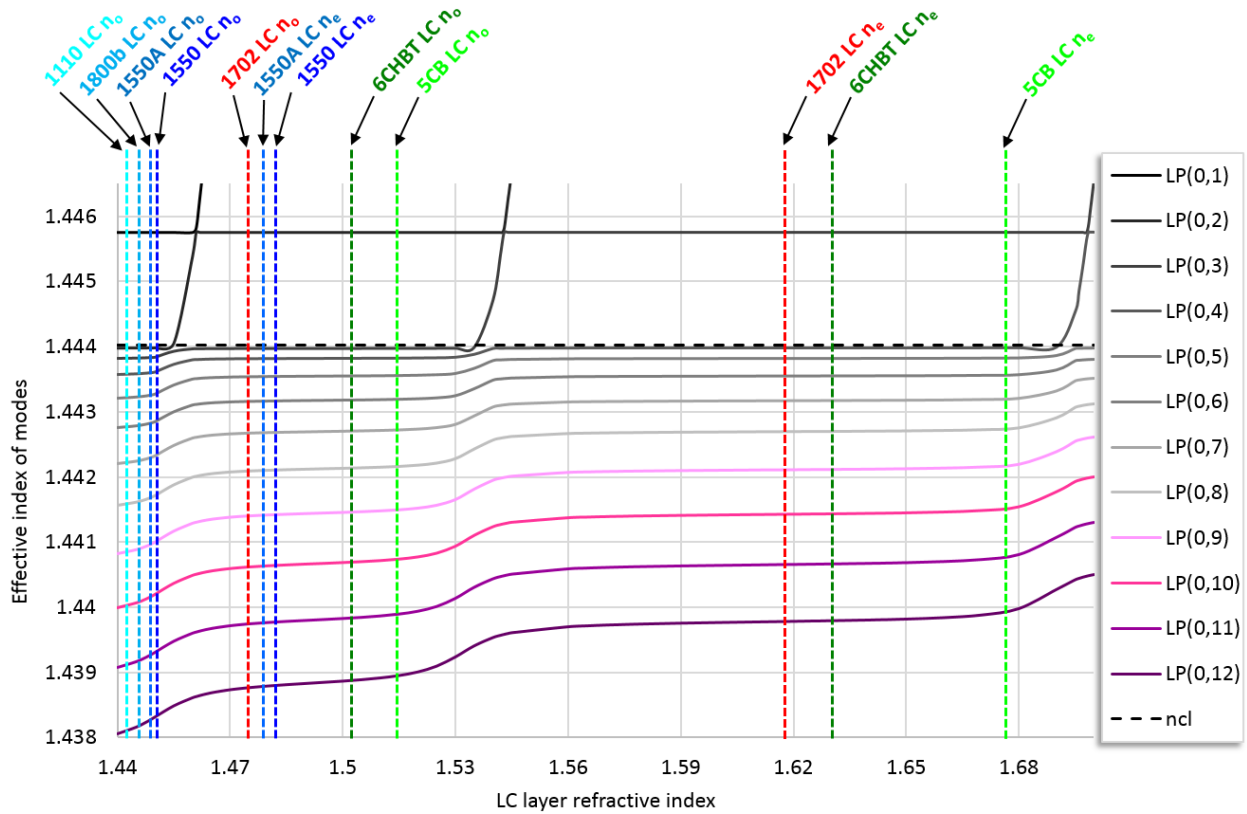


Fig. 6.3.3 Mode structure plot versus LC layer refractive index. The LC layer thickness is fixed to be $2 \mu\text{m}$.

RIs values for all LCs considered are marked with dash lines.

When the fiber host or grating fabrication methods are considered, the LPFGs show a very similar response to the LC layer presence. However, the impact of the LC layer on the LPFG spectral properties increased with decreasing period of the host LPFG. When the UV-induced LPFG with period of $226.8 \mu\text{m}$ was chosen as a host grating, the stronger response of the grating to the LC layer was measured. In this case, the vanishing of the attenuation band with dual-resonance peak was observed almost for all the LC layers applied (with exception for the 1550A LC layer with estimated thickness of $1.8 \mu\text{m}$ – see Fig. 6.5.7). Such an effect should not be surprising when we keep in mind that this type of attenuation band is characterized by the highest sensitivity to any external factors. As a result, the possibility to track this type of attenuation band is limited, since a narrow range of LPFG and LC layer parameters will meet a condition for the coupling of the cladding mode near its phase turning point; nevertheless, the possibility

to track the dual-resonant attenuation band for such LC-LPFGs designs could be obtained by tune them with temperature or/and electric field – see Section 6.4 and 6.5.

In addition to the analysis presented above, there is another issue which has to be discussed. When the LC layer was applied on the grating surface, the depth of attenuation bands decreased for all the LC-LPFGs experimentally studied. The consequence of this attenuation bands vanishing is negative in terms of their detection. When LC-LPFGs transmission spectra were simulated this effect was not observed. This is due to the fact that in this theoretical work it was assumed that the refractive index of LC layer is purely real. In reality there are scattering and material losses from the LC layer and they have an impact on the attenuation band depths. Apart from the imaginary part of the LC layer material, other additional effects may contribute to the vanishing of the attenuation bands, such as radiation losses of the cladding modes. However, this assumption permits to understand more easily the effects of the LC layer on a LPFG, and it still describes adequately the experimental results.

6.4 LC-LPFGs designed for thermal tuning

The thermal sensitivity response is an important behavior that must to be considered when a LPFG is designed to operate as a sensor in the presence of the LC layer. The sensitivity to temperature is determined by the composition of the LC-LPFG. The impact of the most important parameters in the context of the LC-LPFG thermal control is summarized in Tab.6.4.1. In general:

- Period of the grating determines the order of modes which can be investigated in the spectral range of interest (with a higher order mode, the measured temperature response of the LPFG increases).
- The host fiber determines the direction of the resonances shift which is associated with the difference in the thermo-optic coefficient of the core and cladding material (blue shift occurs with temperature rise for LPFG based on the PS1200/1500 fiber while for the LPFG written on the SMF28 fiber the red shift is measured versus temperature). The magnitude of this difference also corresponds with the magnitude of the LPFG thermal sensitivity (e.g. LPFGs fabricated on the PS1200/1500 fiber are characterized by the higher thermal sensitivity than the LPFGs produced on the SMF28 fiber).
- The thermal characteristic of the LC ordinary refractive index n_o (e.g. the rate or sign of n_o changes with the temperature) and the LPFG sensitivity to the presence of the LC layer (mainly depends from RI and thickness LC layer) modify the thermal response of the LPFG itself.

From the statements above, it can already be noticed that the LC-LPFG thermal sensitivity can be designed with remarkable flexibility. In particular, as was already predicted in Section 5.3, the LC-LPFGs can exhibit:

- positive or negative responses to the temperature (regardless of the type of the host fiber used to produce the LPFG),
- enhancing of thermal sensitivity,
- switching of their transmission spectrum in specific temperatures,
- compensating for their thermal effect by a proper choice of the LC layer.

In this section the experimental results are presented, which empirically confirm the LC-LPFG features listed above.

6.4.1 Towards tuning of the thermal sensitivity of LPFGs by using LC

In this section it is demonstrated that the LC-LPFG temperature sensitivity may be tailored in a wide range by a suitable choice of the LPFG host and the LC material.

Thermal tuning rate of change of the attenuation bands in the LC-LPFG transmission spectrum will be mainly determined by the:

- refractive indices thermal characteristic of the LC material selected as a grating coating (in addition, of course, to the thermal sensitivity of the LPFG itself). For example, if as a layer of the LPFG the HB LC is chosen, continuously tunable functionalities of the LC-LPFGs could be expected in the temperature range corresponding with the LC nematic phase. When the LB LC is selected as a grating layer, this principle should also apply, except for the temperature in which the n_o thermal characteristics intersect with the thermal characteristic of the n_{cl} (theoretical description of this property is presented in Section 5.3.4 and its experimental investigation is shown in Section 6.4.2).
- thickness of the LC layer will define the temperature induced LC RIs variation range where the mode transition phenomena can take place. As a result, by properly defining this value, the LC-LPFG thermal sensitivity magnitude can be adjusted as well.

Simultaneously, the presence of the LC layer on the bare grating will have an impact on the attenuation band shift direction. A detailed description of relations between the host fiber and LC layer properties,

which determine the direction of attenuation bands displacement, was already explained in the Section 5.3.4. Here they are schematically summarized in Tab 6.4.1, in order to clearer present the LC-LPFG thermal behaviour.

Tab. 6.4.1 Summarized relation between the host fiber and LC layer properties, which determine the direction of attenuation bands shift (without and with temperature variations). The K_T [nm/°C] is the thermal sensitivity of the LC-LPFG.

**Depends strongly on the temperature-induced rate changes in the n_{LC} value.*

| | RI for the air/LC layer | Host fiber | |
|--------------------------|-------------------------|---|---|
| | | SMF-28 | PS1250/1500 |
| no temperature variation | 1 | - | - |
| | $n_{LC}(T) \uparrow$ | Blue shift of the λ_{res} | |
| | $n_{LC}(T) \downarrow$ | Red shift of the λ_{res} | |
| temperature increase | 1 | Red shift of the λ_{res} | Blue shift of the λ_{res} |
| | $n_{LC}(T) \uparrow$ | *from $K_T \downarrow$ to $K_T \uparrow$ but with opposite sign | $K_T \uparrow$ |
| | $n_{LC}(T) \downarrow$ | $K_T \uparrow$ | *from $K_T \downarrow$ to $K_T \uparrow$ but with opposite sign |

The above description of the LC-LPFG thermal response was confirmed by the experimental and theoretical work. In Fig. 6.4.1 measured and calculated transmission spectra for the arc-induced LPFG coated with 1702 LC layer are shown. The host LPFG has period of 400 μm and is based on the SMF-28 fiber. Thanks to the performed simulations, the thickness of the LC layer could be estimated to be of 2 μm . It was also possible to determine that the coupling of the $LP_{0,8}$ mode is associated with the attenuation band investigated here (located in room temperature at 1439.5 nm). From the results presented below it can be instantly noticed that the LC-LPFG thermal response depends primarily on the temperature range of operation. Namely, for a temperature range:

- from 25.0°C to 69.1°C (1st) the attenuation band shifts toward longer wavelengths with temperature rise,
- from 76.5°C to 85.0°C (2nd) the attenuation band shifts toward shorter wavelengths with temperature rise.

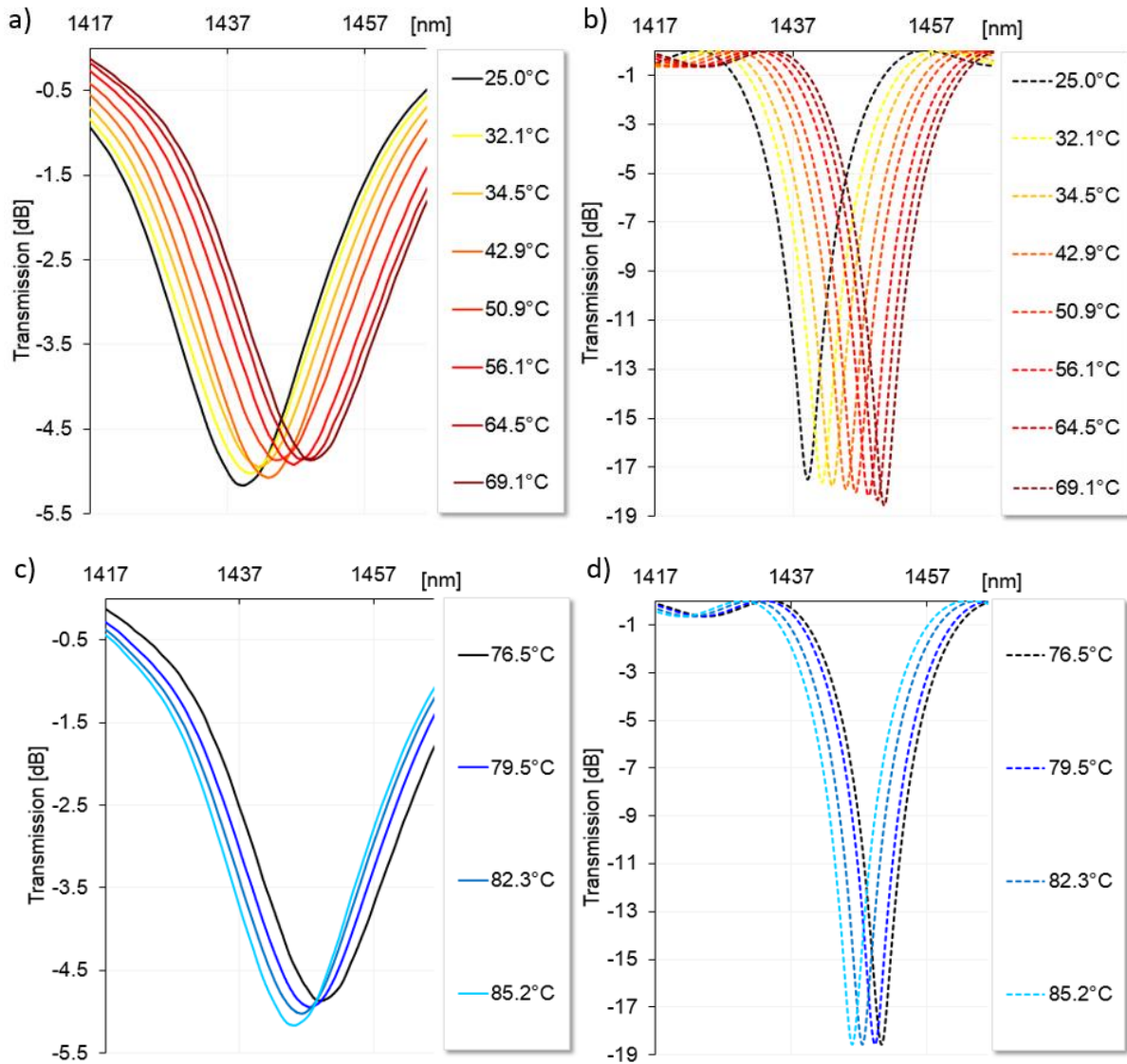


Fig. 6.4.1 Measured (a,c) and simulated (b,d) transmission spectra of the arc-induced LPFG (period: 400 μm ; host fiber: SMF-28) coated with the 1702 LC layer. The thickness of the 1702 LC layer was estimated to be 2 μm .

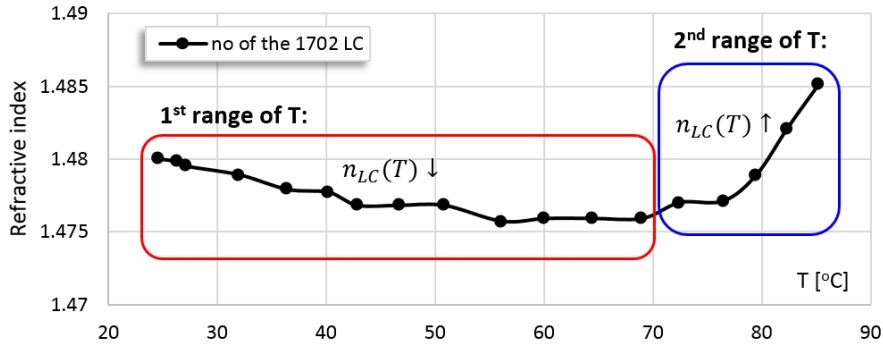


Fig. 6.4.2 Thermal characteristic of the n_o of 1702 LC estimated for wavelength 1550 nm. The temperature range corresponding with the nematic phase of 1702 LC.

This phenomenon can be understood through a close look at the n_o thermal characteristics for the 1702 LC from Fig. 6.4.2, where its estimated values for the wavelength of 1550 nm are shown. Therefore it can be noticed that for the:

- 1st temperature range the n_o decreases with temperature,
- 2nd temperature range the n_o increases with temperature.

Consequently, the behaviour of the thermal tuning of such a LC-LPFG design is in accordance with the principles set out in Tab. 6.4.1.

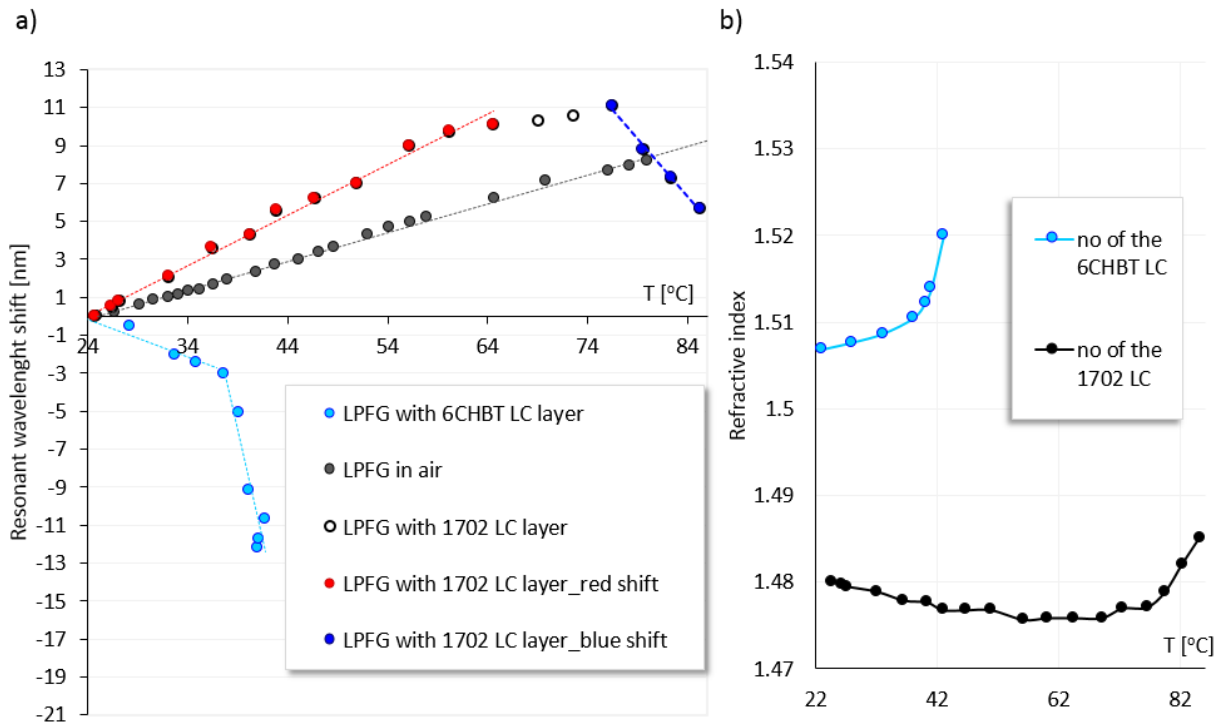


Fig. 6.4.3 a) Measured thermally induced shifts of the resonant wavelength for this LPFG in air and coated with 1702 LC or 6CHBT LC. b) Thermal characteristics of the n_o for the 1702 LC and 6CHBT LC.

Measured thermal induced shift of the resonant wavelength for this LPFG in air and coated with 1702 LC is shown in Fig. 6.4.3. Clearly, for the 1st temperature range of operation the impact of the LC surrounding medium overrides the inherent thermal sensitivity of the grating. For the 2nd temperature range the presence of the LC layer changes the sign of LPFG thermal response. The magnitude of the attenuation band shift induced by the temperature is also higher than that of the LPFG itself. Additionally, the temperature-induced resonant wavelength shifts measured for the same LPFG host but coated with 6CHBT LC is shown in Fig. 6.4.3 (transmission spectra versus temperature for this sample are presented in Section 6.4.2). The n_o of the 6CHBT LC always increases with temperature. As a result, thermal response of the LPFG with 6CHBT LC layer has a negative sign in the whole temperature range investigated here (which corresponds to the LC nematic phases). Thus, the thermal tuning of this sample is similar to tuning the LPFG coated with 1702LC layer, when its transmission spectra are measured in the 2nd temperature range of operation. The main difference is the magnitude of their thermal sensitivities. For 6CHBT LC layer the LC-LPFG thermal sensitivity is much greater than for the 1702 LC layer. This is mainly due to the fact that the n_o rate of change induced by temperature is much higher for the 6CHBT LC than for the 1702 LC (comparison of the n_o thermal characteristics for the 1702LC and 6CHBT LC is shown in Fig. 6.4.3b). As a result high-efficient thermal tuning could be achieved for the LPFG coated with 6CHBT LC.

Tab. 6.4.2 Thermal sensing properties of arc-induced LPFG based on SMF-28 fiber in air and coated by the 1702LC layer and by the 6CHBT LC layer. The grating period is of 400 μm .

| | Surrounding medium | | | | |
|--|--------------------|------------------|-----------|----------------|-----------|
| | air | 1702 LC layer | | 6CHBT LC layer | |
| T range of operation [°C] | 25.0-90.0 | 25.0-69.1 | 76.5-85.0 | 24.0-33.0 | 33.0-41.5 |
| Thermal sensitivity K_T [nm/°C] | 0.1608 | 0.2649 | -0.6106 | -0.2049 | -2.2783 |
| Mode corresponding with the measured attenuation band | LP ₀₇ | LP ₀₈ | | | |
| Resonant wavelength [nm] of the band measured at room T | 1435.0 | 1439.5 | | 1417.4 | |

It also has to be noted that the thermal sensitivity dependence of the LC-LPFGs shows a non-linear behavior. In general, such a behavior has to be expected since the response of the LPFG to the LC refractive index and the thermal characteristic of the LC refractive indices are non-linear. However, it is possible to distinguish the respective temperature ranges for which LC-LPFGs will exhibit a near-linear thermal

response. This will allow to estimate the values of LC-LPFG thermal sensitivities. Tab. 6.4.2 provides a summary of the measured thermal sensitivities for the LC-LPFGs discussed above.

Interesting results were also achieved when the UV-induced LPFG coated by the 1702 LC layer was tuned by temperature. This grating had short period of $226.8 \mu\text{m}$ and in the air its transmission spectrum exhibits a dual-resonant attenuation band (see Fig. 6.2.5). Unfortunately, after coating the LPFG with the 1702 LC, the dual-resonant attenuation band was not observed anymore. Thanks to the performed simulation, it was found that this attenuation band (corresponding with the $\text{LP}_{0,11}$ mode) is centered at 1672 nm , therefore its resonant wavelength was outside of the experimentally investigated spectral range. Further calculations of the thermal effect also showed that its resonant wavelength is close to the phase-matching turning point at room temperature (the thickness of the LC layer was estimated to be of $2.1 \mu\text{m}$). Consequently, by exploring the LC-LPFG thermal sensitivity, the dual resonant band could be generated again in the LC-LPFG transmission spectrum. With increasing the temperature value it splits into the left- and right peaks which move in the opposite directions (see Fig. 6.4.4).

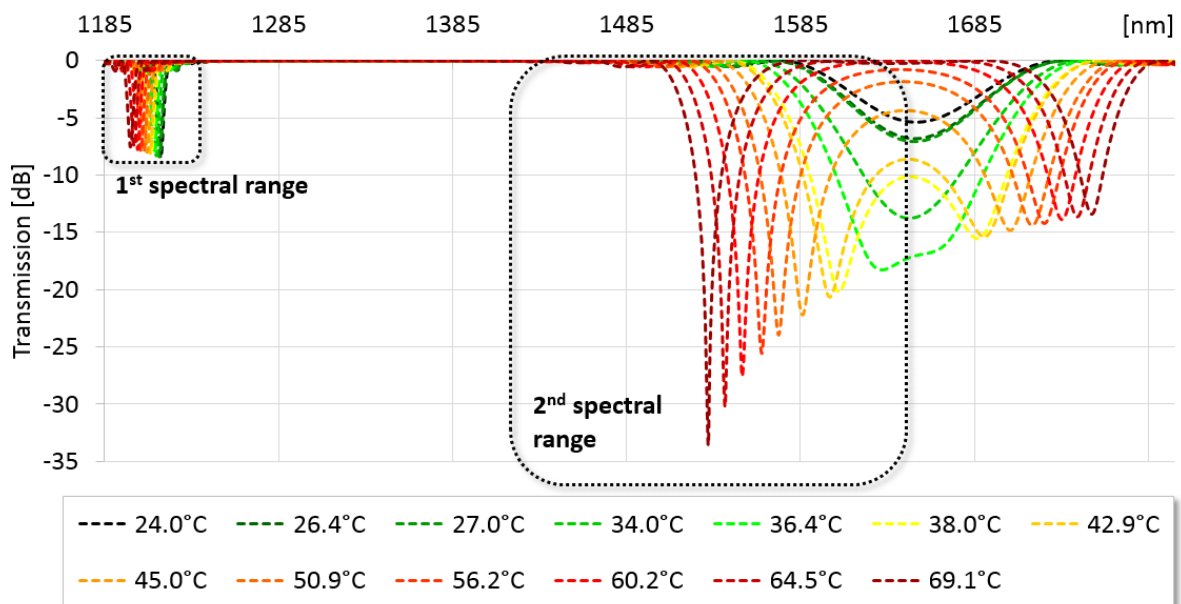


Fig. 6.4.4 Simulation of the LC-LPFG thermal response. The host LPFG has UV induced period of $226.8 \mu\text{m}$ and based on the PS1200/1550 fiber. As a LC layer the 1702 LC was chosen. . The thickness of the 1702 LC layer was estimated to be $2.1 \mu\text{m}$.

The theoretical calculations presented above are in accordance with the experimental work. As is presented in Fig. 6.4.5, where experimental LC-LPFG transmission spectra versus temperature are shown:

- for the spectral range from 1185 nm to 1240 nm (designated in Fig.6.4.4 as a 1st one) it was possible to track thermally induced changes of the attenuation band corresponding with the LP_{0,10} mode. This band shows blue shift with increasing temperature.
- for the spectral range from 1400 nm to 1600 nm (designated in Fig.6.4.4 as a 2nd one) when the temperature rises, the “new” attenuation band can be observed. As can be deduced from the analysis presented above, this is the left-side peak of the dual-resonant attenuation band blue shifted when the ambient temperature rises.

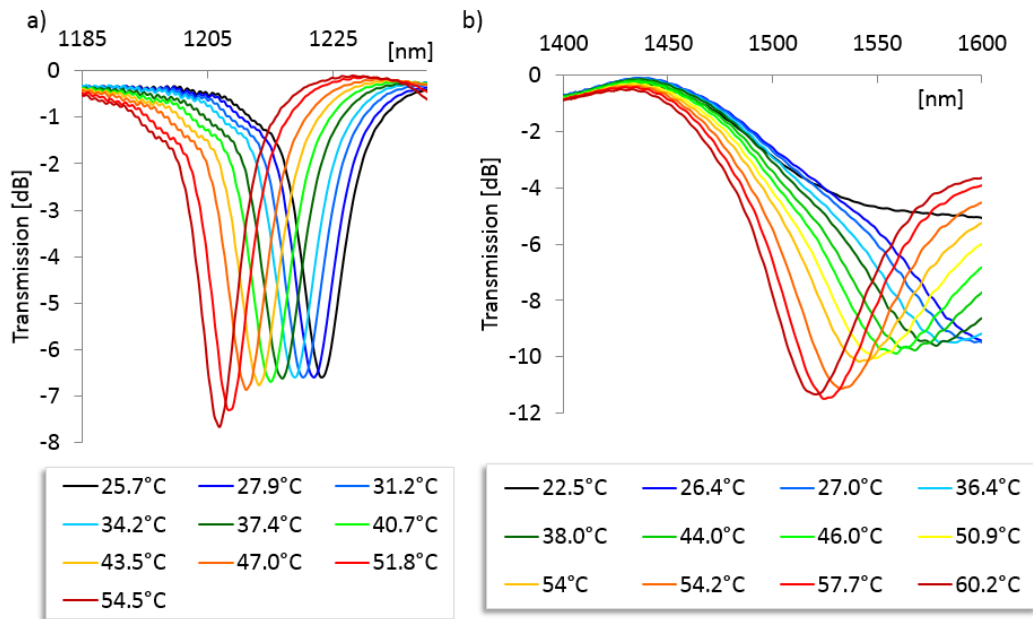


Fig. 6.4.5 Measured transmission spectra of the UV-induced LPFG (with period of 226.8 μm ; based on PS1250/1500 fiber) coated with 1702 LC versus temperature.

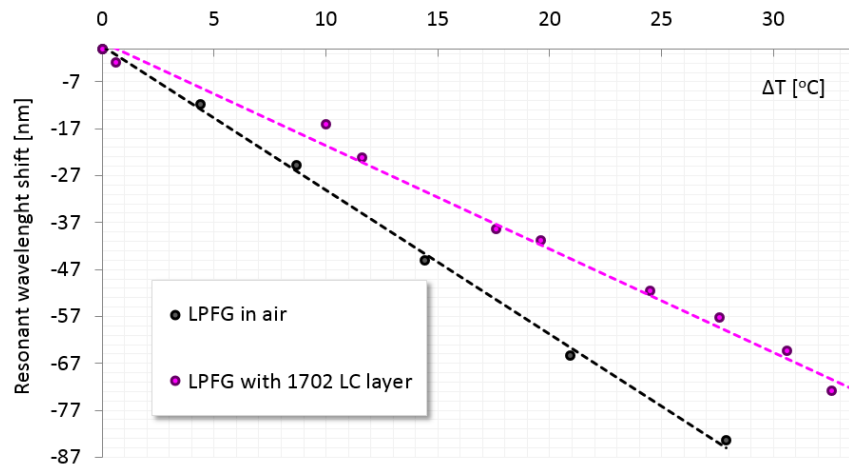


Fig. 6.4.6 Measured temperature induced shifts in the 2nd spectral range for the UV-induced LPFG (with period of 226.8 μm ; based on PS1250/1500 fiber) in air and with 1702 LC.

The blue shift measured for this sample should not be surprising, even if the n_o thermal characteristic of the 1702 LC increases within temperature operational range (the temperature variation investigated here corresponds with the 1st temperature range of operation indicated in Fig. 6.4.2). First, the internal thermal sensitivity of the LPFGs based on boron co-doped fibers is relatively high (its thermal sensitivity is several times higher than for the gratings based on the SMF-28 fibers). Secondly, the temperature-induced rate of change in the n_o value for 1702 LC are less significant than for other MB LCs used in the experimental work (e.g. for the 1702 LC the maximum change in the n_o value from 22°C to 42°C is more than 4 times smaller than this change over this same temperature range for the 6CHBT LC). As a result, the measured LPFG thermal sensitivity decreases when the 1702 LC layer is added to its structure. The measured temperature induced shifts for the LPFG in air and with 1702 LC are shown in Fig. 6.4.6 and Tab. 6.4.3 shows a comparison of thermal sensitivity values estimated for these two cases.

Tab.6.4.3 Thermal sensitivities measured for the UV-induced LPFG (with period of 226.8 μm ; based on PS1250/1500 fiber) in the 2nd spectral range when the grating is in air and with 1702 LC layer.

| | K_T [nm/°C] | Mode of operation |
|---------------|---------------|--------------------|
| air | -3.0673 | LP _{0,10} |
| 1702 LC layer | -2.2030 | LP _{0,11} |

A significant enhancement of the thermal sensitivity was also observed for the LPFG placed into the capillary filled with the LB LC mixture 1110. The host grating was fabricated by UV laser and had a period of 368 μm . In Figs. 6.4.7-6.4.9 the measured transmission spectra versus the temperature are presented for this sample. The simulated transmission spectra for results shown in Fig. 6.4.9 are also provided in the Fig. 6.4.10. As can be seen, a high variation in depth and resonant wavelengths of the attenuation bands was measured for this sample when temperature increased. The observed thermal sensitivity for such a LC-LPFG design based on the different response of the attenuation bands associated with modes with even and odd radial numbers. As was described in Section 5.4 (where a detailed theoretical explanation of these results is provided) modes with even radial numbers for this LC-LPFG are around the transition region. There is an additional phenomenon of vanishing of the attenuation bands. This phenomenon was not taken into account in the simulation (the LC refractive index was assumed to be purely real). In addition, the vanishing of the attenuation bands is also caused by the fact that the 1110 LC refractive indices are very close to the refractive index of the fiber clad. Moreover, at temperatures around 26°C (in the nematic phase) and 52°C (in isotropic phase) the LC refractive index is equal to the refractive index of

the clad. Therefore some disagreement can be noticed when the simulated (Figs. 5.3.13) and the measured transmission spectra are compared. Nevertheless, there is still a satisfactory correspondence between them.

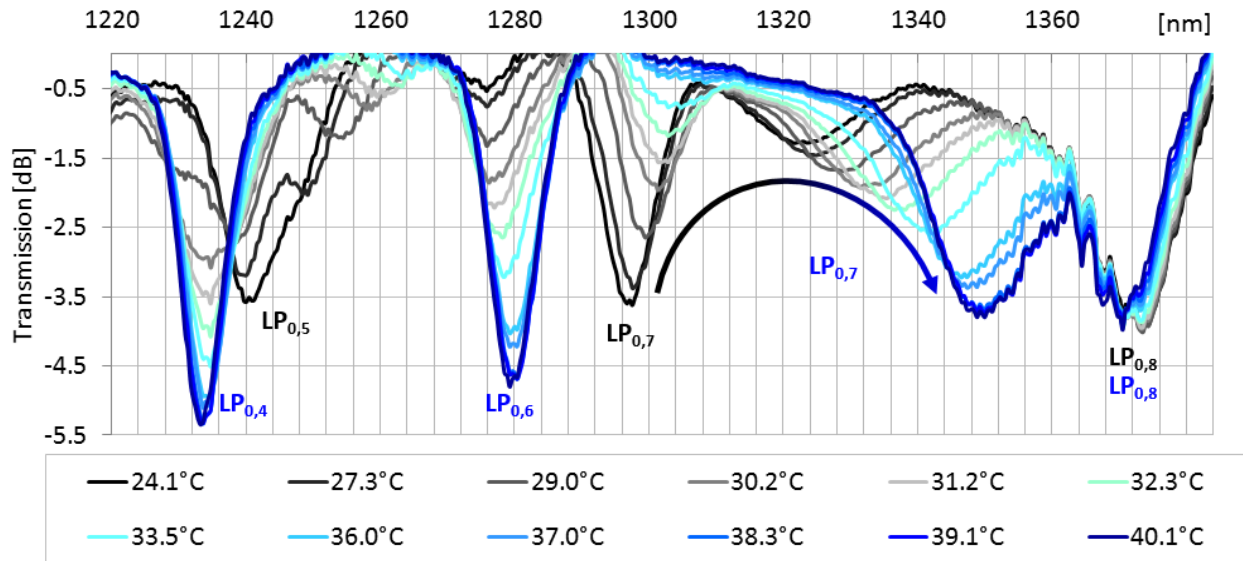


Fig. 6.4.7 Measured thermal response of the LPFG placed in the capillary and filled with 1110 LB LC. The spectral range covers attenuation bands associated with the lower modes order. The temperature range covers the nematic phase of the 1110 LB LC.

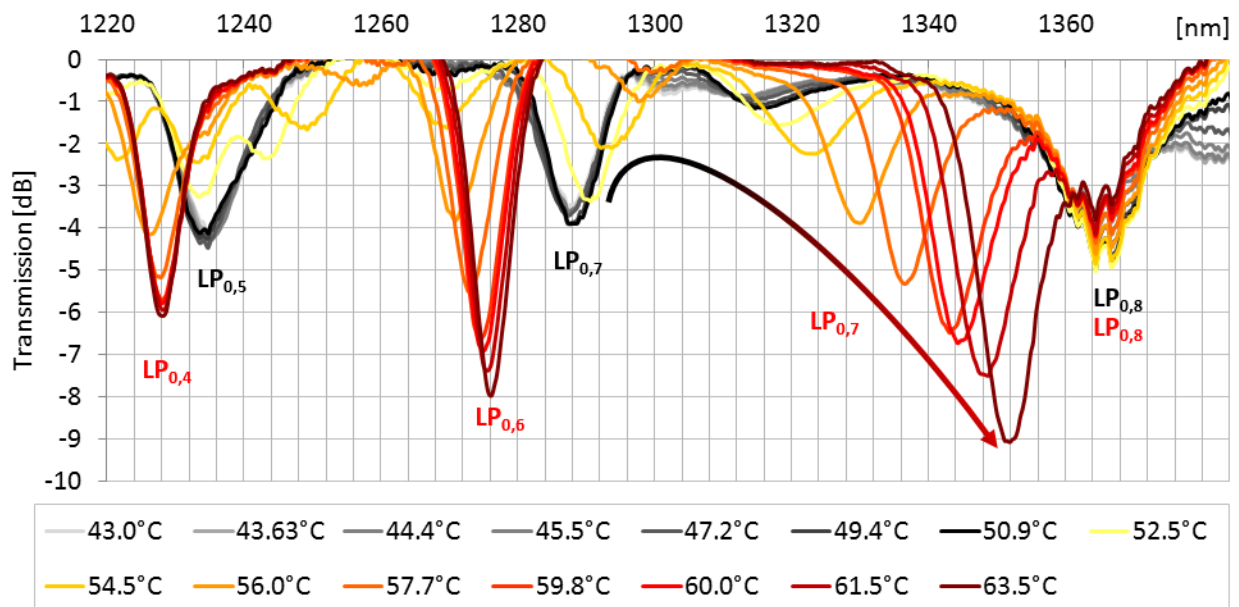


Fig. 6.4.8 Measured thermal response of the LPFG placed in the capillary and filled with 1110 LB LC. The spectral range covers attenuation bands associated with the lower modes order. The temperature range covers the isotropic phase of the 1110 LB LC.

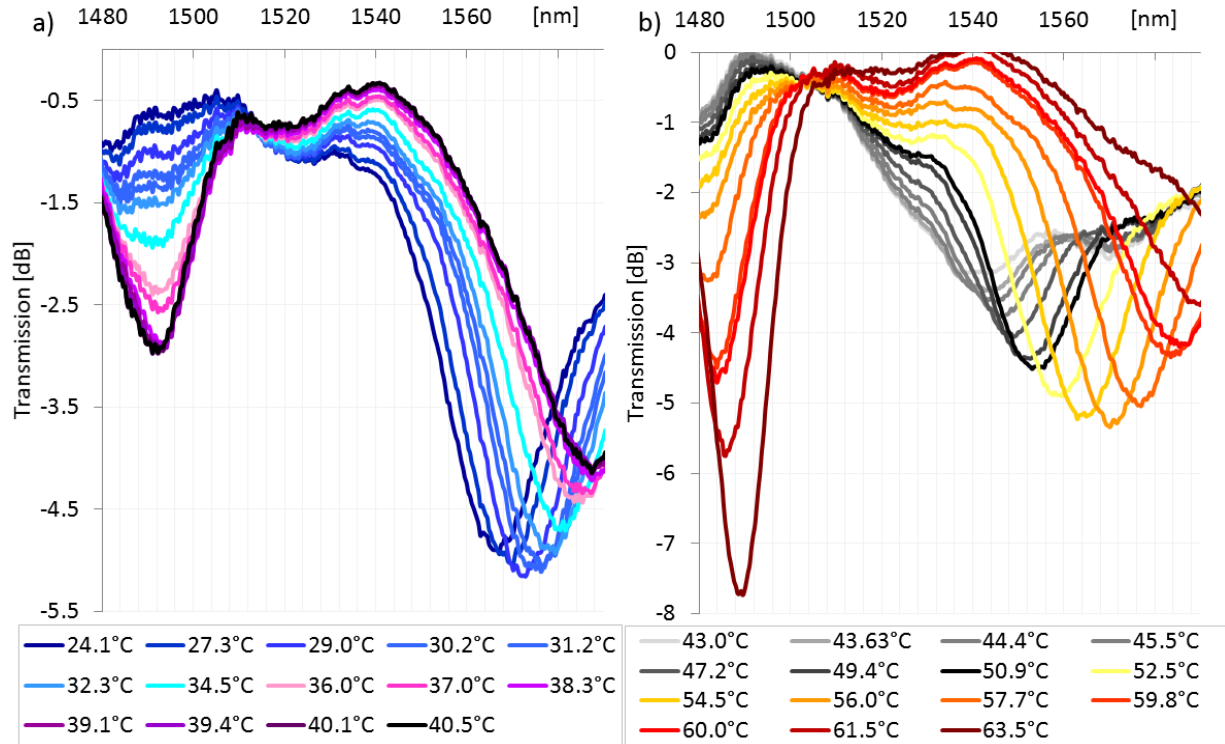


Fig. 6.4.9 Measured thermal response of the LPFG placed in the capillary and filled with 1110 LB LC. The spectral range covers attenuation bands associated with the higher modes order. The temperature range covers the nematic (a) and the isotropic (b) phases of the 1110 LB LC.

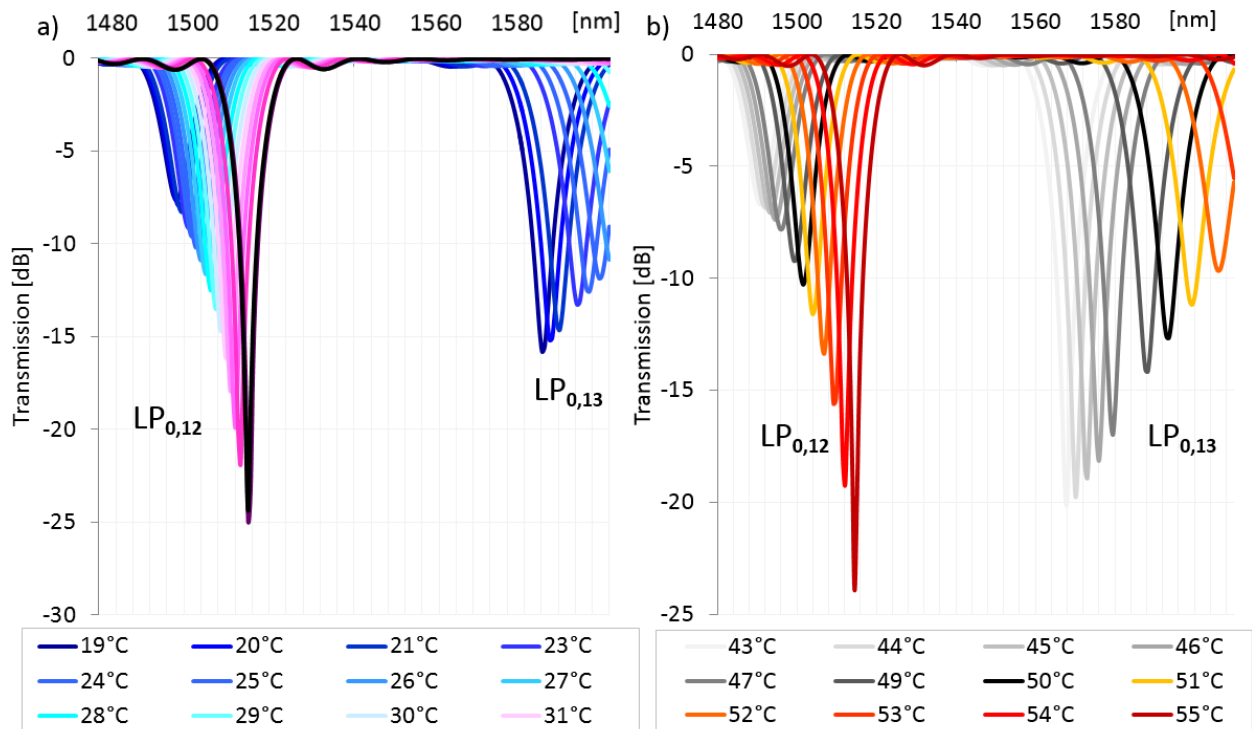


Fig. 6.4.10 Simulated thermal response of the LPFG placed in the capillary and filled with 1110 LB LC.

For example, the simulated effect of the LC-LPFG thermal tuning repeatability observed for the nematic and isotropic phase of the LC, was clearly observed in the experiment as well (compare Fig. 6.4.7 with Fig. 6.4.8 and Fig. 6.4.9a with Fig. 6.4.9b). This feature could be achieved thanks to the unique thermal characteristic of the 1110 LB LC used here (see Fig. 5.3.14). Namely, the 1110 LB LC n_o values coincides with the 1110 LC n_{iso} values. Consequently, the main difference between the LC-LPFG thermal response measured in the nematic and isotropic phases of the 1110 LC display a displacement in their attenuation bands'. This displacement is due to the thermal sensitivity of the host LPFG. As a result, all attenuation bands measured in the isotropic phase are blue shifted relative to those measured in the nematic phase (according with the thermal response of the LPFG based on the 1250/1500 fiber). In addition, a different dynamics of the thermally induced changes was observed when the LC-LPFG transmission spectra measured in the nematic and isotropic phases are compared. This effect is associated with a different slope of the thermal characteristic curve for the n_o and n_{iso} . Finally, it is also clearly seen that the depths of the attenuation bands measured in the isotropic phase of the LC are deeper than those recorded for the temperature range corresponding with the LC nematic phase. This is due to the fact that LC in the isotropic phase is characterized by smaller scattering losses. Through the theoretical analysis carried out for this sample it was also possible to determine a mode associated with the measured attenuation bands (designated in Figs. 6.4.7, 6.4.8, 6.4.10). It seems therefore that the reorganization between the modes with even and odd radial numbers occurs in the experiment and this effect is also in accordance with the theoretical calculation.

6.4.2 Switching the LC-LPFG transmission spectrum in specific temperatures

By operating close to the proper chosen temperature value, the switching capability of the LC-LPFG can be achieved. In Fig. 6.4.7 the experimental and simulated transmission spectra versus temperature for the arc-induced LPFG coated with 6CHBT LC layer are shown. The grating had a period of $400\ \mu\text{m}$ and was based on the SMF-28 fiber. The thickness of the LC layer for the theoretically investigated LC-LPFG model was estimated to be of $2\ \mu\text{m}$. The LC-LPFG thermal response was measured over a temperature cycle from 22°C to 53°C , therefore in the nematic and isotropic phases of the 6CHBT LC (the clearing temperature T_c for this LC is 43°C).

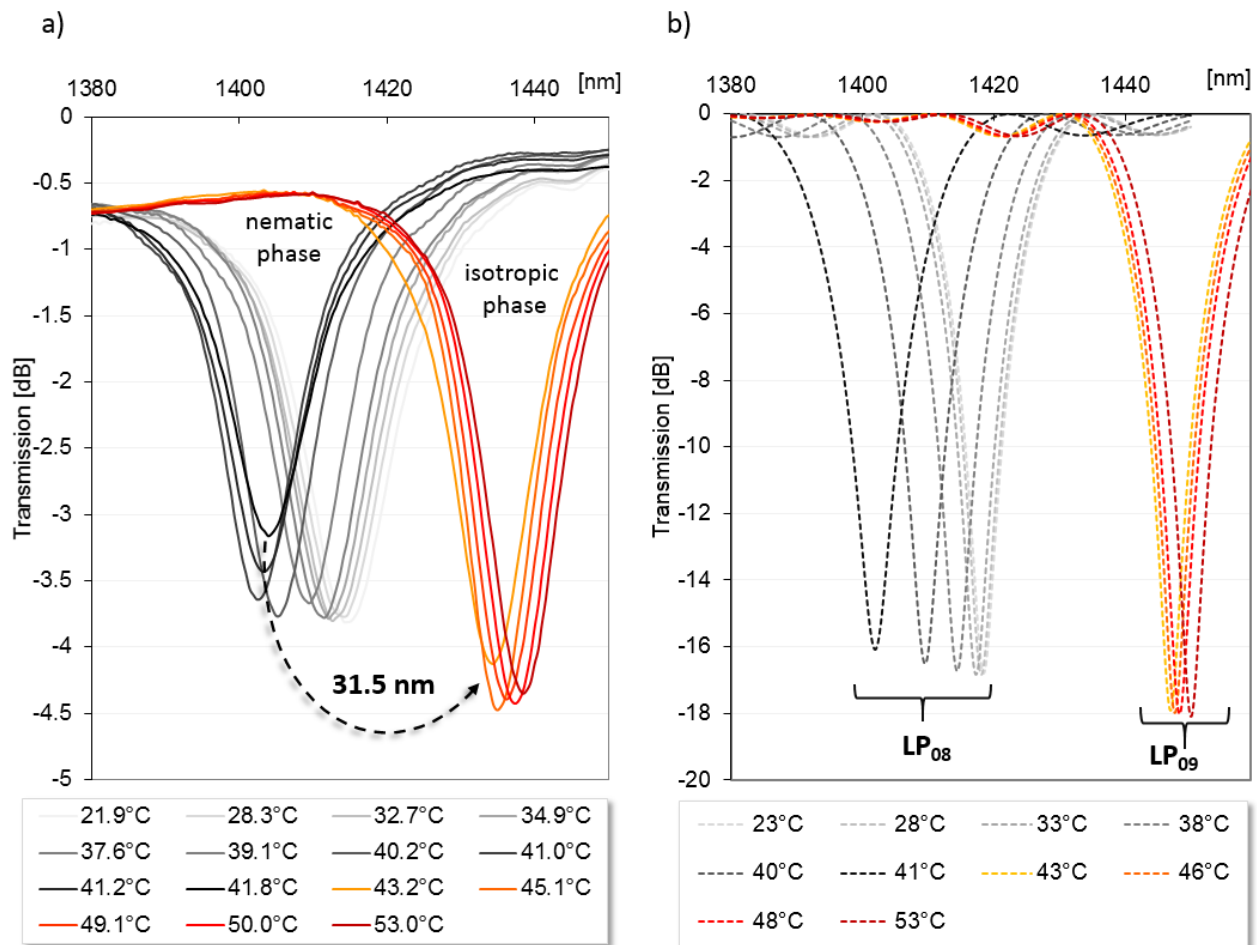


Fig. 6.4.7 Experimentally measured (a) and calculated transmission spectra versus temperature for the arc-induced LPFG (based on SMF-28; with period of $400\ \mu\text{m}$) with 6CHBT LC layer.

As can be noticed from the results presented above, fast switching of the attenuation band at T_c occurs over a temperature cycle of only 1.5°C . The attenuation band is red shifted up to $31.5\ \text{nm}$. This effect is

due to the fact that at T_c the sudden jump in the n_o value occurs. Thanks to the performed simulation, it was found that the transition of the cladding modes happens at this point (see Fig. 6.4.8). Precisely, in the investigated spectral range, the attenuation band corresponding with the LP₀₈ mode switches to the attenuation band which is associated with the LP₀₉ mode. It can be also remarked that the magnitude of the transition increases with the increasing mode order.

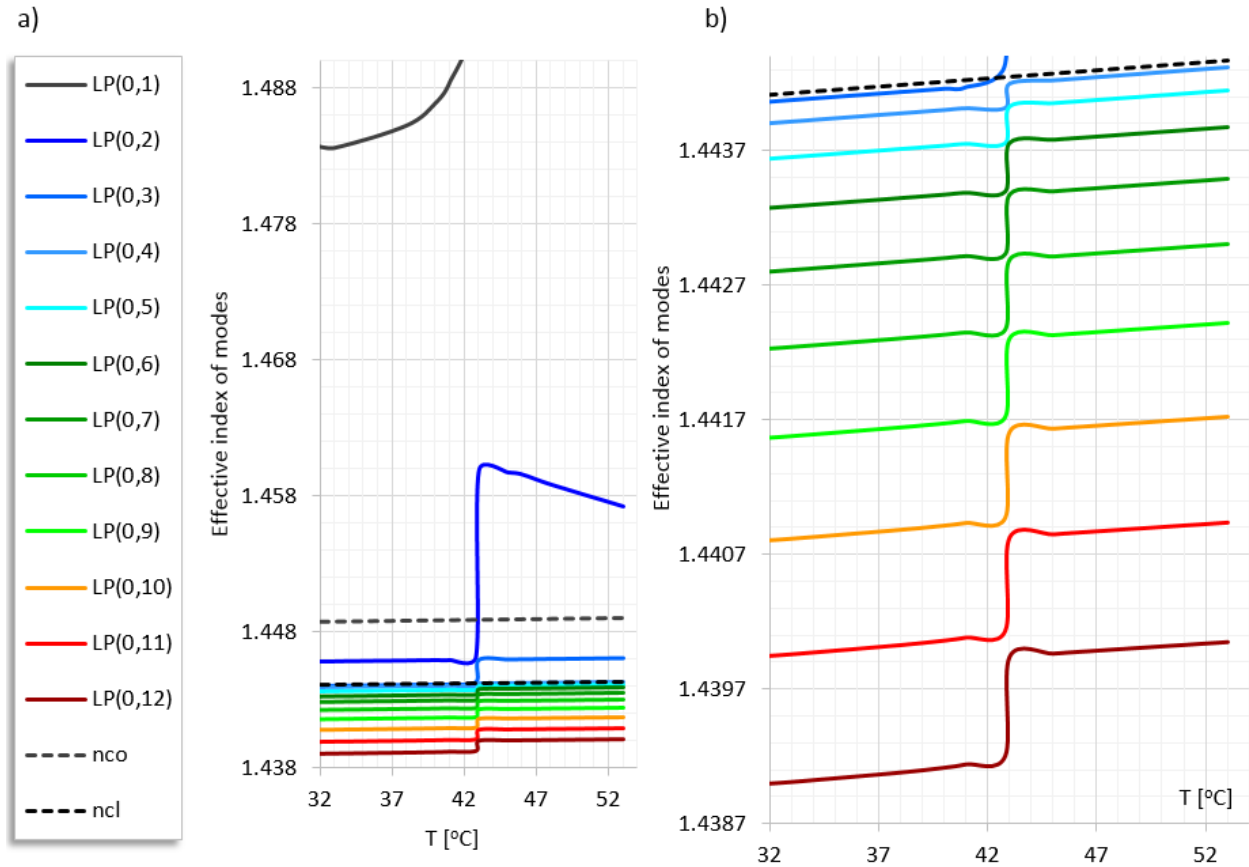


Fig. 6.4.8 Mode structure plot versus temperature for the arc-induced LPFG (based on the SMF-28 fiber) coated with 6CHBT LC layer. In (a) it is calculated for the 12 first modes while in (b) the thermal dependence for cladding modes effective indices is only presented.

Moreover, thermal tuning of such a LC-LPFG design is different in the nematic and the isotropic phases of the 6CHBT LC (as is clearly visible in Fig. 6.4.9, where the temperature-induced resonant wavelength shifts measured for this LC-LPFG are shown). Specifically, within the temperature range corresponding with the 6CHBT LC:

- nematic phase the attenuation band is shifted toward shorter wavelengths,
- isotropic phase the attenuation band is shifted toward longer wavelengths,

This LC-LPFG thermal response is directly related to the n_o thermal characteristic for the 6CHBT LC (presented in Fig.6.4.3) and is in accordance with Tab. 6.4.1, where relations between the host fiber and LC layer properties were summarized. In Tab. 6.4.4 the measured thermal sensitivity values (distinguished for the temperature ranges for which they show a near-linear dependence) are summarized as well.

Tab. 6.4.4 Thermal sensing properties of arc-induced LPFG (with grating period of $400\ \mu\text{m}$; based on SMF-28 fiber) coated by the LC 6CHBT LC layer.

| | temperature range of operation [°C] | | |
|---|-------------------------------------|-------------|------------------|
| | 21.9 - 37.6 | 37.6 – 41.8 | 43.2 – 53.0 |
| Thermal sensitivity K_T [nm/°C] | -0.2049 | -2.2783 | 0.4302 |
| Mode corresponding with the measured attenuation band | LP ₀₈ | | LP ₀₉ |

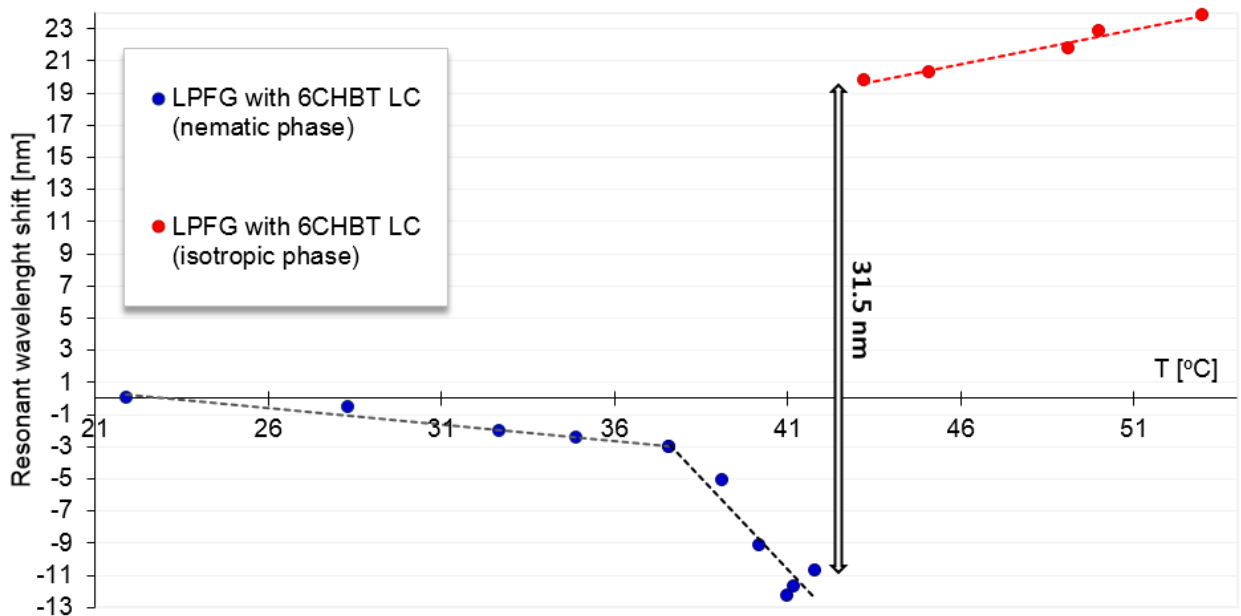


Fig. 6.4.9 Measured thermal induce shifts of the resonant wavelength for arc manufactured LPFG (with grating period of $400\ \mu\text{m}$; based on SMF-28 fiber) coated by the LC 6CHBT LC layer.

Interesting results were also achieved for the UV-induced LPFG with period of $226.8 \mu\text{m}$. As a coating material the 1550 LB LC mixture was chosen in this case. In Fig. 6.4.10 the thermal response of such a LC-LPFG design is presented. As can be seen, a strong modification of the LC-LPFG transmission spectrum occurs between temperatures from 36°C to 49°C : one band at 1229.5 nm , designated as 1^{st} one is splitting to two other bands, designated as $1^{\text{st.a}}$ and $1^{\text{st.b}}$. In addition one more band starts appearing, designated as 2^{nd} , and at 63°C it reaches the λ_{res} of 1426 nm . It has to be noted that in this experiment the temperature range of operation was within the LC nematic phase (unlike for the previously presented LC-LPFG, where switching occurred at T_c). Therefore, it can be stated that this unusual change of the transmission spectrum indicates the cladding modes transition phenomenon.

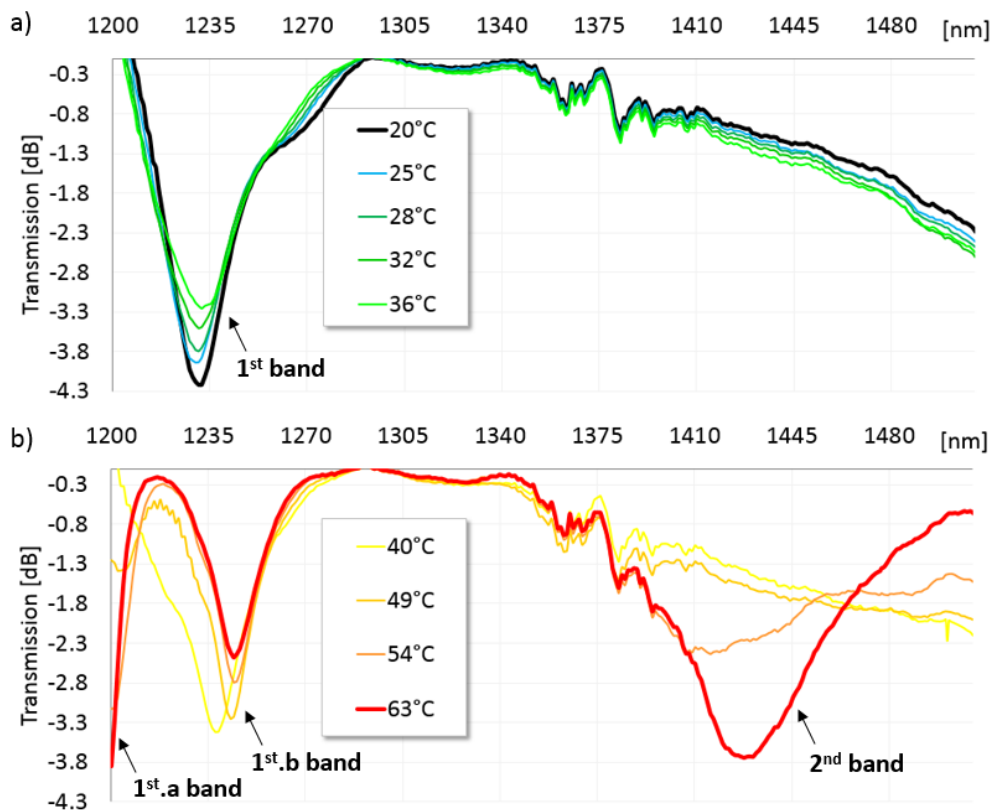


Fig. 6.4.10 Transmission spectra of the UV-induced LPFG (based on the PS1250/1500 fiber and with period of $226.8 \mu\text{m}$) coated with 1550 LC layer

In order to confirm this thesis, a series of simulations for this LC-LPFG were performed. As was expected, they showed that the transition of the cladding modes can occur within the investigated temperature range (see Fig. 6.4.11). Precisely, the transition from LP_{02} mode to LP_{01} mode with increasing temperature is clearly seen. The effect of the transition for the rest of the modes is not so pronounced. This could be

explained if we noticed that the thermal dependence of the LC layer RI, decreased the effective index of the modes. At the same time, the change of temperature increases their values and consequently reduces the transition effect. Nevertheless, the change of the mode structure is significant enough to have a clear impact on the transmission spectrum of the designed LC-LPFG.

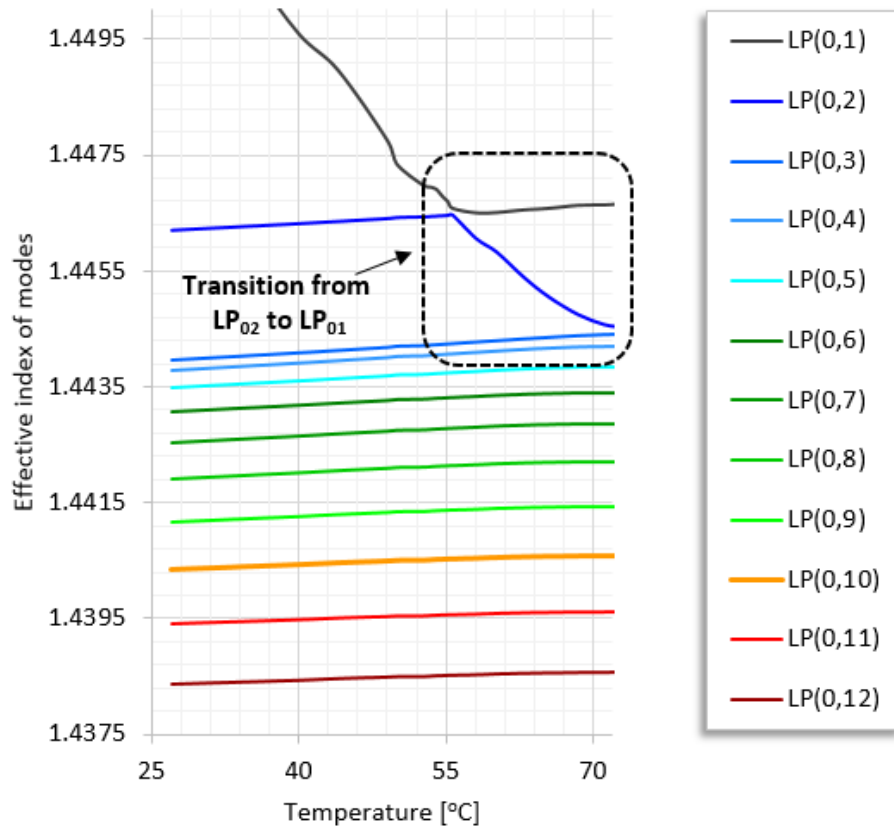


Fig. 6.4.11 Mode structure of the 12 first modes as a function of the temperature for the UV-induced LPFG (based on the PS1250/1500 fiber and with period of 226.8 μm) coated with 1550 LC layer.

The simulated LC-LPFG transmission spectra are shown in Fig. 6.4.12 The thickness of the 1550 LC layer was estimated to be of 3.5 μm . These values should not be surprising since the 1550 LC is characterized by a low n_o value (the lower the RI of layer, the higher thickness of the layer is required to reach the transition region). The experimental spectral range studied is marked there by a grey dash square. It was found that attenuation bands indicated in Fig. 6.4.10 as a 1st and 2nd are associated with the LP_{0,10} and LP_{0,11} modes, respectively.

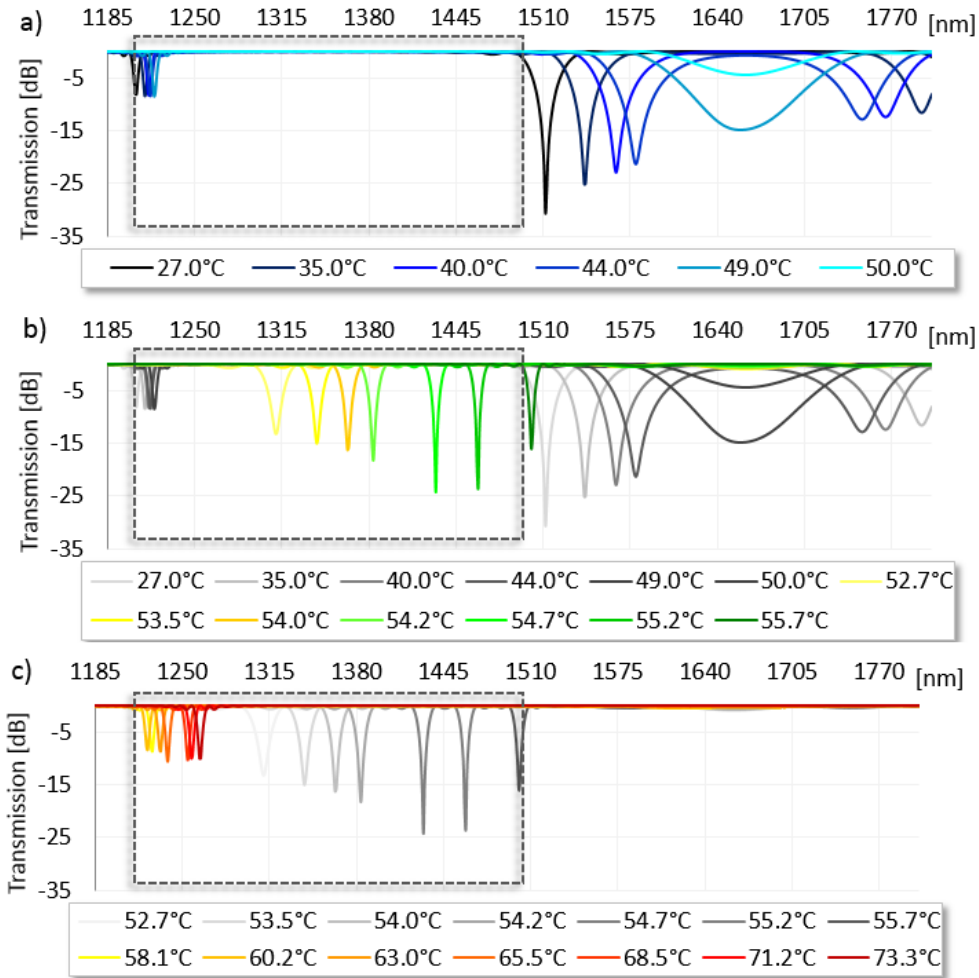


Fig. 6.4.12 Transmission spectra of the UV-induced LPFG (based on the PS1250/1500 fiber and with period of $226.8 \mu\text{m}$) coated with 1550 LC layer.

From Fig. 6.4.12 three main steps can be distinguished when this sample is tuned by temperature. With an increase of the temperature value:

STEP 1 (Fig. 6.4.12a): from 27°C to 50°C the 2nd dual-resonant attenuation band resonance, disappears (for this reason it was impossible to track its spectral range investigated experimentally). Simultaneously, the 1st attenuation band is slightly red shifted by the temperature change.

STEP 2 (Fig. 6.4.12b): From 52.7°C to 55.7°C the 1st attenuation band vanishes from the investigated spectral range. Concurrently, the 2nd attenuation band reappears (precisely it's the left-side peak) and is red shifted by an increase in temperature.

STEP 3 (Fig. 6.4.12c): Above 58.1°C only the 1st attenuation band is observed in the spectral window – corresponding with the 1st.a band measured in the experiment.

Hence it seems that the STEP 2 indicates a temperature variation where the transition of the cladding modes happens. Based on the analysis presented above, it can therefore be inferred that the experimentally measured LC-LPFG spectra are mainly between the STEP 1 and STEP 2. Consequently, there is a correspondence between the theoretical and the experimental results. By comparing them carefully some disagreements should be however noted, namely:

- In the experimentally measured spectra the border between steps is not clear. It rather appears that they overlap. For example, the simulations have failed to reveal the splitting of the 1st attenuation band. This effect is probably due to the fact that the LP_{0,10} mode is still in the reorganization process (which took longer than it was theoretically predicted). In addition, the LP mode approximation is limited in its accuracy within the modes transition region. By using the more precise hybrid-mode method it was shown in [110] that for LPFG coated with HRI layer there can be more than one resonance wavelength for the same cladding mode if the transition comes from a higher to a lower mode (which is this case, see Fig. 6.4.11).
- The difference between the measured and simulated temperatures, where the effects described above took place, can be eminent. These deviations can be explained by the fact that there are many parameters that can influence the thermal response of the LC-LPFG and not all of them can be perfectly determined (e.g. dopant concentration of the host fiber which strongly affect the LPFG thermal response, LC dispersion properties or orientation order of the LC molecules which have essential impact to the LC RI value). However, it has to be emphasized that the simulations of the LC-LPFGs are difficult and computational heavy task, even more so when their thermal response is analyzed as well. Therefore, the primary effort was put here to determine the principle of operation of its thermal tuning rather than an exact match of the results. Performed calculations allowed to qualitatively observe the thermal tuning of the devices LC-LPFG designed for this project. Furthermore, it is also worth noting that the effect of the appearance of the 2nd attenuation band in the LC-LPFG spectrum, takes place in a very narrow temperature range (around ~2°C according to the simulation). Thus, the accuracy of the measurements carried out in the experiment could be insufficient to follow (or keep track of) this phenomenon precisely.

The effective switching feature was also achieved for the UV-induced LPFG coating with LB LC mixture 1110. In this case the period of the grating was 368 μm. The LC layer for this sample was formed by filling the glass capillary where the LPFG was initially introduced with the LC (a detailed description of such a LC

layer application technique on the LPFG is presented in Section 6.1.4). This method gives the LC layer a thickness of $\sim 4.5 \mu\text{m}$. It has to be noted that the LC-LPFG structure studied here (see Fig. 5.1.1) now presents five layers (corresponding with the fiber core, the fiber clad, the LC layer, the silica glass layer surrounded by the 5th layer of air). A detailed theoretical analysis for this LC-LPFG sample was presented in Section 5.3.5. However, it seems justified to repeat a few basic observations as the following result interpretation will build upon these principles. First, when such a LC-LPFG device is thermally tuned, the attenuation bands associated with the modes with even and odd numbers will manifest a different thermal sensitivity. Secondly, the characteristic of the lower-order modes can change from a mode with an even radial number to a mode with an odd radial number during this transition.

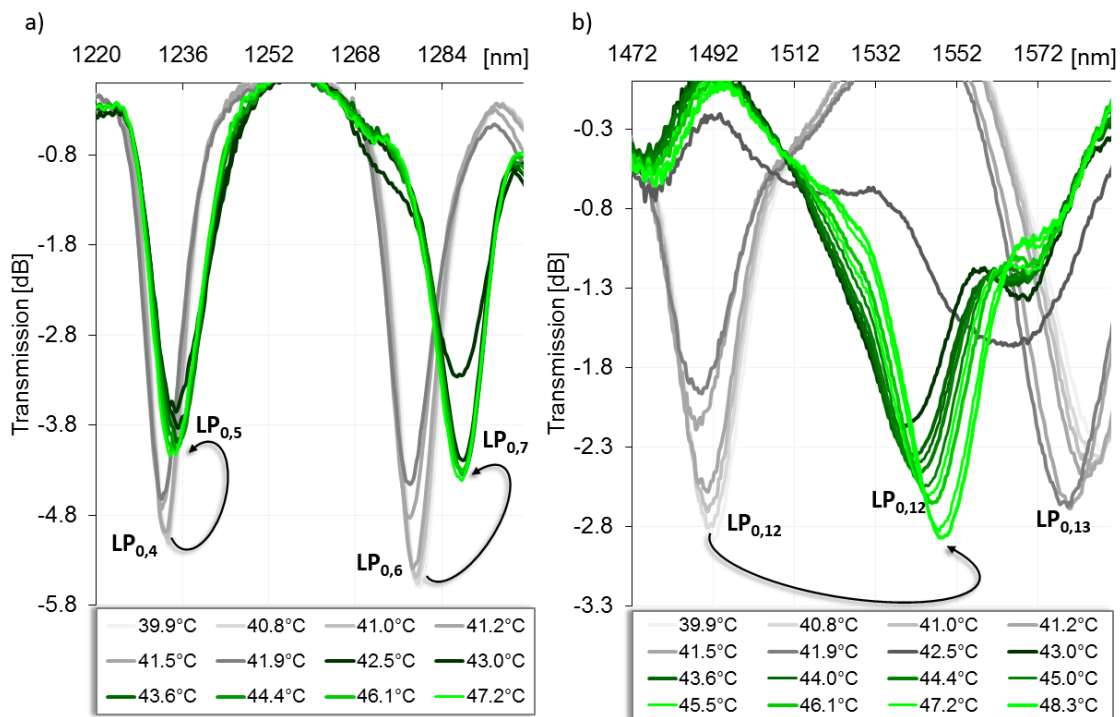


Fig. 6.4.13 Switching of the attenuation bands in the transmission spectrum of the UV-induced LPFG (with period of $386 \mu\text{m}$) coated by the 1110 LC close to 43°C (which is the T_c of the 1110 LC)

In Fig. 6.4.13. The transmission spectra versus the temperature for the LC-LPFG sample discussed here are presented. Through the theoretical work it was also possible to determine the modes associated with the measured attenuation and they are designated in Fig 6.4.13 as well. In this experiment the temperature range of operation was close to the 1110 LB LC T_c which is 43°C . At this point a fast switching was achieved over a temperature cycle of only 2°C . It is worth adding that the switching effect can also be obtained for this LC-LPFG by operating close to the temperature where the transition of modes with odd and even

radial numbers occurs. For example, by further heating the sample up to around a temperature of 52°C, an enhancement of the thermal sensitivity of the LC-LPFG was observed again (see Fig. presented in Section 6.4.1). In contrast to the switching effect at T_c , a smoother change of the LC-LPFG transmission spectrum was recorded then, over a temperature cycle of 8°C. In Fig. 6.4.14 the thermally induced attenuation bands (corresponding with $LP_{0,4-0,7}$ modes and with $LP_{0,11-0,12}$ modes) a shift measured for this LC-LPFG is presented, with maximum shift up to 73.5 nm. Therefore, it is clearly seen that the results described above provide efficient illustration of the LC-LPFG transmission spectra switching methods.

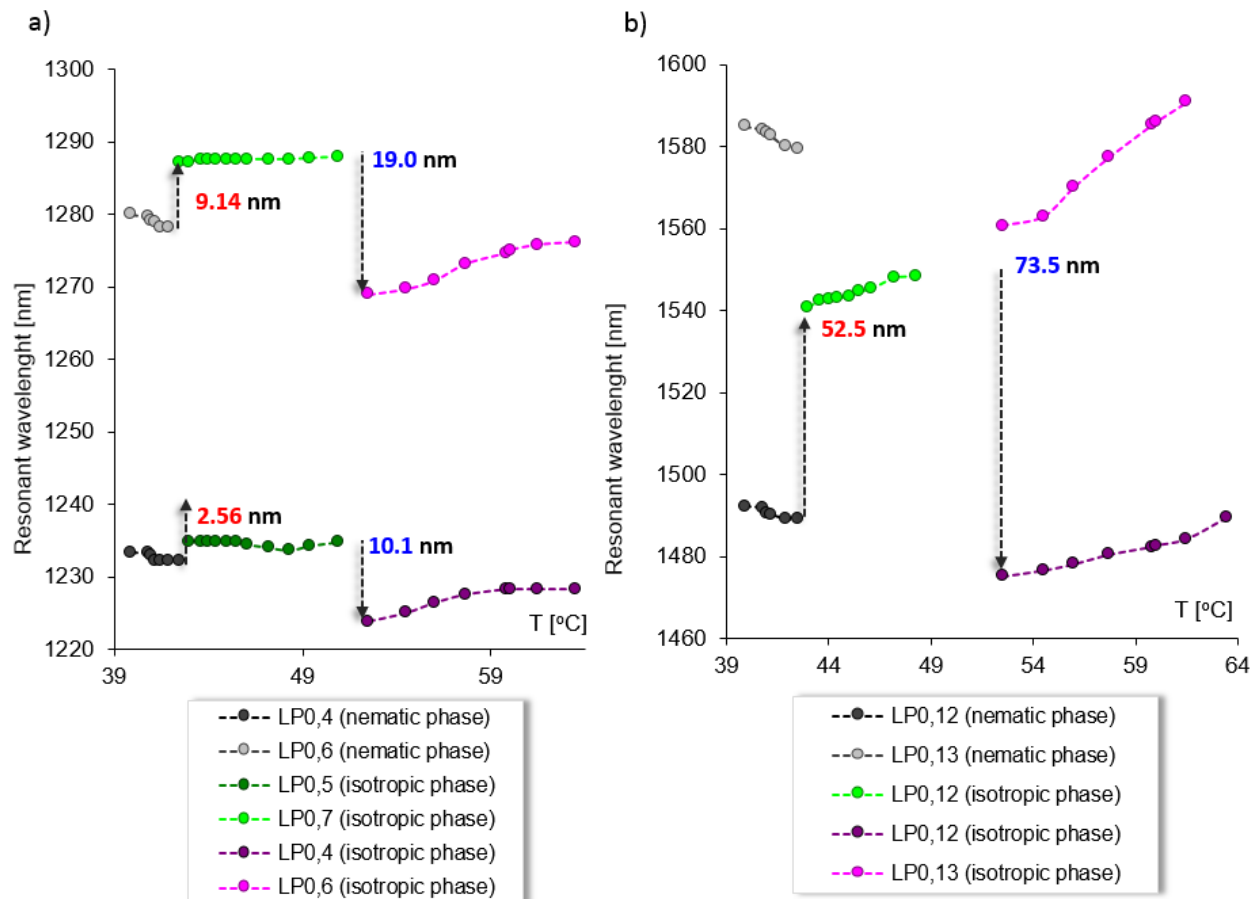


Fig. 7.4.15 Resonant wavelength of attenuation bands versus temperature for the LC-LPFG based on the combination of the UV-induced LPFG ($\lambda = 368 \mu\text{m}$) with 1110 LC mixture.

6.4.3 Compensating of the thermal effect in LPFGs by a proper choice of the LC layer

The thermal response of the LPFG can be also decreased by adding a properly chosen LC layer to its structure. The experimental observation of this effect was measured for the LPFGs based on the PS1200/1500 fiber. In Fig. 6.4.16a the measured transmission spectra of this type of UV-induced LPFG with a thin layer of 1800b LC mixture for different temperatures are presented. The period of the investigated grating was $226.8 \mu\text{m}$. As can be noticed from the results presented below, just after adding the 1800b LC layer to the grating, the efficiency of mode coupling intensity decreases significantly in comparison to air (by around of 7dB). However, when the sample started to be heated, the attenuation band reappeared in the LC-LPFG transmission spectrum. Above the temperature of 38°C , a new attenuation band measured in the spectral range from 1180 nm to 1240 nm could be easily tracked since its depth increased significantly. Moreover, the thermal response of this attenuation band in the temperature range from 38°C to 68°C was almost nullified for such LC-LPFG device.

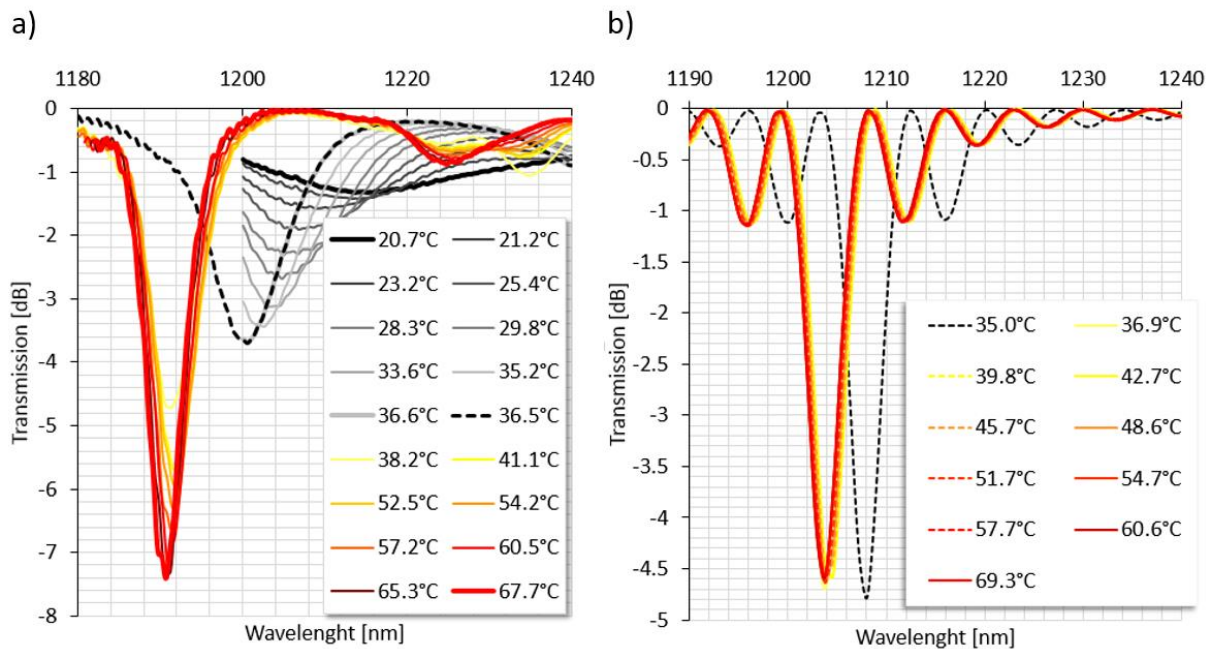


Fig. 6.4.16 Experimental (a) and calculated transmission spectra versus temperature of the LPFG (based on PS1200/1500 fiber; with period of $226.8 \mu\text{m}$) with 1800b LC layer. The 1800b LC layer thickness was estimated to be of $1.3 \mu\text{m}$

As can be seen from Fig. 6.4.17a the thermal tuning of this LPFG in air and with the 1800 LC layer is significantly different in the investigated spectral range. In Fig. 6.4.17b a comparison between the temperature sensitivities of the LPFG studied here in air and with 1800b LC layer is also shown. The

thermal response of the LC-LPFG (giving an experimental sensitivity as $-0.0413 \text{ nm}/^\circ\text{C}$) is more than 10 times lower than the sensitivity measured for the LPFGs in air (having an experimental sensitivity as $-0.4219 \text{ nm}/^\circ\text{C}$). This property could be valuable, since the environmental temperature shifts in the wavelengths of the LPFG resonant bands could be eliminated in various sensors, improving their metrological properties.

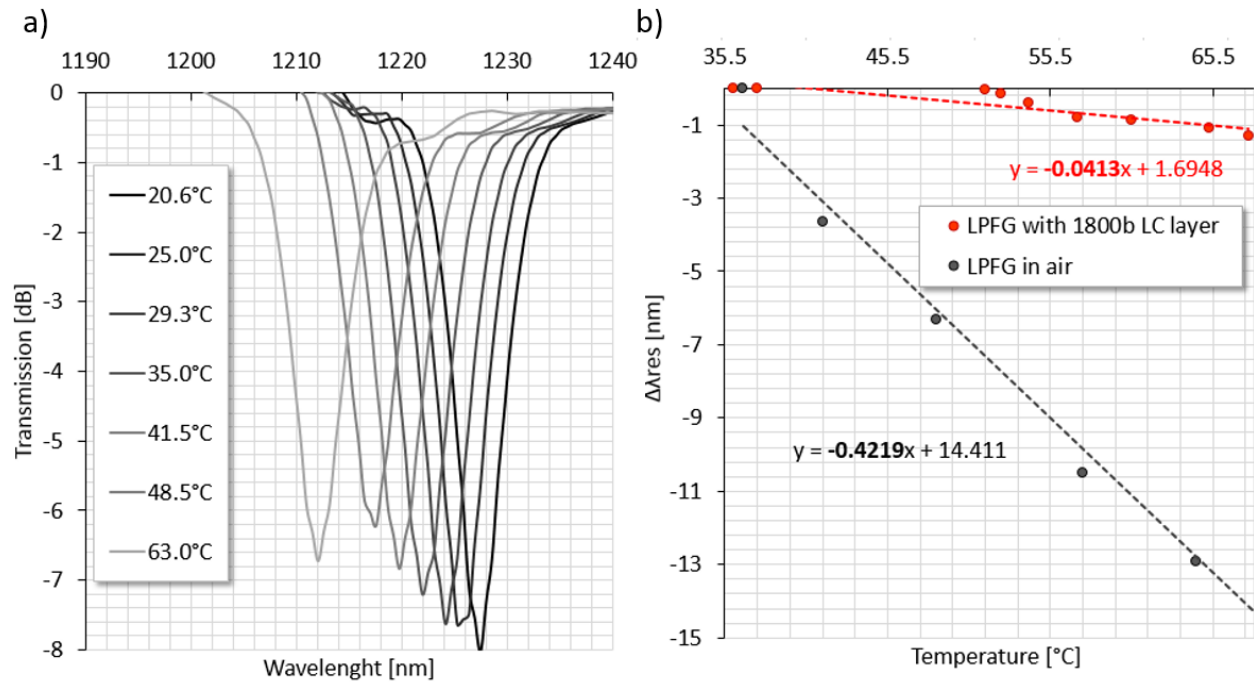


Fig.6.4.17 Experimentally measured (a) transmission spectra versus temperature of the LPFG (based on PS1200/1500 fiber; with period of $226.8 \mu\text{m}$) in air b) Thermal sensitivities for this LPFG measured in air and with 1800b LC layer.

The behaviour presented above can be explained by considering the fact that while the LC-LPFG is heated, two effects will take place. First, from the host fiber perspective, the LPFGs based on the Be/Ge co-doped fiber exhibits shifts towards lower resonant wavelengths with increasing temperature. Second, from the LB LC mixture perspective, the value of the ordinary refractive index n_o of the 1800b LC mixture decreases with the temperature. Thus, the presence of the LB LC layer around the LPFG should cause the temperature shifts towards higher wavelengths. It seems that for the measured attenuation band the impact of these two effects is almost cancelled out in the wide range of the temperature operation. This assumption was also confirmed by the preformed simulations shown in Fig. 6.4.16b. In the theoretical considerations of such LC-LPFG design, the LC layer thickness was estimated to be of $1.3 \mu\text{m}$ and the

tracking attenuation band was associated with the coupling of the $LP_{0,9}$ mode. Clearly, the experimental transmission data for such a LC-LPFG design stays in agreement with the simulations carried out. A small difference between the measured and simulated spectra (mainly in terms of the attenuation band position in the spectral range investigated here) is generally attributed to a small uncertainty in the data about the fiber and grating parameters. A similar effect of decreasing the temperature sensitivities of the LPFG was observed by adding to its structure layer of LB LC 1550 (this LC mixture have similar properties to the 1800b LC in terms of n_o magnitude and its thermal characteristic). In this case the UV induced period of the investigated LPFG was of $368 \mu\text{m}$. The transmission spectra versus temperature for such LC-LPFG device are presented in Fig. 6.4.18. In Fig. 6.4.19 dependence of the resonant wavelength versus temperature for such designed LC-LPFG is presented as well (giving an experimental sensitivity as $-0.4219 \text{ nm}/^\circ\text{C}$), compared simultaneously with the thermal sensitivity of the host LPFG measured in air.

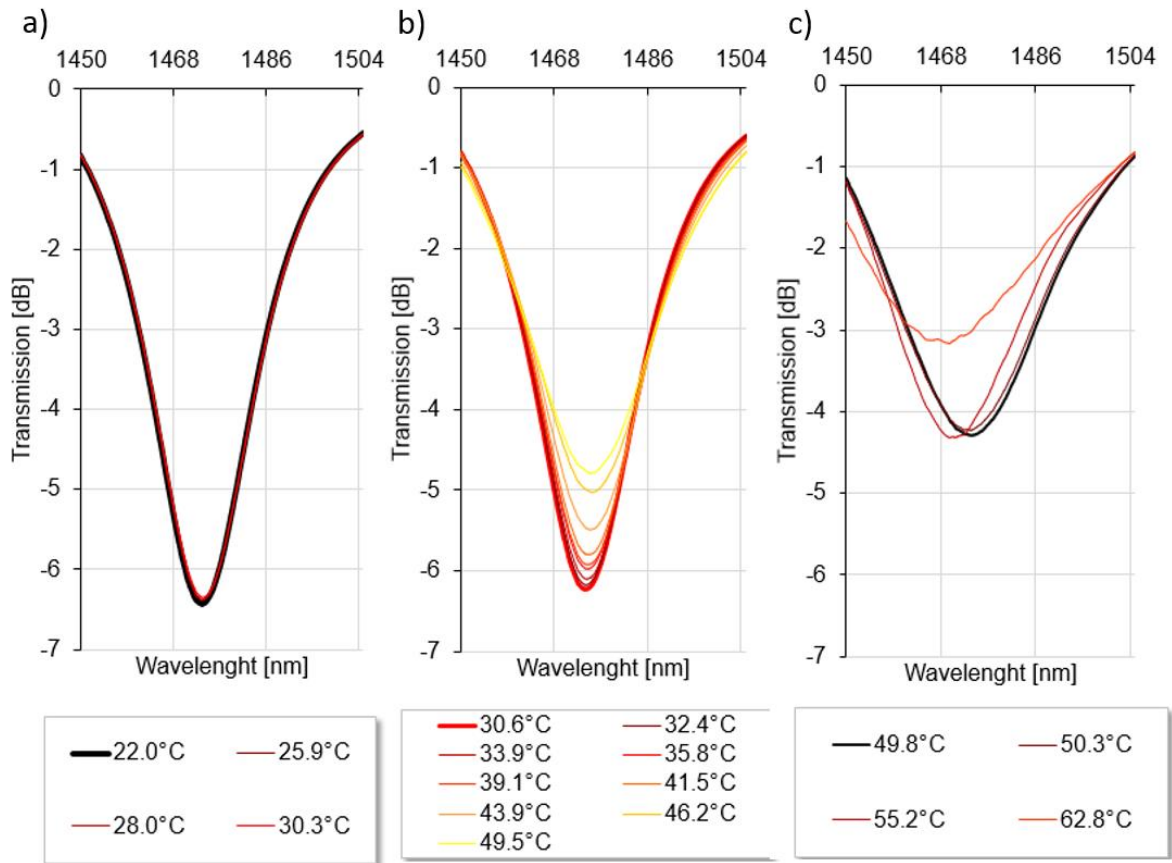


Fig. 6.4.18 Measured transmission spectra versus temperature for the LPFG (based on PS1200/1500 fiber; with period of $368 \mu\text{m}$) with 1550 LC layer.

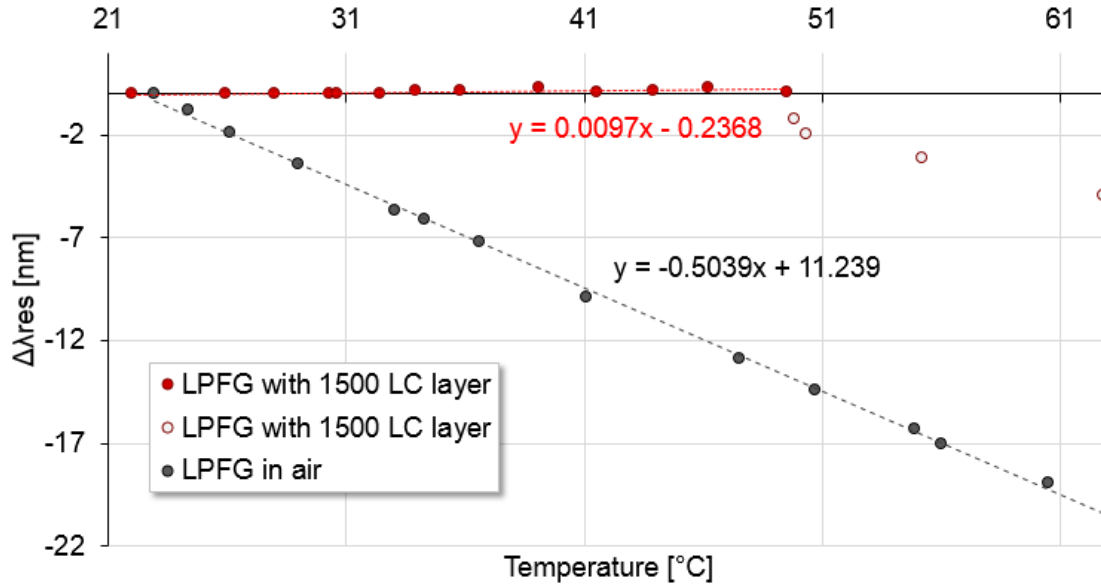


Fig. 6.4.19 Thermal sensitivity of the LPFGs (based on PS1200/1500 fiber; with period of 368 μm) measured in air and with 1550 LC layer.

From the Figures shown above, three different thermal responses can be distinguished:

- From 22.0°C to 30.3°C the attenuation band is almost immune to the temperature variations in terms of its resonant wavelength and depth.
- From 30.6°C to 49.5°C the resonant wavelength of the attenuation band remains nearly unmoved with the temperature increasing but its depth is slightly affected by the temperature variation (decreases by approx. 1.5 dB over a temperature change of 25.5°C)
- Above 49.8°C the resonant wavelength of the attenuation band is blue shifted with temperature increasing and its depth changes occurs.

The LPFG based sensor principle typically relies on changes in the position of the attenuation. Therefore it can be stated that the temperature compensation effect for the LC-LPFG discussed here can occur from 22.0°C to 49.5°C. In this range the thermal sensitivity of the LPFG decreases by almost 52 times thanks to the presence of the 1550LC layer. This experimental results prove once again that by coating with a suitable LC layer LPFG a novel method to compensate the inherent temperature sensitivity of the host grating can be provided. This feature is very attractive since often the spectral stability (especially in term of temperature changes) is of prime importance when the LC-LPFG are designed for a practical application.

6.5 LC-LPFGs designed for electrical tuning

The distinctive feature of the LC-LPFGs is that their spectral properties can be tuned by the external electric field. By applying an external electric field to the LC-LPFG, the LC molecules reorient accordingly to the field. If the alignment of the LC molecules is changed, the effective index of the LC is changed as well. Consequently, change in the LC-LPFG transmission spectrum is expected to happen.

This hypothesis has been confirmed during the course of the experimental work. Its results are presented in this section. In the first part of this study, the electrical tuning of the LPFGs placed in the LC cell will be presented. Furthermore, it will be shown that an enhancement of the electrical sensitivity of the LC-LPFGs can be achieved by decreasing the thickness of the LC layer in the order of few μm . Moreover, it will be demonstrated that the electrical tuning of the LC-LPFGs can be tailored by a suitable choice of the operational temperature. Parallel to the experimental work, a series of simulations were conducted and provided theoretical explanation of the observed effects.

6.5.1 Electrical modulation of the transmission properties for LPFG placed in an LC cell

In this part of the experiment the LC-LPFG electrical sensing properties are studied, when the grating is placed in the LC cell (the LC cell constructed to carry out these experiments was presented in Fig. 6.1.2). The LCs that serve here as a grating surrounding material are typical nematic LCs: 5CB and 6HBT. Both refractive indices (n_o and n_e) of these LCs are higher than n_{SiO_2} . Let's note also that the thickness of the LC layer for such a design of the LC-LPFG may be approximated to be infinite. Consequently, the cladding modes partly become radiation modes and can be guided by the Fresnel reflection. As a result, the strength of a mode coupling should be possible to be controlled by varying the boundary condition of the cladding.

In Fig. 6.5.1, the example of the electrically tuned transmission spectra for the arc-induced LPFGs in a LC cell filled with 5CB LC is presented. As can be seen, the coupling strength depends on the strength of an applied electric field through the dielectric interaction with the 5CB LC. In the absence of an electric field, the 5CB LC molecules are aligned along the fiber axis. Then, the propagating transverse cladding mode experiences the n_o of the surrounding 5CB LC. As the external electric field increases above a specific value (according to the Fredericks transition rule), the 5CB LC molecules tend to reorient perpendicularly to the fiber axis and the alignment of the 5CB LC is changed from planar to orthogonal. In this case the cladding modes parallel to the electric field are enhanced. That's why the strength of the mode coupling

increases and consequently the depth of the attenuation bands become deeper. In addition, the resonance wavelength remains almost unchanged under the variation of an external electric field. In Tab. 6.5.1 the measured modulation of the attenuation band depth measured for samples is given.

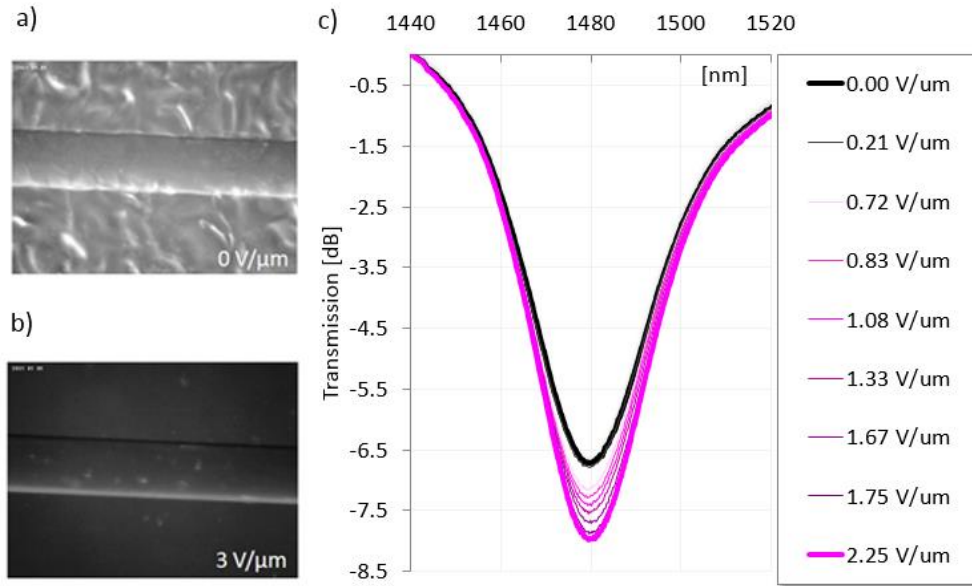


Fig. 6.5.1 In (a) and (b) pictures of the arc-induced LPFG (with $\Lambda = 400 \mu\text{m}$; based on the SMF-28 fiber) placed in the LC cell (filled with 5CB) are shown without and with electric field applied. In (c) the transmission spectrum versus electric field for this same sample is demonstrated.

Tab. 6.5.1 The modification of the depth under the external electric field (from $0 \mu\text{m}/\text{V}$ to $2 \mu\text{m}/\text{V}$), measured for the last band in the transmission spectra of LPFGs in LC cell.

| No | LPFG | | | LC material | Modification of the depth under E-field |
|----|-------------|--------|-----------------------------|-------------|---|
| | host fiber | method | Λ [μm] | | |
| 1 | SMF | arc | 400 | 6CHBT | 15.0 % |
| 2 | SMF | arc | 400 | 5CB | 15.6 % |
| 3 | PS1200/1500 | arc | 375 | 6CHBT | 19.9 % |
| 4 | PS1200/1500 | UV | 226.8 | 5CB | 23.4 % |

In addition, from results presented above the following schema of the LC-LPFG response to an increasing voltage can be also established:

- **STEP 1:** Just after the voltage is applied, no significant changes in the LC-LPFG transmission spectrum are observed. This is due to the fact that at very low voltages, most of the LC molecules are un-tilted and still have a planar alignment. Therefore, the variations in the transmission spectrum are not clearly observable when the voltage is below the specific threshold value V_T , according to Frederick's transition rule.
- **STEP 2:** When the electric field is increased above the V_T , a shift of the attenuation band and modification in its depth can be observed. This behavior can be attributed to non-collective reorientation of LC molecules. Consequently, when the applied voltage exceeds the threshold value, the reorientation of all the molecules is not instantaneous and disturbs the propagation conditions.
- **STEP 3:** When the applied voltage is high enough, further increasing of the voltage does not affect anymore the LC-LPFG transmission spectrum. This phenomenon can be explained by the fact that a sufficiently high voltage ensures a homogeneous orientation of the LC. Consequently, most of the LC molecules achieve a perpendicular orientation and they reach a new equilibrium state.

This schema of the LC-LPFG electric tuning can be also used when results concerning the LPFG with a LC layer (presented in the next Section) are interpreted. The only difference that can be expected is that the spectral change of the attenuation bands can additionally occur in the case of the LPFG coated with LC layer.

6.5.2 Electrical modulation of the transmission properties for the LPFG with a LC layer

In this part it will be shown that an enhancement of the electrical sensitivity of the LC-LPFGs can be achieved by decreasing the thickness of the LC layer in the order of few μm . A key fact in achieving an electrical control for the LPFG coated with thin LC layer, is the dependence of the LPFG's spectral properties on:

- a) its sensitivity to the SRI (resulting mainly from its period value),
- b) the LC layer thickness (d),
- c) the RI of the LC layer (n_{LC}),
- d) the birefringence of the LC, (Δn).

If these parameters are properly chosen, a reorganization of the cladding modes occurs between off- and on-voltage states. It is possible since the electric field increases the LC layer refractive index. The consequence of this change is the shift of the effective indices of the cladding modes to the higher values. This effect leads to the transition of the lowest-order cladding mode (higher effective index) to be guided within the LC layer instead of cladding area only. As the lowest-order cladding mode moves to be guided within the LC layer, a reorganization of the effective index of the rest of the modes take place. They shift their effective index values towards the effective index of the immediate higher effective index mode. The same is true for the resonance wavelength values since there is a close relation between the resonance wavelength of the attenuation bands and the effective index of the cladding mode. Consequently, the presence of the electric field will induce a new set of attenuation bands in the LC-LPFG transmission spectrum. The attenuation bands in the on-voltage state can be thus centered at different resonant wavelengths than the attenuation bands visible without electric field. Moreover, if the LC-LPFG response to the electric field occurs within the transmission region the LC-LPFG, the electric sensitivity can be enhanced significantly. In order to verify the outline of the LC-LPFGs electric control presented above, a series of experiments were performed and supported simultaneously by the theoretical analysis (in terms of modelling the LC-LPFGs sensing capability of the external electric field).

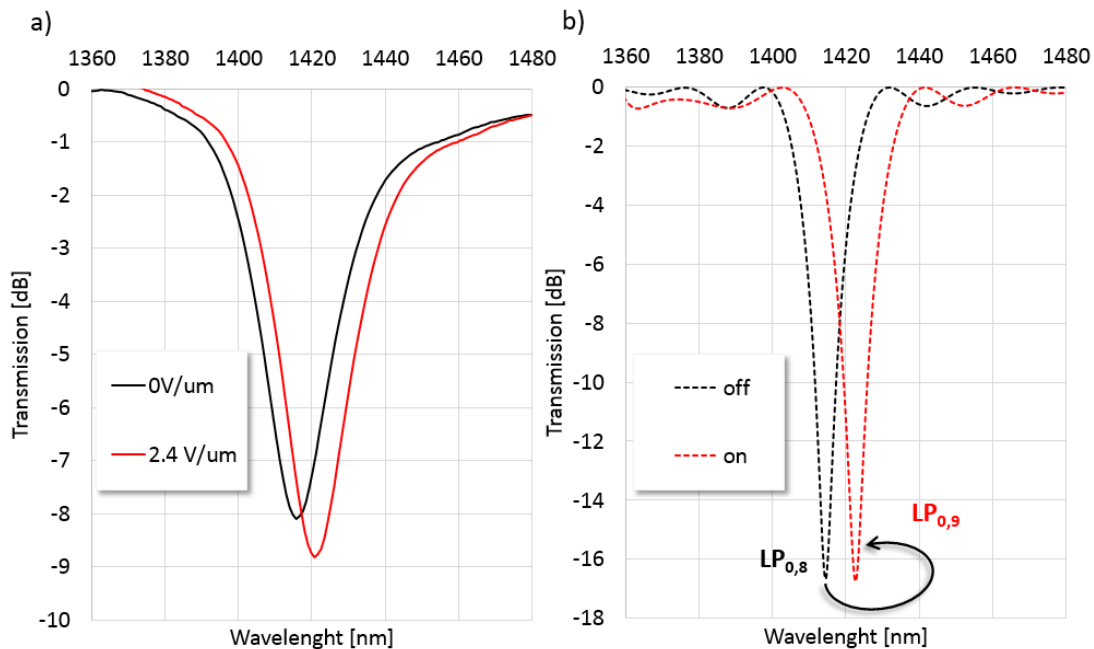


Fig. 6.5.2 Experimentally measured (a) and simulated (b) effect of the LC-LPFG electric tuning. The host LPFG based on SMF-28 fiber, is arc-induced and have period of $400 \mu\text{m}$. As a LC layer the 5CB LC is chosen with estimated thickness of $1.9 \mu\text{m}$.

In Fig. 6.5.2 the transmission spectra for the LC-LPFG measured without and in the presence of the external electric field are shown. The LPFG used in this experiment was based on the SMF-28 fiber with period of 400 μm . It was fabricated by the arc method. As a LC layers, the 5CB LC was chosen. With help of the calculations performed (the simulated transmission spectra for this LC-LPFG are shown Fig. 7.5.1 b) the thickness of the LC layers was estimated to be of 1.9 μm . The LC layer RIs values used in the simulation correspond with the values of n_o (in the off-voltage state) and close to the value of the n_e (in the on-voltage state, see also Section 5.3.6) measured at room temperature. Clearly, it is visible that such a LC-LPFG design provides electric tuning effects in the spectral range of interest. Namely, a red shift of the attenuation band, up to nm, was electrically induced. Such a modulation of the LC-LPFG occurs since an electric field increased the LC layer RI to a value sufficient to reorganize the cladding modes. As a result, in the on-voltage state, a new set of attenuation bands is observed in the LC-LPFG transmission spectrum. These attenuation bands correspond now with the higher order modes than those visible in the off-voltage state. Particularly, for the LC-LPFG sample discussed here the attenuation band corresponding to the $LP_{0,8}$ mode is electrically switched closely with its wavelength (with positive shift) to the attenuation band associated with the $LP_{0,9}$ mode.

By further examining the LC-LPFG response to the electric field it was found that a direction of the attenuation band displacement is strongly dependent on the sample design. In Fig. 6.5.3 the transmission spectra versus the electric field for this same host LPFG, but this time with the 1702 LC layers are shown. In this experiment the LPFG was coated several times with 1702 LC, increasing in this way the thickness of the layer. The values of the LC thicknesses, established with help of numerical simulations (simulated LC-LPFGs transmission spectra are presented in the Fig. 7.5.4), are 2 μm and 2.4 μm . It was also found that the observed attenuation band in the off-voltage state corresponds with the $LP_{0,8}$ mode. In the on-voltage state, the attenuation band is associated with the $LP_{0,9}$ mode and the $LP_{0,10}$ mode when the thickness of the LC layer was 2 μm and 2.4 μm , respectively. When the switching occurs from the $LP_{0,8}$ mode resonance to the $LP_{0,9}$, the blue shift displacement is measured, up to 7 nm (Fig. 6.5.3a). For the higher LC layer thickness value (switching this time is from the $LP_{0,8}$ mode to the $LP_{0,10}$) the attenuation band is electrically red shifted, up to 10 nm (Fig.6.5.3b).

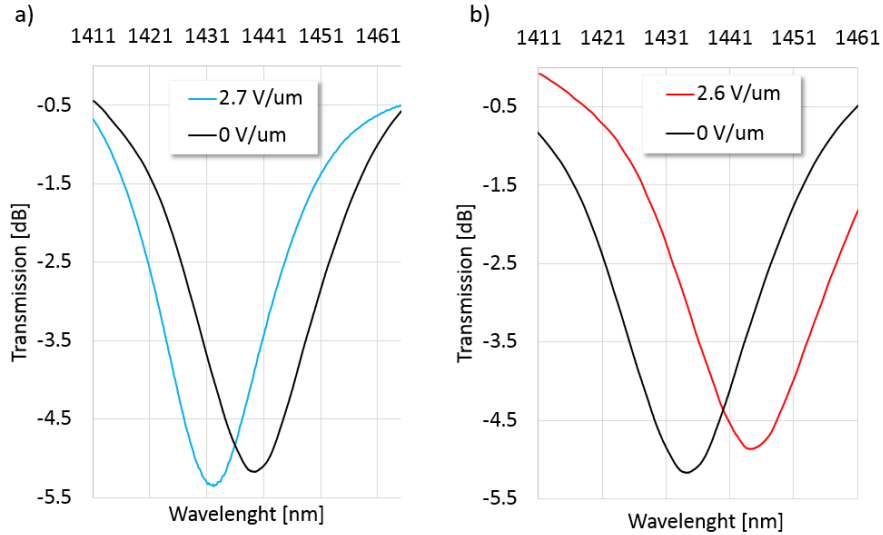


Fig. 6.5.3 Experimental results of the electric tuning the LPFG (arc induced; based on SMF28 fiber; with period of 400 μm) coated with the 1702 LC with thickness of 2.0 μm (a) and 2.4 μm (b).

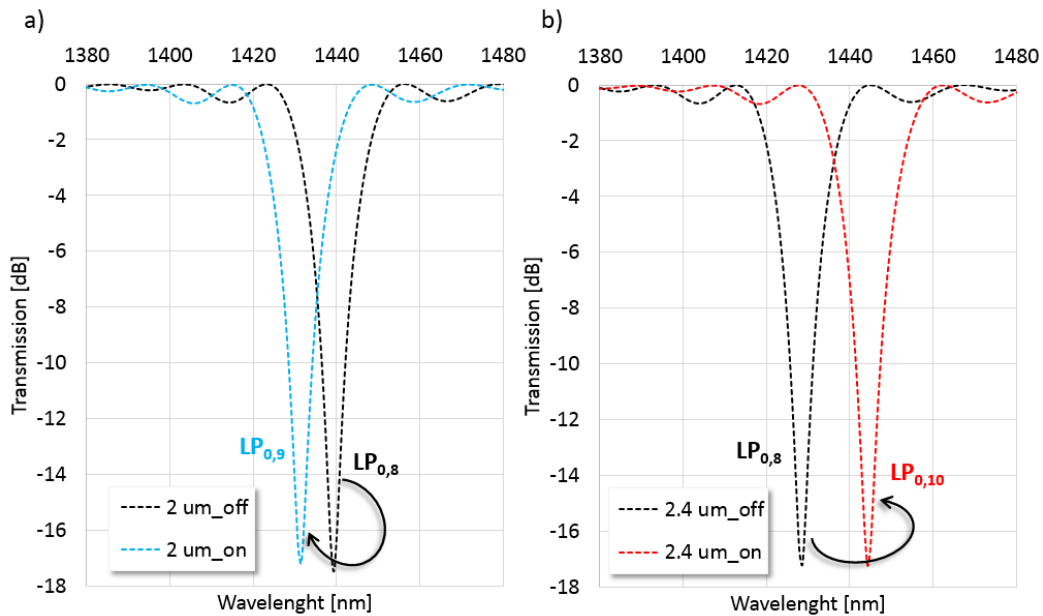


Fig. 6.5.4 Simulated effect of electrical tuning the LPFG (arc induced; based on SMF28 fiber; with period of 400 μm) coated with the 1702 LC with thickness of 2.0 μm (a) and 2.4 μm (b).

In order to explain the results presented above, let's carefully examine the modes' effective index dependence of the LC layer thickness (in particular for $LP_{0,8}$ mode in off-voltage state and modes close to it in the on-voltage state, $LP_{0,9}$ and $LP_{0,10}$) presented in Fig. 6.5.5. This plot has been calculated separately for two cases. Namely, two different values of the LC RI layer where set to the simulation, corresponding

with an off- (marked in the Fig. 6.5.5 with dashed lines) and an on-voltage (marked in the Fig. 6.5.5 with solid lines) states. The range of LC layer thickness variation studied here is from 1.9 μm to 2.5 μm . The experimentally investigated LC layer thickness is indicated in Fig. 6.5.5c by the vertical dashed black lines. The point of intersection of these lines with the modes characteristics determines the modes' effective refractive indices for which the attenuation bands should appear in the measured LC-LPFG transmission spectrum. These points are marked in the Fig. 6.5.5c by blue and red dots for the off- and on-voltage states, respectively. From the calculation performed, it is possible to distinguish three different ranges of the LC layer thickness, which will provide various LC-LPFG responses to the electric field presence. In particular:

- the 1st range will exhibit the highest sensitivity to the external electric field. This is due to the fact that for these thickness values the transition of the cladding modes occur. Therefore, if the LC layer thickness would be of $\sim 2.24 \mu\text{m}$ (which is the value where the effective indices of the $\text{LP}_{0,9}$ mode and the $\text{LP}_{0,10}$ mode are half way in their transition region for the on-voltage state) the attenuation band associated with the $\text{LP}_{0,8}$ should vanish in the presence of the electric field. Such an effect is expected since there is an additional phenomena of vanishing of attenuation bands within the transition region (which is the case for the the $\text{LP}_{0,9}$ mode and the $\text{LP}_{0,10}$ in the on-voltage state). The consequence of these attenuation bands vanishing is negative in terms of their detection. Nonetheless, high variations in amplitude can be also exploited in the same manner as wavelength shift in sensor applications.
- the 2th.a (approximated up to thicknesses of 2.15 μm) and 2th.b (approximated from the thicknesses of 2.35 μm) LC layer thickness ranges should demonstrate smaller sensitivity to the external electric field than it is in the 1st range. However, these LC layer thickness values provide an opportunity to detect the attenuation bands in a LC-LPFG transmission spectrum. In addition, a measurable displacement of the attenuation bands should be still possible to observe. The main difference for the LC layer thickness ranges considered here is revealed when the direction of the electrically induced band-shift is considered. Exactly, for:
 - the 2th.a range the attenuation band should demonstrate a blue shift in accordance with the fact that the effective index of the $\text{LP}_{0,8}$ in the off-voltage state is lower than the effective index of the $\text{LP}_{0,9}$ in the on-voltage state.
 - the 2th.b LC layer thickness range the attenuation band should demonstrate a red shift in accordance with the fact that the effective index of the $\text{LP}_{0,8}$ in the off-voltage state is higher than the effective index of the $\text{LP}_{0,10}$ in the on-voltage state.

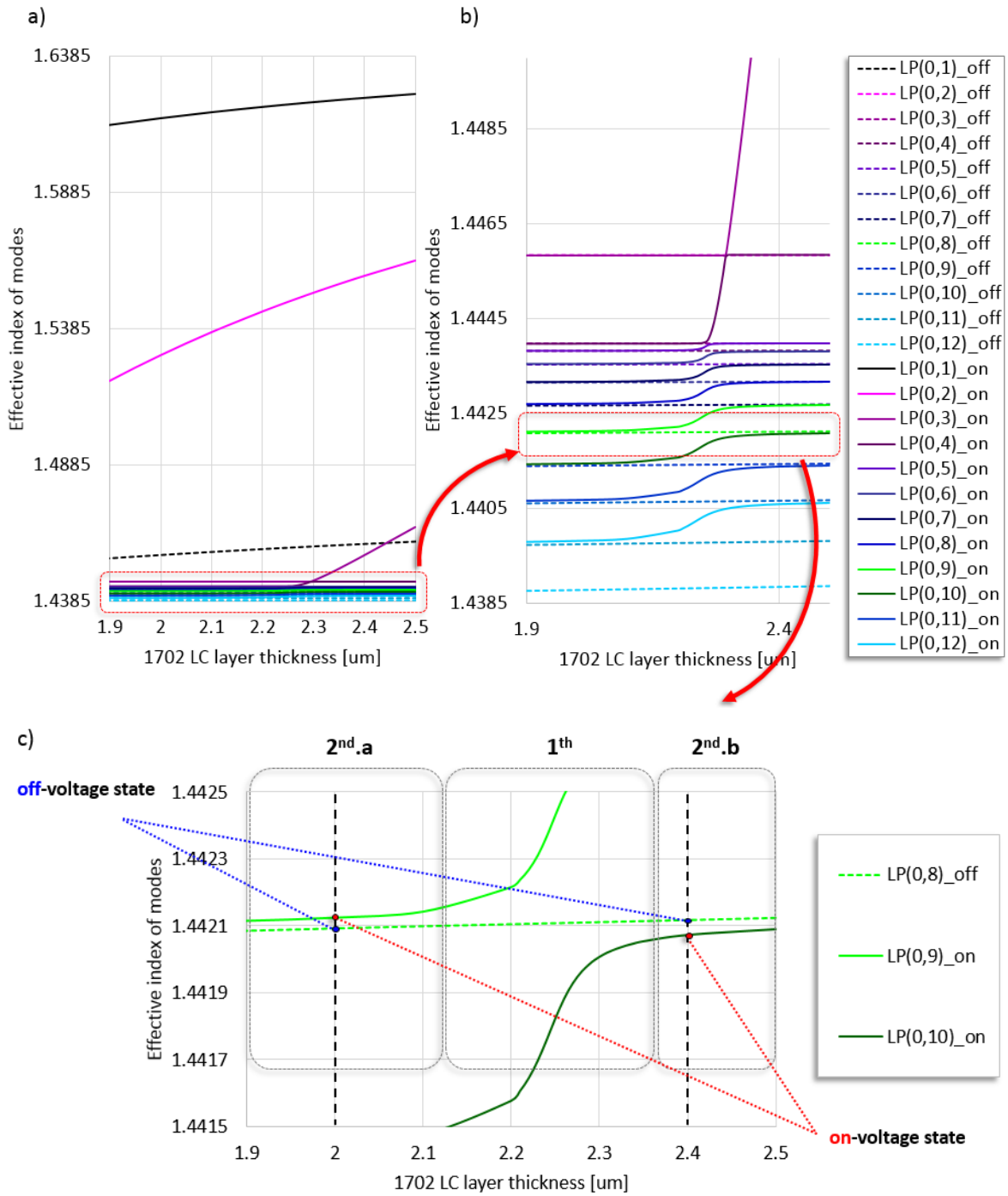


Fig. 6.5.5 Mode structure plot versus layer thickness with the fixed 1702 LC layer refractive index for off- and on-voltage states.

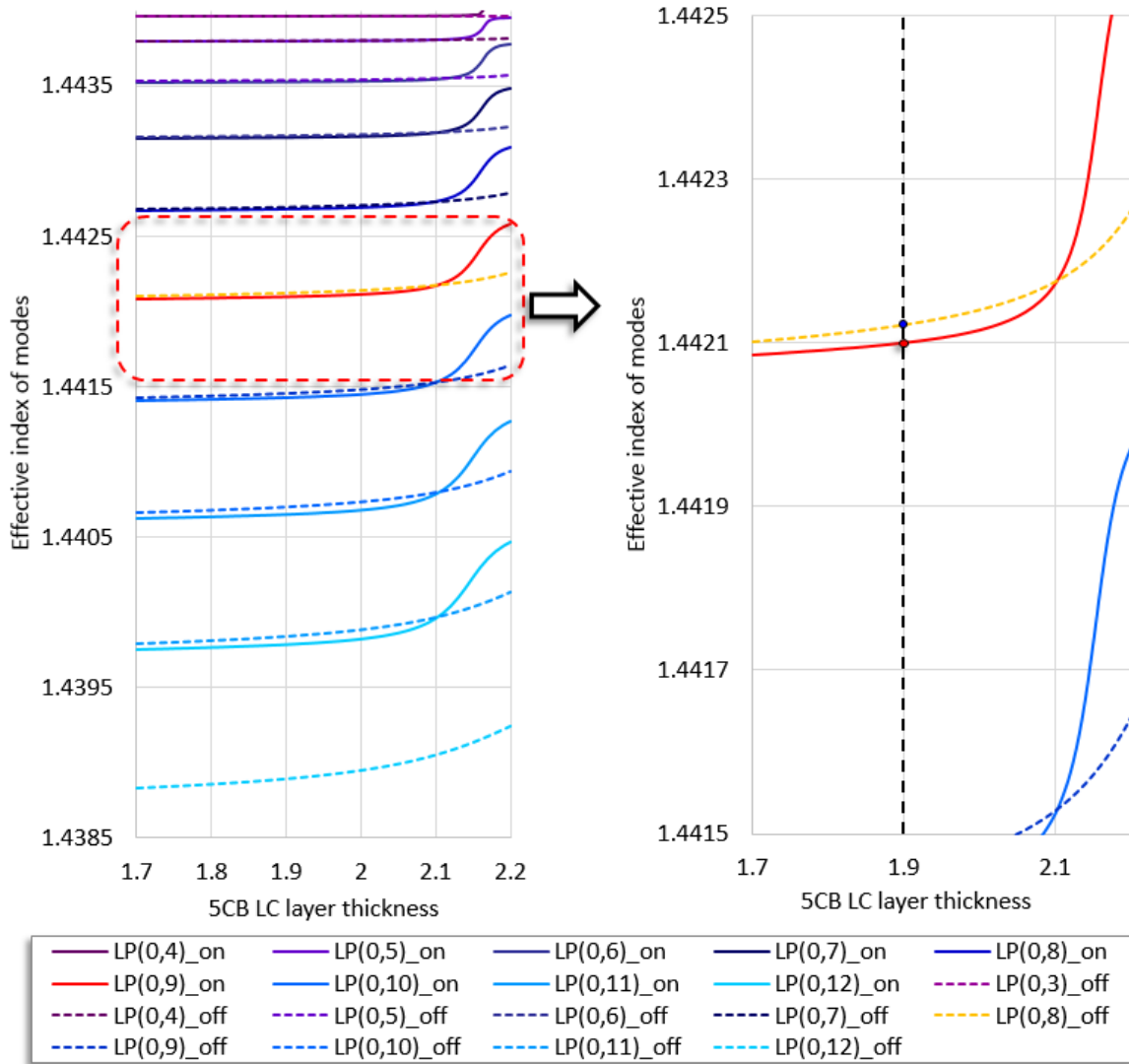


Fig. 6.5.6 Mode structure plot versus layer thickness with the fixed 5CB LC layer refractive index for off- and on-voltage states.

From the presented analysis it can therefore be concluded that the measured spectra for the LPFG coated with the 1702 LC layer thickness of:

- 2.0 μm (Fig. 6.5.3a) corresponds to the electrical response, demonstrated within the 2th.a LC layer thickness range.
- 2.4 μm (Fig. 6.5.3b) corresponds to the electrical response, demonstrated within the 2th.b LC layer thickness range.

This interpretation of the tuning attenuation band mechanism by the electric field is also consistent with the results previously obtained for the LPFG with 5CB LC layer (Fig. 6.5.2). In the Fig. 6.5.6 the mode

structure plot versus 5CB LC layer thickness was calculated in the off- and on voltage states. The studied range of 5CB LC layer thickness variation was from 1.7 μm to 2.2 μm . For the experimentally investigated 5CB LC layer thickness (indicated there by the vertical dashed black line), the modes' reorganization should occur, from the $\text{LP}_{0,8}$ mode to the $\text{LP}_{0,9}$ mode, in the presence of an electric field. At this point the effective index of the $\text{LP}_{0,9}$ mode in the on-voltage state is also lower than for the $\text{LP}_{0,8}$ mode in the off-voltage state. Consequently, the electrically induced red displacement of the attenuation band should actually be observed for this sample.

In order to further examine the impact of the electric field on the LC-LPFG spectral properties, a series of experiments was also conducted when a short period of the grating (226.8 μm and 222 μm) was chosen. This type of LPFGs exhibits enhanced sensitivity. This is due to the fact that in their transmission spectrum we can observe attenuation bands which are associated with higher-order modes. Higher order modes are showing greater sensitivity to any external perturbation. In addition, when the coupling of such a higher-order mode occur near the phase-matching turning point, the attenuation band contains dual resonant peaks at two separate wavelength values. Consequently, by operating at wavelengths near to the mode phase-matching turning point, higher sensitivity of the LC-LPFG to the electric field should be observed. In Fig. 6.5.7 measured and simulated transmission spectra of the LPFG coated with 1550A LC versus E-field are presented. In this experiment, the LPFG with the period of the 226.8 μm was chosen. As a host fiber, a boron co-doped photosensitive fiber (*Fibercore* PS1250/1500) was used and the grating was written into it by an Eximer laser. By fitting both experimental and simulated figures, the 1550A LC layers thickness could be estimated to be of as 1.8 μm . Results shown in Fig. 6.5.7 indicate that an electric field can induce significant changes in the transmission spectrum. In the off-voltage state two attenuation bands are visible (Fig. 6.5.7b). Thanks to the performed simulation (presented in Fig. 6.5.7a), it could be established that the measured attenuation bands at 1207 nm and at 1359 nm results from the coupling of the $\text{LP}_{0,9}$ and $\text{LP}_{0,10}$ modes, respectively. By applying the electric field to the sample, the RI of the LC layer increases. Therefore, the reorganization of the modes occurs. As a result, in the on-voltage state the attenuation band corresponding with the $\text{LP}_{0,10}$ is offset from the attenuation band measured in the off-voltage state by almost 130 nm. The attenuation bands associated with the $\text{LP}_{0,9}$ mode is no longer visible in the spectral range of interest. In addition, by increasing the electric field, an additional attenuation band appears in the LC-LPFG transmission spectrum (as is shown in Fig. 6.5.7c). Comparing the simulated and experimental transmission spectrum, it can be deduced that this attenuation band corresponds with the $\text{LP}_{0,11}$.

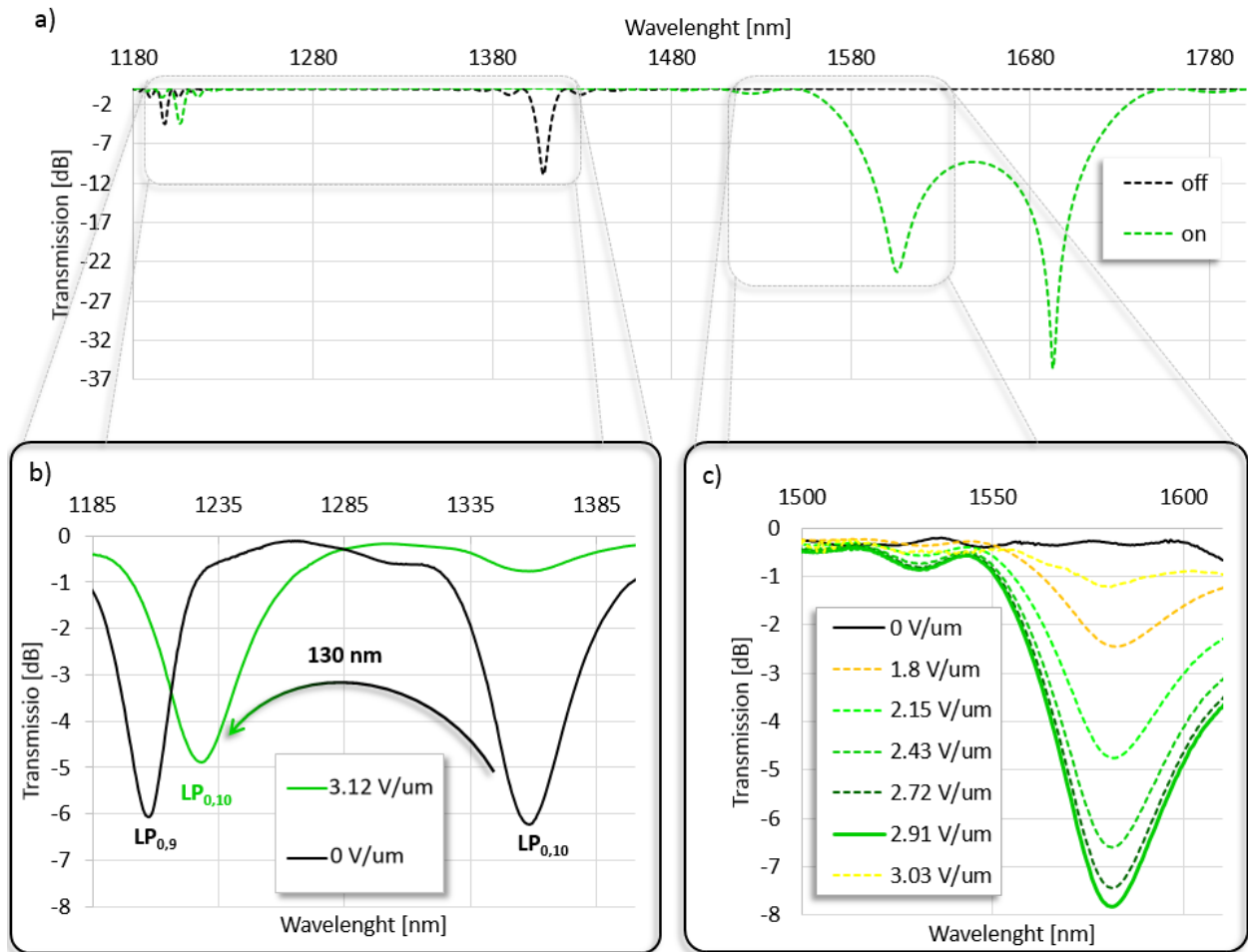


Fig. 6.5.7 Simulated (a) and experimental measured (b-c) transmission spectra for the LPFG (UV induced grating based on the PS1200/1500 fiber with period of $226.8 \mu\text{m}$) with 1550A LC layer ($d=1.8 \mu\text{m}$) versus E-field.

The electric tuning ability could be also observed for this same host LPFG coated with the 1702 LC layer. The thickness of the LC layer in this case was estimated to be of $2.1 \mu\text{m}$. The electrical switching of the attenuation band and its repeatability are clearly shown in Fig. 6.5.8b, where the transmission spectrum was measured in the sequences of the off- and on-voltage states. As can be seen from Fig. 6.5.8c, the attenuation band induced by the electrical field is blue shifted by around 8 nm with respect to the band measured without the electric field. From the performed simulations, it was found that the attenuation band measured in off-voltage states is associated with the $LP_{0,10}$ mode, while in the on-voltage state the attenuation band corresponds with the $LP_{0,11}$ mode. In addition, one more band in the off-voltage state (centered at the wavelength of 1660 nm) is visible in the theoretically calculated LC-LPFG transmission spectrum (presented in Fig. 6.5.8a). Unfortunately, the empirical examination of this band was not

possible since its resonant wavelength is outside from the spectral range available in the experiment. However, the experimental examination of this theoretically predicted attenuation band will be presented in the next section, where the LC-LPFG thermal sensitivity is explored furthermore in order to increase the LC-LPFG response to an electric field.

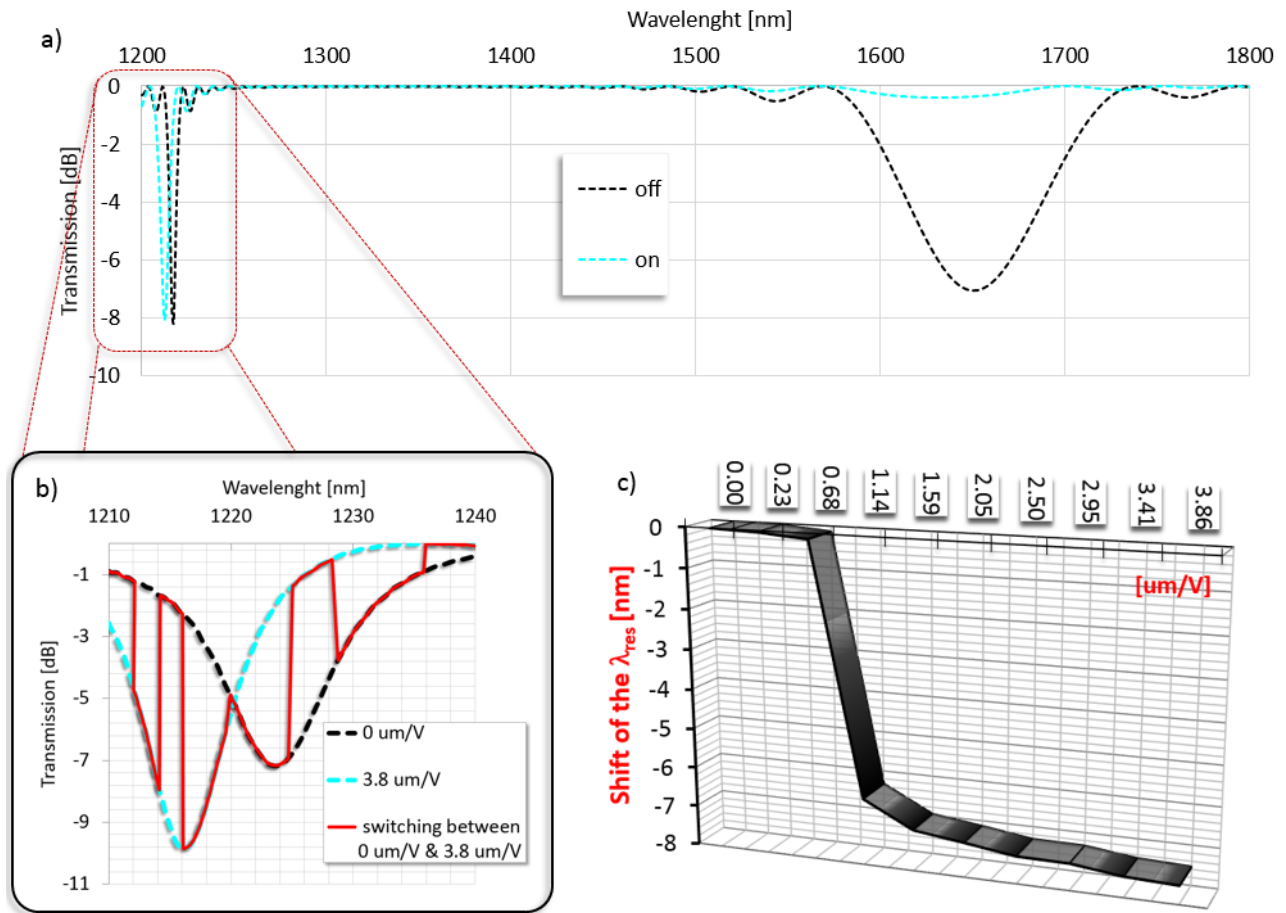


Fig. 6.5.8 Simulated (a) and experimental measured (b) transmission spectra for the LPFG (UV induced grating based on the PS1200/1500 fiber with period of $226.8 \mu\text{m}$) with 1702 LC layer ($d=2.1 \mu\text{m}$) versus E-field. In (c) the electrical field induced shift of the attenuation band is shown.

Effective tuning of the LC-LPFG was also achieved for the arc induced LPFG host with period of $222 \mu\text{m}$. This grating was coated with the 1550A LC layer with a thickness approximately of $2 \mu\text{m}$. The Fig. 6.5.9 shows that the depth of the attenuation band was reduced significantly in the presence of an electric field. Through the theoretical work, it was found that the attenuation band measured in the off-voltage state results from coupling of the $LP_{0,11}$ mode. This result can be interpreted by the fact that the change in the LC layer under the influence of an electric field gives a value of the refractive index for which the modes

are close to the transition region (which should decrease significantly the visibility of the attenuation bands). Additionally, the mode which should take its place (precisely the $LP_{0,12}$ mode) is also close to its turning point and was not formed yet in the LC-LPFG transmission spectrum.

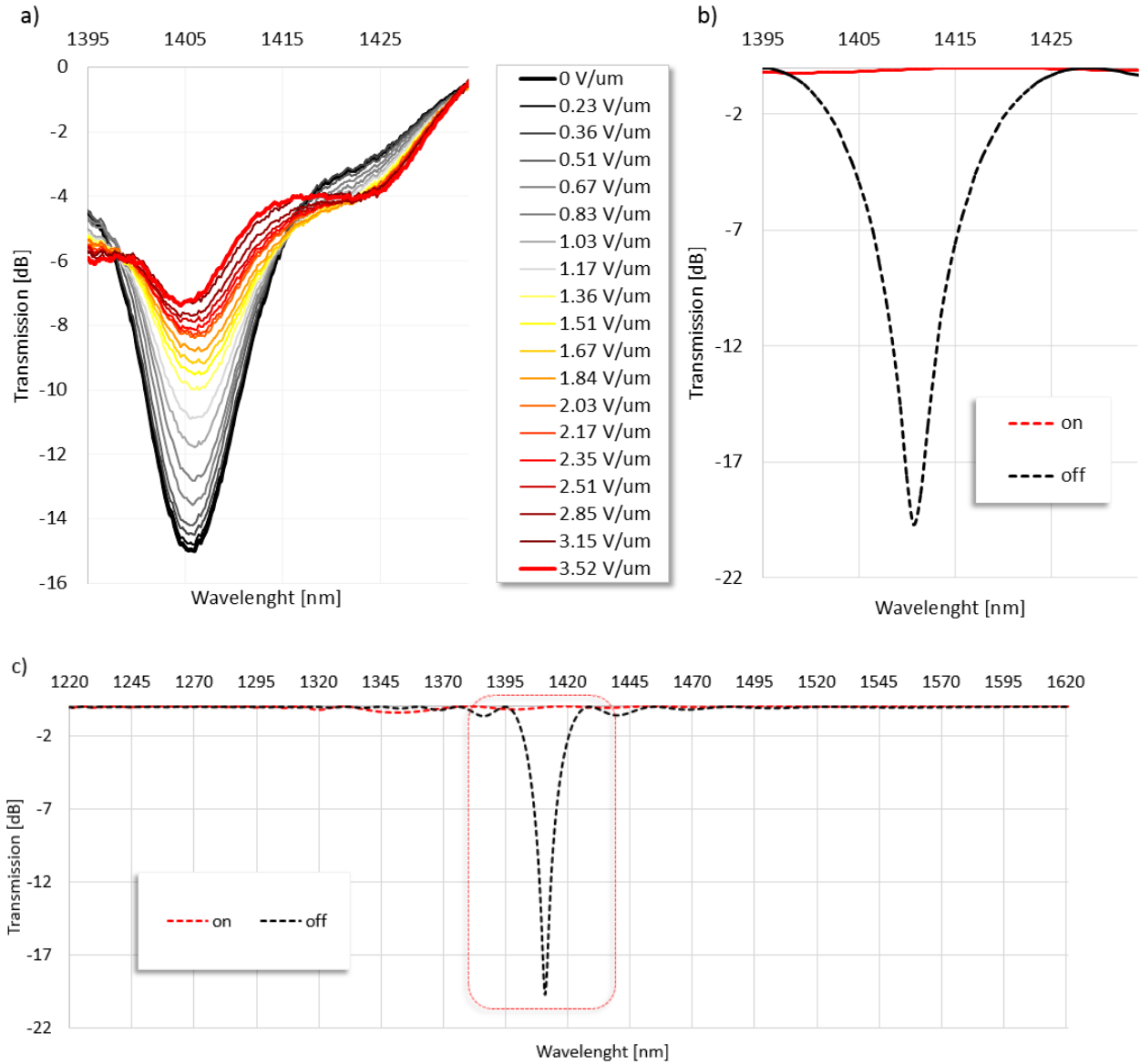


Fig. 6.5.9 Measured (a) and simulated (b,c) transmission spectra versus electric field for the arc induced LPFG with period of 222 μm coated with 1702 LC layer.

6.5.3 Enhanced LC-LPFG electrical properties by a properly chosen temperature of the operation

The ranges of the LC-LPFG electrical tuning are determined by the spectral position of the attenuation band that is monitored. Below it will be shown that, by a properly chosen temperature of operation, the resonant wavelength of attenuation bands may be adjusted to a certain extent. Note that the temperature range of operation, when the LC-LPFG is designed to operate in the E-field is limited to the LC nematic phase. The technique proposed here will allow to tune the LC-LPFG electric sensitivity as well.

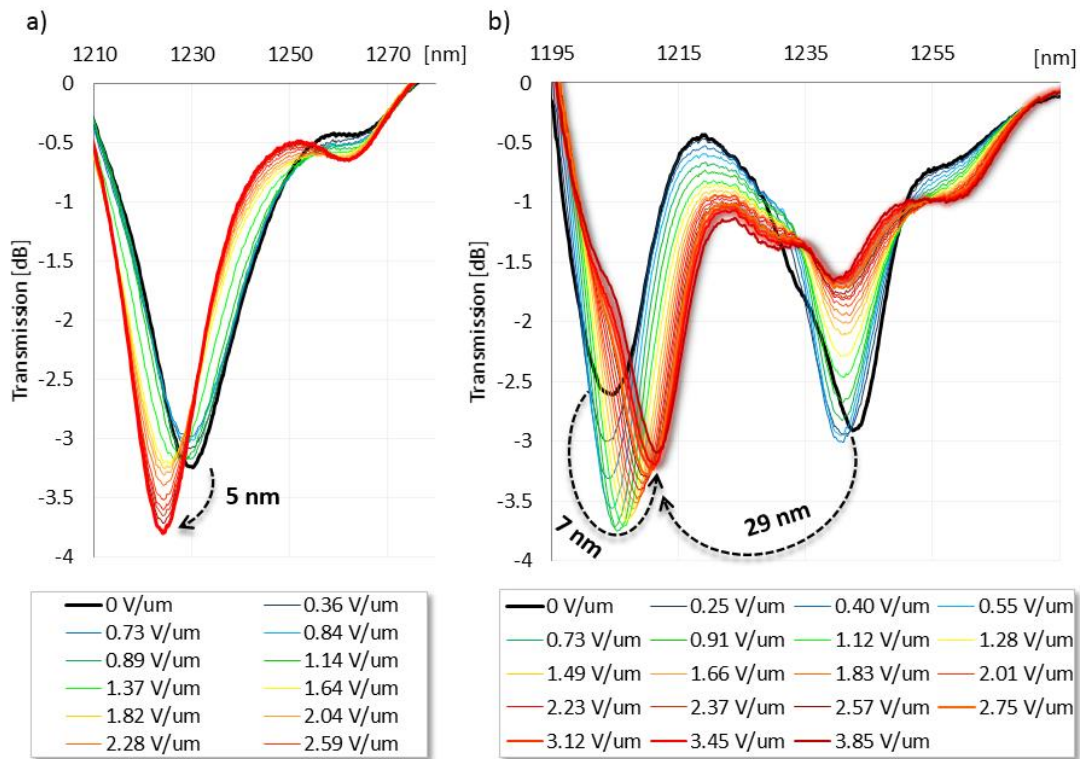


Fig. 6.5.10 Experimentally measured transmission spectra of the UV-induced LPFG (based on the PS1250/1500 fiber; with period of 226.8 μm) coated by the 1550 LC versus external electric field when the temperature was stabilized at 25°C (a) and 60°C (b).

The enhanced electric sensing capability of the LC-LPFG becomes evident when we look on the Fig. 6.5.10. In this Figure the measured LC-LPFG transmission spectra are shown in the off- and on-voltage states at two different temperatures. The LC-LPFG used in this experiment are based on the combination of the LPFG coated with the 1500 LC layer. The thickness of the LC layer was established by the simulations to be of 3.5 μm . The host grating has a period of 226.8 μm and was UV-induced on the PS1200/1500 fiber. From the results presented here it is visible that different ambient temperature can significantly change

the LC-LPFG electric response. The performed simulations show that an electrical switching of this LC-LPFG is based on the reorganization of the modes from the $LP_{0,10}$ mode (in the off-voltage state) to the $LP_{0,11}$ mode (in the on-voltage state). At 25°C the blue shift was measured, up to 5 nm (6.5.10a). When the ambient temperature was stabilized at 60°C the RI value of the LC layer without E-field is set close to the cladding modes' transition region (as was already discussed in the Section 6.4.1). Consequently, splitting up of the band associated with the $LP_{0,10}$ resonance was experimentally confirmed. When the electric field was applied to the sample this effect vanished and a new attenuation band, corresponding with the $LP_{0,11}$ resonance, was visible in the spectral window (Fig. 6.5.10b). These results indicate that for such a LC-LPFG device, the electrical spectral tunability could be increased by a proper adjustment of the ambient temperature.

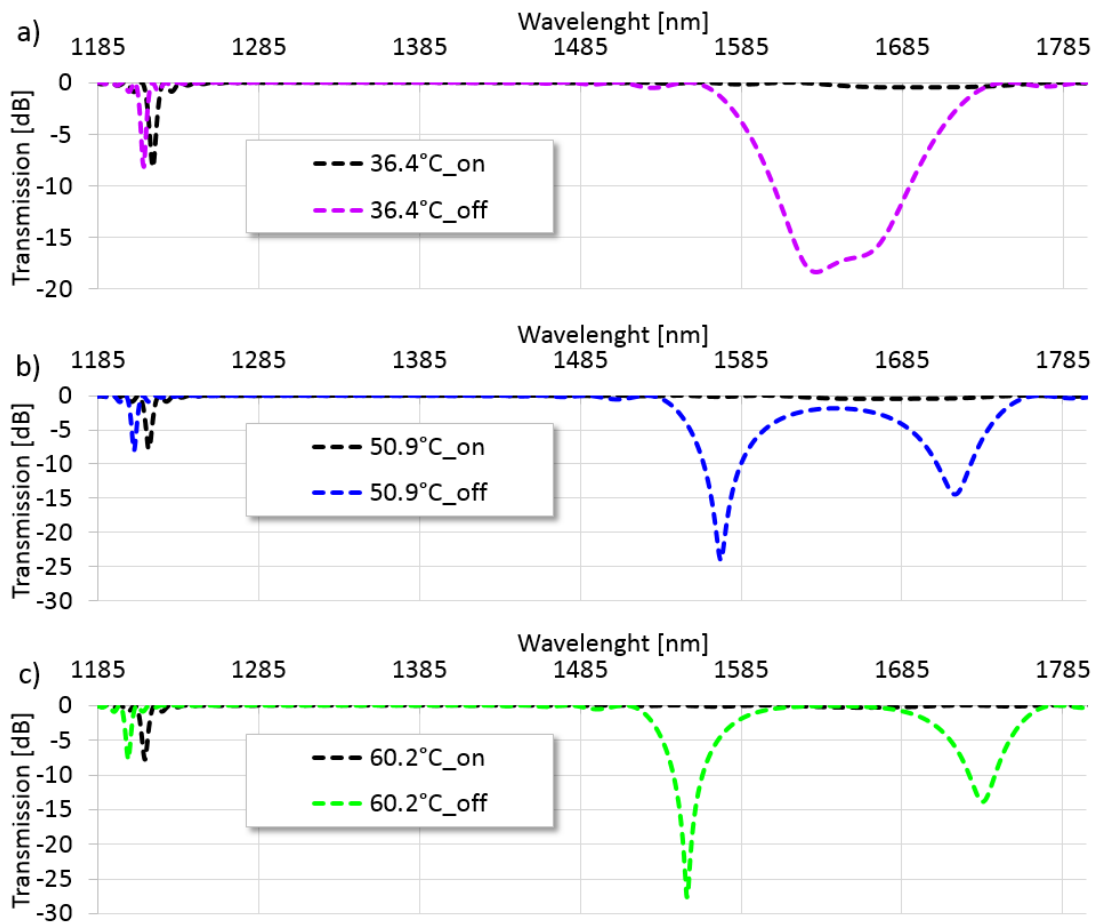


Fig. 6.5.11 Simulated transmission in the off- and on-voltage states for the UV-induced LPFG (based on the PS1250/1500 fiber; with period of 226.8 μm) coated with 1702 LC layer. The thickness of the LC layer was established to be of 2.1 μm . The results were calculated for three different ambient temperature: 36.4°C (a), 50.9°C (b) and 60.2°C (c)

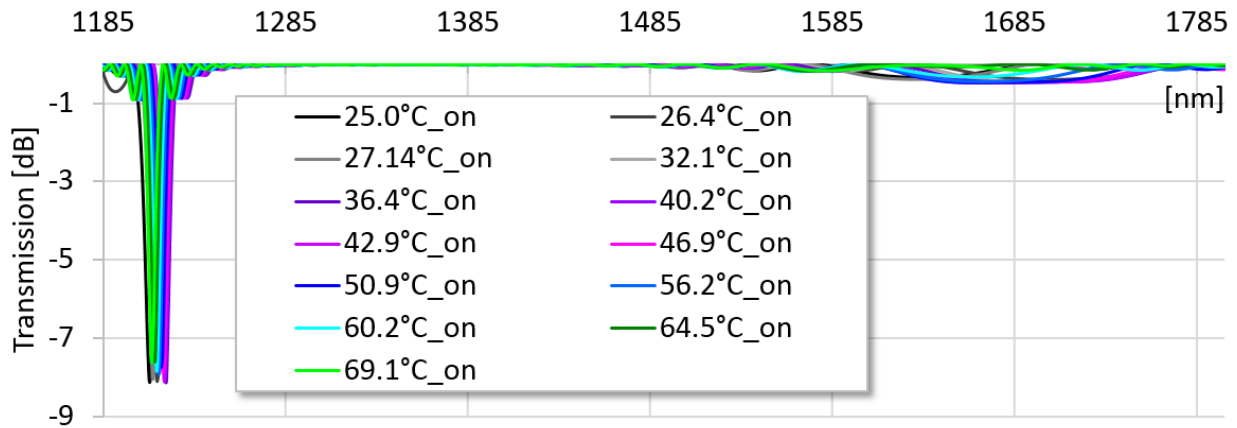


Fig. 6.5.12 Simulated transmission in the on-voltage state versus temperature for the UV-induced LPFG (based on the PS1250/1500 fiber; with period of $226.8 \mu\text{m}$) coated with 1702 LC layer. The thickness of the LC layer was established to be of $2.1 \mu\text{m}$.

In the next step, this same host LPFG was coated with 1702 LC of $2.1 \mu\text{m}$ thickness. In this experiment, thanks to the thermo-optic properties of the LC layer, the RI of the LC layer was also altered by temperature. Simultaneously, the host LPFG responds to the changes in the environmental temperature. As a result, the LC-LPFG transmission spectrum could be modified in order to gain optimum tuning conditions by the electric field. The results presented in Section 6.4.1 show already that by appropriately selecting the ambient temperature, the empirical study of the attenuation band associated with $\text{LP}_{0,11}$ mode will become possible to investigate. The biggest benefits from tracking this attenuation band is that its resonant wavelength is close to the phase-matching turning point. At this moment the attenuation band should exhibit the highest rate of changes to any external perturbations. Consequently, by exploring the LC-LPFG thermal sensitivity, the dual resonant band is generated in the LC-LPFG transmission spectrum. With temperature increasing the central wavelengths of the peaks of the dual resonance band move in the opposite directions. When the temperature is stabilized at the optimal values, the electric field can be subsequently applied to the sample. In Fig. 6.5.11 the simulated transmission spectra for this LC-LPFG in off- and on-voltage states are shown. They were calculated for three different temperatures, namely 36.4°C , 50.9°C and 60.2°C . Simultaneously, the experimentally measured LC-LPFG transmission spectra under this same condition are shown in Fig. 6.5.13. The experimentally investigated spectral range is designated in Fig. 6.5.11 by dash black rounded rectangle. In the presence of an E-field, the dual-resonance attenuation band disappears (this effect is also confirmed by performed simulation of the LC-LPFG thermal response in the on-voltage state, presented in Fig. 6.5.12). This feature gives the possibility to effectively switch this attenuation band by applying an external field to the LC-LPFG. Simultaneously,

its resonant wavelength can be easily altered for the particular needs by adjusting the ambient temperature. It is shown in Fig. 6.5.13 that the wavelength of operation could be fixed at 1520.8 nm, 1564.4 nm and at 1588.4 nm for a temperature of 36.4°C, 50.9°C and 60.2°C, respectively.

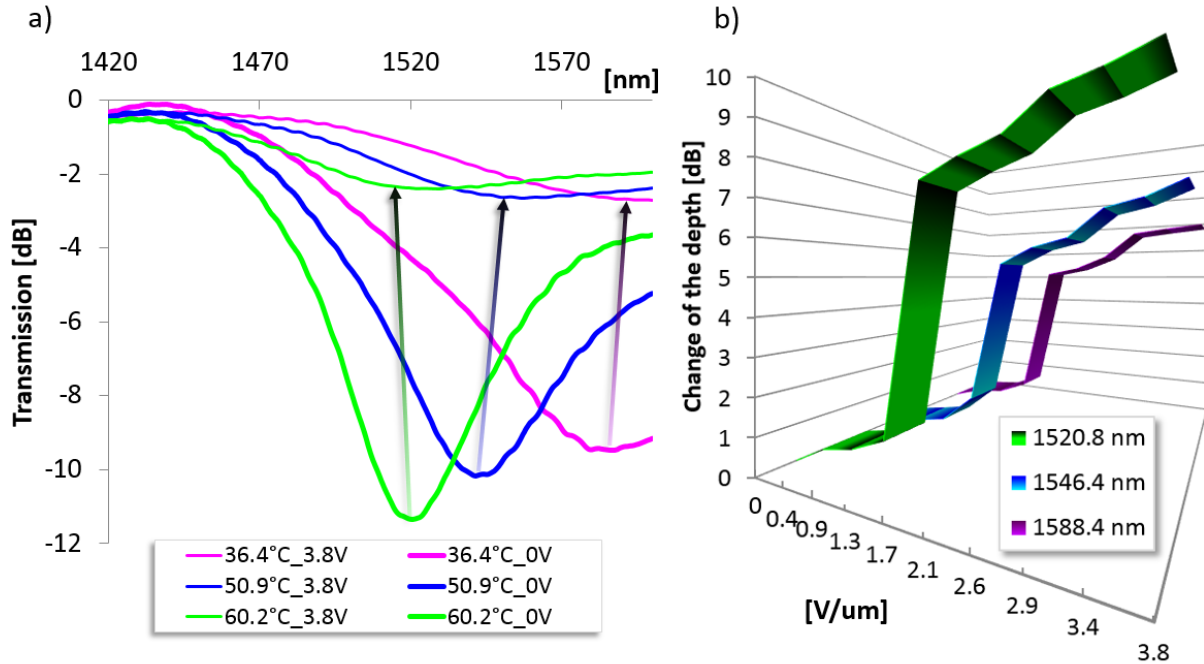


Fig. 6.5.13 a) Transmission spectra in the off- and on-voltage state measured for the UV-induced LPFG (based on the PS1250/1500 fiber; with period of 226.8 μm) coated with 1702 LC layer when the ambient temperature was stabilized to be 36.4°C, 50.9°C and 60.2°C.

b) The attenuation band depth change versus electric field measured for three different values of temperature (36.4°C, 50.9°C and 60.2°C) which correspond with three different values of wavelength operation (1520.8 nm, 1564.4 nm and 1588.4 nm).

Chapter 7 CONCLUSION

7.1 Original contribution and significance of the work

In this Thesis the LPFGs with the LC layers added from the outside to their structure, and referred here to as a liquid crystal long-period fiber gratings (LC-LPFG), have been intensively investigated. The attractiveness of the LC-LPFGs results from the fact that they combine the unique advantages of the long-period fiber gratings and liquid crystals. The biggest practical advantage of LC-LPFGs is the ability to dynamically tune their propagation characteristics, e.g. by an external electric field.

At the beginning of this research (see Section 1.2) the most important objectives realized through these studies were defined. They all have been fully accomplished, which is confirmed by the obtained results - the most significant achievements are listed below. They clearly contribute to the current state-of-art within the LC-LPFGs topic in terms of the LC-LPFG design, the LC-LPFG sensing properties' and the LC-LPFG theoretical analysis.

✓ **Original contribution from the LC-LPFG device design viewpoint**

- developing the methods for coating of the LPFGs with a thin LC layers

The efficiency of LC-LPFG tuning has to be considered in the context of the LC layer thickness. This parameter determines how the cladding modes are guided within the LC-LPFG structure. For example if the grating is placed in the LC cell, the LC layer can be assumed to be infinite. As a result, for gratings surrounded by MB LCs (since RIs for these LC types are higher than the n_{cl} , cladding modes can be guided only thanks to Fresnel reflection effect), variations in the LC RIs will only change considerably the attenuation band depth (see Fig. 6.5.1). However, when the thickness of the LC layer is decreased sufficiently, a strong improvement in the sensitivity of LC-LPFGs can be obtained. Due to the refractive-reflective regime at the cladding-LC layer interface the cladding modes in the LC-LPFG are bound within the structure comprising the core, the cladding and the layer. The induced changes in the RI of such a thin LC layer should thus also lead to a considerable shift of the attenuation bands.

Within this work, two method are developed in order to obtain a thick enough LC coating on the LPFG (presented in Section 6.1.4): placing the LPFG inside a capillary and filling it with LC or coating directly the bare LPFG with a thin LC layer. It has to be mentioned that the LC-LPFG created by the second method

was demonstrated previously in [32]. This Thesis contains a comprehensive and extensive study of this concept, in terms of investigation of various LC materials (see Fig. 6.3.3) combined with different LPFG types (see Tab. 6.1.4). Broad studies focus on the optimization LC-LPFG sensing properties by choosing the appropriate LC layer thicknesses are presented within this work as well.

- implementation of the “double-resonant” LPFGs

The ability of the LPFG to perform as a sensor is highly dependent on the grating period. For shorter periods, coupling takes place to higher order cladding modes. In this case, coupling to a single cladding mode can occur at two wavelengths (so called “double-resonant” effect) within the spectral range investigated. The attenuation band corresponding with this phenomena will exhibit the highest sensitivity to any external perturbation. This feature was exploited here in the context of the LC-LPFGs (see Fig. 6.2.5 and e.g. Figs. 6.5.8, 6.5.13). The combination of “double-resonant” LPFGs with the LCs is investigated here for the first time, to the author’s best knowledge.

- using prototype LB LC mixtures as a LPFG coating

In this work the use of hybrid LC-LPFGs is aimed at taking advantage of two different LCs classes: those with MB and those with LB, providing in this way the widest LC index range variation investigated so far. In contrast to the MB LCs, for which both RIs are greater than the RI of silica glass, the ordinary RI of LB LC mixtures is close to the refractive index of the silica glass and in some temperature range, it is even lower. It has been shown that combination of this LC types with LPFGs allowed to obtain novel and valuable effects. For example, an electrically induced displacement of 130 nm in the attenuation band of the LC-LPFG transmission spectrum could be obtained by coating the UV-induced LPFG with 1550A LB LC (Fig. 6.5.7). Interesting results were also accomplished for the LPFG placed inside the capillary filled with 1110 LB LC (Figs 6.4.5 – 6.4.7 and Fig. 6.4.13). For such a LC-LPFG device design the attenuation bands associated with modes with the even and odd radial numbers manifest different thermal sensitivities. Moreover, the modes’ characteristic was changed from a mode with an even radial number to a mode with an odd radial number while the LC-LPFG sample was heated. Using this novel approach, the sensitivity of the LC-LPFG can be increased considerably.

✓ **Original contribution from the LC-LPFG sensing properties’ viewpoint**

The spectral characteristics of the LPFG transmission spectrum are dependent on the RI of the external medium. Consequently, one can expect that varying the LC’s thermo- and electro-optical properties will

induce a modification of the LPFG response. This hypothesis was confirmed by the experiments carried out in this work. The most interesting effects that have been accomplished in the course of this study, include:

- Changing the sign and the magnitude of the LPFG thermal response by adding the LC layer to its structure – realized within **objective 1.1**.
- Compensating the thermal effect in the LPFGs by a proper choice of a LC layer – realized within **objective 1.1**.
- Fast switching of the LC-LPFG transmission spectrum in specific temperatures (e.g. in the clearing temperature of the LC used as a grating layer) – realized within **objectives 1.1 and 1.3**.
- Achieving electrical modulation of the depth of the attenuation bands and spectral positioning of the resonant wavelengths for gratings coated with thin LC layers. This effect is possible since the cladding modes transition occurs when the external electric field is applied to the LC-LPFG. As a result, the LC-LPFG is able to operate between two sets of attenuation bands corresponding with on- and off-voltage states – realized within **objectives 1.2 and 1.3**.
- Improving the LC-LPFGs electric switching capabilities by a proper choice of the temperature range operation – realized within **objectives 1.2 and 1.3**.

✓ **Original contribution from the LC-LPFG theoretical analysis viewpoint**

The LC-LPFG theoretical model has to be developed. So far there is a lack of publications devoted exactly to this topic.

The LC-LPFG model developed and analyzed within this work is based on the thin layer coated LPFG concept. A detailed description of the LC-LPFG theoretical analysis can be found in Chapter 5, and in Chapter 6 these theoretical results were put in context of the experimental work. In order to find correspondence between the experimental and the theoretical LC-LPFGs transmission spectra the following problems were solved:

- Simulating as accurately as possible the LC-LPFG transmission spectra in regards to the parameters of the fiber itself (e.g., cladding/core radius and RI, dopant concentration), changes in the fiber induced by the formation of the LPFG (e.g., grating period, fiber length, changes in

the core–cladding RI difference or fabrication methods) and adequate parameterization of the LC layer (through the carefully examined the impact of its refractive index and thickness values) – realized within **objective 2.1**.

- Modelling the LC-LPFG thermal sensitivity effect. The theoretical analysis shows that thanks to the presence of a properly chosen LC layer, the thermal response of the grating can be (in principal) adjusted over a very wide temperature sensitivity range: starting from a significant increase of the LC-LPFG thermal sensitivity down to its compensation. The effect of the fast switching the LC-LPFG transmission spectrum in specific temperature ranges was successfully simulated as well (see e.g. Fig. 6.4.7) – realized within **objective 2.2**.
- Modelling the LC-LPFG electrical effect. It was demonstrated that the electrically switching attenuation bands' effect in the LC-LPFG transmission spectrum occurs mainly thanks to the cladding modes' transition. The birefringence magnitude for the LCs investigated experimentally was from 0.0611 to 0.170. Therefore, the external electric field changed the LC layer RI by the value which should usually lead to the transition of the lowest-order cladding mode (higher effective index) to be guided within the LC layer. As the lowest-order cladding mode moves to be guided within the overlay, a reorganization of the other cladding modes occurs. As a result, the LC-LPFG is able to operate between two states of the attention bands, namely off- and on-voltage states. Moreover, it was also explained how the direction of the electrically induced attenuation band displacement (toward red/blue part in the LC-LPFG transmission spectrum) depend on the LC-LPFG design (see e.g. Figs. 6.5.4 and 6.5.5) – realized within **objective 2.2**.
- Modelling the LPFG placed inside the capillary filled with LC and providing a thermal sensitivity dependence for such a LC-LPFG device design. It was demonstrated that the presence of the capillary fundamentally changes the modes' characteristic. Precisely, this outer layer separates them into two groups of modes with even and odd radial numbers (e.g. the transition for modes with even and odd radial numbers occur at different moments with the LC layer refractive index variation: see Fig. 5.4.1 and Fig. 5.4.2). This novel effect obviously has an impact on the thermal response of such a LC-LPFG design. It was shown that by varying temperature, the characteristic of the modes can be changed from a modes with an odd radial number to an even radial number (see Figs. 5.4.3 and 5.4.5) – realized within **objective 2.3**.

The main software tool chosen in order to analyze the problems listed above is the OptiGrating v.4.2. This software is specifically designed for modeling integrated fiber optic devices that are assisted by optical

gratings. The simulated LC-LPFG structures (see Fig. 5.1.1) were composed by four layers, in the case of the LPFG coated with a thin LC layer (corresponding with the fiber core, the fiber clad and the LC layer surrounded by the four layers of air), and by five layers, in the case of the LPFG placed in the silica glass capillary with an inner LC layer (corresponding with the fiber core, the fiber clad, the LC layer, the silica glass layer surrounded by the five layers of air). It is worth mentioning that up to now, the 5-layer model was never analyzed before in the context of the LC-LPFGs.

In conclusion, the obtained results provide a deeper understanding of a proper choice of the LC-LPFG components, along with an adjustment of their parameters. The necessary characteristics of the thermo- and/or electro-optic sensing behavior of the LC-LPFGs were presented as well. Therefore, this study should be useful for further development of such advanced tunable devices that have no counterpart on the current market of active fiber components. The major benefit of these devices is that their spectral properties can be adjusted and controlled with an outstanding level of flexibility. Moreover, the optical signal is formed and modified directly in the fiber (all-in-fiber), avoiding in this way a variety of complex alignment issues. They can also be easily coupled to the fibers (useful whenever there is a need for superior fiber optic systems). They can be created with considerably low production costs as well, since they are based on the elements that are already produced with advanced manufacturing capabilities and well-developed know-how technology. From a wider perspective, the work presented here can contribute to the fabrication and practical implementation of LC-LPFGs as photonic devices which can be created as individual components (including tunable filters, all-in fiber attenuators, threshold sensors, temperature and electric field sensors, switches, all-optical multi-parameter sensors and so on), as well as a complement to already existing fiber optic systems. Such flexible fiber optic photonic structures are expected to meet the need for miniaturized, reliable, flexible, alignment-free devices. Further active research in this field can lead to unique and innovative technologies applicable in optical communication and sensing technologies.

7.2 Further research directions

The proposed designs of the LC-LPFGs offer very interesting properties, useful characteristics, and therefore introduce a new level of sensitivity and an improvement in performance. However, as with any research, some unexpected phenomena and problems could be observed during the course of the investigation – many of them present new research opportunities and perhaps even novel tuning attributes. The most interesting future research directions are:

- Achieve a better control of the LC layer thickness and improve the repeatability of its application

The coating technique on the surface of the fiber with LC is challenging and the method is still not settled enough (nonetheless, the LC layer thickness on the LPFGs investigated could be established through the LC-LPFGs modeling process). In this work, the rubbing technique was applied. The next possible improvement involves the pre-coating of the LPFG with a thin orientation layer for a LC e.g. by using the polyimide resin [120]. In addition, many of these materials possess high refractive indices. This could be a supplementary advantage to their use, as it increases the LPFG sensitivity to higher values of the LC refractive indices and may even provide new tuning effects.

- Investigation of the LC-LPFGs polarization properties

In the cases when high values of birefringence or Polarization Dependent Losses are desirable, the LC-LPFG polarization properties could be well exploited. For this purpose, the LC with high birefringence and dielectric anisotropy would be the best choice. Additionally, in order to achieve LCs molecules' orientation effectively, modified by an electric field, a different electrode configuration could be used, e.g.: four electrodes arranged in the v-groove assembly or two short parallel electrodes together with two conductive rods placed on both sides of the LC-LPFG (the theoretical calculation of the electric field distribution in the photonic crystal fiber filled with LC for these electrode sets was presented in [107]). Then, depending on the electrode supply configuration, the direction of the electric field (and thus also polarizer axis) could be changed from 0° to 45° or 90° . Such a LC-LPFG packed design would serve as a tunable polarizer with variable polarization axis.

- Study of the LC-LPFG theoretical model having a complex refractive index

For all the LC-LPFGs experimentally studied, when the LC layer was applied on the grating, the depth of attenuation bands decreased. This is due to the fact that there are scattering and material losses from the LC layer which have an impact on the attenuation band depths. Additionally, the strong variation of the

attenuation bands depth was observed when the LC-LPFG was tuned within the mode transition region. When LC-LPFGs transmission spectra were simulated these effects were not observed since the LC layer refractive index was assumed to be purely real. This assumption allows to more easily understand the effects of the LC layer on a LPFG, and it still describes adequately the experimental results. However, the case for LPFG with LC layer having a complex refractive index would be worth studying in the future. This would additionally allow the simulation of the modes' vanishing phenomena.

- Theoretical study of the LC-LPFG by using a hybrid mode model

For the LC-LPFGs theoretical analysis, a linearly polarized (LP) mode model supported by experimental data was used. This model has been shown to yield satisfactory results when the LC-LPFG spectral properties were simulated. Nevertheless, some disagreements between the simulated and experimental results were evident (as an example, let the UV-induced LPFG coated with 1550 LC layer - Figs. 6.4.10 and 6.4.12 be recalled: the simulations have failed to remark the effect measured experimentally of the attenuation band splitting up when this LC-LPFG sample was heated). While comparing the LP mode model with the hybrid mode model, it was presented that if the weak guidance condition was not fulfilled, low order modes should show a two-step transition rather than the one step transition predicted by the LP mode model [43]. Therefore, the computationally more involved hybrid mode model should be used in the next step of the LC-LPFGs simulations in order to provide more accurate results.

- Investigation of different LCs and/or host LPFGs combinations

By choosing different LCs and/or host LPFGs new types of tuning effects could be obtained. In this work, the LCs were applied selectively in the nematic or isotropic phases. The results already showed numerous interesting features when they were combined with LPFGs. However, the variety of LCs is large: ferroelectric LCs [108] or chiral nematics with helical structure [109] are only a few examples of LC materials that could be used. In contrast to the variations of the mesophases, new types of LPFGs could be applied in order to make use of other tuning properties. For example, it could be interesting to fabricate LPFG based on the fiber made from glass with high refractive index. Such a grating would be a very suitable candidate to be combined with LC, since it could offer sensitivity to the highest values of LC refractive index. It may be also worthwhile to coat the LPFG based on PCF fiber with a LC layer. It was demonstrated that this kind of gratings exhibits extraordinary features. For example, it has been found that the resonance wavelength of a LPFG in PCF is blue-shifted when the grating period is increased, which is contrary to that of a LPFG based on conventional fibers. Moreover, the LPFG based on PCF could solve the problem of the thermal cross-sensitivity between the host grating and LC layer.

References

1. "The Nobel Prize in Physics 2009". *Press release of the Royal Swedish Academy of Sciences*. 6 October 2009, http://nobelprize.org/nobel_prizes/physics/laureates/2009/press.html.
2. V. Vali, R.W. Shorthill. "*Fiber Ring Interferometer*". *Appl. Opt.*, Vol. 15, pp. 1099-1100, 1976
3. S.A. Vasiliev, O.I. Medvedkov, I.G. Korolev, A.S. Bozhkov, A.S. Kurkov, E.M. Dianov. "*Fiber gratings and their applications*". *Quantum Electronics.*, Vol. 35, 12, pp. 1085-1103, 2005
4. K.S. Chiang, 2Q. Liu. "*Long-period grating devices for application in optical communication*". *Proc. ICOCN 2006*, pp. 128-133, 2006
5. T. Erdogan. "*Fiber grating spectra*". *J. Lightwave Technol.*, Vol. 15, 8, pp. 1277-1294, 1997
6. T. Erdogan. "*Cladding-mode resonances in short- and long-period fiber grating filters*". *J. Optical Society of America A.*, Vol. 14, 8, pp. 1760-1773, 1997
7. T. Erdogan. "*Cladding-mode resonances in short- and long-period fiber grating filters: Errata*". *J. Optical Society of America A.*, Vol. 17, 11, p. 2113, 2000.
8. A. N. Vengsarkar, P. J. Lemaire, J. P. Judkins, V. Bhatia, T. Erdogan, J. E. Sipe. "*Long-period fiber gratings as band-rejection filters*". *J. Lightwave Technol.*, Vol. 14, 1, pp. 58-65, 1996
9. X. Shu, L. Zhang, I. Bennion. "*Sensitivity characteristics of long-period fiber gratings*". *J. Lightwave Technol.*, Vol. 20, 2, pp. 255-266, 2002
10. S. W. James, R. P. Tatam. "*Optical fibre long-period grating sensors: characteristics and application*". *Meas. Sci. Technol.*, Vol. 14, pp. R49–R61, 2003
11. V. Bhatia. "*Applications of long-period gratings to single and multi-parameter sensing*". *Opt. Express.*, Vol. 4, pp. 457-466, 1999
12. O. Frazão, G. Rego, M. Lima, A. Teixeira, F. M. Araújo, P. André, J. F. Rocha, H. M. Salgado. "*EDFA gain flattening using long-period fibre gratings based on the electric arc technique*". *Proc. London Communications Symposium 2001*. University College of London, England, pp. 55-57, 2001
13. X. J. Gu. "*Wavelength-division multiplexing isolation fiber filter and light source using cascaded long-period fiber gratings*". *Optics Letters.*, Vol. 23, 7, pp. 509-510, 1998
14. Brent L. Bachim and Thomas K. Gaylord "Polarization-dependent loss and birefringence in long-period fiber gratings", *Applied Optics*, Vol.42, No. 34, pp. 6816-6823, 2003
15. J. L. Arce-Diego, D. Pereda-Cubian and M. A. Muriel "Polarization effects in short- and long-period fibre gratings: a generalized approach" *J. Opt. A: Pure Appl. Opt.* 6, pp. S45-S51, 2004
16. T. A. Eftimov, W. J. Bock, J. Chen, P. Mikulic. "*Müller–Stokes analysis of long-period gratings Part I: Uniformly birefringent LPGs*". *J. Lightwave Technol.*, Vol. 27, pp. 3752-3758, 2009

17. T. A. Eftimov, W. J. Bock, P. Mikulic, J. Chen, Tinko A. Eftimov, Wojtek J. Bock, Predrag Mikulic, and Jiahua Chen. "*Müller–Stokes analysis of long-period gratings Part II: Randomly birefringent LPGs*". J. Lightwave Technol., Vol. 27, pp. 3759-3764, 2009
18. O. Lehmann. "Über fließende Krystalle". Zeitschrift für Physikalische Chemie., Vol. 4, pp. 462–472, 1889
19. I.C. Khoo, S.T. Wu. "*Optics and Nonlinear Optics of Liquid Crystals*". Singapore: World Scientific Publ., 1997
20. I. Palarie, C. Florea. "*Refractive indices determination of a new nematic liquid crystal*". J. Optoelectronics and Advanced Materials, Vol. 7, 2, pp. 997-1007, 2005
21. J. Li, C-H. Wen, S. Gauza, R. Lu, and S-T. Wu "*Refractive Indices of Liquid Crystals for Display Applications*," J. Display Technol., Vol. 1, pp. 51-61 , 2005
22. M. Gu, Y. Yin, S.V. Shiyonovskii, O. D. Lavrentovich. "*Effects of dielectric relaxation on the director dynamics of uniaxial nematic liquid crystal*". Physical Review., Vol. 76, pp. 061702-1-061702-12, 2007
23. M. Klasen, M. Bremer, A. Gotz, A. Manabe, S. Naemura. "*Calculation of optical and dielectric anisotropy of nematic liquid crystal*". Jpn. J. Appl. Phys., Vol. 37, pp. L945-L948, 1998
24. R. Wang, T. J. Atherton, M. Zhu, R. G. Petschek, C. Rosenblatt. "*Naturally occurring reverse tilt domains in a high-pretilt alignment nematic liquid crystal*". Phys. Rev. Lett., Vol. 75, pp. 1-5, 2007
25. D. K. Shenoy, J. V. Selinger, K. A. Grüneberg, J. Naciri, R. Shashidhar. "*Coarsening of reverse tilt domains in liquid-crystal cells with heterogeneous alignment layers*". Phys. Rev. Lett., Vol. 82, pp. 1716–1719, 1999
26. J. Weirich, J. Lagsgaard, L. Wei, T. Tanggaard Alkeskjold, T. X. Wu, S-T. Wu, A. Bjarklev. "*Liquid crystal parameter analysis for tunable bandgap fiber devices*". Opt. Express., Vol. 18, pp. 4074-4087, 2010
27. O. Duhem, J.F. Hennion, M. Warengem, M. Douay, L. Rivoallan. "*Long period fiber gratings modulation by liquid crystal cladding*". Proc. 6th IEEE Conf. on Telecommunications. 451, pp. 195-196, 1998
28. S. Yina, K-W. Chung, X. Zhu. "*A novel all-optic tunable long-period grating using a unique double-cladding layer*". Opt. Commun., 196, pp. 181-186, 2001
29. Hak-Rin Kim, Y. Kim, Y. Jeong, S. Baek, Y. Wook Lee, B. Lee, S-D. Lee. "*Suppression of the cladding mode interference in cascade long period fiber gratings with liquid crystal cladding*". Mol. Cryst. Liq. Cryst., Vol. 413, pp. 399-406, 2004
30. S.Z. Yin, K.W. Chung, X. Zhu. "*A highly sensitive long period grating based tunable filter using a unique double-cladding layer structure*". Opt. Commun., Vol. 188, 5-6, pp. 301-305, 2001
31. A.A. Abramov, A. Hale, R.S. Windeler, T.A. Strasser. "*Widely tunable long-period fiber gratings*". Electron. Lett., 35, pp. 81-82, 1999

32. H. Luo, X. Li, S. Li, J. Chen. "Analysis of temperature-dependent mode transition in nanosized liquid crystal layer-coated long period gratings". *Appl. Opt.*, 48, pp. F95-F100, 2009
33. Y. Jeong, B. Yang, B. Lee, H. S. Seo, S. Choi, K. Oh. "Electrically controllable long-period liquid crystal fiber gratings". *IEEE Photonics Technology Letters.*, Vol. 12, 5, pp. 519-521, 2000
34. D. Noordegraaf, L. Scolari, J. Lægsgaard, L. Rindorf, T. T. Alkeskjold. "Electrically and mechanically induced long period gratings in liquid crystal photonic bandgap fibers". *Opt. Express.*, Vol. 15, pp. 7901-7912, 2007
35. D. Noordegraaf, L. Scolari, J. Lægsgaard, T. T. Alkeskjold, G. Tartarini, E. Borelli, P. Bassi, J. Li, S-T. Wu. "Avoided-crossing-based liquid-crystal photonic-bandgap notch filter". *Opt. Lett.*, Vol. 33, pp. 986-988, 2008
36. H. Hochreiner, M. Cadab, P. D. Wentzella "Tuning the response of long-period fiber gratings for chemical sensing applications". *Proc. of SPIE*, Vol. 6765, 676504, pp.1-15, 2007
37. N. D. Rees, S. W. James, R. P. Tatam, and G. J. Ashwell, "Optical fiber long-period gratings with lang-muirbloodgett thin-film overlays," *Opt. Lett.* 27, pp. 686-688, 2002
38. I. del Villar, M. Achaerandio, I. R. Matías, and F. J. Arregui, "Deposition of overlays by electrostatic self-assembly in long-period fiber gratings," *Opt. Lett.* 30, pp. 720-722, 2005
39. I. Del Villar, I. R. Matías, F. J. Arregui. "Optimization of sensitivity in long period fiber gratings with overlay deposition". *Optics Express.*, Vol. 13, pp. 56-69, 2005
40. I. del Villar, I. R. Matias, F. J. Arregui, and M. Achaerandio, "Nanodeposition of materials with complex refractive index in long-period fiber gratings", *J. Lightwave Technol.* 23, pp. 4192-4199, 2005
41. A. Cusano, A. Iadicicco, P. Pilla, L. Contessa, S. Campopiano, A. Cutolo, and M. Giordano, "Cladding mode reorganization in high-refractive-index-coated long-period gratings: effects on the refractive-index sensitivity," *Opt. Lett.* 30, pp. 2536-2538, 2005
42. A. Cusano, A. Iadicicco, P. Pilla, L. Contessa, S. Campopiano, A. Cutolo, and M. Giordano. "Mode transition in high refractive index coated long period gratings," *Opt. Express.*, Vol. 14, pp. 19-34, 2006.
43. I. del Villar, I. R. Matias, and F. J. Arregui, "Influence on cladding mode distribution of overlay deposition on long-period fiber gratings," *J. Opt. Soc. Am. A* 23, pp. 651-658, 2006.
44. I. del Villar, I. R. Matias, and F. J. Arregui, "Enhancement of sensitivity in long-period fiber gratings with deposition of low-refractive-index materials," *Opt. Lett.* 30, pp. 2363-2363, 2005.
45. A. Cusano, A. Iadicicco, P. Pilla et al., "Coated long-period fiber gratings as high-sensitivity optochemical sensors," *Journal of Lightwave Technology*, vol. 24, no. 4, pp. 1776-1786, 2006
46. I. D. Villar, I. R. Matias, and F. J. Arregui, "Long-period fiber gratings with overlay of variable refractive index," *IEEE Photonics Technology Letters*, vol. 17, no. 9, pp. 1893-1895, 2005.

47. J.-L. Tang and J.-N. Wang, "Measurement of chloride-ion concentration with long-period grating technology," *Smart Materials and Structures*, vol. 16, no. 3, pp. 665–672, 2007.
48. X. T. Wei, T. Wei, H. Xiao, and Y. S. Lin, "Terbium doped strontium cerate enabled long period fiber gratings for high temperature sensing of hydrogen," *Sensors and Actuators B*, vol. 152, no. 2, pp. 214–219, 2011.
49. R.M.Carter, R. R. J.Maier, P. Biswas et al., "Increased sensitivity of long period grating hydrogen sensors through coupling to higher order claddingmodes," in *22nd International Conference on Optical Fiber Sensors*, vol. 8421 of *Proceedings of SPIE*, pp. 1–4, Beijing, China, October 2012.
50. M. Konstantaki, A. Klini, D. Anglos, and S. Pissadakis, "An ethanol vapor detection probe based on a ZnO nanorod coated optical fiber long period grating," *Optics Express*, vol. 20, no. 8, pp. 8472–8484, 2012.
51. G. Zhu, X. Li, C. Tao, J. Huang, and J. Yang, "Optical fiber methane sensor based on SAN film containing cryptophane-E-(OEt)₆," *Chinese Optics Letters*, vol. 10, no. 10, Article ID100601, 2012.
52. G. Rego, "A Review of Refractometric Sensors Based on Long Period Fibre Gratings", *The Scientific World Journal*, Article ID 913418, pp.1-14, 2013
53. C. S. Cheung, S. M. Topliss, S. W. James, R. P. Tatam "Response of fiber-optic long-period gratings operating near the phase-matching turning point to the deposition of nanostructured coatings" *J. Opt. Soc. Am. B*, Vol. 25, No. 6, pp. 897- 902
54. S. Khaliq, S. W. James, R. P. Tatam. "Enhanced sensitivity fibre optic long period grating temperature sensor". *Meas. Sci. Technol.*, Vol. 13, pp. 792–795, 2002.
55. M. Śmietana, W. J. Bock, P. Mikulic. "Comparative study of long-period fiber gratings written in a boron co-doped fiber by an electric arc and UV irradiation". *Meas. Sci. Technol.*, Vol. 21, pp. 1-8, 2010
56. W. Bock, J. Chen, P. Mikulic, T. Eftimov, M. Korwin-Pawłowski, "Pressure sensing using periodically tapered long-period gratings written in photonic crystal fibers". *Meas. Sci. Technol.*, Vol. 18, pp. 3098–3102, ISSN 1361-6501, 2007
57. L-Y.Shao, A.Laroche, M.Smietana, P.Mikulic, W.J.Bock, J.Albert, "Highly Sensitive Bend Sensor with Hybrid Long Period and Tilted Fiber Bragg Grating", *Optics Comm. (NL)* vol. 283, pp. 2690-2694, 2010
58. M. Szymańska, K. Krogulski, P. Mikulic, W.J. Bock, M. Śmietana, "Sensitivity of Long-period Gratings Modified by their Bending", *Procedia Engineering*, Vol. 87, pp.1180-1183, 2014
59. V. Bhatia, A.M. Vengsarkar "Optical fiber long-period grating sensors". *Optics Letters*, Vol. 21, pp. 692-694, 1996
60. A. Iadiciocco, S. Campopiano, A. Cutolo, M.L. Korwin-Pawłowski, W.J. Bock, A. Cusano. "Refractive Index Sensitivity in Thinned UV and Arc Induced Long-Period Gratings: A Comparative Study. *International Journal on Smart Sensing and Intelligent Systems*, Vol. 1, pp. 354-369, 2008

61. P. Pilla, P. F. Manzillo, V. Malachovska, A. Buosciolo, S. Campopiano, A. Cutolo, L. Ambrosio, M. Giordano, A. Cusano "Long period grating working in transition mode as promising technological platform for label-free biosensing". *Optics Express*, Vol. 17, No. 22, pp. 20039-20050, 2009
62. S. A. Vasiliev, E. M. Dianov, O. I. Medvedkov, V. N. Protopopov, D. M. Costantini, A. Iocco, H. G. Limberger, R. P. Salathe. "Properties of the cladding modes of an optical fibre excited by refractive-index gratings". *Quantum Electron.*, Vol. 29, pp. 65-68, 1999
63. H. J. Patrick, A. D. Kersey, F. Bucholtz. "Analysis of the response of long period fiber gratings to external index of refraction". *J. Lightwave Technol.*, Vol. 16, 9, pp. 1606-1612, 1998
64. R. C. Kamikawachi, G. R. C. Possetti, M. Muller, J. L. Fabris. "Non-linear behavior of long period fiber grating thermal sensitivity in different surroundings". *J. Microwaves and Optoelectronics.*, Vol. 6, 1, pp. 336-345, 2007
65. B. H. Lee, Y. Liu, S. B. Lee, S. S. Choi, J. N. Jang. "Displacements of the resonant peaks of a long-period fiber grating induced by a change of ambient refractive index". *Optics Letters* 22(23)., Vol. 22, 23, pp. 1769-1771, 1997
66. H. J. Patrick, A. D. Kersey, F. Bucholtz, K. J. Ewing, J. B. Judkins, A. M. Vengsarkar. "Chemical sensors based on long-period fibre grating response to index of refraction". *Conf. on Lasers and Electro-Optics. CThQ5*, pp. 420-421, 1997
67. O. Duhem, J. F. Henninot, M. Warengem, M. Douay. "*Demonstration of long-period-grating efficient couplings with an external medium of a refractive index higher than that of silica*". *Applied Optics.*, Vol. 37, 31, pp. 7223-7228, 1998
68. D. B. Stegall, T. Erdogan. "*Leaky cladding mode propagation in long-period fiber grating devices*". *IEEE Photonics Technology Letters.*, Vol. 11, 3, pp. 343-345, 1999
69. R. Hou, Z. Ghassemlooy, A. Hassan, C. Lu, K.P. Dowker. "*Modelling of long-period fibre grating response to refractive index higher than that of cladding*". *Meas. Sci. Technol.*, Vol. 12, pp. 1709-1713, 2001
70. K. Okamoto. "Fundamentals of optical waveguides". San Diego: Academic Press, 2000.
71. R.M. Measures. "Structural monitoring with fiber optic technology". San Diego: Academic Press, 2001
72. G. Keiser. *Optical fiber communications*. (3rd ed.). Boston: McGraw-Hill, 2000.
73. D. Marcuse, D. Gloge, E.A. Marcatili. "Guiding properties of fibres. In Miller, S.E. & Chynoweth, A.G. (Eds.), *Optical fiber telecommunications*. New York: Academic Press, 1979.
74. K. Kawano, T. Kitoh. "Introduction to Optical Waveguide Analysis: Solving Maxwell's Equation and the Schrödinger Equation". Wiley, 978-0-471-40634-1, 2001
75. D. Gloge. "Weakly guiding fibers". *Applied Optics.*, Vol. 10, 10, pp. 2252-2258, 1971
76. H. A. Haus, W. P. Huang, S. Kawakami, N. A. Whitake. "Coupled-mode theory of optical waveguides". *J. Lightwave Technol.*, Vols. LT-5, 1, pp. 16-23, 1987.

77. R. Kashyap. "Fiber Bragg gratings". San Diego : Academic Press, 1999.
78. K. P. Chen, P. R. Herman, R. Tam, J. Zhang. "Rapid long-period grating formation in hydrogen-loaded fibre with 157nm F2-laser radiation". *Electronics Letters.*, Vol. 36, 34, pp. 2000-2001, 2000
79. J. Albert, B. Malo, K. O. Hill, F. Bilodeau, D. C. Johnson. "Comparison of one-photon and two-photon effects in the photosensitivity of germaniumdoped silica optical fibers exposed to intense ArF excimer laser pulses". *Applied Physics Letters.*, Vol. 67, 24, pp. 3529-3531, 1995.
80. Y. Zhu. „Fabrication of Long-Period Gratings and their Applications in Optical Fibre Communications and Sensing Systems“. Faculty of Engineering, Rand Afrikaans University Johannesburg Republic of South Africa. 2002. PhD Thesis.
81. I. J. G. Sparrow. "Development and Applications of UV Written Waveguides". Faculty of Engineering, University of Southampton. 2005. PhD Thesis.
82. D. L. Williams, B. J. Ainslie, R. Armitage, R. Kashyap, R. Campbell. "Enhanced UV photosensitivity in boron codoped germanosilicate fibres". *Electron. Lett.*, Vol. 29, p. 45, 1993
83. K. Awazu, H. Kawazoe, M. Yamane. "Simultaneous generation of optical absorption bands at 5.14eV and 0.452eV in 9SiO₂:GeO₂ glasses heated under an H₂ atmosphere". *J. Appl. Phys.*, Vol. 68, pp. 2713-2718, 1990
84. E. Salik, D. S. Starodubov, V. Grubsky, and J. Feinberg. "Increase of photosensitivity in Gedoped fibres under strain". *Optical Fibre Communication Conference (OFC2000)*, Vol. TuH5., 2000
85. G. Rego, P. Caldas, O. Ivanov, and J. L. Santos, "Investigation of the long-term stability of arc-induced gratings heat treated at high temperatures," *Optics Communications*, vol. 284, no. 1, pp. 169–171, 2011
86. M. Smietana, W. J. Bock, P. Mikulic, and J. Chen, "Increasing sensitivity of arc-induced long-period gratings-pushing the fabrication technique toward its limits," *Measurement Science and Technology*, vol. 22, no. 1, Article ID015201, 2011
87. G. Rego. "Arc-Induced Long-Period Fibre Gratings. Fabrication and Their Applications in Optical Communications and Sensing". Department of Electrical and Computer Engineering, Faculty of Engineering, University of Porto. 2006. PhD Thesis.
88. G. Humbert, A. Malki. "Electric-arc-induced gratings in non-hydrogenated fibres: fabrication and high-temperature characterisations". *Journal of Optics A: Pure and Applied Optics.*, Vol. 4, 2, pp. 194-198, 2002
89. G. Rego, O.V. Ivanov, P.V.S. Marques. "Demonstration of coupling between to symmetric and antisymmetric cladding modes in arc-induced long-period fiber gratings". *Opt. Express.*, Vol. 14, pp. 9594-9599, 2007
90. V. Grubsky and J. Feinberg, "Rewritable densification gratings in boron-doped fibers," *Optics Letters*, vol. 30, no. 11, pp. 1279–1281, 2005

91. Y. Jiang, Q. Li, C. H. Lin, E. Lyons, I. Tomov, H. P. Lee. "A novel strain induced thermally tuned longperiod fibre grating fabricated on a periodic corrugated silicon fixture". *IEEE Photon. Technol. Lett.*, Vol. 14, 7, pp. 941-943, 2002
92. G. Kakarantzas, T. E. Dimmick, T. A. Birks, R. Le Roux, P. St. J. Russell. "Miniature all-fibre devices based on CO₂ microstructuring of tapered fibres". *Opt. Lett.* 2001, Vol. 26, 15, pp. 1137-1139, 2001
93. C. Y. Lin, G. W. Chern, L. A. Wang. "Periodical corrugated structure for forming sampled fibre Bragg grating and long-period fibre grating with tunable coupling strength". *J. Lightwave Technol.*, Vol. 19, 8, pp. 1212-1220, 2001
94. S. Savin, M. J. F. Digonnet, G. S. Kino, H. J. Shaw. "Tunable mechanically induced long-period fiber gratings". *Opt. Lett.*, Vol. 25, 17, pp. 710-712, 2000
95. V. I. Kopp, V. M. Churikov, G. Zhang, J. Singer, C. W. Draper, N. Chao, D. Neugroschl, A. Z. Genack. "Chiral Fiber Gratings: Perspectives and Challenges for Sensing Applications". *Proceedings of SPIE.*, Vol. 6619, pp. 66190B-1 - 66190B-8, 2007
96. J. K. Bae, S. H. Kim, J. H. Kim, J. H. Bae, S. B. Lee, J. M. Jeong. "Spectral shape tunable band-rejection filter using a long-period fiber grating with divided coil heaters". *IEEE Photon. Technol. Lett.*, Vol. 15, 3, pp. 407-409, 2003
97. H. S. Kim, S. H. Yun, I. K. Kwang, B. Y. Kim. "All-fiber acousto-optic tunable notch filters with electronically controllable spectral profile". *Opt. Lett.*, Vol. 22, 19, pp. 1476-1478, 1997
98. K. R. Sohn, K. T. Kim. "Thermo-optically tunable band-rejection filters using mechanically formed longperiod fiber gratings". *Opt. Lett.*, Vol. 30, 20, pp. 2688-2690, 2005
99. J. G. Delly. "The Michel-Lévy interference color chart. The microscopist's magical color key". [<http://www.modernmicroscopy.com/main.asp?article=15>], on-line journal Modern Microscopy , 2003.
100. Olympus Microscopy Resource Center. Michel Levy Chart. [Online] <http://www.olympusmicro.com/primer/java/polarizedlight/michellevylarge/index.html>.
101. J. McAndrew. "Differential dispersion measurement of refractive index". *American Mineralogist.*, Vol. 57, pp. 231-236, 1972.
102. J. G. Delly. "The Michel-Lévy interference color chart. The microscopist's magical color key". [<http://www.modernmicroscopy.com/main.asp?article=15>], on-line journal Modern Microscopy , 2003.
103. A. Anawati. *Alignment in cylindrical geometry and dielectric properties* . Chalmers University of Tecnology, Sweden. 2005. M.Sc. thesis.
104. J. Liou, T. Chang, T. Lin, and C. Yu "Reversible photo-induced long-period fiber gratings in photonic liquid crystal fibers". *Optics Express*, Vol. 19, No. 7, pp. 6756-6761, 2011

105. E. Anemogiannis, E. N. Glytsis, and T. K. Gaylord, "Transmission characteristics of long-period fiber gratings having arbitrary azimuthal/ radial refractive index variation," *J. Lightw. Technol.*, vol. 21, no. 1, pp. 218–227, Jan. 2003.
106. J. W. Fleming "Dispersion in GeO_2-SiO_2 glasses", *Appl. Opt.*, Vol. 23, No. 24, pp. 4486 - 4493, 1984
107. S. Ertman, T. R. Woliński " Electric field control of liquid crystal infiltrated photonic crystal fibers by using various electrode configurations" *Proc. SPIE 7120*, doi: 10.1117/12.804500, 2008
108. S. Wróbel, A. Fąfara, M. Marzec, W. Haase, R. Dąbrowski, W. Drzewiński, B. Gestblom, M. Makrenek. "Ferroelectric and antiferroelectric phases studied by dielectric spectroscopy". *Phase Transitions.*, Vol. 80, pp. 791-797, 2007
109. M. Marzec, A. Mikułko, S. Wróbel, A. Szymańska, R. Dąbrowski Molecular structure and physical properties of chiral liquid crystalline compounds. "Molecular structure and physical properties of chiral liquid crystalline compounds". *Mol. Cryst. Liq. Cryst.*, Vol. 480, pp. 140-148, 2008
110. I. Del Villar, J.M. Corres, M. Achaerandio, F. J. Arregui, I. R. Matias „Spectral evolution with incremental nanocoating of long period fiber gratings”, *Opt. Express*, 14 (25), pp. 11972-11981, 2006
111. X. Shu, T. Allsop, B. Gwandu, L. Zhang, and I. Bennion, "Room-temperature operation of widely tunable loss filter", *Electron. Lett.* Vol. 37, pp. 216-218, 2001
112. B.H., Lee, Y. Chung, W.-T. Han, and U.C. Paek, "Temperature sensor based on self-interference of a single long-period fiber grating", *IEICE Transactions on Electronics E83-C(3)*, pp. 287-292, 2000
113. M.N. Ng, and K.S. Chiang, "Thermal effects on the transmission spectra of long-period fiber gratings", *Optics Communications* 208, pp. 321-327, 2002
114. Y. J. Kim, U.C. Paek, and B.H. Lee, "Measurement of refractive-index variation with temperature by use of long-period fibre gratings. *Optics Letters* 27(15), pp.1297-1299, 2002
115. G.W. Yoffe, P.A. Krug, F. Ouellette, and D.A. Thorncraft, "Passive temperature-compensating package for optical fiber gratings", *Applied Optics*, 34(30), pp. 6859-6861, 1995
116. X. Shu, T. Allsop, B. Gwandu, L. Zhang, and I. Bennion, "Room-temperature operation of widely tunable loss filter", *Electronics Letters* 37(4), pp. 216-218, 2001
117. X. Shu, T. Allsop, B. Gwandu, L. Zhang, and I. Bennion, "High-temperature sensitivity of long-period gratings", 2001
118. Adrian Van Brakel, "Sensing characteristics of an optical fibre long period grating Michelson refractometer", doctor thesis in the Rand Afrikaans University, Faculty of Engineering, 2004
119. M. Chychłowski, S. Ertman, T. R. Woliński. "Analysis of liquid crystals orientation in microcapillaries". *Photonics Letters of Poland.*, Vol. 2, 1, pp. 31-33, 2010
120. C. Tyszkiewicz, E. Maciak, P. Karasiński, T. Pustelny. "Determination of the refractive index of the SE1211 resin using an SPR spectroscopy". *Molecular and Quantum Acoustics.*, Vol. 26, pp. 267-271, 2005

121. M. Śmietana, W. J. Bock, P. Mikulic and J. Chen. "Increasing sensitivity of arc-induced long-period gratings - pushing the fabrication technique toward its limits". *Meas. Sci. Technol.*, Vol. 22, 015201, 2011
122. S. Pissadakis, M. Konstantaki and G. Violakis. "Recording of type IIA gratings in B–Ge codoped optical fibres using 248 nm femtosecond and picosecond laser radiation". *Proc. ICTON 2006*, pp. 183, 2006
123. T. L. Huynh. "Dispersion in photonic systems". Technical report MECSE-10-2004, Dept. of Electrical and computer systems engineering, Monash University, Clayton, Australia, 2004
124. I. del Villar. "Ultrahigh-sensitivity sensors based on thin-film coated long period gratings with reduced diameter, in transition mode and near the dispersion turning point". *Opt. Express*, 23 (7), pp. 8389-8398, 2015

PhD publication list

Publications in journals from the Philadelphia (ISI) list

1. T. R. Wolinski, S. Ertman, P. Lesiak, A. W. Domanski, **A. Czapla**, R. Dabrowski, E. Nowinowski-Kruszelnicki, J. Wojcik, "Photonic liquid crystal fibers - a new challenge for fiber optics and liquid crystals photonics", *Opto-Electron. Rev.* 14, 329-334 (2006)
2. T. R. Woliński, S. Ertman, **A. Czapla**, P. Lesiak, K. Nowecka, A. W. Domański, E. Nowinowski-Kruszelnicki, R. Dąbrowski, J. Wójcik, "Polarization effects in photonic liquid crystal fibers", *Meas. Sci. Technol.* 18, 3061–3069 (2007)
3. T. R. Woliński, **A. Czapla**, S. Ertman, M. Tefelska, A. W. Domański, E. Nowinowski-Kruszelnicki, R. Dąbrowski, "Tunable highly birefringent solid-core photonic liquid crystal fibers", *Opt. Quantum Electron.* 39, 1021-1032 (2007)
4. T. R. Woliński, **A. Czapla**, S. Ertman, M. Tefelska, A. W. Domański, J. Wójcik, E. Nowinowski-Kruszelnicki, R. Dąbrowski, "Photonic liquid crystal fibers for sensing applications", *IEEE Trans. Inst. Meas.* 57, 1796 – 1802 (2008)
5. T. R. Woliński, S. Ertman, M. Tefelska, **A. Czapla**, D. Budaszewski, A.W. Domański, R. Dąbrowski, E. Nowinowski-Kruszelnicki, J. Wójcik, "Polarizing and depolarizing optical effects in photonic liquid crystal fibers", *Mol. Cryst. Liq. Cryst.* 489, 495-508 (2008)
6. S. Ertman, **A. Czapla**, T. R. Woliński, T. Nasiłowski, H. Thienpont, E. Nowinowski-Kruszelnicki, R. Dąbrowski, "Light propagation in highly birefringent photonic liquid crystal fibers", *Opto-Electron. Rev.* 17, 150-155 (2009)
7. D. Budaszewski, A. W. Domański, **A. Czapla**, S. Ertman, T. R. Woliński, T. Nasilowski, H. Thienpont, "Depolarization of light in microstructured fibers filled with liquid crystals", *Opto-Electron. Rev.*, 17, 156-160 (2009)
8. **A. Czapla**, T. R. Woliński, W. J. Bock, Edward Nowinowski-Kruszelnicki, R. Dąbrowski, and J. Wójcik, "Long-Period Fiber Gratings with Low-Birefringence Liquid Crystal", *Mol. Cryst. Liq. Cryst.*, 502, 65–76, (2009)

9. **A. Czapla**, W. J. Bock, P. Mikulic, T. R. Woliński, "Towards Tuning of Thermal Sensitivity of the Long Period Fiber Gratings Using a Liquid Crystal Layer", *Bulletin of the Polish Academy of Sciences Technical Sciences*, 58, 1-6 (2010)
10. **A. Czapla**, T. R. Woliński, E. Nowinowski-Kruszelnicki, W. J. Bock, "A novel electrically tunable long-Period Fiber Grating with thin liquid crystal layer", *Acta Physica Polonica A*, 118, 1104-1107, (2010)
11. **A. Czapla**, W. J. Bock, T. R. Woliński, R. Dąbrowski, E. Nowinowski-Kruszelnicki, "Spectral Tuning of the Long-Period Fiber Gratings by Using Low Birefringence Liquid Crystals ", *Acta Physica Polonica A*, 4, 590-592, (2011)
12. **A. Czapla**, W. J. Bock, T. R. Woliński, R. Dąbrowski, E. Nowinowski-Kruszelnicki, „Tuning cladding-mode propagation mechanisms in liquid crystal long-period fiber gratings”, *Journal of Lightwave Technology*, 1, 1 (2012)
13. **A. Czapla**, W. J. Bock, T. R. Woliński, P. Milulic, R. Dąbrowski, „Improving the electric field sensing capabilities of the long-period fiber grating coated with a liquid crystal layer” – submitted to *Optic Express* (December, 2015)

Publications in refereed journals and conference proceedings

1. **A. Czapla**, P. Mikulic, W.J. Bock, T.R. Wolinski, „Studies of long-period fiber grting devices coated with the liquid crystal layer tuned near the phase-matching turning point”, *proc. IEEE Xplore, Photonic North International Conference on Optical Fibre Sensors*, <http://dx.doi.org/10.1109/PN.2015.7292510>, 2015
2. S. Ertman, K. Bednarska, **A. Czapla**, T.R. Wolinski, „Photonic liquid crystal fibers tuning by four electrode system produced with 3D printing technology”,*proc. SPIE, 24th International Conference on Optical Fibre Sensors*, <http://dx.doi.org/10.1117/12.2195189>, 2015
3. S. Ertman, M. Bielska, **A. Czapla**, K. Domosławski, M. Chychłowski, K. Reszka, T. R. Woliński, „Photochemical bonding of special optical fibers”, *Photonics Letters of Poland*, 6 (3), pp. 114-116, 2014

4. **A. Czapla** , W. J. Bock and T. R. Wolinski , "*Designing sensing properties of the long-period fiber gratings coated with the LC layers*", proc. SPIE, <http://dx.doi.org/10.1117/12.977928>, 2012
5. T. R. Wolinski, S. Ertman, D. Budaszewski, M. Chychłowski, **A. Czapla**, R. Dabrowski, A. W. Domański, P. Mergo, E. Nowinowski-Kruszelnicki, K. Rutkowska, M. Sierakowski, M. Tefelska, „*Emerging photonic devices based on photonic liquid crystal fibers*” Photonics Letters of Poland, 3 (1), pp. 116-118, 2011
6. **A. Czapla**, W. J. Bock, T. R. Woliński, R. Dąbrowski and E. Nowinowski-Kruszelnicki , "*Liquid crystal long-period fiber grating as a sensing element for electric field and temperature measurements*", SPIE; <http://dx.doi.org/10.1117/12.887546>, 2011
7. **A. Czapla**, T. R. Woliński, R. Dąbrowski, E. Nowinowski-Kruszelnicki, W. J. Bock, „*Electrically tunable filter based on a long-period fiber grating with a thin liquid crystal layer*”, Photonics Letters of Poland, 2 (3), pp. 116-118, 2010
8. A. Domański, **A. Czapla**, K. Prokopczuk, T. Poczęsny, W. J. Bock, T. R. Woliński, „*Długookresowe siatki światłowodowe jako czujniki drgań w materiałach kompozytowych*”, Pomiar Automatyka Kontrola, nr 07, pp. 809 -811, 2010
9. T. R. Woliński, D. Budaszewski, M. Chychłowski, **A. Czapla**, S. Ertman, P. Lesiak, K. Rutkowska, M. Sierakowski, M. Tefelska, A.W. Domanski, „*Photonic liquid crystal fibers: Towards highly tunable photonic devices*” Proc. Of International Conference on Photonics ,ICP, IEEE Xplore, ICP2010-82, pp. 1-5, 2010
10. **A. Czapla**, W. J. Bock , T. R. Woliński, P. Miculic „*High-Efficiency Thermal Tuning of a Long-Period Fiber Grating Using a Liquid Crystal Layer*”, Photonics Letters of Poland, 1 (2), pp. 100-102, 2009
11. T. R. Woliński, D. Budaszewski, M. Chychłowski, **A. Czapla**, R. Dąbrowski, A. W. Domański, S. Ertman, P. Lesiak, E. Nowinowski-Kruszelnicki, K. Rutkowska, M. Sierakowski, M. Tefelska, J. Wójcik, „*Fotoniczne światłowody ciekłokrystaliczne – stan badań i perspektywy rozwoju*”, Proc. of XII Scientific conference Optical Fiber and Their Application, Karasnośród, Vol I, pp. 13-25, 2009
12. **A. Czapla**, T. R. Woliński, W. J. Bock, E. Nowinowski-Kruszelnicki, R. Dąbrowski, J. Wójcik, “*Long-period Fiber Gratings using Liquid Crystals*”, Proc. SPIE, vol. 7124, 7124-06, 2008

13. **A. Czapla**, W. J. Bock, T. R. Woliński, P. Mikulic, "Towards spectral tuning of long-period fiber gratings", Proc. of Canadian Conference [Electrical and Computer Engineering, CCECE 2008](#), pp. 001015 – 001018, 2008
14. M. M. Tefelska, M. Chychłowski, **A. Czapla**, R. Dąbrowski, S. Ertman, E. Nowinowski-Kruszelnicki, J. Wójcik, T.R. Woliński, „Hydrostatic pressure effects in photonic liquid crystal fibers”, Proc. SPIE, vol. 7120, 7120-07, 2008
15. T. R. Woliński, S. Ertman, M. Tefelska, P. Lesiak, **A. Czapla**, A. W. Domański, E. Nowinowski-Kruszelnicki, R. Dąbrowski, and J. Wójcik, „Photonic liquid crystal fibers for electric field and hydrostatic pressure sensing”, Proc. SPIE, vol. 7004, 70043W, 2008
16. L. R. Jaroszewicz, K. Stasiewicz, T. R. Woliński, K. Czupryński, P. Marć, **A. Czapla**, and E. Nowinowski-Kruszelnicki, „Novel all in-line photonic crystal fiber interferometer with liquid crystal transducer”, Proc. SPIE, Vol. 7004, 70046O, 2008
17. Tomasz R. Woliński, M. Chychłowski, **A. Czapla**, R. Dąbrowski, A.W. Domański, S. Ertman, K. Godyń, E. Nowinowski-Kruszelnicki, M. Tefelska, J. Wójcik, "Fotoniczne światłowody ciekłokrystaliczne jako całościowe światłowodowe układy czujnikowe" (Photonic liquid crystal fibers for all-fiber sensing applications), Elektronika 6, s. 199, 2008
18. **A. Czapla**, S. Ertman, T. R. Woliński, J. Wójcik, and R. Dąbrowski, "Influence of temperature and electrical fields on spectral properties of microstructured optical liquid-crystals fibers", Proc. SPIE, Vol. 6608, 6608-06, 2007
19. **A. Czapla**, T. R. Woliński, S. Ertman, K. Nowecka¹, M. Tefelska, P. Lesiak, A. W. Domański, J. Wójcik, Edward Nowinowski-Kruszelnicki, R. Dąbrowski „Sensing applications of photonic crystal fibers infiltrated with liquid crystals”, Proc. of International Measurement Technology Conference, IMTC 2007, May 1-3, Warsaw, Poland, 2007
20. S. Ertman, T. R. Woliński, **A. Czapla**, K. Nowecka, E. Nowinowski-Kruszelnicki, J. Wójcik, „Liquid crystal molecular orientation in photonic liquid crystal fibers with photopolymer layers”, Proc. SPIE, Vol. 6587, 658706, 2007

21. S. Ertman, **A. Czaplą**, K. Nowecka, P. Lesiak, A. W. Domański, T. R. Woliński, R. Dąbrowski *“Tunable highly-birefringent Photonic Liquid Crystal Fiber”*, Proc. of International Measurement Technology Conference – IMTC 2007, May 1-3, Warsaw, Poland, 2007
22. T. R. Woliński, S. Ertman, **A. Czaplą**, A. W. Domański, J. Wójcik, R. Dąbrowski, E. Nowinowski-Kruszelnicki *“Photonic liquid crystal fibers as a sensing element for electric field measurement”*, Proc. of International Measurement Technology Conference – IMTC 2007, May 1-3, Warsaw, Poland, 2007
23. T. R. Woliński, **A. Czaplą**, S. Ertman, A. W. Domański, J. Wójcik, R. Dąbrowski *“Spectral properties of photonic liquid crystal fibers”*, Proc. SPIE Vol. 6587, 658705, 2007
24. T. R. Woliński, **A. Czaplą**, S. Ertman, K. Nowecka, M. Tefelska, P. Lesiak, A. W. Domański, J. Wójcik, Edward Nowinowski-Kruszelnicki, R. Dąbrowski *„Tunable Highly Birefringence Solid-Core Photonic Liquid Crystal Fibers”*, Proc. of Symposium on Microstructured and Nanostructured Optical Fibers, 1 – 6 July, Singapur, 153-161, 2007
25. T. R. Woliński, K. Brzdąkiewicz, P. Lesiak, S. Ertman, **A. Czaplą**, K. Nowecka, A. W. Domański, *„Light propagation in photonic crystal fibers infiltrated with nematic liquid crystals”*, Proc. of 6th International Conference Numerical Simulation of Optoelectronic Devices, Nanyang Technological University, Singapore, 2006
26. T. R. Woliński, P. Lesiak, K. Ślusarz, S. Ertman, **A. Czaplą**, A. W. Domański, E. Nowinowski-Kruszelnicki, R. Dąbrowski, J. Wójcik, *„Polarization effects in photonic liquid crystal fibers”*, Proc. of 18th International Conference on Optical Fiber Sensors, Cancún, México, October 23-27, 2006
27. **A. Czaplą**, S. Ertman, T. R. Woliński, J. Wójcik, R. Dąbrowski, *„Właściwości spektralne mikrostrukturalnych światłowodów ciekłokrystalicznych w obecności temperatury i pola elektrycznego”*, X Konferencja Naukowa „Światłowody i ich zastosowania”, Kranobród, Tom I, s. 87-93, 2006
28. A. W. Domański, D. Budaszewski, **A. Czaplą**, S. Ertman, P. Lesiak, K. Nowecka, K. Szaniawska, T. R. Woliński, *„Badanie propagacji światła częściowo koherentnego w światłowodowych strukturach ciekłokrystalicznych”*, X Konferencja Światłowody i ich zastosowania, Krasnobród, Tom I, s. 94-101, 2006

List of acronyms

- ASE** amplified spontaneous emission
- CMT** coupled mode theory
- DFN** dual frequency nematic
- EDFA** erbium-doped fiber amplifier
- FBG** fiber Bragg grating
- HRI** high refractive index
- LB** low-birefringence
- LC** liquid crystal
- LC-LPFG** liquid crystal long-period fiber grating
- LPFG** long-period fiber grating
- MB** medium-birefringence
- NLC** nematic liquid crystal
- OSA** optical spectrum analyzer
- PBG** photonic band gap
- PCF** photonic crystal fiber
- PLCF** photonic liquid crystal fiber
- PSF** photosensitive fiber
- RI** refractive index
- RTD** reverse tilt domain
- SC** super-continuum
- SMF** single-mode fiber
- SRI** surrounding refractive index
- TFBG** tilted fiber Bragg grating
- TIR** total internal reflection
- UV** ultraviolet
- WDM** wavelength division multiplexing